AIR MOTION IN A FOUR STROKE DIRECT INJECTION DIESEL ENGINE

by

JOHN ALAN DERHAM

A Doctoral Thesis

Submitted in partial fulfilment of the requirements

for the award of

Doctor of Philosophy of Loughborough University of Technology

November, 1972

Supervisor: J. C. DENT, Ph.D., C.Eng.

SUMMARY

The investigation presented attempts to develop a suitable mathematical model which may be relied upon to predict the air motion within the cylinder of a motored, four stroke direct injection Diesel Engine.

Using a method of hot wire anemometry, a three wire anemometer was developed for measuring the magnitude and direction of the three dimensional velocity vector within a variable density flow similar to that encountered inside a motored engine cylinder and an exhaustive experimental program undertaken to justify the technique. The results of the experimental program showed that the magnitude of the three dimensional velocity vector may be measured within an accuracy of $\pm$ 9% whilst the direction may be determined within $\pm$ 12%. Applying the method to an engine cylinder, measurements of the air motion were recorded over a range of engine speeds (500 - 1500 r.p.m.) and the effect of a masked inlet valve and supercharging the engine at 10 p.s.i.g. were also investigated. In order to predict the air motion within the engine cylinder, a mathematical model was developed which assumed that momentum of the air entering the engine cylinder was conserved and that a forced vortex velocity profile existed during the induction and compression periods, whilst friction was accounted for between the air and the containing surfaces of the cylinder during the compression period.

Comparison was made between the computed results using the mathematical model and the angular velocity computed from the velocity measurements made at differing radial locations. Agreement between computed and measured results were found to be good. The largest errors encountered were approximately 20% and these were confined to the

initial stages of the induction period (approximately the first 100 degrees crank angle) where it was concluded that an orderly flow pattern had not developed and the flow was three dimensional. However, during the latter part of the induction period and the compression period, an orderly flow pattern was developed and, during the latter stages of the compression period (after approximately 300 degrees crank angle) the flow pattern was basically two dimensional and a low vertical angle (less than 10 degrees) was measured.

Substitution of the plain inlet valve for a masked valve increased the swirl velocity, but the increase was dependant upon the mask location. When the mask was positioned along the direction of the inlet port axis, the maximum increase in swirl was measured.

Supercharging the inlet manifold to a pressure of 10 p.s.i.g. also increased the swirl velocity and, at an engine speed of 1000 r.p.m., this increase was approximately 100% at the top dead centre position during the compression period.

It was concluded that the mathematical model could be relied upon to predict a representative value of the angular velocity throughout the induction and compression periods providing that the effects of friction were accounted for and that the effect of inlet valve masking and supercharging at 10 p.s.i.g. increased the angular velocity but did not alter the orderly flow pattern developed when the engine was operated under normal conditions.

During the latter stages of the compression period, a radial component of the flow (squish) was measured and this compared well with the computed squish using the model proposed by Fitzgeorge and Allison (9) (which neglects friction). However, when the piston was

in the top dead centre position, a component of the swirl was measured and it was concluded that the swirl and squish (radial component of flow) could not be isolated from each other but instead combine together to form a spiral pattern as the air is transferred from the outer cylinder into the combustion chamber.

A C K N O W L E D G E M E N T S

The author wishes to express his thanks to:

Dr. J. C. Dent for his guidance throughout the project,

Mr. P. Norton and all other members of the laboratory staff for manufacturing hardware,

Mr. K. Topley for his photographic work,

Miss M. Tivey for typing the completed thesis,

Mr. C. J. Morris for his suggestions and help in developing the mathematical model.

PUBLICATION

The following paper entitled "A Method for Checking the Consistency of Velocity Computations from Hot Wire Anemometer Measurements in Variable Density Flows" was accepted for publication in the Journal of Physics E: Scientific Instruments, 1972.

NOTATION

A	Cross-sectional area of inlet port	(m^2)
a	Radius of the cylinder	(m)
b	Radius of the combustion chamber	(m)
Cd	Coefficient of discharge	(-)
C_f	Skin Friction	(-)
Cp	Specific heat of air at constant pressure	($KJ/kg\,^oK$)
D	Diameter of cylinder	(m)
d	Diameter of combustion chamber	(m)
I	Mass moment of inertia	(kgm^2)
k	Thermal conductivity	($w/m^2\,^oC/m$)
$\dot{m}$	Mass flow rate	(kg/s)
m_t	Induced mass	(kg)
N	Engine Speed	(r.p.m.)
P	Pressure	(KN/m^2)
S(θ)	Distance from piston top to cylinder cover	(m)
T	Temperature	(^oK)
t	time	(s)
U	Entry velocity of induced air	(m/s)
V	Volume	(m^3)
w	Angular velocity	(rad/s)
γ	Ratio of the specific heats	(-)
Δ	Incremental step or finite difference	(-)
θ	Crank angle and incidence of a velocity vector to a single sensing wire	(^{o})
α	Temperature coefficient of resistance	($/^oC$)
μ	Dynamic viscosity of air	kg/m s
ρ	Density	(kg/m^3)

τ	Shear Stress	(N/m^2)
ϕ	Entry angle of induced air	(^{o})
$\not{\phi}$	Angle between inlet port axis and line joining cylinder axis to inlet port axis.	(^{o})

SUFFICES

b	refers to the combustion chamber
c	refers to the engine cylinder
g	refers to the instantaneous gas temperature
IVC	refers to inlet valve closing
n	refers to instantaneous value at crank angle θ and cylinder contents
o	refers to normal temperature and pressure conditions (ambient 20^oC, 14.7ps
w	refers to the anemometer wire temperature
T.D.C.	refers to top dead centre
B.D.C.	refers to bottom dead centre

L I S T O F C O N T E N T S

1.0 INTRODUCTION

1.0 INTRODUCTION

1.1 General Comment

The internal combustion engine has been in use as a prime mover for well over fifty years and, despite its extensive use, the detailed mechanism of the combustion and heat transfer processes occurring inside the engine cylinder have not been completely understood. This situation arises due to the complexity of the process involved and also because of the empirical nature of engine development over the years. The need for engines developing higher specific output and in the future, with low exhaust emission levels, has led to a more fundamental appraisal of the combustion process within the engine cylinder.

1.2 Effects of Air Motion on Combustion in a Diesel Engine

In 1934, Alcock demonstrated that the air motion inside the cylinder of a high speed Diesel Engine was necessary for efficient combustion because it promoted rapid mixing of the air and fuel within the combustion chamber. Over the years, various methods have been developed to promote air/fuel mixing in the Diesel Engine and these may be summarised as follows:-

(i) Induction swirl

(ii) Compression swirl and squish

(iii) Indirect injection

Induction swirl is developed throughout the induction period by suitable inlet port design which imparts a tangential component to the incoming air. A similar tangential component can also be developed by the use of a masked or shrouded inlet valve, which produces an optimum direction in which the air can enter the cylinder.

The swirl is increased throughout the compression period by suitable piston design and, as top dead centre is approached, the transfer of air from the outer cylinder area to the combustion space in the region of the centre of the piston is referred to as squish.

Indirect injection may also be used to promote air/fuel mixing by the suitable design of a pre-combustion chamber which is connected to the cylinder by a short passage. As the piston approaches top dead centre during the compression period, the air is transferred to the pre-chamber where the fuel is simultaneously injected.

Each particular engine design will have its own optimum conditions of swirl which will provide an efficient combustion process. However, to achieve this optimum swirl for a particular engine design, extensive engine development and cold flow rig testing are required. This procedure is expensive and a more fundamental knowledge of the swirl process is a necessary part of reducing engine development costs and providing a more detailed understanding of the combustion process.

1.3 Object of the Investigation

The object of this investigation is to make an accurate appraisal of the air motion within the engine cylinder of a four stroke, direct injection Diesel Engine and to investigate some of the factors influencing this motion. The results of a comprehensive experimental study are presented in which extensive use was made of hot wire anemometry in the determination of cylinder airflow magnitude and direction. A theoretical model for the air motion is developed which includes the effects of fluid friction at the air and surface interfaces within

the cylinder and relates the air motion in the cylinder to easily measured engine parameters (speed, cylinder geometry and valve timing) so as to facilitate its use in design computations.

2.0 LITERATURE SURVEY AND THE OBJECTIVES OF THE INVESTIGATION

2.0 LITERATURE SURVEY AND THE OBJECTIVES OF THE INVESTIGATION

2.1 Currently Accepted Definitions of Swirl and Squish

In order to understand the air motion within the cylinder of a Diesel Engine, it is important to define the components of the existing air motion, which are generally accepted to be swirl and squish.

Fig. 2.1 illustrates an idealised port and cylinder where swirl is initiated during the induction period by admitting the air so that it has a tangential component of velocity to the cylinder wall. The air in Fig. 2.1 is induced by the downward movement of the piston, the inlet port being inclined at an angle ϕ to the horizontal and the air speed denoted by U. The values of U and ϕ will obviously affect the swirl rate within the engine cylinder.

The effect of varying the angle ϕ may be understood by considering the extreme values $\phi = 0^{o}$ and $\phi = 90^{o}$. In the latter case, there is no swirl and in the former case there would be no axial component of inlet velocity and the tangential component U cos ϕ would have its maximum value U, with maximum swirl being the result. The conception of idealised swirl breaks down for very small angles of entry but it is clear that for a maximum swirl ϕ should be as small as possible. With an intermediate value of ϕ, the air motion within the cylinder is a combination of the effects of the components U cos ϕ and U sin ϕ, the former produces swirl and the latter an axial component of the type produced when $\phi = 90^{o}$, the axial component not affecting the swirl but only the number of revolutions of the air motion per cylinder length.

The distance of the idealized port from the cylinder axis must necessarily influence the swirl, and the diameter of an engine port is usually such that only two valves can be accommodated on the same diameter. However, in a vast majority of engines, the placing of an injector coincident with the cylinder axis necessitates the valve centres being approximately equal to half the cylinder radius and thus allows little scope for variation.

During the compression period the swirl developed throughout the inlet period is assumed to be increased in accordance with the conservation of angular momentum and change of moment of inertia that occurs when the mass of air is transferred from the outer cylinder into the combustion chamber in the piston crown, as the piston approaches the top dead centre position. It is possible therefore to extend the definitions of swirl to include both induction swirl and compression swirl, the former developed during the induction period and the latter continuing throughout the compression period.

Whilst swirl occurs throughout the induction and compression periods of the engine cycle, squish is only developed during the latter part of the compression period and is a simple process to define. Consideration of Fig. 2.2 illustrates that squish consists of a radial movement of the air across the piston crown resulting from a transfer of air from the outer cylinder area into the piston recess which forms the combustion chamber. This transfer of air occurs as the piston approaches the top dead centre position during the compression period and consequently squish only occurs during that part of the engine cycle.

In summarising, it may be said that the air motion within the engine cylinder which is most likely to affect the air and fuel

mixing, is comprised of an initial induction swirl followed by compression swirl. Finally, as the piston approaches top dead centre during the latter part of the compression period, a squish component develops along with the compression swirl.

2.2 Summary of the Literature Surveyed

In 1934, Alcock (1) demonstrated conclusively with the aid of a swirl meter that swirl exists within the cylinder of an engine. He concluded that, with regard to engine output performance, an optimum swirl ratio (number of revolutions of the swirl meter per minute/number of revolutions of the engine per minute) exists for a particular combustion system and this swirl ratio is independent of engine speed, size and load. It is therefore a characteristic of the particular combustion system.

Lee (7) 1938, also demonstrated that air motion exists within the cylinder of a four stroke spark ignition engine, using a high speed photographic technique and tracers injected with the air entering the cylinder. This method permitted measurement to be made with reasonable accuracy and the effect of a masked inlet valve showed an increase in the measured swirl rate whilst the use of a modified inlet port produced some vertical motion within the engine cylinder, particularly during the induction period.

Dicksee (8), 1949, postulated a possible pattern of the air motion within an open combustion chamber engine and he substantiated this with a single frame photograph obtained using fine drops of paint on the piston crown and motoring the engine at speed for several minutes. This technique, whilst justifying

Dicksee's (8) postulation allowed no quantitative measurements of the swirl to be made.

In 1962, Fitzgeorge and Allison (9) presented the first theoretical model for the air motion in the engine cylinder which could be used in conjunction with the results from a cold blowing test rig. The results of this study supported those of Alcock (1) and Dicksee (8) and suggested that, whilst an orderly swirl pattern might exist during the induction and initial compression periods, a more complicated toroidal pattern occurs within the combustion chamber as the piston approaches the top dead centre position during the compression period.

Alcock and Scott (10), 1962, presented a comprehensive photographic study of the combustion process within the engine cylinder using several different types of direct injection combustion chamber geometry. The results justified the hypothesis of an orderly flow within the open combustion chamber system. However, they also showed a distinct absence of the toroidal motion postulated by Alcock (1), Dicksee (8) and Fitzgeorge and Allison (9). Instead, Alcock and Scott (10) presumed that the air entered the combustion chamber in a spiral manner and then continued to rotate at an increased speed.

Finally, Horvatin and Hussmann (11) successfully installed a hot wire anemometer system within an engine cylinder and used this method to determine accurately the air motion under motoring conditions. The results, whilst suggesting a forced vortex profile existed within the engine cylinder, also showed a total absence of toroidal motion during the latter part of the compression period, thus supporting the

photographic evidence of Alcock and Scott (10).

In order to justify future investigations of the air motion within the engine cylinder of a four stroke, direct injection Diesel Engine, the above literature was reviewed in considerable detail and a critical appraisal made of each publication. The detailed survey may be found in the following Section 2.3.

2.3 Detailed Literature Survey

2.3.1 ALCOCK, J.F. (1), 1934

Alcock (1) in 1934 stated that air movement is required in both petrol and oil engines in order to promote satisfactory combustion. However, an important difference exists between the two systems and that is, in the ready mixed charge of the petrol engine, the duty of the air flow is to disperse the flame nuclei, whilst in the oil engine, the temperature is everywhere sufficiently high to effect ignition wherever the air and fuel come together and therefore the duty of the air movement is to bring them together. For this reason, an orderly movement or swirl is required in the oil engine as opposed to the indiscriminate turbulence which suits the petrol engine. Three methods of swirl production were postulated by Alcock (1) and these are:-

(i) Induction swirl, produced by oblique air inflow to the cylinder during the induction period (or scavenge period in the case of two stroke engines).

(ii) Compression swirl, produced during the compression period by forcing the air through a restricted passage and into a pre-combustion system and is successfully demonstrated in such systems as the Lister, the Ricardo 'Comet' and the Thornycroft.

(iii) Combustion swirl, produced by the combustion and subsequent expansion of the air. The Lanova engine is the only one using this principle.

In order to measure the rate of swirl within an oil engine, Alcock (1) proposed two measuring devices suitable for use within a motored engine. The first was a freely rotating vane located within the combustion chamber and carried on a spindle which passes through a sealing gland to an external counting mechanism, refer Fig. 2.3. The vane revoltuions per minute were measured whilst the engine was motored at a particular speed. It is obvious that the measured speed is not the true swirl at the end of the compression period, which is of particular importance when considering the combustion process, but instead some kind of mean of the swirl throughout the entire engine cycle. Alcock (1) concluded however that the two values appear to be in some roughly constant relationship, since it was found that different engines, with similar combustion arrangements, all required much the same swirl rate as measured by the above method. The second method was to measure the force exerted by the air on a fixed vane and this idea is described in detail by Sass (2) and illustrated in Fig. 2.4.

The latter method has two important advantages over the first, that it can be used in cases where the swirl axis is occupied by a piston rod or other obstruction and secondly it can give some

indication of the swirl variation during the engine cycle. However, it is difficult to allow for the swirl reducing effects of the fixed vane and the inertia of the moving parts would seriously affect the indication at high engine speeds. In addition to their use on motored engines, both methods can be employed on cold rig tests, air being supplied to the inlet ports from an external source. The freedom of experiment is of course far greater in these tests than that encountered on a motored engine but Alcock (1) stated that, to his knowledge, there was no reliable method for deducing motoring swirl rates from experiments carried out on cold test rigs.

Having adopted a paddle wheel similar to that illustrated in Fig. 2.3, Alcock (1) investigated in detail the development of swirl within the cylinder of an oil engine using a single sleeve inlet valve principle and a vortex combustion chamber, refer Fig. 2.5 and 2.3 respectively. Alcock (1) suggested that, if the viscosity and compressibility effects were negligible, the velocity inflow at any point during the induction period would be proportional to the engine speed but its direction unaffected by this. The number of swirl revolutions per minute would then be proportional to the engine speed and the swirl ratio, defined as

$$\text{Swirl ratio} = \frac{\text{Number of revolutions per minute of the swirl meter}}{\text{Number of revolutions per minute of the engine}}$$

would remain constant. Similarly, if the linear dimensions of the engine were doubled, the inflow velocity would be doubled and also the diameter of the swirl would be doubled; hence the number of revolutions of the air per minute would remain unchanged.

Several important factors which could be altered within an existing engine and thereby produce a change in the swirl ratio were also suggested and the first of these is the inlet valve timing. Delaying the inlet timing showed an increase in the inflow velocity during the early part of the induction period, when the swirl effect is generally highest and this resulted in an increase in the measured swirl ratio. Alteration of the combustion chamber diameter affects the velocity within the chamber, since the air rotating within the cylinder will have a fixed angular momentum and, if this mass is transferred to the small diameter combustion chamber, neglecting frictional losses, the angular velocity will increase, since momentum must be conserved. In engines using a poppet inlet valve, it is generally accepted that the valve itself has no ability to produce swirl, although this can be achieved when a plain inlet valve is used in conjunction with an inlet port located so as to direct the air tangentially into the cylinder. Alternatively, a masked inlet valve could be used to direct the air in a particular direction and Alcock (1) concluded that, whilst he could find no evidence of the use of a masked inlet valve in motoring studies, preliminary experimental work using a cold test rig showed that increases of 50-60% could be achieved in the swirl ratio using a masked valve.

With particular reference to the experimental investigation of the 'Vortex' chamber, refer Fig. 2.3, Alcock (1) suggested that the air does not rotate as a solid body within the chamber but rather as a free vortex. This was suggested by the increase in measured values of swirl when paddle wheels using smaller diameter vanes were used, although this could also be an indication of the frictional and inertial effects being reduced by the smaller vanes

Further investigation also suggested that the air moves in a spiral pattern within the combustion chamber and this may be explained by:

(i) the piston approaching the top dead centre position expels the trapped air in the cylinder, thus creating an inflow at the bottom of the combustion chamber,

(ii) the friction of the outside walls of the combustion chamber reduces locally the swirl ratio and therefore the centrifugal pressure gradient and this causes the air to move inwards at the ends and outwards in the middle.

The combined effect of these two facts gives the circular path, illustrated in Fig. 2.6, the central outflow being displaced upwards by the squish inflow at the bottom of the combustion chamber.

Using a swirl pre-combustion chamber, Alcock (1) developed a mathematical model for the swirl developed throughout the compression period and this model was based on the assumption of conservation of momentum between the cylinder and the pre-combustion chamber. The model gave exceptionally high values of swirl ratio (55 for a typical 'Comet' design) and experimental work performed on a similar chamber (theoretical swirl ratio = 42) recorded a measured value of 14, approximately 30% of the theoretical. This error is likely to arise due to the absence of frictional considerations in the mathematical analysis and whilst these may not be particularly high due to the cylinder wall, it is likely to be a serious deficiency regarding the mass transfer through the throat, connecting the cylinder and the pre-combustion chamber, and the friction that will result due to the surface of the paddle wheel vanes.

Alcock's (1) major conclusions from his experimental work carried out primarily on a single sleeve valve engine incorporating a vortex chamber combustion system were as follows:

(i) Swirl is developed during the induction period and a secondary pattern of air motion occurs during the latter stages of the compression period,

(ii) An optimum swirl ratio, determined with respect to the engine performance, was found to exist and this ratio was practically independent of engine size, speed and load. It was concluded therefore to be a characteristic of that particular combustion system.

(iii) The most effective way of increasing the swirl ratio was to reduce the diameter of the combustion chamber, although similar results could be achieved by delaying the inlet timing of the engine.

(iv) For engines incorporating a poppet valve, there was evidence from cold rig tests to suggest that the use of a masked inlet valve could, with correct adjustment, provide considerable improvements to the swirl ratio.

The discussion of Alcock's (1) paper following its presentation at several Institution of Mechanical Engineers' meetings raised some interesting questions regarding the development of swirl and these are outlined below along with supporting criticism.

Mr. T. F. Hurley (3) said that he had been responsible for a series of tests carried out to determine the effect of various forms of turbulence, including swirl, on petrol engine performance. The engine tested was a Ricardo E5 sleeve valve incorporating

a combustion chamber identical in shape with the vortex head illustrated in Fig. 2.3 so that, under certain conditions, the air movements should be exactly similar to that described by Alcock (1).

Hurley (3) criticised both methods of measuring swirl presented by Alcock (1) since they disturbed the distribution of air velocity; the swirl meter by compelling the whole of the air to move with the same angular velocity and the Sass meter by obstructing the air flow. Hurley (3) used a technique involving a Pitot tube (*further detail of this may be found on Page 157 of Alcock's (1)* paper) and measured the velocity at several radial locations within the combustion chamber. Fig. 2.7 illustrates the results obtained and, unlike the free vortex profile suggested by Alcock (1), observation shows that the velocity decreased as the centre of the chamber was approached, that is an approximation to a forced vortex was obtained. After a certain position however, the curve departed from that of a forced vortex and tended to rise. With a forced vortex, the curve should descend to a zero value at the centre of the combustion chamber. It must be remembered however that the curves represent an average of the velocities throughout the engine cycle and, whilst there is evidence to suggest a compound vortex (combination of free and forced vortex) exists throughout the engine cycle, it is possible that a forced vortex may be predominant during the induction period and a free vortex during the compression and expansion periods. However, this hypothesis could only be justified by detailed analysis of the air motion throughout the engine cycle which cannot be achieved using either the swirl meter or the pitot tube.

Mr. R. Cooke (4) supported Alcock's (1) remarks concerning the probability of inward radial flow caused by the friction of the cylinder walls and illustrated in Fig. 2.6.

Cooke (4) said concrete evidence of this radial motion had been obtained by placing a glass plate over the cylinder head and coating the underside with oil. Particles of carbon were put in the oil to assist visibility and, when the engine was motored, the oil moved in a series of equiangular spirals towards the central nucleus. Consequently, it appears that the assumption of a secondary motion within the combustion bowl is fully justified.

Wing. Commr. T.R. Cave-Browne-Cave (5) criticised the measuring techniques adopted by Alcock (1) because he considered the presence of the vane would destroy the free vortex which he considered would be the natural flow pattern with the Vortex combustion chamber. Instead of using a vane, he suggested the possible use of a hot wire anemometer which would have a far greater response to the flow pattern than a swirl meter and it was interesting to note that such a technique was considered feasible at this time.

A further communication by Mr. P. M. Baker (6) suggested that a small paddle wheel which could be located at various radii and heights within the combustion chamber might yield results which would be of importance in defining the profile of the air motion. Baker (6) himself had employed Pitot tubes for the measurement of gas velocity but, like Cave-Browne-Cave (5), he suggested the possible use of a hot wire anemometer, although he considered that serious problems would be encountered regarding the calibration of such an instrument for use inside a variable density flow likely to be found within a motored engine.

In summarising the work presented by Alcock (1) and the discussions and communications to this work, it is apparent

that the majority opinion confirms the development of swirl during the induction period, which continues throughout the compression period. However, little detailed knowledge is available concerning the profile of the air motion during the individual periods of the engine cycle, for instance Alcock (1) suggested a free vortex to exist within the combustion chamber whilst Hurley (3) presumed a compound vortex was a more representative description. Regarding the question of secondary motion within the combustion chamber, the evidence appears conclusive that the air spirals into the combustion chamber and that there is probably a more complicated toroidal motion existing. Unfortunately little knowledge is available concerning this motion due to the lack of response of the swirl meter to a radial component of the flow. Throughout the experimental work, Alcock (1) adopted to use a single sleeve valve engine for the development of the swirl during the induction period and no evidence is presented for a comparison between this arrangement and the more conventional poppet valve engine. It is considered likely, however, that the comments regarding swirl and secondary motion within the combustion chamber should apply to almost any engine, since the swirl, having been developed inside the cylinder is affected only by the piston and combustion chamber geometry during the compression period. It is also more usual to find the combustion chamber located within the piston crown on a poppet valve engine instead of the cylinder head as is the case with the single sleeve engine used by Alcock (1). However, the transfer of mass from the outer cylinder into the combustion chamber should be similar regardless of the combustion chamber being located in the cylinder head on the piston crown.

Whilst Alcock (1) has provided a quantity of information regarding the swirl and presented a variety of suggestions for improving the air and fuel mixing process, it is obvious that a considerable amount of work has yet to be performed in order to clarify and substantiate his basic ideas. Since the swirl meters mentioned in the paper are both unable to respond accurately to the air motion, it would seem feasible to investigate the suggestions of Cave-Browne-Cave (5) and Baker (6) and attempt to use a hot wire anemometer within the engine cylinder. This latter method should be invaluable regarding the clarification of the outstanding problems outlined above.

2.3.2 LEE, D.W. (7), 1938

In 1938, Lee (7) conducted a study of the air motion within an engine cylinder of a 4 stroke, spark ignition engine. The engine was equipped with a glass cylinder and the air movements were studied whilst the engine was motored at a particular speed. Movement of the air was made visible by mixing white goose feathers with the entering air and high speed motion films taken so that the air currents might be studied in detail and their velocities measured. A swirl meter was also used to indicate the rate of rotation of the air about the cylinder axis. In order to produce different types of air motion within the cylinder, Lee (7) constructed several masked valves which had mask angles varying

between 180^{o} and 90^{o} and also a plain inlet valve and a modified inlet port, the latter being altered with the use of modelling clay. In conjunction with the films of the air motion, the fuel spray was recorded on film during the inlet period, so that some estimation could be made of the effects of the air motion on the fuel spray.

From the experimental work, Lee (7) concluded that the air movement developed during the induction period continued throughout the compression period and was a distinct aid to the distribution of the fuel spray injected into the cylinder. Measurements of the velocities of the induced air showed they were approximately proportional to the engine speed and the use of a masked inlet valve arranged to direct the incoming air tangentially into the cylinder, resulted in the air rotating rapidly about the cylinder axis at an increased rate compared to that developed when plain inlet valves were used; this maximum rate of rotation occuring at approximately 110 degrees crank angle after the commencement of the inlet period, refer Fig. 2.8. The results illustrated in Fig. 2.8 also suggest that the inlet velocity is higher than the velocity of the air movements occuring towards the end of the compression period and this may be explained as follows. During the latter part of the compression period, the feathers become enclosed in a smaller volume and so it becomes impossible to perform a detailed analysis of the individual feathers after 320 degrees crank angle. Secondly, for the successful investigation of the air motion using tracers, it is assumed that the density of the tracer material is approximately equal to that of the air under investigation and during the compression period the density of the air will change appreciably due to its compression within the cylinder. Consequently the tracer density material is no longer equal to that of the air

and this results in serious inaccuracies occuring in the measuring technique.

Using a plain inlet valve and a modified inlet port, which directed the incoming air into the cylinder at an angle of approximately 45 degrees to the vertical, resulted in rotation of the air about the cylinder axis but this was also accompanied by considerable turbulence and some vertical air movement, however the turbulence subsided during the compression period. The tests carried out using the swirl meter were not considered to be as accurate as the results from the high speed film and were therefore only used to make an approximate comparison with the swirl ratio calculated from the films.

Summarising Lee's (7) work, it is clear to see that the air and fuel mixing process can be greatly improved by the development of induced air motion within the engine cylinder and consequently the work is of considerable importance. However, several disadvantages exist regarding the experimental techniques and improvements would have to be made in a future investigation using this method. For instance, using the feathers mixed with the induced air, a maximum engine speed of only 1000 r.p.m. could be reached since the feathers became blurred traces on the film at higher speed. This is a serious disadvantage because the representative speed of a spark ignition engine of the size used is likely to be in excess of 3000 r.p.m.; however, with the development of more sophisticated photographic techniques, it is unlikely that this problem could not be overcome. Attempts were made to photograph both the motion of the feathers and the fuel spray together but this was not possible because the feathers hid all trace of the fuel spray.

Consequently, these photographs had to be made separately which relied upon good cycle to cycle repeatability of the air motion. The velocities of the air motion derived from the study of individual frames from the film are not true velocities for two important reasons:-

(i) all the motion parallel to the camera axis was neglected,

(ii) in all accelerated movements, the feathers lagged behind that of the air because of their greater density.

These problems could be overcome by selecting for the measurement purposes only those feathers which appeared to move perpendicular to the camera axis and also by selecting the more rapidly moving feathers. Finally, the most serious criticism results from the inability to measure any velocities of the air motion whilst the piston was within 40 degrees crank angle of the top dead centre position, and such a situation occurred because, in this position of the piston, the feathers were no longer visible as individual traces. This period of the cycle is of considerable importance because it is during the latter part of the compression period that ignition will occur and hence the details of the air and fuel mixing are of considerable importance.

It must be concluded therefore that this type of photographic technique, like that of the paddle wheel, can only give an approximate indication of the air movement within the engine cylinder and cannot be relied upon to produce accurate magnitudes and directions of the air motion within the engine cylinder.

2.3.3 DICKSEE, C. B. (8), 1949

Dicksee (8) presents a comprehensive review of the effects of the open combustion chamber in relation to the performance of the Diesel Engine. Investigating the effects on the brake mean effective pressure of an engine, Dicksee (8) concluded that the most effective way of promoting increased performance was to alter the air motion within the engine cylinder using a masked inlet valve. The masked valve having superiority to the modified inlet port since the former can be rotated through a variety of positions whilst modifications to the latter are more difficult to manufacture.

Having developed a suitable swirling motion during the induction period by using a masked inlet valve, Dicksee (8) suggested that the swirl would continue throughout the compression period and with a deep bowled combustion chamber with a conical mound, would result in the air travelling into the combustion chamber in a spiral pattern. Photographic evidence produced using small drops of paint on the piston crown and then motoring the engine at speed for several minutes supported this assumption and is illustrated in Fig. 2.9. During the compression period, the air is transferred from a rotating mass having a diameter equal to that of the cylinder into a mass of smaller diameter equal to that of the combustion chamber and, theoretically, by the law of conservation of momentum, this results in an increase in rotational velocity proportional to the squares of the two diameters. Dicksee (8) suggests that considerable losses due to friction will accompany the transfer and the increase in rotational velocity will be considerably less than the theoretical. The actual speed would

not be easy to determine but the ratio according to Dicksee (8) is more likely to be that of the two diameters.

In addition to the rotary motion of the air Dicksee (8) suggests that there is a well defined secondary motion similar to that suggested by Alcock (1) which plays an important part in the air and fuel mixing process. The movement is complex and is caused by the frictional effects of the fluid rotating against the combustion chamber walls which results in a centrifugal pressure against the wall near the middle of its length. Because this centrifugal pressure is higher in the middle than at the two ends there is a flow outward from the middle towards the ends. The air near the middle endeavours to maintain its correct pressure and so throws air outward to the wall, the supply being maintained by a flow axially inwards toward the middle from either end. This movement, combined with the rotary movement, produces a double helical movement inwards across the ends and outwards across the centre, the result being a double vortex movement illustrated in Fig. 2.10.

Dicksee (8) concludes from his experimental measurement of engine output performance that the secondary motion is beneficial to the engine performance and is supported by a marked falling off in performance if the conical mound is removed from the floor of the combustion chamber. Consequently, it appears that the function of the mound seems to assist the air to turn at the bottom of the combustion chamber and so produce the maximum amount of secondary movement.

Whilst Dicksee (8) presents some excellent photographic evidence to support his hypothesis of an orderly

swirl and spiral movement within the combustion chamber, no attempt is made to measure quantitatively the rotating motion within the engine cylinder. Consequently, Dicksee's (8) only estimation of the improvements of the air and fuel mixing resulting from the developed air motion originates from the performance tests carried out on the engine and these tests are obviously laborious and a costly procedure. It is not possible therefore to justify the method as a suitable approach for future investigations.

2.3.4 FITZGEORGE, D. and ALLISON, J.L. (9), 1962/63

Fitzgeorge and Allison (9) recognised the necessity for a satisfactory air motion within the engine cylinder and attempted to present a theoretical analysis of the air motion occurring within the engine cylinder which could be related to an experimental investigation performed on a cold blowing rig.
The authors developed a test rig consisting of a pipe through which air could be blown at a predetermined rate and on one end of which a cylinder head assembly could be mounted. Using a swirl meter located inside the pipe, an assessment was made of the swirl producing ability of the inlet port under steady state conditions. It is important to mention, however, that this would not necessarily be a reliable indication of the swirl generated by the inlet port when incorporated on an engine under operating conditions because of the frictional and inertial effects of the swirl meter and the fixed opening of the inlet valves. During the cold rig test, the momentum of the air supplied to the rig will pass continuously down the pipe, whilst in the engine cylinder the momentum produced by the air entering the cylinder through the inlet valve, which incidentally will vary from one crank angle position to another, remains inside the cylinder. Hence, if two identical cylinder heads were fitted, one to the cold test rig and one to an engine, then for a particular flow rate and valve opening, since the ability to produce angular momentum would be the same in each case, the momentum flow past the swirl meter would equal the instantaneous rate of acquisition of momentum by the air inside the cylinder. In a mathematical form this can be expressed by:

$$\frac{1}{2} G b^2 w_r = \frac{d}{dt} (I w_c) \qquad \text{——————} \quad 2.1$$

where G is the mass per second entering the cold test rig

b is the radius of the rig pipe

w_r is the mean angular velocity of the swirl meter

Iw_c is the instantaneous angular momentum of the air inside the engine cylinder.

Integrating both sides of equation 2.1 gives

$$\frac{b^2}{2}\int_o^t Gw_r\,dt = \int_o^{Iw_c} d(Iw_c) = Iw_c \qquad \text{——————2.2}$$

Therefore, $$w_c = \frac{b^2}{2}\int_c^t \frac{Gw}{I}_r\,dt \qquad \text{——————2.3}$$

This gives an expression for the instantaneous swirl within the cylinder during the induction period and depends upon the results of mean angular velocity (w_r) of the swirl meter and the mass flow rate (G) obtained from the cold test rig.

Assuming the pressure distribution during the induction and compression periods to be spatially uniform and that the angular velocity is the same for each particle of air, the authors show that the angular momentum of the air at any instant is given by, (refer Appendix 5A for derivation)

$$Iw_c = \frac{w_c\, m_t}{2}\,\frac{\left(\frac{\Pi\, b^4\, s(\theta)}{v} + a^2\right)}{\left(\frac{\Pi\, b^2\, s(\theta)}{v} + 1\right)} \qquad \text{——————2.4}$$

where w_c is the instantaneous angular velocity

m_t is the mass of air within the cylinder

b is the radius of the engine cylinder

a is the radius of the combustion bowl

$s(\theta)$ is the distance between piston and cylinder head

v is the volume of the combustion chamber.

Hence, using equation 2.3 the angular velocity can be computed at any instant throughout the induction period and the computation extended for the compression period using equation 2.4 and noting that the integral Gw_r will be constant throughout this period and equal in value to that computed at inlet valve closing.

In order to complete the theoretical analysis of the air motion within the cylinder, the authors investigated the radial transfer of the air as the piston approaches the top dead centre position during the compression period. This motion is referred to as squish and by neglecting the presence of spatial pressure differences, which were shown to be negligible, the squish was computed on a mass transfer basis between the outer cylinder and the combustion chamber and the geometrical dimensions of the piston. The equation derived for squish is given by the following expression and its derivation may be found in Appendix 5B.

$$U_r = \frac{1}{2r}\left(\frac{b^2 - r^2}{As(\theta) + v}\right)\frac{v}{s(\theta)}\frac{ds(\theta)}{dt} \qquad \text{——————2.5}$$

where U_r is the radial velocity

r is the characteristic radius for the velocity

A is the cross sectional area of the cylinder

$\frac{ds(\theta)}{dt}$ is the piston velocity

Using the equations 2.3, 2.4 and 2.5 both the swirl and squish were calculated for an engine speed of approximately 2000 r.p.m. and are illustrated in Figs. 2.11 and 2.12. Fig. 2.12 shows the swirl calculated for several inlet port configurations and Fig. 2.11 illustrates the variation of squish with crank angle position before the top dead centre position for different piston crown and cylinder head clearances.

From the theoretical analysis undertaken, the authors conclude that squish will increase with,

(i) diminishing 'bump clearance' between the cylinder head and piston crown,

(ii) decrease in the combustion bowl diameter.

The maximum squish value will however be limited because, in the case of the 'bump clearance', it is impractical to reduce this distance below 0.075 cm (.030 in) owing to the thermal expansion occurring with increase in engine temperature. Reduction of the combustion bowl diameter can only be made at the expense of increased piston height, since the compression ratio of the engine must be maintained and increase in the piston height will obviously lead to an increase in the height of the engine.

Using the equations 2.3 and 2.4 for the calculation of swirl, it may be observed that the swirl speed during the induction period may be increased by

(i) increasing the air inflow capacity of the inlet valve or alternatively by supercharging the engine,

(ii) extending the range of crank angle (or valve lift) over which the cylinder head has a swirl producing capability.

The former suggestion has the obvious limitation of physical size and normally the largest size of inlet valve that may be accommodated in the cylinder head is used. The second suggestion indicates the possible advantage of using a masked valve and this would definitely improve the computed swirl, provided that the volumetric efficiency may still be maintained.

Regarding the pattern of air motion developed within the engine cylinder, Fitzgeorge and Allison (9) assume that the swirl developed during the induction period continues throughout the compression period and is accompanied by a squish motion as the piston approaches the top dead centre position. Ideally, if the two different flow patterns could be isolated from each other, the swirl would result in a rotary motion within the combustion chamber, whilst the squish would produce a double helical movement either side of the combustion chamber centre line. However, the authors make the assumption that the combination of the two movements results in a rotary toroidal movement and, whilst this is a feasible argument, it is also possible that with the high swirl rates calculated for the particular engine configuration ($\triangleq$ 20,000 r.p.m. at top dead centre) the swirl would completely dominate the air movement within the combustion chamber. It is unlikely then that the air would perform the theoretical toroidal motion suggested but instead rotate inside the combustion chamber at a rate governed by the cylinder and piston crown geometry. Conversely, if the swirl were particularly low at the top dead centre position, the reverse situation could occur and the helical movement would become the dominant air motion. However, it is not possible to justify either of these arguments without the adoption of a more sophisticated measuring technique which can predict accurately the direction of the air motion and then it should be possible to clarify the movement within the combustion chamber.

2.3.5 ALCOCK, J.F. and SCOTT, W.M. (10), 1962/63

Alcock and Scott (10) investigated the sequence of the combustion process occurring within a small, high speed Diesel Engine using a high speed photographic technique and, having developed a reliable method, they recorded the combustion process that occurred using three different types of combustion system, these being,

(i) Toroidal direct injection chamber

(ii) 'Meaurer' direct injection chamber

(iii) Pre-combustion chamber

From the individual frames of the combustion film it is possible to make some estimation of the swirl speed within the cylinder although this will be limited to movement occurring at right angles to the camera axis. It was concluded from the measurements that the swirl in the top dead centre position during the compression period on the engine using a vortex chamber was higher than the previous experimental values reported by Alcock (1) using a swirl meter and this conclusion supports the criticism of the swirl meter mentioned previously, emphasising the poor response of the equipment. Analysis of the results using the pre-chamber combustion system revealed that the maximum swirl occurs before 350 degrees crank angle and this agrees closely with the theoretical results computed by Alcock (1) for the 'Comet' pre-combustion chamber.

Following the work of Alcock (1), Dicksee (8) and Fitzgeorge and Allison (9), it appeared to be generally accepted that, during the latter part of the compression period, the swirl would be accompanied by a secondary squish motion and the combination of these would cause the air to move in a rotating toroidal manner within the

combustion chamber. Detailed analysis of the films made by the authors during this period of the engine cycle reveal a distinct lack of any toroidal motion and even the inclusion of various air markers (paper confetti or atomised silicone fluid) into a motored engine fitted with a transparent head, failed to indicate any radial motion of air during the squish period, i.e. 330 degrees crank angle to top dead centre. However, there was evidence of a definite outward squish just after the top dead centre position but this was considerably less in magnitude than the computed squish using a theoretical expression similar to that developed by Fitzgeorge and Allison (9). Alcock and Scott (10) therefore concluded that there is no substantial evidence of the presence of inward squish in a normal direct injection combustion chamber and this would explain the total absence of toroidal motion in the combustion photographs. However, observation of Fig. 2.13, which illustrates a piston crown and cylinder head arrangement which have been prepared with paint and motored in an engine for several minutes, suggests that the air spirals into the combustion chamber and this supports the photographic evidence of Dicksee (8). This also supports the argument made in Section 2.3.4 that the air motion cannot be defined by either swirl or squish but is a combination of the two components and consequently the spiral pattern suggested by the photographic evidence is perfectly reasonable and justified.

Whilst the experimental procedure developed by Alcock and Scott (10) produced some spectacular sequences of the combustion process within the combustion chamber, it must be concluded that the detailed determination of the air pattern is not possible. The swirl rate can only be measured approximately due to the two dimensional recording ability of the camera and consequently the photographic method, whilst supporting the presence of an orderly

air motion within the cylinder can only determine approximate mean swirl rates and would be of little use in any detailed investigation of the air motion.

2.3.6 HORVATIN, M. and HUSSMANN, A.W. (11), 1968

Horvatin and Hussmann (11) investigated the air motion within the cylinder of a motored Diesel Engine using a hot wire anemometer and thus made considerable progress in the attempt to gain a detailed understanding of the air motion inside the cylinder. The hot wire probes were located through the cylinder head at a variety of locations and could be adjusted to penetrate into the cylinder to a maximum depth of 6.2 cm, refer Fig. 2.14. Using only a single wire probe rotated about its axis until it gave a maximum signal, the authors concluded that this signal will be composed of a horizontal and vertical velocity component. Therefore, the measured velocity vector will form an angle with the plane of measurement which is parallel to the cylinder head. However, on the assumption that the measured velocities inside the cylinder are always in excess of the piston velocity by a factor of at least 3, the authors concluded that the maximum error of the velocity in the measuring plane will always be less than 10% and, in the majority of cases,only approximately 3% .

From the experimental results taken at a depth of 1 cm below the cylinder head and illustrated in Fig. 2.15, it can be observed that a distinct orderly swirl is developed during the induction

period and this pattern continues throughout the entire compression stroke. During the latter part of the compression period when the air is transferred from the outer cylinder area into the combustion chamber, there occurs in accordance with the law of conservation of angular momentum the expected rise in angular velocity as the moment of inertia of the air is decreased. Check calculations according to the theory of conservation of angular momentum were performed by the authors at two crank angle positions and these showed good agreement with the experimental results, although the authors suggested that losses would occur due to friction on the cylinder wall and leakage past the piston rings at top dead centre. Whilst the hot wire anemometer appears to be an ideal method for predicting the air motion within the engine cylinder, the experimental technique of Horvatin and Hussmann (11) could be considerably modified to include a piston mounted probe, located close to the piston crown surface and this would have two main advantages over the probe located through the cylinder head:

(i) Traversing the cylinder would reveal a more detailed study of the air motion adjacent to the piston at all crank angle positions throughout the cycle. This would avoid making the assumption of a solid body rotation to exist within the cylinder when analysing the experimental results.

(ii) By mounting the probe sufficiently close to the piston surface, it would not be necessary to have the probes plunging into recesses in the cylinder head and a complete study could then be made of the air motion at the top dead centre during the compression stroke. This latter position would be of extreme importance regarding the distribution of the air and fuel mixing process and must therefore be regarded as an extremely important criterion for any future investigation.

2.4 Conclusions of the Literature Survey

Having reviewed the relevant publications concerned with the measurement of swirl within the cylinder of an internal combustion engine, several important conclusions can now be made. It was mentioned previously that the swirl meter can only provide an estimation of the mean swirl occurring during the engine cycle and will be subjected to both inertial and frictional losses which both produce errors in the measured results. The swirl meter cannot therefore be used to determine accurately the swirl pattern within the engine cylinder.

The use of tracers injected with the incoming air has the disadvantage, due to their density, of not following exactly the air motion and tend to be thrown out towards the cylinder wall and there is also the disadvantage of the tracer density being constant whilst that of the air will change considerably, particularly during the compression period. Consequently the tracers cannot be relied upon to produce accurate information within the cylinder. The incorporation of a transparent cylinder head and sleeve also limits the speed capability of the engine and this produces unrepresentative results from within the cylinder.

Photographic evidence of the combustion process within the cylinder is extremely useful in justifying the presence of an orderly motion but again, because of the restriction to two dimensional photography, the method cannot be relied upon to produce a quantitative study of the air motion.

Unlike the previous methods for measuring the swirl speed, the hot wire anemometer has immense flexibility due to its size and

its ability to respond to frequencies in the order of 25 kilocycles per second suggests that the anemometer would easily respond to the changes of velocity occurring throughout the engine cycle. It must be concluded therefore that any future investigation into the air motion within an engine cylinder must be accomplished with the use of a hot wire anemometer system. Furthermore, experience has been gained in the use of hot wire anemometers in the pre-chamber of a single cylinder Diesel Engine at Loughborough and this substantiates the decision to adopt the hot wire anemometer for future investigations.

Detailed analysis of the results presented by the various authors with regard to the direct injection open combustion chamber system reveals that it is generally accepted that swirl is developed during the induction period either with the use of an inlet port arranged to admit the air tangentially into the cylinder or with the use of a masked inlet valve. A special case of the four stroke engine is that mentioned by Alcock (1) where a single sleeve valve arrangement was adopted to provide the tangential component of the air. The swirl developed during the induction period continues to exist throughout the compression period, its magnitude being increased as the air is transferred from the outer cylinder area into the combustion chamber. This transfer is assumed to be governed by the law of conservation of momentum although several authors, notably Dicksee (8), Fitzgeorge and Allison (9) and Horvatin and Hussmann (11) suggest that losses will accompany the transfer due to frictional effects on the cylinder wall and the possibility of leakage past the piston rings as the piston approaches the top dead centre position during the compression period.

According to Alcock (1), Dicksee (8) and Fitzgeorge and Allison (9), as the top dead centre position is approached during the compression period, a squish component will be developed and this

will combine with the swirl to produce a rotary toroidal motion within the combustion chamber. However, the photographic work of Alcock and Scott (10) showed a distinct lack of toroidal motion and this was supported by Horvatin and Hussmann (11) who assumed that as the air was transferred to the combustion chamber, it continued to rotate at an increased rate. Alcock and Scott (10) suggested that the absence of the toroidal motion might be due to the frictional loss, heat transfer or leakage past the piston rings as the air was compressed. However, a more feasible explanation is that outlined in Section 2.3.4, where it was suggested that the swirl might be the dominant motion within the combustion chamber and therefore the squish, because it is small in comparison to the swirl, would contribute little to the final motion. This argument is supported by the high swirl rates predicted by Fitzgeorge and Allison (9) and would justify the experimental results of Alcock and Scott (10) and Horvatin and Hussmann (11), where the toroidal motion appears to be negligible.

Having established that swirl is a distinct aid to the distribution of the air and fuel within the engine cylinder, Alcock (1) defined the profile of the swirl within the vortex combustion chamber as a free vortex, since the use of smaller diameter swirl meters resulted in increased swirl rates. This was not supported by Hurley (3), refer Section 2.3.1, who suggested a compound vortex was a more representative description of the swirl profile within the vortex combustion chamber. Whilst doubt exists therefore as to the swirl profile,

it must be remembered that both Alcock's (1) and Hurley's (3) results are obtained from average measurements throughout the engine cycle and do not provide detailed information for any particular period of the engine cycle. Horvatin and Hussmann (11), however, present a series of results, refer Fig. 2.15, which definitely suggest that a forced vortex profile would be a representative description of the swirl profile during the induction and compression periods. It must be concluded that the results of Horvatin and Hussmann (11), because they apply for both the engine cylinder and combustion chamber and are instantaneous measurements during the induction and compression periods, are the more representative for the type of combustion chamber under investigation.

2.5 Recommendations for the Investigation

From a detailed study of the literature, the following final conclusions were made regarding the undertaking of a further investigation into the air motion within the cylinder of a four stroke, direct injection Diesel Engine.

(i) A hot wire anemometer system would be developed and mounted at various positions on the piston crown in order that a complete study of the air motion within the entire cylinder might be made throughout the engine cycle.

(ii) Having developed a suitable measuring technique, this would be used to measure the flow pattern over a range of engine speeds.

(iii) Investigations within the combustion bowl would be made in order to justify or disprove the hypothesis of squish and toroidal motion.

(iv) In order to promote an increased swirl within the cylinder, it is proposed that a masked inlet valve would be used located in a number of angular positions and the effect upon the swirl recorded.

(v) Investigation into the increase in swirl developed using a supercharging system would also be made since this method would increase the supply of air delivered to the engine cylinder.

2.6 Further Literature Published after Undertaking the Present Investigation

2.6.1 WATTS, R. and SCOTT, W. M. (12), 1970

Watts and Scott (12) investigated the air motion and fuel distribution requirements of a high speed, direct injection Diesel Engine. Their study is an extension of the work undertaken by Alcock and Scott (10) reviewed in Section 2.3.5 and the authors make use of the photographic technique developed previously to produce more detailed information of the combustion process as the injected fuel impinges on the cylinder wall. In order to make an estimation of the swirl requirements within the engine, the authors used a cold blowing test rig, similar in design to that used by Fitzgeorge and Allison (9) and measured the swirl producing ability of the cylinder head using a swirl meter. The results of this test were plotted against piston displacement and are illustrated in Fig. 2.16. Analysis of the performance tests carried out on the engine led Watts and Scott (12) to conclude, as suggested by Alcock (1) in 1934, an optimum swirl ratio exists for a particular combustion system. This optimum is obviously important and over and under swirl of the air both result in equally disastrous results in the engine performance.

Watts and Scott (12) also investigated in detail the flow developed by a variety of inlet port and valve configurations and conclude that sufficient swirl may be obtained from wide combination of these. However, little information is presently available to predict accurately the swirl developed by any one particular inlet valve and port combination and this information they conclude is vital for the economic design of fuel injection systems. Further research is

obviously necessary in the field of swirl measurement and its development and this justifies the proposed investigation of the air motion within the engine cylinder.

2.6.2 HEUBNER, K.H. and McDONALD, A.T. (13), 1970

Heubner and McDonald (13) investigated the existence of air motion within the cylinder of a model engine using a hot wire anemometer, a variety of paddle wheels each having a different radius paddle and high speed photographic evidence of tracers injected into the engine cylinder. A model engine was designed to avoid large compressive forces and the valve timing of the model arranged to produce an intake and exhaust period for each revolution of the crankshaft. Suitable modification could be made to the cylinder head so that a masked inlet valve or an alternative inlet port could easily be accommodated and the effect upon the swirl noted.

The authors state that detailed information concerning the air motion within the engine cylinder can only be obtained when measurements are made at a variety of locations in the cylinder and whilst this cannot be disputed, the results from the model presented can hardly be representative of a 4 stroke cycle engine, since only two cycles were incorporated in the model, these being the induction and exhaust periods.

Heubner and McDonald (13) concluded from their experimental work that the hot wire anemometer technique can be applied with reasonable accuracy to determine the flow velocities in the

model cylinder during the induction period, however, Horvatin and Hussmann (11) have previously shown that it is possible to determine actual velocity measurements from a motored engine. It must be concluded therefore that the model engine, whilst simplifying the experimental programme, has little to offer in the way of meaningful measurements within the cylinder of an engine. Neither does the model adopted here provide any further understanding of the air motion within the combustion chamber during the latter stages of the compression period and this appears to be a major failing of the work presented, particularly since some differences of opinion exist regarding the air motion within the combustion chamber.

2.6.3 SHIMAMOTO, Y. and AKIYAMA, K. (14), 1970

Shimamoto and Akiyama (14) measured the squish component developed when an open chamber combustion system was used and compared this to the theoretical computation of squish which was corrected for leakage past the piston rings and heat transfer to the cylinder wall. The authors used a modified four stroke Diesel Engine which had both the inlet and exhaust valves removed and inlet ports machined into the lower part of the cylinder so that the pressure was atmospheric when the piston was in the bottom dead centre position. Consequently, the modified engine performed only the compression and expansion periods of the four stroke cycle and these periods were repeated without exchange of the trapped air. Only the amount of air equivalent to the leakage through the piston rings was supplied through the ports.

In order to measure the squish components, the authors used a method which relied upon the movement of a thin plate which changed the inductance of a solenoid and consequently gave an output voltage which could be displayed on an oscilloscope. The velocity detector was located through the cylinder head and the thin plate of the detector positioned 1.5 mm from the combustion chamber wall at a height equal to the piston crown in the top dead centre position. Consequently, providing that the plate was perpendicular to a cylinder radius, it would respond to the squish component developed by the air during its transfer from the outer cylinder into the combustion chamber during the compression period.

The authors computed a theoretical squish in a similar manner to that of Fitzgeorge and Allison (9), refer Appendix 5B, and corrected for the leakage of air past the piston rings and heat transfer to the cylinder wall. The results of the experimental and theoretical squish are illustrated in Fig. 2.17 and it may be observed that the error incurred by neglecting the losses is a maximum for the combustion chamber having a combustion chamber diameter cylinder dia. ratio = 0.45 and cylinder head and piston crown clearance of 1 mm. This error is approximately 8% and for other combustion chamber configurations, the error is considerably smaller.

The authors concluded that, whilst the velocity decrement due to leakage and heat transfer may appear to be considerable during the latter part of the compression period (20 degrees before top dead centre), the absolute value of the squish decrement is too small to seriously affect the computed, uncorrected component and this is justified by the experimental evidence. Consequently, the squish developed in an actual engine may not be much different from the

theoretical squish predicted using the equation 5B3 of Fitzgeorge and Allison (9), refer Appendix 5B. This latter statement would probably be true if it were possible to isolate the squish component as the authors have successfully done in the experimental investigation. However, as mentioned in Section 2.3.4, it is more likely that the air motion occurring during the compression period of a four stroke cycle would consist of a spiral pattern as the air is transferred into the combustion chamber and not ideal swirl or squish. The evidence presented by the authors therefore can only be relied upon to justify the theoretical squish equation and conclude that the errors encountered due to leakage and heat transfer will have a negligible effect on the computed magnitude of the squish component.

2.6.4 OHIGASHI, S.; HAMAMOTO, Y. and TANABE, S. (15), 1972

Noting that all the previous investigations of the effects of air swirl were carried out on either cold rig tests, simulated models or motored test engines, the authors developed a technique for measuring the magnitude and direction of the air motion within the cylinder of a fired engine using a method of electrical discharge, where a probe located in the engine cylinder measures the current flowing due to the ion cloud which is produced by the electrical discharge and is free to move with the air motion.

The swirl velocities over a range of crank angle degrees before top dead centre during the compression period were measured in the motored and fired test conditions at various speeds and the results illustrated in Fig. 2.18. It was observed that the

air moved in a tangential direction to the cylinder wall and little noticeable differences were found between the measured values in both motored and fired conditions during the later stages of the compression period. This observation suggests that the velocity immediately before ignition in a fired engine can be estimated from that obtained in an identical motored run. It should be noted that the results illustrated in Fig. 2.18 include a theoretical squish velocity computed from equation 2.5 derived by Fitzgeorge and Allison (9). However, this theoretical result is only included as a reference and not intended to be a theoretical estimate of the measured result. This comparison would be impossible since the experimental results are for air swirling within the chamber, whilst the theoretical results are computed on the assumption of radial motion into the combustion chamber from the outer cylinder.

The swirl velocity and its direction, which was varied by rotating a masked valve, were also measured and are illustrated in Fig. 2.19. In this series of the tests, a piston without a combustion bowl was used to eliminate the possibility of any secondary motion being produced, within the combustion chamber. Consequently, the engine compression ratio was reduced in order to prevent the piston crown and measuring instrument coming into contact with each other. Observation of Fig. 2.19 shows that a position of the mask exists which will produce the maximum swirl possible.

Whilst the method outlined above appears to be a major development in the measurement of swirl, it must be mentioned that because of the size of the measuring instrument and its location through the cylinder head, it is impossible to make any detailed measurements whilst the piston is within 30 degree crank angle of the top dead centre position. This latter period can only be measured using a flat topped

piston crown which, along with a lowered compression ratio would produce unrepresentative results. Consequently, it must be concluded that the technique developed by the authors does not introduce any revolutionary method for measurement of swirl within the engine cylinder. Indeed, with the conclusion of approximately identical velocities for both the motored and fired test data during the latter part of the compression period, it would appear that it is satisfactory to continue investigating the air motion with a motored engine using a hot wire anemometer system and subsequently relate this to the engine in the fired test condition.

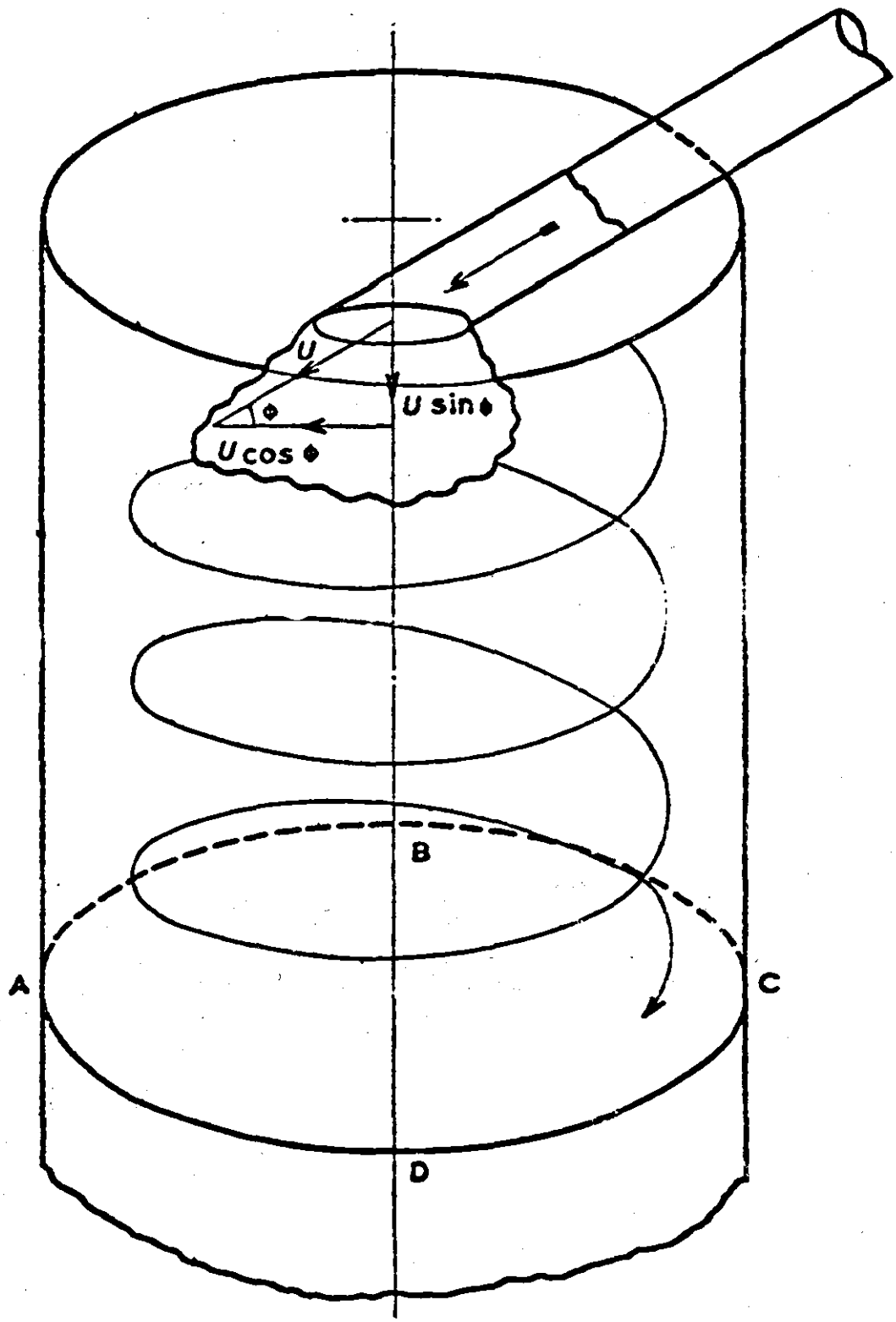

2.1 Air Motion inside the Engine Cylinder

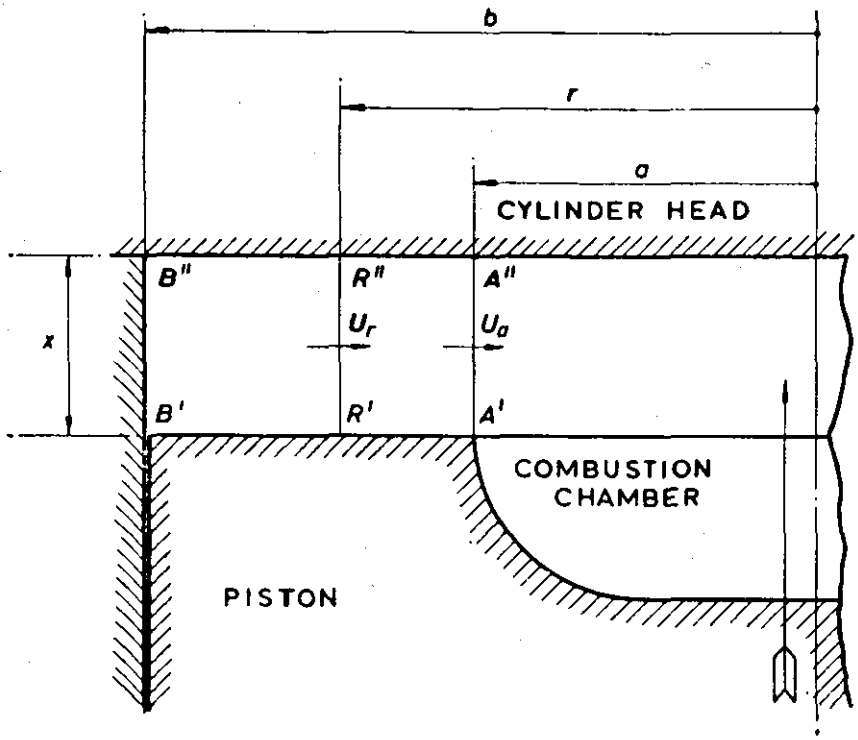

2.2 Cylinder Head and Combustion Chamber Geometry

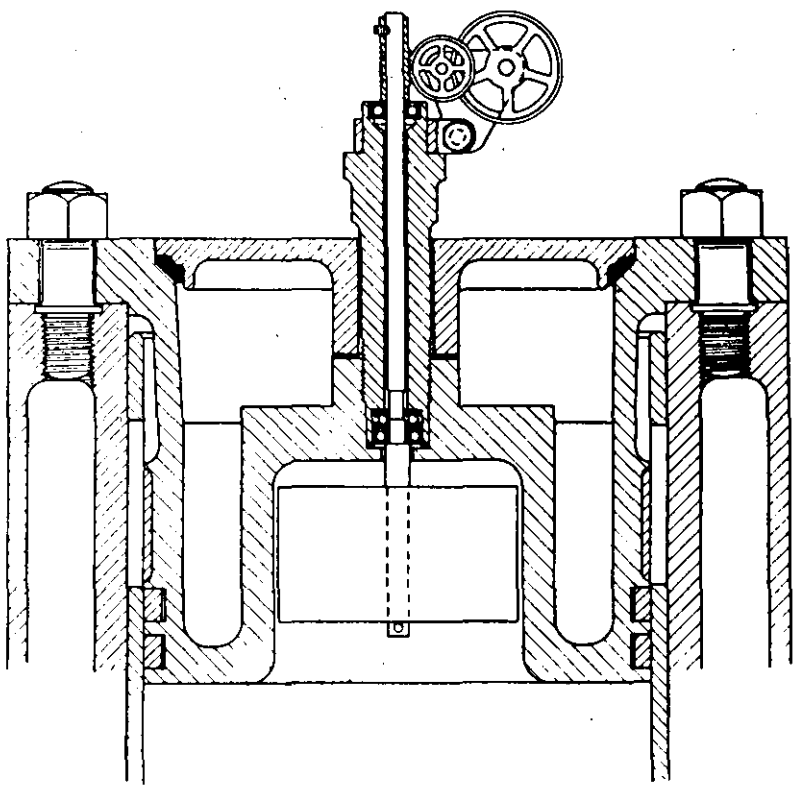

2.3 'Vortex' Combustion Chamber and Swirl Meter

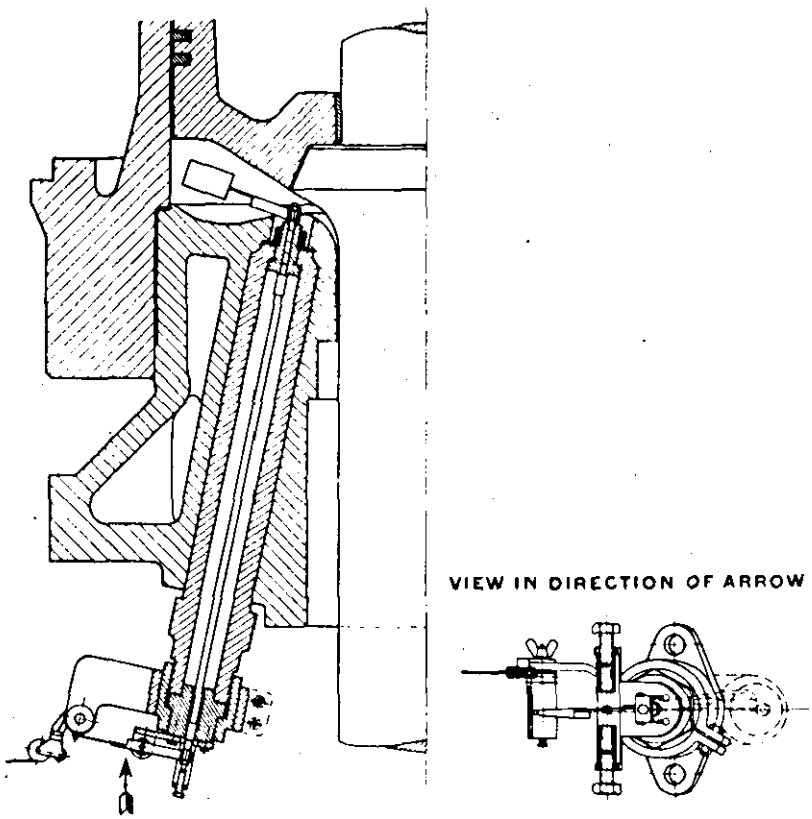

2.4 'Sass' Swirl Meter

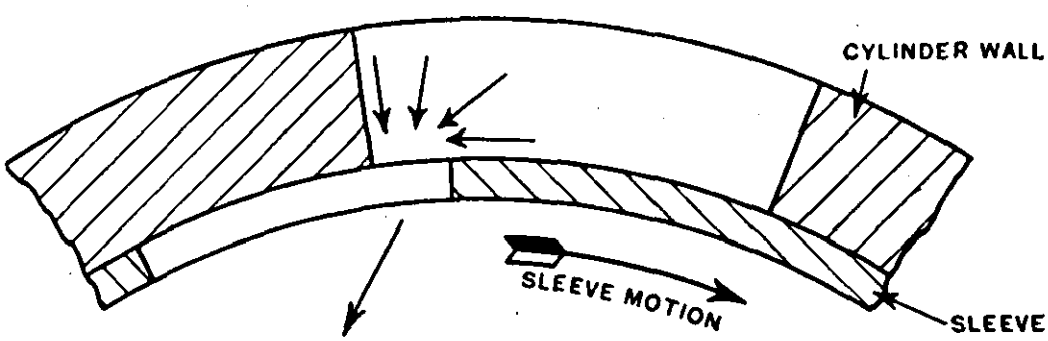

2.5 Single Sleeve Valve Engine

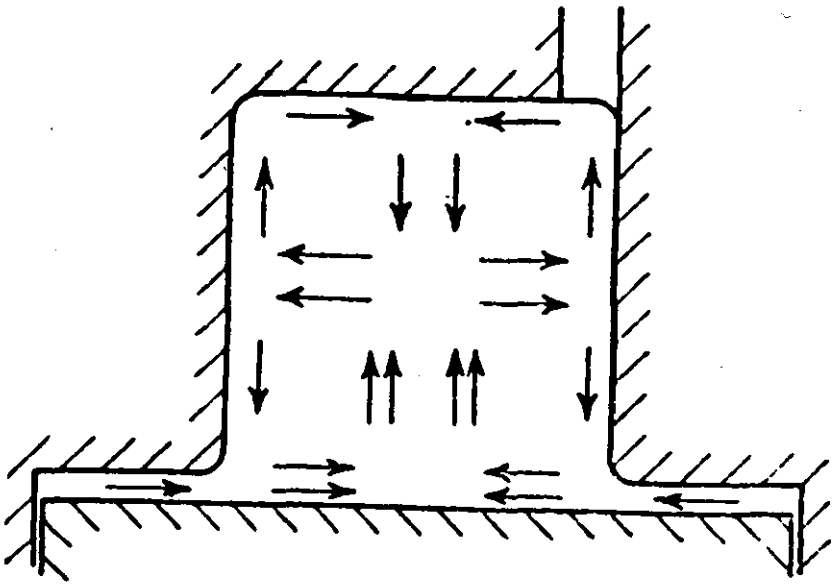

2.6 Complex Squish Motion inside the 'Vortex' Combustion Chamber

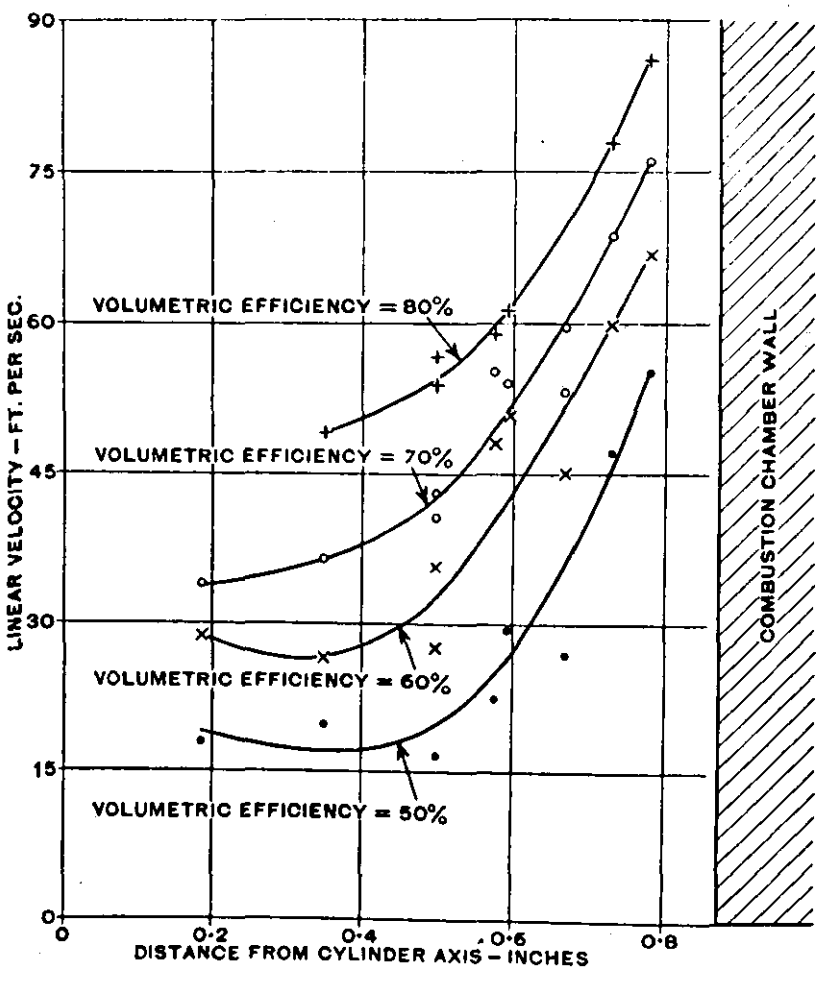

2.7 Hurley's (3) Results for a 'Vortex' Combustion Chamber

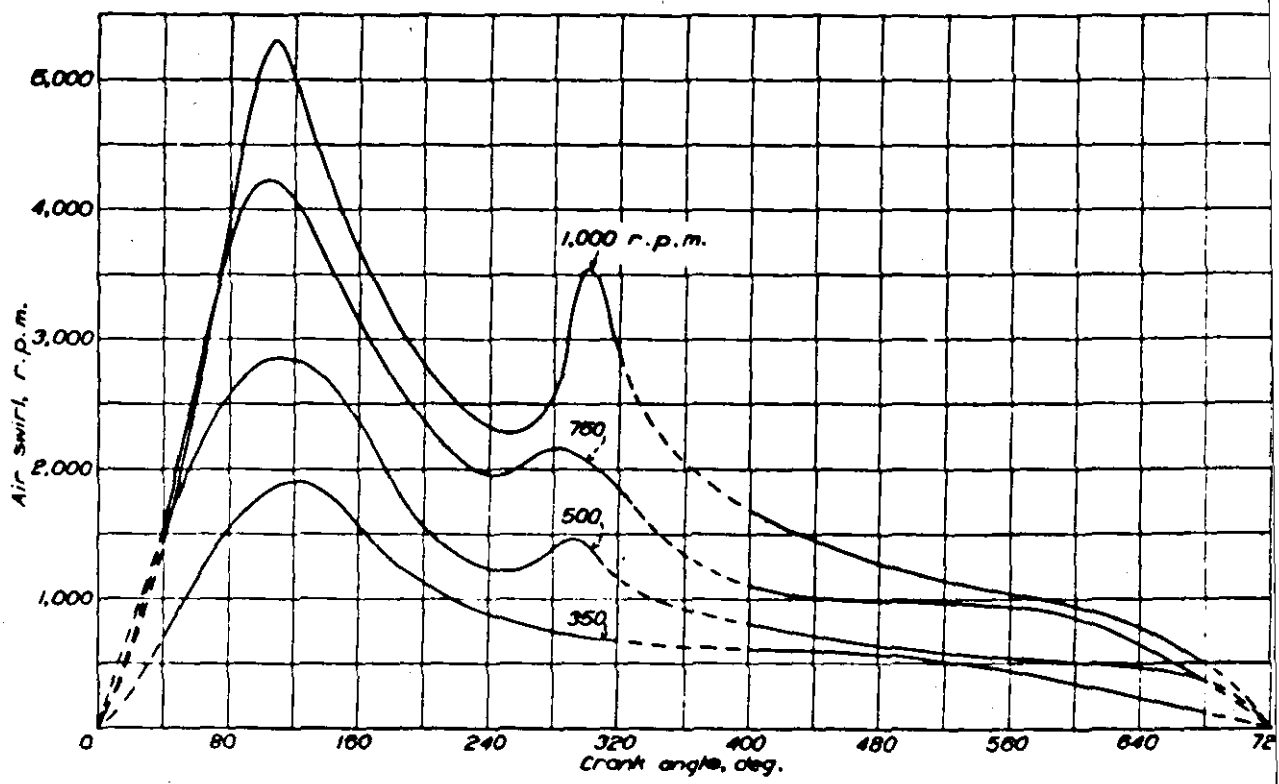

2.8 Lee's (7) Results for Measured Swirl

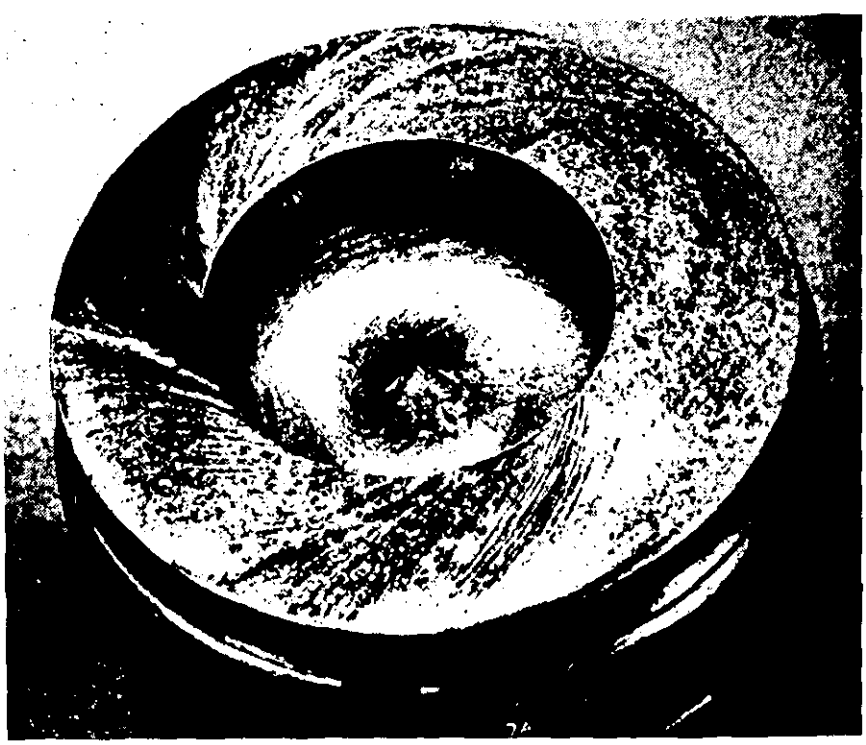

2.9 Dicksee's (8) Results showing a Spiral Flow into the Combustion Chamber

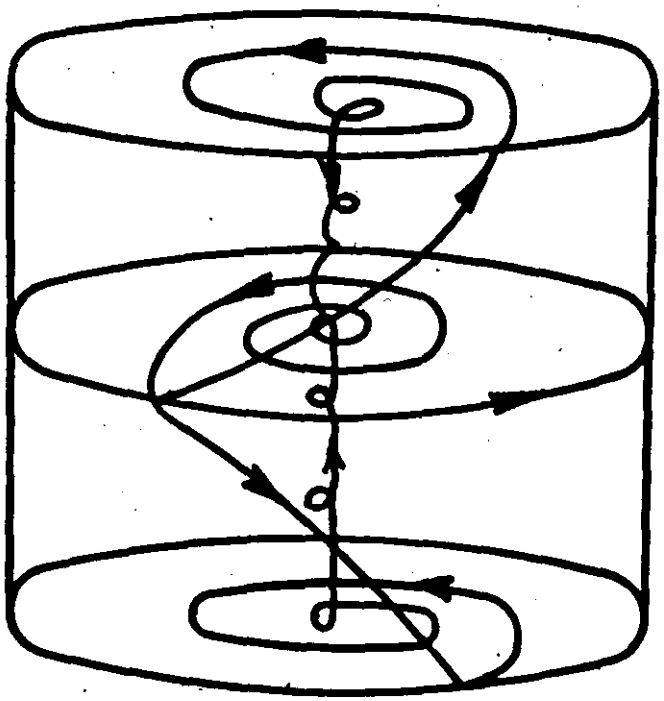

2.10 Dicksee's (8) Postulation for the Air Motion inside the Combustion Chamber

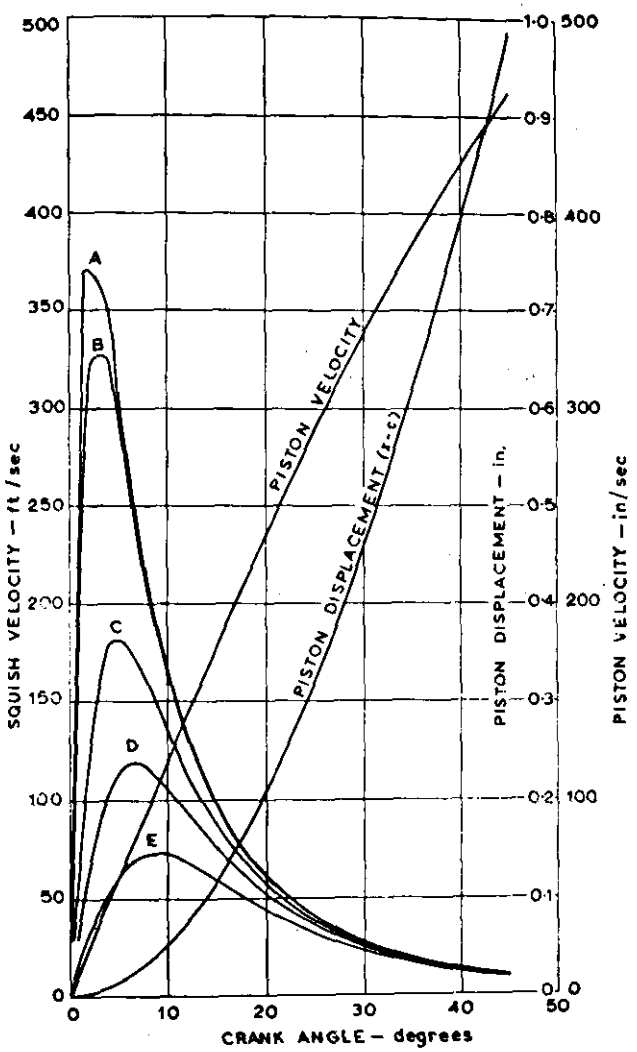

A, c = 0·004 in. B, c = 0·005 in. C, c = 0·015 in.
D, c = 0·030 in. E, c = 0·060 in.

2.11 Fitzgeorge and Allison's (9) Theoretical Squish Computations

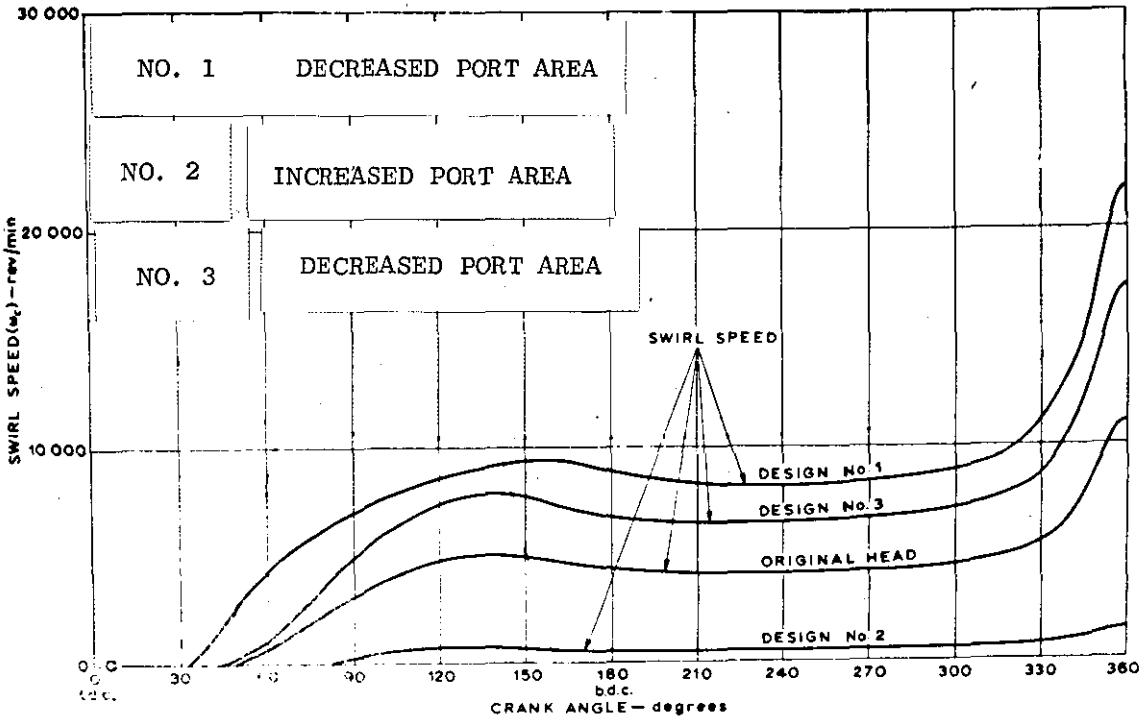

2.12 Fitzgeorge and Allison's (9) Theoretical Swirl Computations

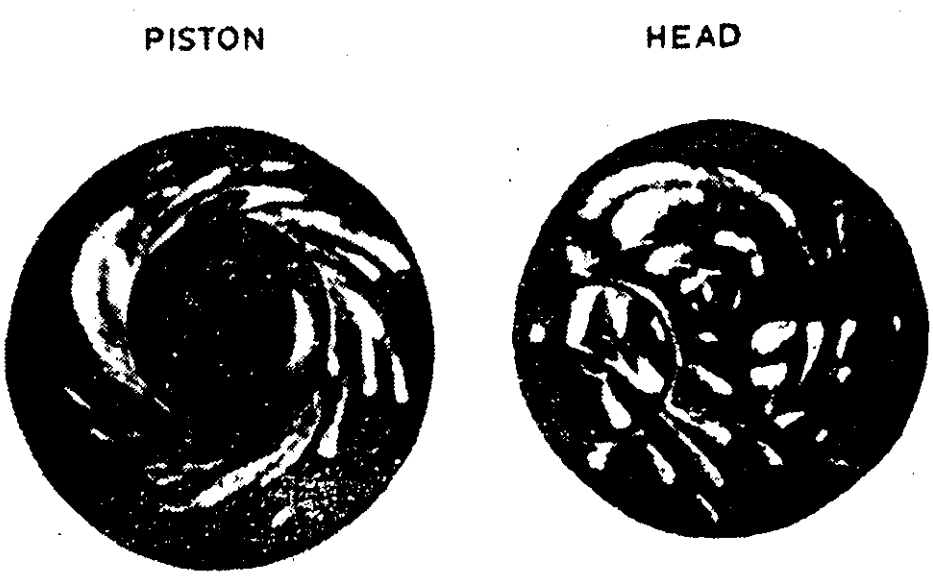

a 0·04 piston/head clearance.

2.13 Alcock and Scott's (10) Results showing a Spiral Flow into the Combustion Chamber

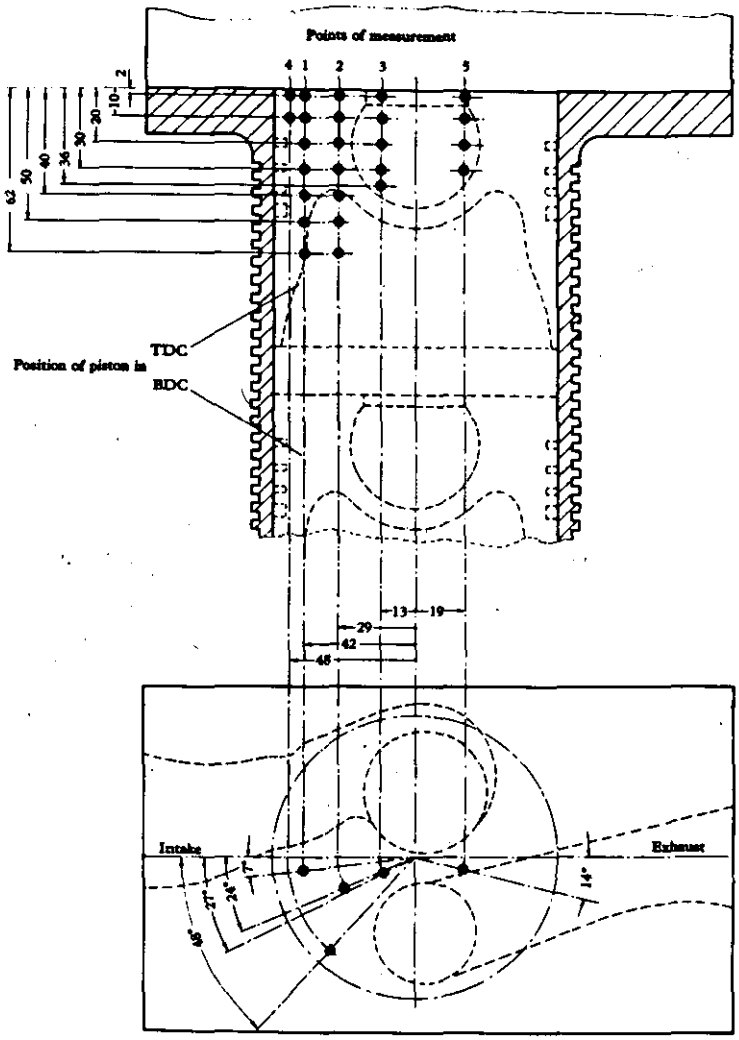

2.14 Anemometer Locations used by Horvatin and Hussmann (11)

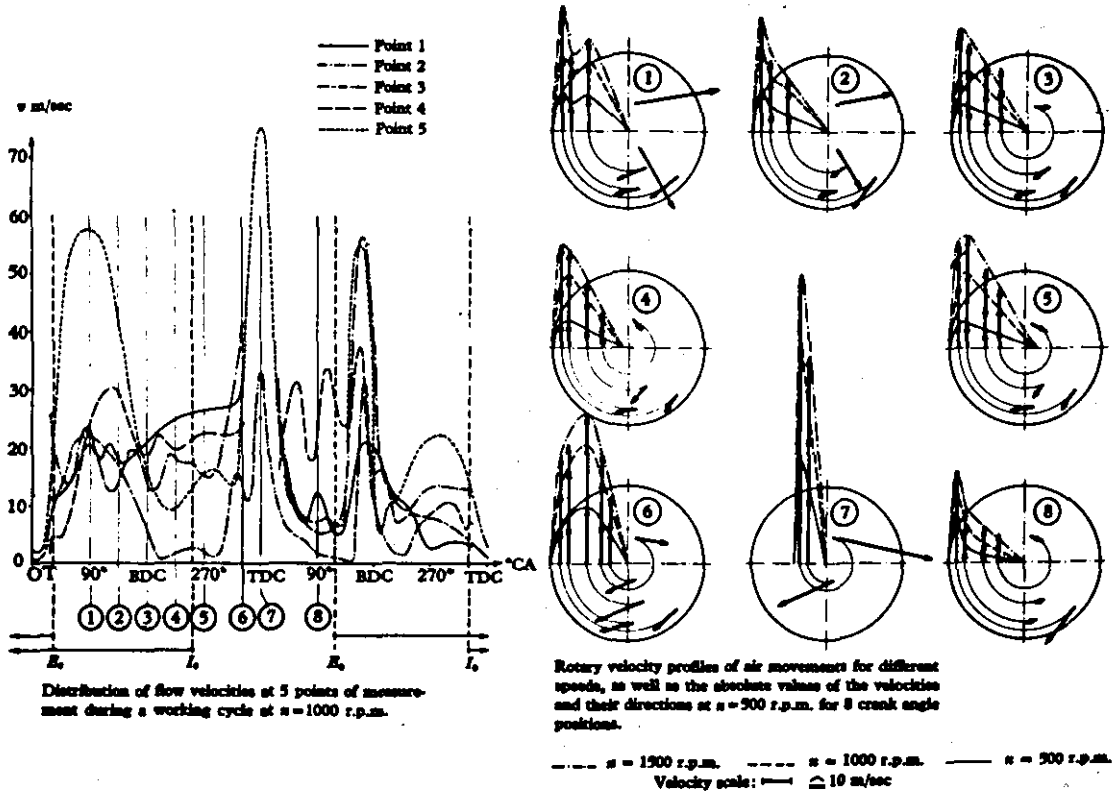

2.15 Horvatin and Hussmann's (11) Swirl Results

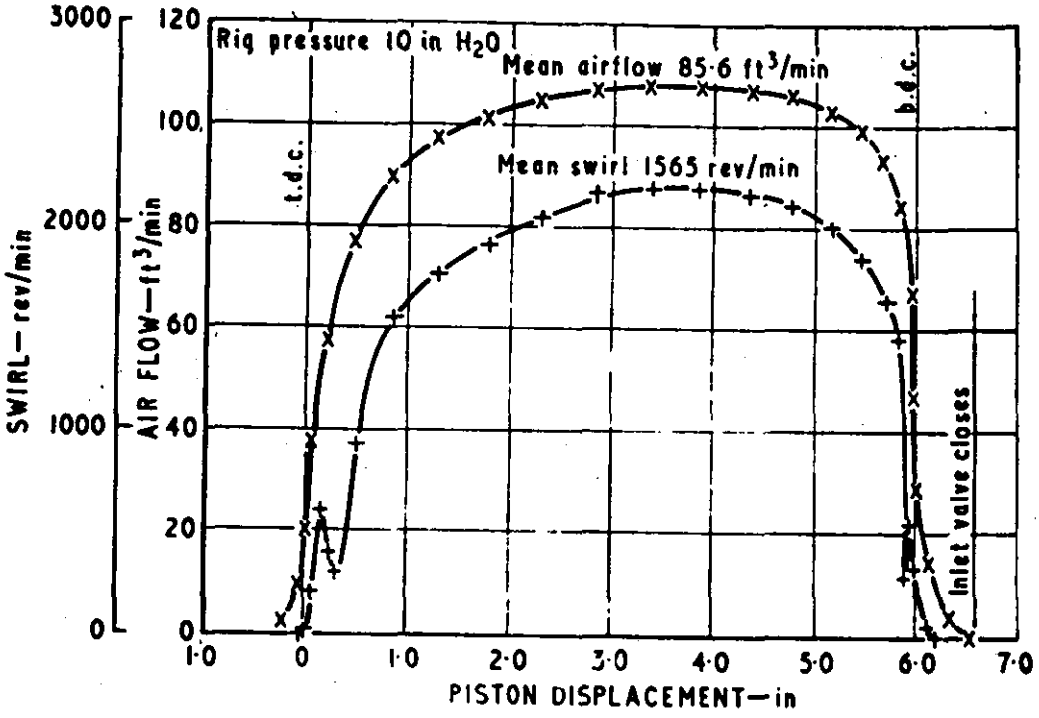

2.16 Typical Rig Swirl and Flow Measurements from Watts and Scott (12)

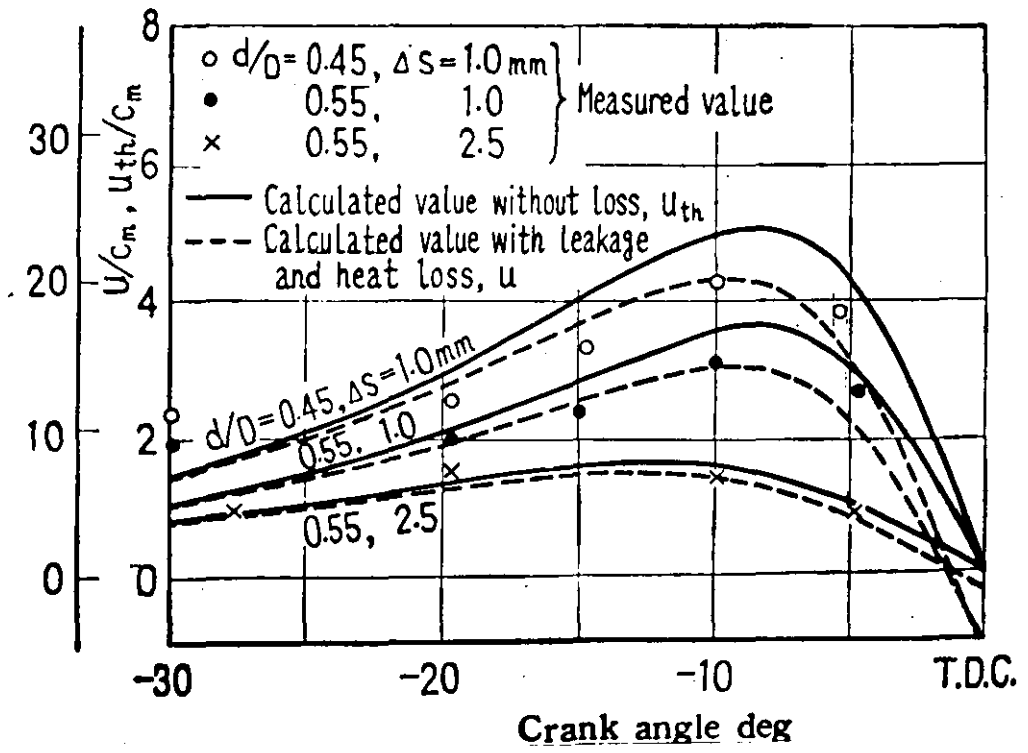

2.17 Shimamoto and Akiyama (14) Squish Results

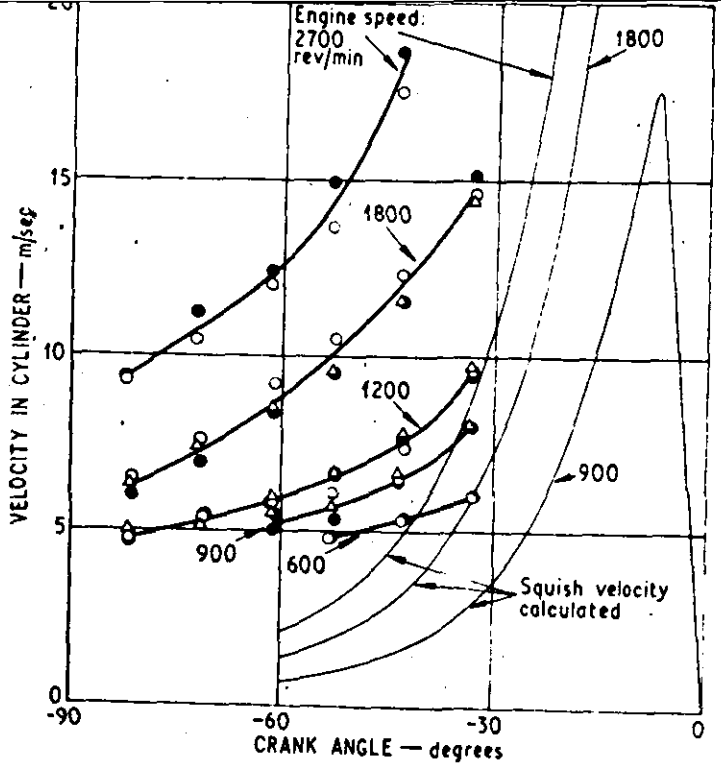

○ Motoring.
● Firing, fuelling: 0·0258 g/cycle.
△ Firing, fuelling: 0·0342 g/cycle.
| Volumetric efficiency: 79 per cent.

2.18 Ohigashi et al (15) Swirl Results

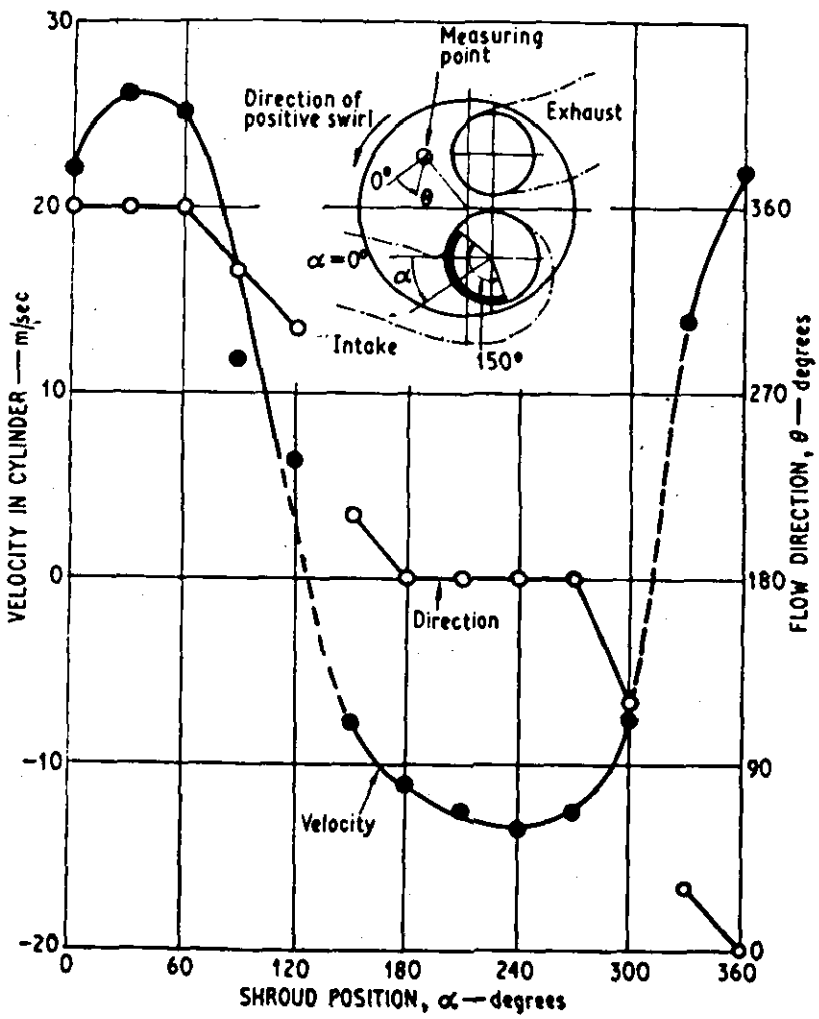

Engine speed: 1800 rev/min.
Volumetric efficiency: 83 per cent.
Flat piston.
Motoring.

2.19 Effect of Valve Masking on the Results of Ohigashi et al (15)

3.0 MEASUREMENT OF AIR FLOW USING A HOT WIRE ANEMOMETER

3.0 MEASUREMENT OF AIR FLOW USING A HOT WIRE ANEMOMETER

3.1 The Hot Wire Anemometer

In the recommendations of Section 2.5, it was concluded that any future investigation of the air motion within the cylinder of a motored engine would require the use of a hot wire anemometer in order that the air velocity might be measured in magnitude and direction. Attempts have been made to install an anemometer within an engine cylinder and it was suggested by Cave-Browne-Cave (5) and Baker (6) refer Section 2.3.1, in a discussion of Alcock's paper (1) as early as 1934 that such a technique might be developed. However, Baker (6) pointed out that the calibration of such an anemometer would be extremely difficult, due to the rapidly varying pressure and temperature of the cylinder contents throughout the engine cycle.

Horvatin and Hussmann (11), 1968, demonstrated that such an anemometer system might be developed by mounting the anemometers through the cylinder head and they overcame the problem of pressure and temperature variation by calibrating their anemometers in a high temperature and pressure wind tunnel. Hence, they were able to make any necessary corrections for the conditions encountered.

Hassan (16), 1968, developed a reliable method of anemometry using the basic principles of Davies and Fisher (17) and he corrected for the varying temperature and pressure using instantaneous values of these along with a temperature loading factor, which is presented in detail by Hassan and Dent (18). In order to compute the gas velocity within the engine, Hassan (16) found that it was necessary to measure the instantaneous gas temperature and pressure of the air within the engine cylinder and then, using the bridge voltage signal from the

hot wire anemometer, he was able to predict the instantaneous gas velocity. Hassan (16) measured the bridge voltage using a constant temperature anemometer system designed by Davies and Fisher (17), the gas temperature using a simple resistance thermometer and a Wheatstone Bridge and the gas pressure using a C.A.V. strain gauge pressure transducer. A more comprehensive description of these techniques may be found in Hassan's thesis (16).

Since the existing equipment of Hassan's (16) was readily available for use within the Mechanical Engineering Department, it was decided to adopt this equipment and develop the basic principles for the measurement of the air motion within the cylinder of a four stroke Diesel Engine.

3.2 Three Dimensional Measuring Technique

Unlike the pre-chamber of the engine used by Hassan (16) where it was known that the air motion would be ideally one dimensional at a particular location, it must be assumed that the flow within an engine cylinder would be three dimensional. Consequently, a method must be developed to measure both magnitude and direction of a three dimensional velocity vector. Horvatin and Hussmann (11) overcame this problem by mounting their anemometers through the cylinder head and rotating them until a maximum signal was obtained, from which they concluded the velocity vector was now perpendicular to the anemometer sensing wire. This method is laborious and does not allow the velocity vector direction to be located with any great accuracy as was discussed in Section 2.3.6.

Lobo (19), 1966, recognised the three dimensional characteristics

of the air flow within the engine cylinder and attempted to develop a suitable method for measuring this using an extremely complicated 5 wire theory. A programme of experimental work was undertaken by Lobo (19) to justify the theory and resulted in the same anemometer wire being located in 5 different angular positions, from which results were recorded and an overall vector determined. Whilst this method avoided any ambiguity as to the direction of the vector, it was decided that the installation of such a system into the cylinder of an engine would be extremely difficult and have little advantage over the previous method of Horvatin and Hussmann (11). Assuming that the air motion within the cylinder would consist primarily of a swirl in a particular direction, it was concluded that a simple three dimensional model could be developed using only three individual anemometers satisfactorily installed within the engine cylinder. Since a good approximation to the flow direction could be made from the published literature in Section 2.0, it was also concluded that any ambiguity of vector direction could be resolved simply by rotating the three anemometers to a different datum position and a further set of readings taken in this new position. Hence the two sets of readings should produce the same magnitude and direction of the velocity vector.

3.2.1 Response of an Anemometer to a Velocity Vector

When measuring the direction of air flow using an anemometer, it is inconvenient to rotate the anemometer wire through a variety of positions in order to obtain a maximum signal from the wire and hence a position where the flow is perpendicular to the sensing wire. Instead an investigation is required into the case where the velocity vector is not normal to the anemometer sensing wire, refer Fig. 3.1 and a suitable equation is required to express the vector in

terms of the angle of incidence θ and the maximum velocity vector U. The following list presents some of the equations, and their limitations, which have been found reliable by a variety of authors.

1. Ulsamer (20) $U_\theta = U(1 - 0.55 \cos^2 \theta)$, $30^\circ < \theta \leq 90^\circ$

2. Hinze (21) $U_\theta^2 = U^2 (\sin^2 \theta + A \cos^2 \theta)$, valid for all angles. However, for practical purposes in the range $10^\circ < \theta \leq 90^\circ$, Hinze (21) considers only the U sin θ component.

3. Kovasnay (22) $U_\theta = \frac{1}{2} U (1 + \sin \theta)$, valid for all angles.

4. Newman and Leary (23) $U_\theta = U(\sin \theta)^{0.914}$, $10^\circ < \theta \leq 90^\circ$

5. Lobo (19) and Pearson (24) $U_\theta = U \sin \theta$, $10^\circ < \theta \leq 90^\circ$

This last equation is the most generally adopted and indeed both Lobo (19) and Pearson (24) have demonstrated that the equation will still predict accurately the velocity component when the angle of incidence is as low as 5°.

In principle, anyone of the above relationships could be adopted to deduce the overall velocity. However, the more complicated the relationship used, the more difficult becomes the three dimensional analysis. Hence, because of its simplicity and on the basis of experimental work carried out in a wind tunnel, the results of which are illustrated in Fig. 3.1, it was decided to adopt the sine relationship,

$$U_\theta = U \sin \theta \qquad \text{——————} \quad 3.1$$

3.2.3 Magnitude of the Velocity Vector

By means of three mutually perpendicular anemometer wires, it is possible to measure the magnitude of the three components of the velocity vector along the wire directions and also the overall magnitude of the velocity vector.

Let U_1, U_2 and U_3 be the velocity readings from the wires in the X, Y and Z directions respectively, and U_X, U_Y and U_Z be the components of the velocity vector along these axes, refer Fig. 3.2. Each wire will then respond to the velocity components perpendicular to it, i.e. the root of the sum of squares of the velocity components along the two directions normal to it, refer Fig. 3.3.

In Fig. 3.3, the components perpendicular to the wire providing the signal will be U_a and U_b, U_c having no effect since it is parallel to the wire.

Hence, we have,

$$U_1^2 = U_y^2 + U_z^2 \qquad \text{——————} \quad 3.2$$

$$U_2^2 = U_x^2 + U_z^2 \qquad \text{——————} \quad 3.3$$

$$U_3^2 = U_x^2 + U_y^2 \qquad \text{——————} \quad 3.4$$

and we can write,

$$U_x^2 = \frac{1}{2}(U_1^2 + U_2^2 + U_3^2) \qquad \text{——————} \quad 3.5$$

$$U_y^2 = \frac{1}{2}(U_1^2 - U_2^2 + U_3^2) \qquad \text{——————} \quad 3.6$$

$$U_z^2 = \frac{1}{2}(U_1^2 + U_2^2 - U_3^2) \qquad \text{——————} \quad 3.7$$

Therefore, the overall velocity vector U may be written

$$U = (U_x^2 + U_y^2 + U_z^2)^{\frac{1}{2}} \qquad \text{——————} \quad 3.8$$

Consequently, by taking the readings from the three anemometers mounted mutually at right angles to each other, it is possible to determine the magnitude of the velocity vector using equation 3.8.

3.2.4 Direction of the Velocity Vector

Owing to the complexity of three dimensional resolution, it is usual to express the direction of a three dimensional velocity vector in terms of its direction cosines l, m and n. Hence if α, β and γ are the angles between the velocity vector U and the X, Y and Z axes respectively, refer Fig. 3.4, then the direction cosines may be defined as:

$$l = \cos\alpha = |U_x| / |U| \qquad \text{——————} \quad 3.9$$

$$m = \cos\beta = |U_y| / |U| \qquad \text{——————} \quad 3.10$$

$$n = \cos\gamma = |U_z| / |U| \qquad \text{——————} \quad 3.11$$

Having now defined the direction cosines of the velocity vector by equations 3.9, 3.10 and 3.11, it would be more convenient to express the direction of the vector by two explicit angles, A in the horizontal plane and B in the vertical plane, refer Fig. 3.4. Simple trigonometry applied to the co-ordinate systems shows that the angles A and B may be written in terms of the direction cosines l, m and n and consequently using equations 3.9, 3.10 and 3.11, A and B can be

expressed in terms of the overall velocity vector and the resolved components of the vector in the X, Y and Z planes. The equations for angles A and B are given by,

$$\cos A = \frac{\cos\alpha}{(\cos^2\alpha + \cos^2\beta)^{\frac{1}{2}}} = \frac{|U_x|}{(U_x^2 + U_y^2)^{\frac{1}{2}}} \qquad \text{——— 3.12}$$

and

$$\cos B = (\cos^2\alpha + \cos^2\beta)^{\frac{1}{2}} = \frac{|U_x|}{|U| \cos A} \qquad \text{——— 3.13}$$

It is now possible using equations 3.8, 3.12 and 3.13 to measure the magnitude of the velocity vector and describe its direction with reference to the horizontal plane.

3.3 Experimental Procedure

Having decided to adopt a method of hot wire anemometer similar to that of Hassan (16) and the three wire method for determination of the velocity vector presented in Section 3.2, it was concluded that a detailed experimental investigation would have to be made to justify the use of the methods involved. Because of the size of the anemometer probe used by Hassan (16) 0.63cm. outside diameter pyrotenax body and copper probe supports of 1.255 mm diameter), it was decided that another type of anemometer probe would have to be developed which differed in two important ways from that of Hassan's (16):

(i) 0.16 cm outside diameter pyrotenax body with nickel chrome probe supports having a diameter of only 0.300 mm could be manufactured.

(ii) a spot welding technique would be used for securing the 10 μm diameter platinum/30% iridium sensing wire to the probe supports.

Consequently, because of its reduced body size, the new probe would provide less interference to the air motion and the reduced probe support diameter would also reduce any masking of the sensing wire which could occur. The decision to spot weld the sensing wire to the probe supports would allow the probe to be built with increased accuracy and the measurement of the sensing wire length and cold resistance measurement could be made with greater reliability. Spot welding, in preference to the soft soldering technique used by Hassan (16) would also permit the probe to be used in a much higher temperature environment and consequently higher compression ratio engine.

3.3.1 Anemometer Probe Calibration

The most important feature of any successful experimental work using a hot wire anemometer is the accurate calibration of the probe in a wind tunnel and determination of the hot operating temperature of the sensing wire. Without this calibration, serious errors may occur in the predicted velocity. Davies and Fisher (17) presented a theoretical method for computing the velocity of a hot wire anemometer probe and showed that the thermal equilibrium of an electrically-heated wire placed in a stream of cooler gas may be expressed by the following relationship:

$$k A_r \frac{d^2 T_w}{dx^2} + \left(\frac{I^2 C_3 \alpha - \Pi dh}{A_r} \right) (T_w - T_g) + \frac{I^2 C_3}{A_r} = 0 \qquad \text{——— 3.14}$$

where k is the thermal conductivity of the gas

A_r is the cross sectional area of the sensing wire

I is the heating current through the wire

ρ is the electrical resistivity of the wire material

d is the sensing wire diameter

h is the average heat transfer coefficient

T is the absolute temperature

α is the temperature coefficient of the wire material

and the suffices

g refers to the gas free stream conditions

w refers to the gas properties at the wire temperature.

In obtaining equation 3.14, the following simplifying assumptions were made by Davies and Fisher (17)

(i) There are no radiation losses,

(ii) The thermal conductivity of the wire material is constant,

(iii) The electrical resistivity of the wire and its temperature are related by the following expression,

$$\rho_w = \rho_g (1 + \alpha T_1) \qquad \text{——— 3.15}$$

where $T_1 = T_w - T_g$

(iv) The sensing wire supports are at the same temperature as the gas stream.

Equation 3.14 can be reduced to the following:

$$\frac{d^2T_1}{dx^2} + K_1 T_1 + K_2 = 0 \qquad \text{———3.16}$$

where $K_1 = \frac{I^2 \rho_g \alpha}{k_t A_r^2} - \frac{\Pi dh}{k_t A_r}$ and $K_2 = \frac{I^2 \rho_g}{k_t A_r^2}$

where k_t is the thermal conductivity of the wire material.

The solution of equation 3.16 gives, with the following boundary conditions,

(i) maximum temperature occurs at the mid wire length of the wire so that $dT/dx = 0$ at that point,

(ii) at the wire supports the wire is at the instantaneous gas temperature Tg.

$$T_1 = \frac{K_2}{K_1} \left(\frac{\cosh (|K_1|^{\frac{1}{2}} x)}{\cosh (|K_1|^{\frac{1}{2}} l} - 1.0 \right) \qquad \text{——————} \quad 3.17$$

which may be integrated along the length of wire and yields the following expression for the mean temperature difference between the wire and gas.

$$T_w = \frac{K_2}{K_1} \left(\frac{\tanh(|K_1|^{\frac{1}{2}} l)}{|K_1|^{\frac{1}{2}} l} - 1.0 \right) \qquad \text{——————} \quad 3.18$$

where $2l$ is the length of the sensing wire.

Since T_w is known from the temperature resistivity relationship (equation 3.15), equation 3.18 can be solved on a digital computer using an iterative procedure to yield the unknown heat transfer coefficient h, which is related to the gas velocity by the following relationship:

$$\frac{hd}{k_w} = \frac{2.6}{\sqrt{\Pi}} \left(\frac{\rho_g U}{\mu_g} \right)^{\frac{1}{3}} \left(\frac{Cp_g \mu_g}{k_g} \right) \qquad \text{——————} \quad 3.19$$

where k_w is the thermal conductivity of the gas at the wire temperature

γ the ratio of the specific heats

ρ_g the gas density

Cp_g the specific heat of the gas at constant pressure

μ_g the viscosity of the gas

k_g the thermal conductivity of the gas

d the wire diameter

and the Eqn. 3.19 is valid in the range,

$$0 \leqslant \left(\frac{\rho_g U d}{\mu_g}\right) \leqslant 50 \qquad \text{——— 3.20}$$

Hence a theoretical calibration curve can be developed for the anemometer probe. In order to verify the calibration, however, the manufactured probe was installed in a Disa wind tunnel, refer Fig. 3.5, and an experimental programme undertaken to determine the output bridge voltage from the Davies and Fisher (17) constant temperature anemometer circuit whilst the tunnel velocity was varied. A typical calibration curve is illustrated in Fig. 3.6 and it can be seen that agreement between the theory and experiment is good and within the experimental error of $\pm$ 5% quoted for the probe and outlined in Appendix 3A.

3.2.3 Measurements using a Three Wire Probe

As mentioned previously in Section 3.2 in order to measure accurately the velocity vector in a three dimensional flow, it is necessary to make three individual measurements in planes mutually at right angles to each other and to add the results vectorially. Three anemometer probes were therefore secured in a holder on a pitch circle

diameter of 0.63cm with the sensing wires inclined mutually at right angles to each other. The assembly was then located inside the wind tunnel using the adaptor illustrated in Fig. 3.7. In order to simulate the effects of a three dimensional flow and check the capabilities of the theoretical method, the probe assembly was rotated through 360^{o} and the signals from the three individual wires recorded at 10^{o} intervals. Consequently, the results obtained from the theoretical method should predict a velocity equal in magnitude to the tunnel velocity whilst the vertical angle B will be zero and the horizontal angle A will be equal to the rotational displacement of the probe assembly from the initial datum position. The experimental work was performed at a variety of tunnel speeds and produced satisfactory results for both the magnitude and horizontal direction of the velocity vector. However, errors of approximately 15-20% were found in the vertical angle. Whilst this latter error was not unreasonable when compared to the error analysis, refer Appendix 3A, performed for the three dimensional method resulting in an overall error of $\pm$ 9.0% for the experimentally determined velocity vector, and $\pm$ 12% for the determination of its direction, it was interesting to note that the error in the vertical angle B was considerably higher than that estimated in the error analysis. Consequently, further investigation was made of the three wire probe.

In order to avoid unnecessary errors in the recording of the results, each individual probe was made to exactly the same specification and operated at the same wire temperature, therefore the error in each probe was assumed to be the same as the two adjacent probes. A special tunnel adaptor was also designed which enabled the probe assembly to be inclined at an angle of 30^{o} to the vertical and this latter modification had a very important contribution to the results, since the vector developed by the tunnel was always

incident at a minimum angle of 30^{o} to each probe sensing wire. Consequently, the errors involved by the vector having a very small angle of incidence (10^{o} and less) to any probe sensing wire were eliminated. The results from the second series of experimental work were considerably more accurate than the initial tests and a typical set of results are illustrated in Fig. 3.8 for a tunnel velocity of 20 m/s.

The experimental programme undertaken for the justification of the three dimensional model was particularly exhaustive and suggested that the three wire method could be successfully applied within the engine cylinder. However, in order to avoid ambiguity of the direction of the measured vector, it would be necessary to rotate the three wire assembly about its own axis and take two separate sets of readings. From the results of these two sets of readings, it should be possible to predict exactly the direction of the measured vector. Rotation of the probe assembly about its axis should also avoid any errors encountered by the signal from any one sensing element being masked by any one of the probe supports. It was evident in the tunnel tests that with the configuration adopted for the probes (location of the individual probe axes on a 0.63 cm diameter pitch circle) masking only occurred in certain unfavourable positions of the probe assembly. However, since the flow direction within the cylinder could be estimated to some extent using the results of previous literature, refer Section 2.0, it should be possible to locate the three wire probe in such a position that probe support masking would be almost impossible. Should masking occur then, the second series of tests would eliminate this possible source of error entirely.

3.3.4 Simulation of the Piston Motion

In anticipation of the three wire probe assembly being mounted on the piston crown, it was considered necessary to investigate the effect that the piston motion would have upon the probe readings. A scotch yoke mechanism was designed and built so that it could be installed as part of the Disa wind tunnel and a single hot wire anemometer mounted on the traversing arm of the mechanism, refer Fig. 3.10. Consequently, as the mechanism was driven at speed, the probe signal was a combination of the tunnel velocity and the velocity of traverse mechanism. The results were investigated at a variety of tunnel and mechanism velocities up to a maximum of 1000 r.p.m. and in all cases the results showed that the velocity indicated by the probe was a simple addition of the tunnel velocity and mechanism velocity. Consequently, it is reasonable to assume that the subtraction of a vertical velocity component equal to the piston speed would have to be made to each of the horizontal probes located inside the engine, the vertical probe not being affected because the component is parallel to this probe and therefore has no effect, refer Section 3.2.3. Inside the engine, the piston speed will vary between zero at top and bottom dead centre and maximum value at approximately the mid-stroke position of the piston. If the piston speed is subtracted vectorially from the overall velocity vector, then it should be possible to obtain the computed overall velocity vector with respect to the cylinder wall and therefore be independant of the piston speed. This computation was undertaken for the most serious case occurring in the cycle when the vertical component due to the piston speed was 6.5 m/s and the resolved horizontal component of the measured velocity vector was 50 m/s. The computed vector relative to the cylinder wall is therefore 49.51 m/s and results in an error of

approximately 1%, therefore it was concluded that this effect could be neglected.

A second method which could be adopted in order to relate the overall velocity vector to the cylinder wall would be to investigate the cooling effect caused by the piston speed on each individual probe signal and subtract the component due to the piston speed. This would result in the three wire computation being performed accurately in both magnitude and direction for the vector relative to the cylinder wall. Analysis of this method was computed for the most serious case, where the piston speed was 6.5 m/s, and required the subtraction of a bridge voltage reading of 0.18 volts when the probe operating temperature was 800°C. This latter method is the easier procedure for determination of the velocity vector relative to the cylinder wall but because the effect reduces the vector by approximately 1%, it was concluded that it was not necessary to perform the analysis for all the results. However, should this method be considered necessary in any future measurements, it would be a simple procedure to perform.

3.3.5 Compensation for Increase in Wire Lead Temperature

Installation of a piston mounted probe would require the extraction of the probe leads via the engine sump and this would result in a rise in the lead resistance as the oil temperature rose due to operation of the engine. Experimental work was therefore carried out to simulate the effect of increased lead temperature on the calibration of an anemometer probe whilst it was mounted in the Disa wind tunnel. The results showed that, for a rise in lead temperature of 25°C, there was negligible change in the calibrated operating temperature

of the probe and so it was concluded satisfactory to neglect any increase in lead temperatures below 25°C. For increases in lead temperature of 60°C and above, however, the calibration curve showed a distinct change, refer Fig. 3.10, and correction was therefore necessary if errors in sensing wire operating temperature were to be avoided. The lead resistance was compensated for using the following equation

$$R_{LH} = R_{LC} (1 + \alpha (T_{LH} - T_{LC})) \qquad \text{3.21}$$

where R_{LH} = resistance of the leads at temperature T_{LH}

R_{LC} = resistance of the leads at temperature T_{LC}

and α = temperature coefficient of resistance for the copper lead

and the results showed that equation 3.14 accurately compensated for any increase in lead temperature.

3.4 Use of a Hot Wire Anemometer in a Variable Temperature and Density Environment

As mentioned in Section 3.1, the major problem encountered with an anemometer system installed within a varying temperature and density environment is that of probe calibration. Hassan (16) recognised the problem and used the instantaneous gas temperature and pressure in his computation of gas velocity using the theory developed by Davies and Fisher (17). However, it was concluded that the original theory was limited to air at ambient temperature and pressure and therefore a temperature loading factor was postulated by Hassan and Dent (18), which could be applied directly to the computed velocity. This correction is

given by

$$V_c = V_{DF} \times \left(\frac{T_w}{T_g}\right)^{0.3} \qquad \text{——— 3.22}$$

where V_c is the corrected velocity

V_{DF} is the computed velocity using Davies and Fisher (17) theory

T_w is the probe operating temperature

T_g is the instantaneous gas temperature.

Hassan and Dent (18) undertook a programme of experimental work in order to justify their correction factor using a high temperature and density wind tunnel and they showed the experimental results were within $\pm$ 12% of the computed results despite the tunnel velocity varying $\pm$ 8%. However, the range of velocities were approximately three times lower than those anticipated to exist within the engine cylinder at a representative engine speed. A more satisfactory experimental programme was undertaken which used the results taken from an engine under motoring conditions and this was published by Dent and Derham (25), and included in Appendix 3B.

The result of the latter experimental work presented a means of checking correction factors applied to wind tunnel calibration tests at ambient conditions to allow for temperature and density variation in the flow and, in the particular application of the motored internal combustion engine, it was found that the correction $(T_w/T_g)^{0.3}$ applied to the velocity computed from Davies and Fisher (17) was perfectly justified.

3.5 Conclusions of the Experimental Programme

Having adopted a system of hot wire anemometry similar to that developed by Hassan (16) and the theory extended to incorporate a three dimensional measuring technique, a comprehensive programme of experimental work was performed and the following conclusions made:

(i) The hot wire anemometer is an extremely sensitive measuring instrument and can be relied upon to reproduce accurate results providing that the hot wire operating temperature is accurately known.

(ii) The equation of $U_\theta = U_{max} \sin \theta$ is justified for angles of incidence above 10^o when the flow is not normal to the probe sensing wire.

(iii) Three probes mounted with their sensing wires mutually at right angles can be relied upon to predict accurately the magnitude and direction of a three dimensional velocity vector. Masking of the sensing wire can occur in specific positions but this can be eliminated by careful positioning of the probe arrangement.

(iv) When the probe was oscillated in the direction of the flow on a scotch yoke mechanism and therefore had a component of velocity, the velocity recorded by the probe was the vectorial addition of the flow velocity and the probe velocity.

(v) Providing that the lead temperature increase is below 25^oC, the effect on the wire operating temperature is

negligible. However, for lead temperature increases above $60^{o}C$, the lead resistance must be increased in accordance with the equation

$$R_{LH} = R_{LC} (1 + \alpha (T_{LH} - T_{LC}))$$

(vi) In the particular application of a motored internal combustion engine, it was found that the correction $(T_w/T_g)^{0.3}$ applied to the velocity computed from Davies and Fisher (17) theory was perfectly justified.

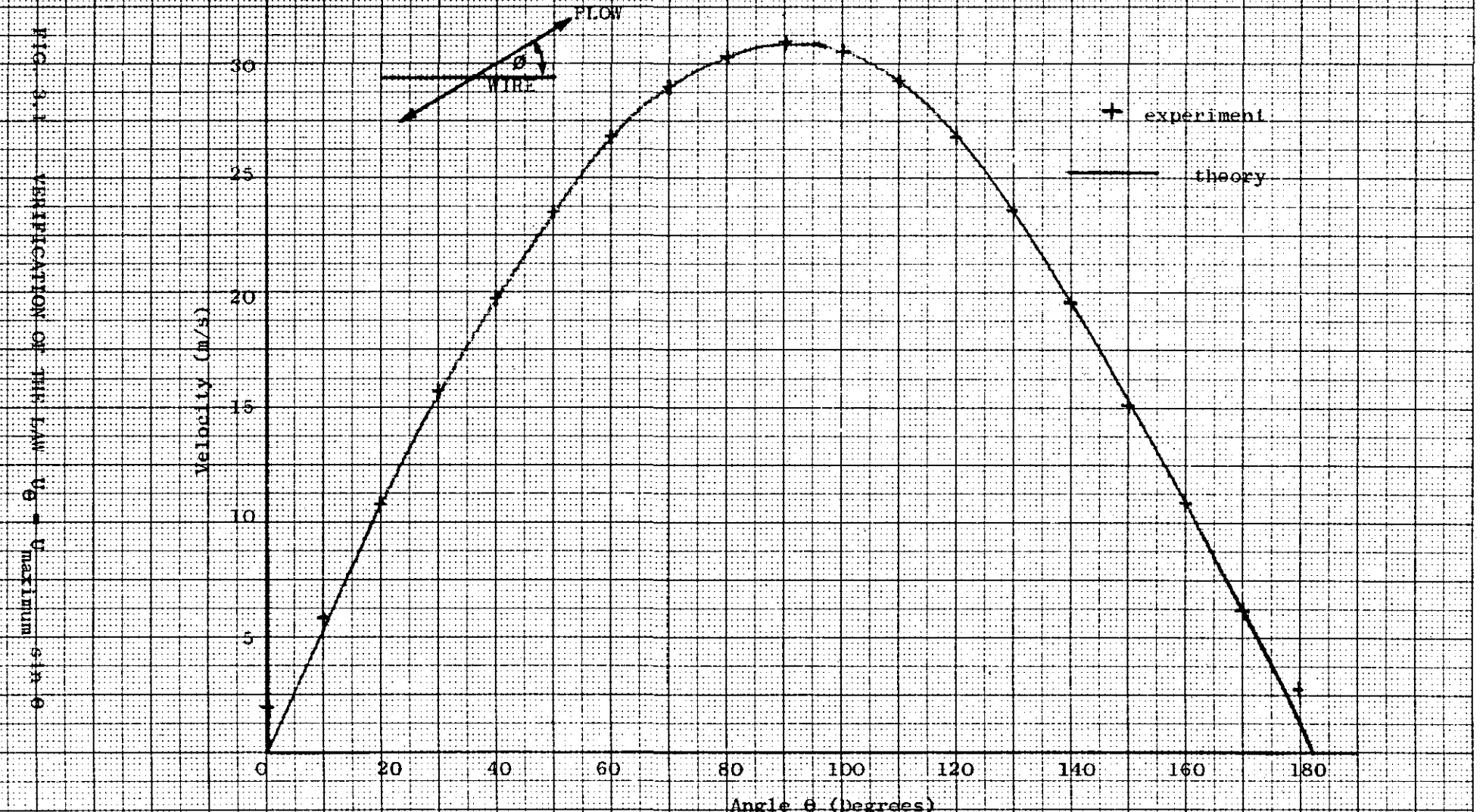

FIG. 3.1 VERIFICATION OF THE LAW $U_\theta = U_{maximum} \sin\theta$

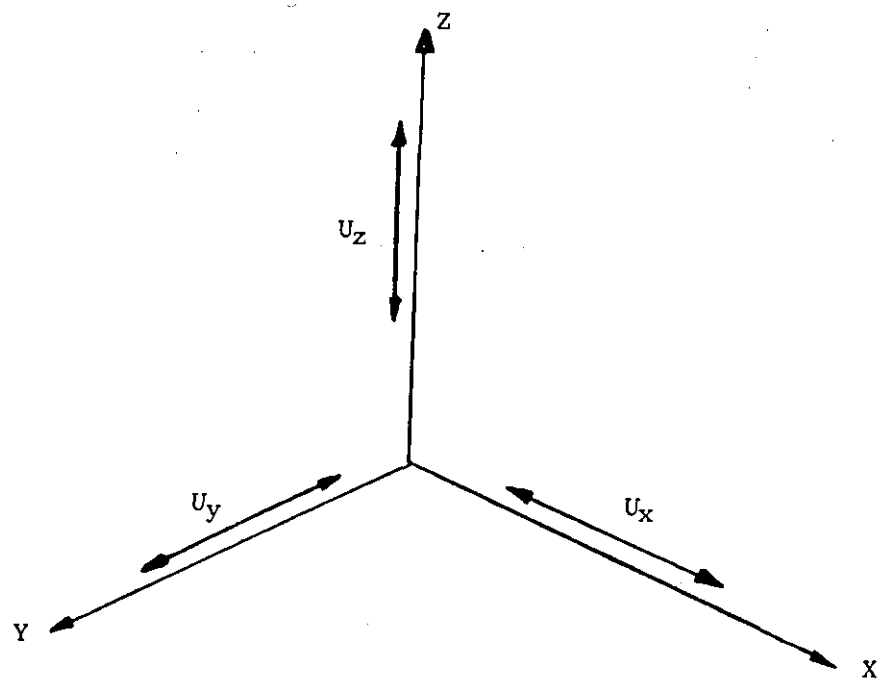

FIG. 3.2 THREE DIMENSIONAL CO-ORDINATE SYSTEM WITH AXES X, Y AND Z

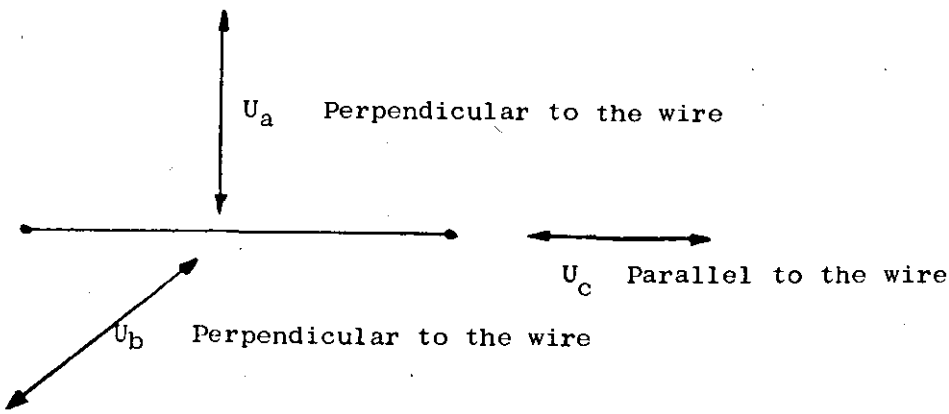

FIG. 3.3 RESOLVED COMPONENTS CONTRIBUTING TO A VELOCITY SIGNAL

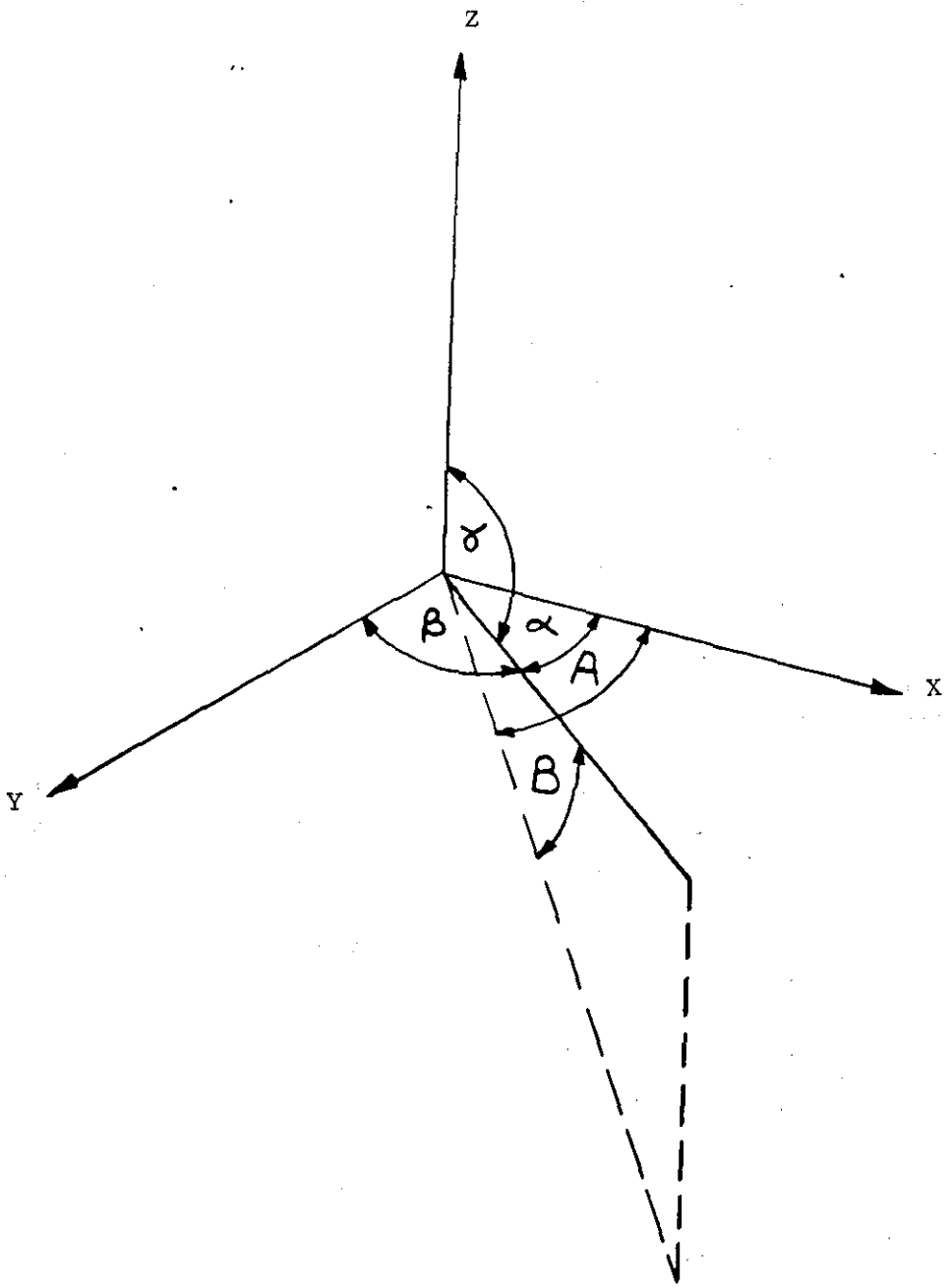

FIG. 3.4 VELOCITY VECTOR IN A THREE DIMENSIONAL CO-ORDINATE SYSTEM

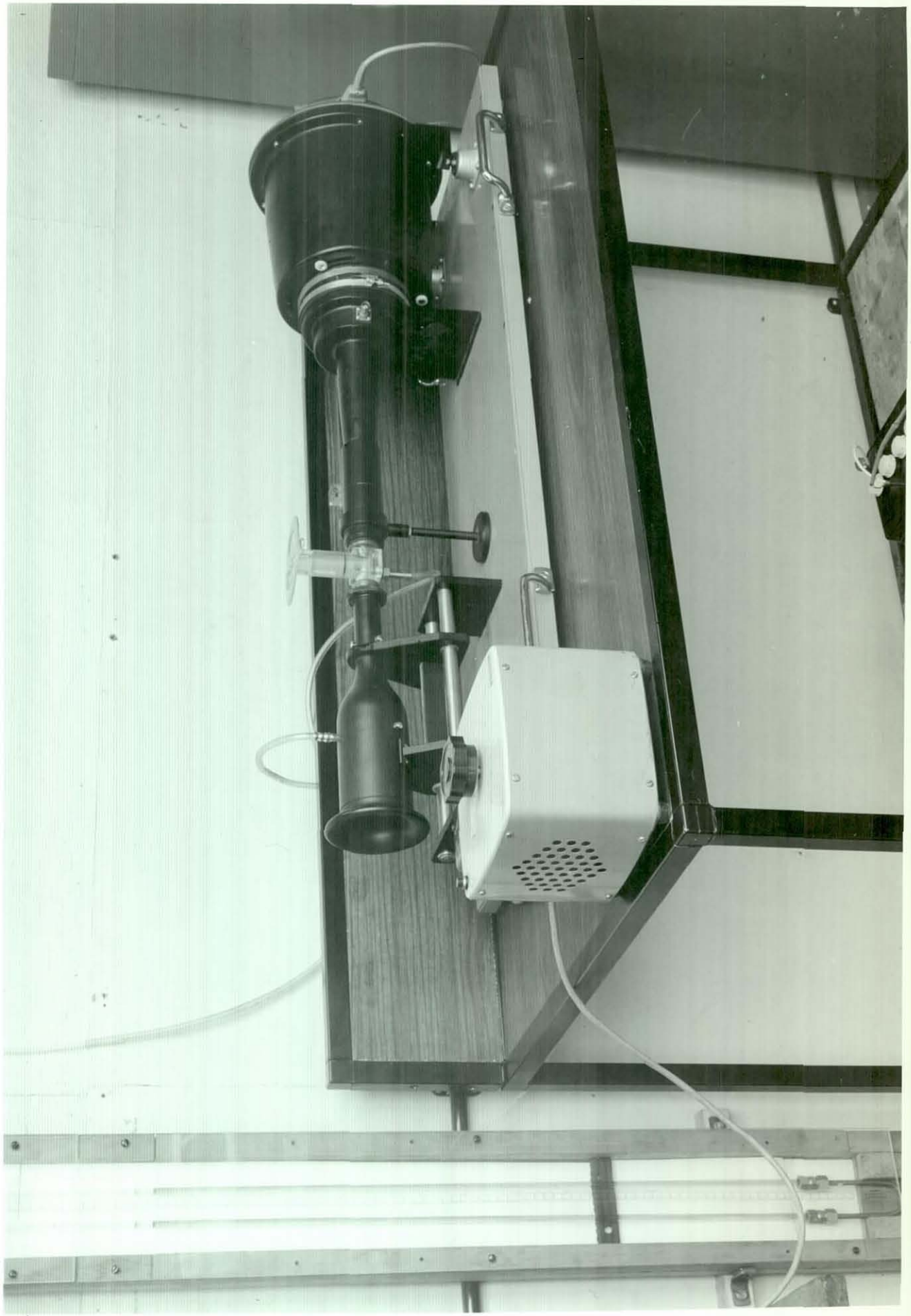

FIG. 3.5 DISA WIND TUNNEL

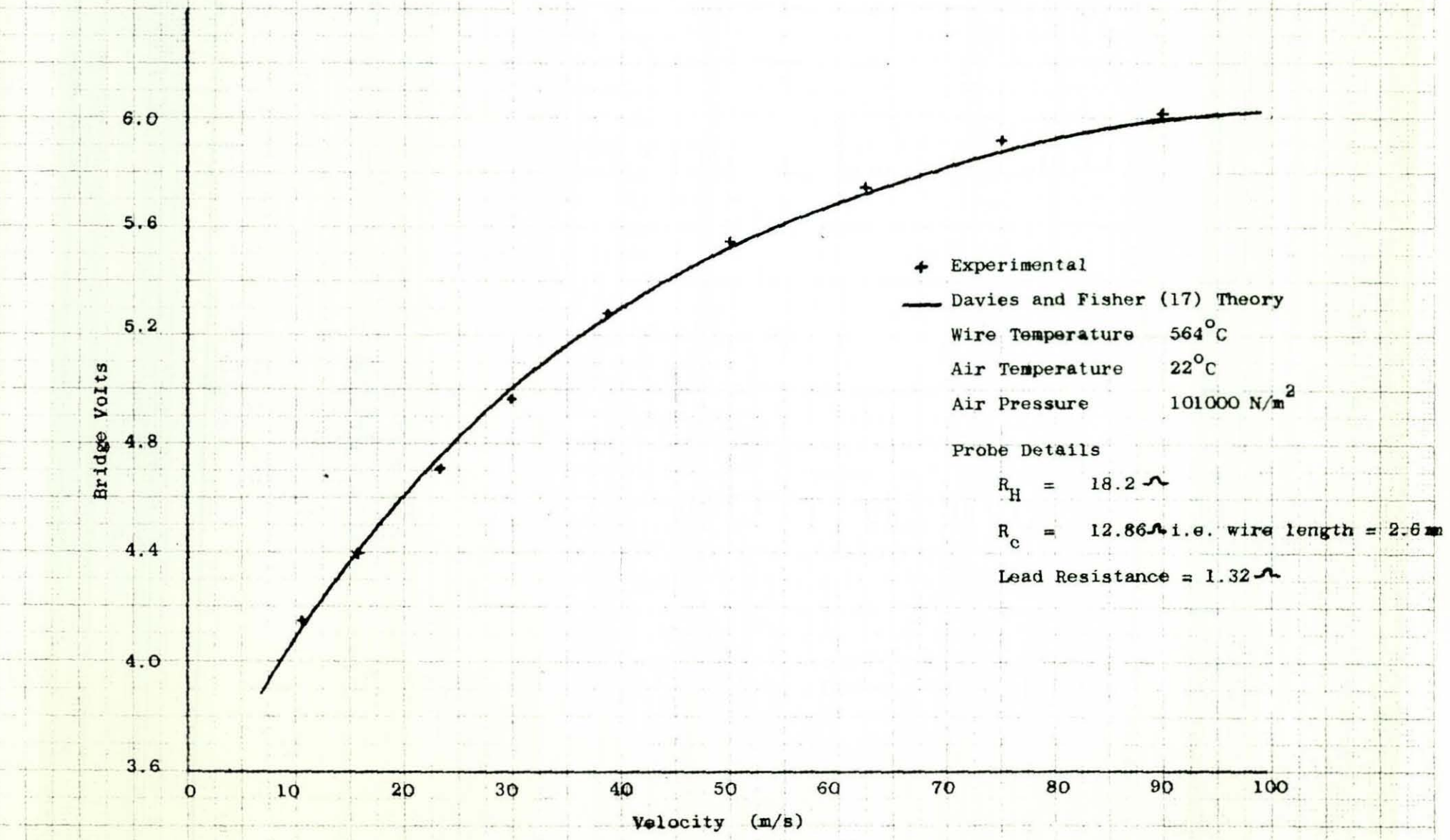

FIG. 3.6 TYPICAL SINGLE WIRE CALIBRATION CURVE

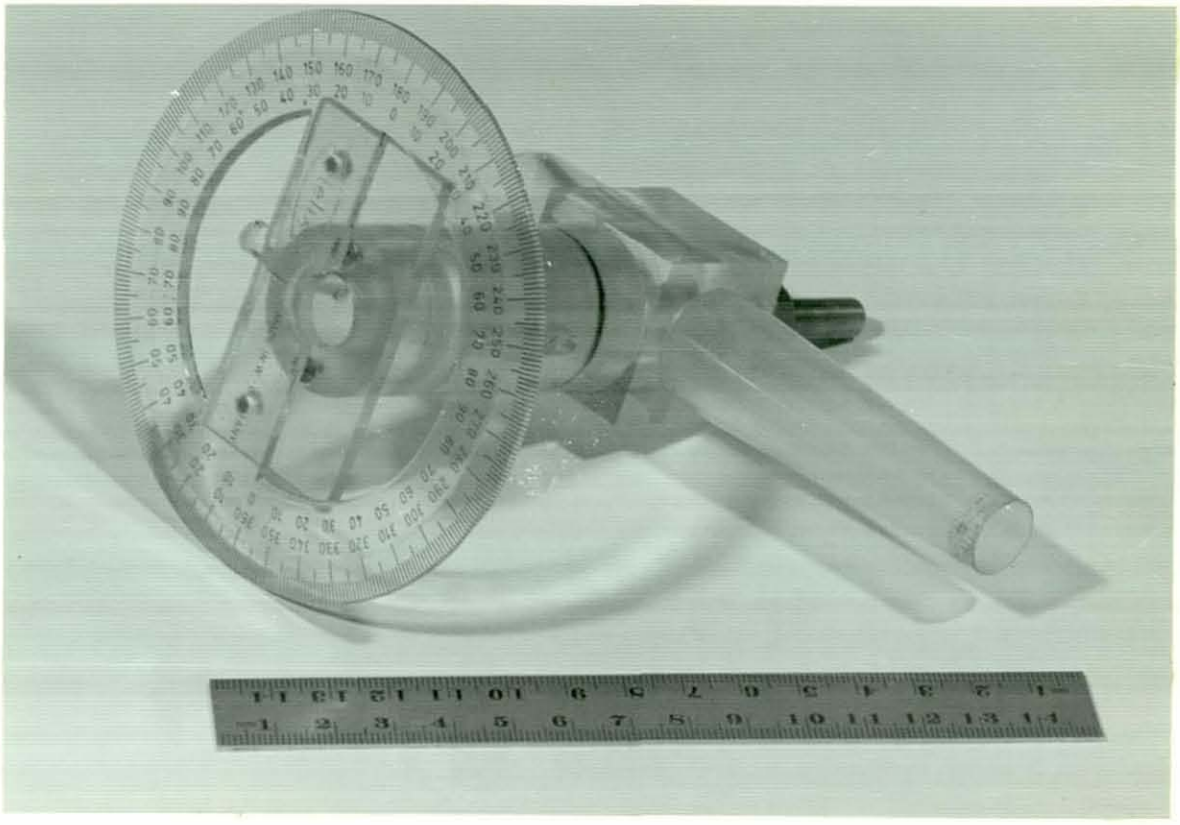

FIG. 3.7 TUNNEL ADAPTOR FOR PROBE MOUNTING

Measured Horizontal Angle when the Inclined Adaptor was Rotated through 360 degrees in the Wind Tunnel

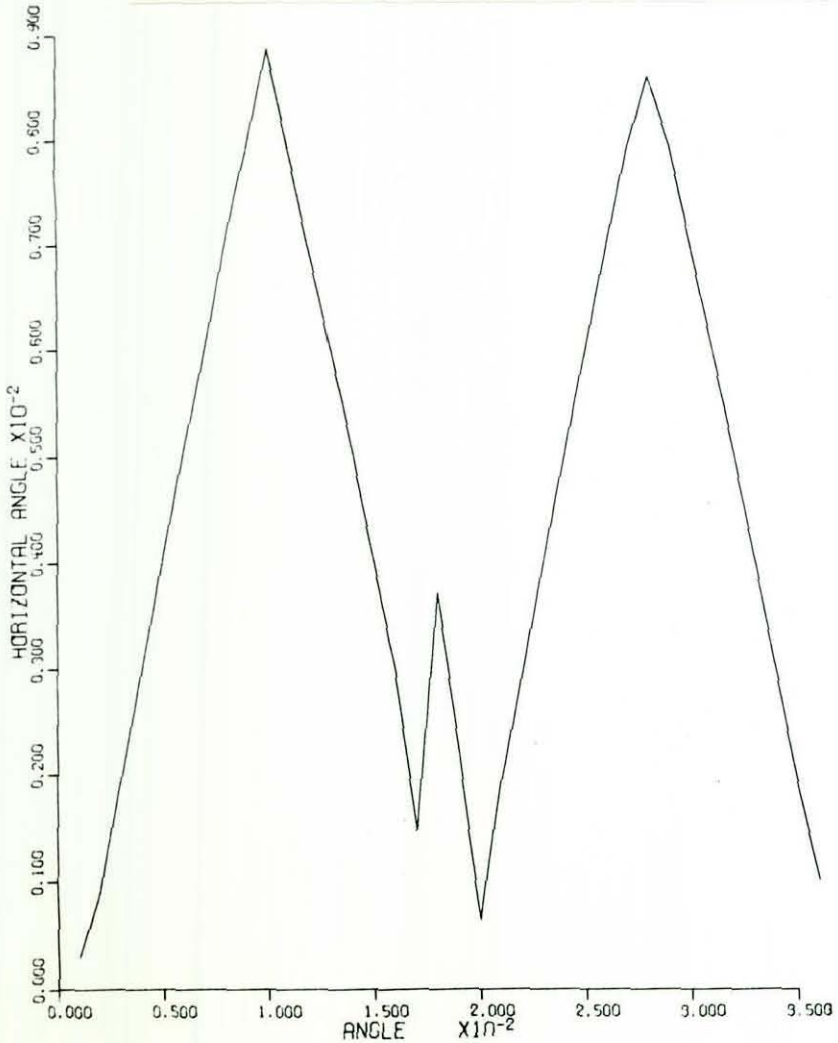

Measured Vertical Angle when the Inclined Adaptor was Rotated through 360 degrees in the Wind Tunnel

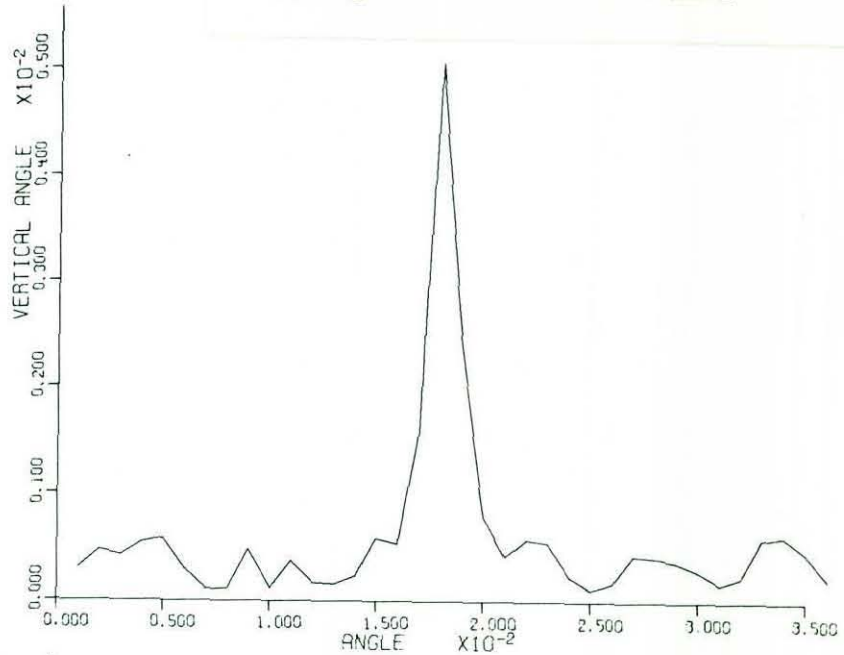

Measured Velocity Vector when the Inclined Adaptor was Rotated through 360 degrees in the Wind Tunnel

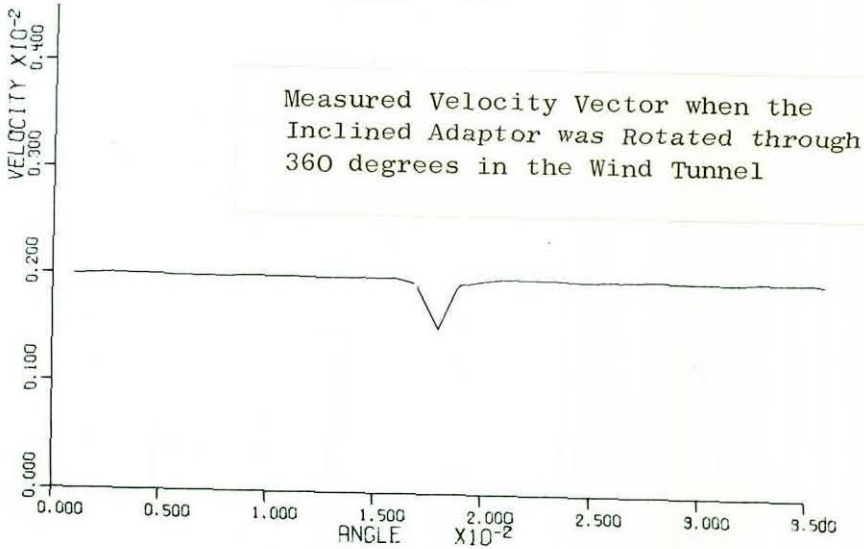

FIG. 3.8 RESULTS FROM THE THREE DIMENSIONAL TUNNEL EXPERIMENTS AT 20 M/S

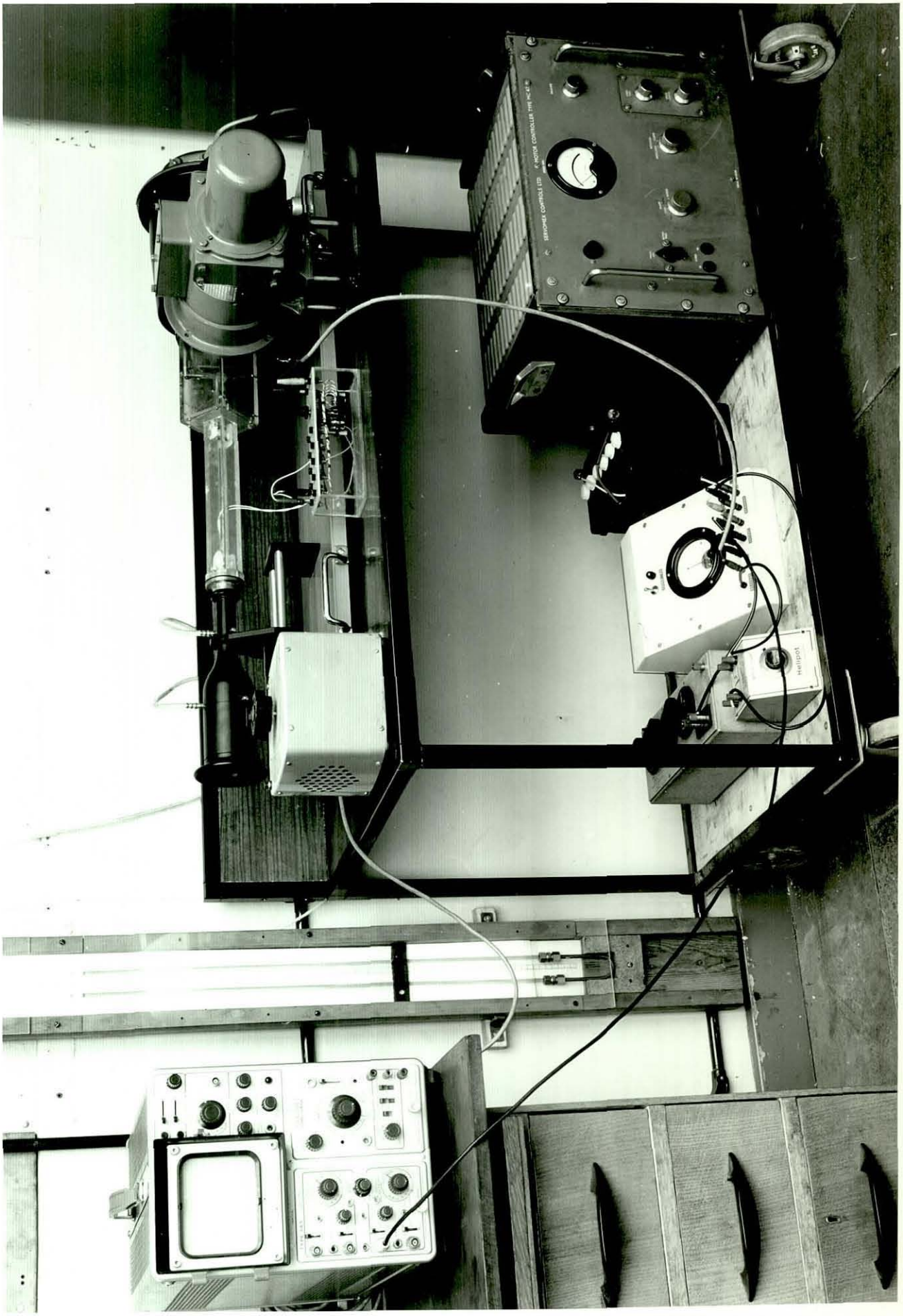

FIG. 3.9 DISA WIND TUNNEL WITH THE SCOTCH YOKE MECHANISM AND DAVIES AND FISHER (17) ANEMOMETER EQUIPMENT

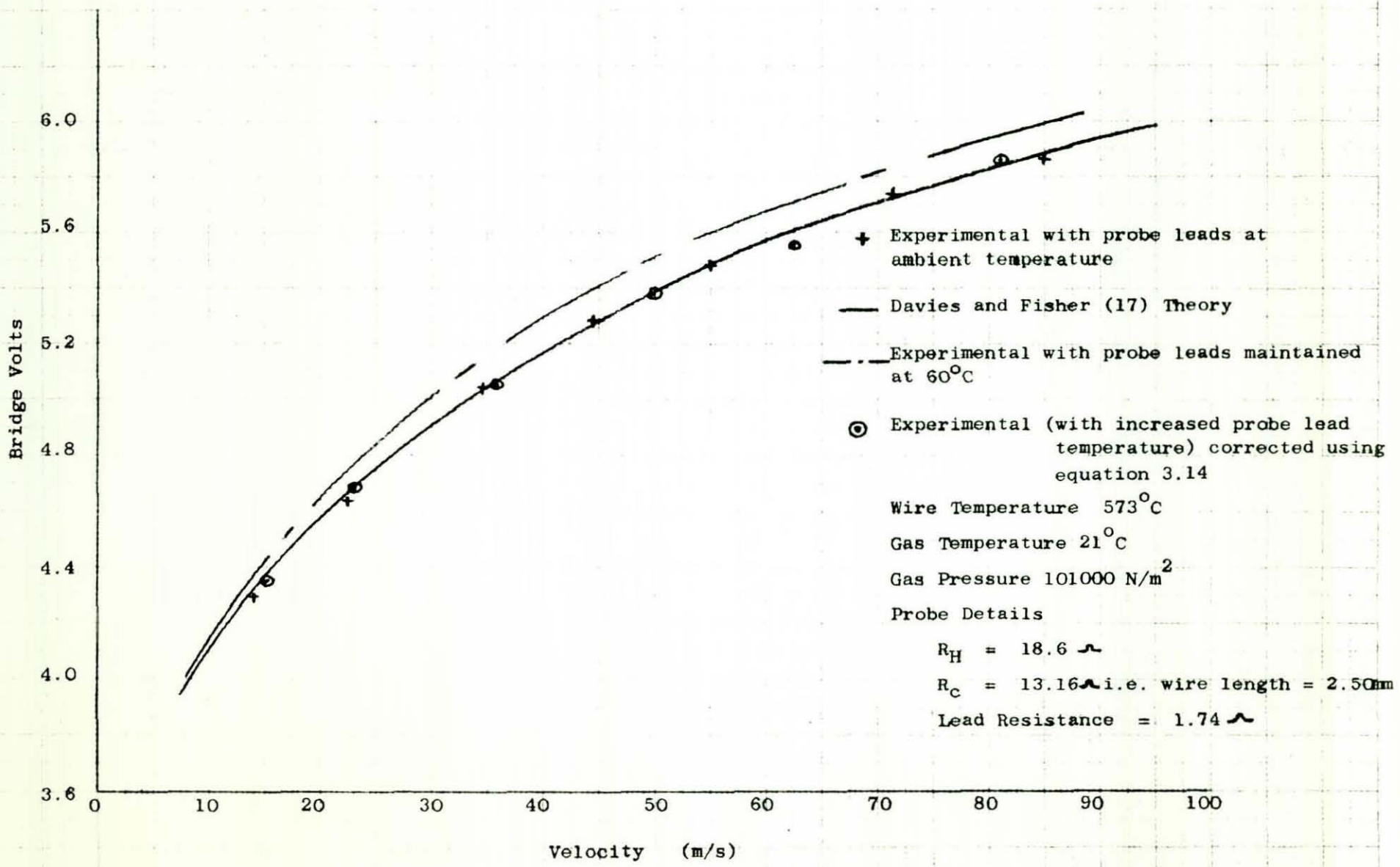

FIG. 3.10 EFFECT OF LEAD RESISTANCE CHANGE ON AN ANEMOMETER CALIBRATION CURVE

4.0 EXPERIMENTAL WORK PERFORMED INSIDE A MOTORED ENGINE

4.0 EXPERIMENTAL WORK PERFORMED INSIDE A MOTORED ENGINE

4.1 The Experimental Engine

4.1.1 Engine Specification

A Ruston and Hornsby 3YWA direct injection Diesel Engine was available for use within the Mechanical Engineering Department and this engine was commissioned for use during the investigation. A general arrangement of the engine with the motoring facility is illustrated in Fig. 4.1 and the engine specification is as follows.

Four stroke, air cooled, overhead valve, three cylinder direct injection Diesel Engine.

Bore	102 mm
Stroke	104.8 mm
Piston displacement	2547 cc
Piston speed at 2000 r.p.m.	6.98 m/s
Inlet valve opening	16° B.T.D.C.
Inlet valve closing	36° A.B.D.C.
Exhaust valve opening	45° B.B.D.C.
Exhaust valve closing	15° A.T.D.C.
Injection commences	27° B.T.D.C.

4.1.2 Modifications of the Engine for Investigation Purposes

In order to undertake the experimental investigation using the engine, it was decided to remove the injection equipment from the engine since it was not anticipated that this would be required during the motoring operation and this made the cylinder head and sleeve more accessible.

4.1.3 Engine Motoring Arrangements

The engine was coupled to a D.C. motor via a complex belt driven system and this resulted in a maximum speed of the engine of approximately 1750 r.p.m. The belt system was necessary due to the poor torque characteristics of the electric motor at low r.p.m. and since no other motor was available the belt drive was the simplest way to overcome the torque created by the engine flywheel, crankshaft and oil drag.

4.1.4 Engine Cycle Degree Marker

A Southern Instruments type M738 Degree Marker was used to record a degree mark every 10^{o} of the crankshaft rotation and was connected to the recording equipment to aid analysis of the experimental results.

4.1.5 Experimental Recording Equipment

A Southern Instruments twin beam oscilloscope was used to display the experimental results and these were recorded using an M731 Universal Oscillograph recording camera. The engine traces

were recorded on RP30 Kodak paper which was approximately 20 inches in length and proved adequate for analysis purposes.

4.2 Gas Velocity Measurement

As mentioned in Section 3.1, the existing electrical equipment for measuring the velocity inside the engine cylinder developed by Hassan (16) was available in the Mechanical Engineering Department and so this was adopted for the investigation. The hot wire anemometer probe was operated using a constant temperature amplifier bridge circuit which maintained the probe sensing element at fixed operating temperature and allowed a record of the bridge output voltage to be displayed on an oscilloscope. In order to compute the velocity using the Davies and Fisher analysis (17) refer Section 3.3.1, the instantaneous gas temperature and pressure were also measured using a simple Wheatstone Bridge and a strain gauge pressure transducer respectively. The equipment is illustrated along with the Southern Instruments recording equipment in Fig. 4.2 and further information regarding the precise mode of operation of the equipment may be found in reference (26) which presents a comprehensive report concerning the measurement of air velocity in a variable density environment.

4.3 Initial Experimental Work

4.3.1 Experimental Work using Hassan's Pre-Chamber

In order to avoid unnecessary destruction of any anemometer probes, it was decided to install a probe within the pre-chamber engine used by Hassan (16) and develop the basic experience required for the measurement of velocity inside the engine cylinder. A single probe was installed in the pre-chamber and the engine motored at a speed of 1000 r.p.m. whilst the results were recorded. Detailed measurements of bridge voltage, gas temperature and gas pressure were made and a typical set of results are illustrated in Fig. 4.3.

4.3.2 Computer Program for the Computation of the Velocity Vector

Analysis of the results was performed by Hassan (16) by measuring individual ordinates at 10^{o} intervals throughout the engine cycle. However, this method proved to be laborious and in order to automate the process, a D.Mac Pencil follower (27) was used to analyse the engine traces. The paper tape output from the D.Mac system was fed directly to a computer program and used in the calculation of the velocity vector.

The program presented in detail in Appendix 4A was developed for measurement of the velocity vector and uses the instantaneous values of voltage, pressure and temperature in order to predict the velocity component. Using the theory developed for three dimensional measurement in Section 3.2, the three velocity components were computed and then added vectorially according to equations 3.8, 3.12 and 3.13 in order to predict the magnitude and direction

of the velocity vector.

4.3.3 Discussion of Results from the Pre-Chamber

The particular pre-chamber engine used develops ideally a one dimensional flow at a particular location and for this reason only a single anemometer probe, arranged so that its sensing wire was perpendicular to the flow direction, was used for the measurement of bridge voltage. The measured signal of bridge voltage is illustrated by curve c in Fig. 4.3. Curves a and b in Fig. 4.3 illustrate the instantaneous gas temperature and pressure respectively. The resulting velocity vector computed from these instantaneous values of bridge voltage, gas temperature and pressure is illustrated in d of Fig. 4.3. and observation shows that the velocity is not directly proportional to the bridge voltage trace. Instead it is obvious that both the gas temperature and pressure contribute significantly to the magnitude of the computed velocity. It was concluded therefore that complete analysis of the results would have to be performed before any estimation could be made of the velocity component from within the engine cylinder and it is not possible to take the bridge voltage trace as a representative indication of the velocity profile developed during the engine cycle. In order to compute the velocity results illustrated in Fig. 4.3.c, the computer program, refer Appendix 4A, was used but the three dimensional vector subroutine was suppressed and only the subroutine for velocity computation used.

4.4 Installation of the Measuring Device

4.4.1 False Piston Crown

Conclusion (iii) of Section 2.5 stated that a piston mounted probe would be required in a variety of radial locations in order that velocity measurements could be made throughout the cylinder during the engine cycle. Because it would be necessary to strip down the engine cylinder assembly in order to transfer the anemometer probes to a different location, it was decided to machine a false piston crown and secure this to the piston skirt by means of 8, 4BA Socket head screws, refer Fig. 4.4. This would reduce the amount of labour involved in transferring the measuring probes to a different location and avoid having to repeatedly remove the entire piston and connecting rod assembly from the engine each time a measurement was to be made at a new location. In order to avoid any unnecessary interference occurring to air motion within the engine cylinder, it was decided to have a three wire probe located at only one particular location at any time, and this meant that special plugs had to be machined to fit into the probe locations not being used. The five radial locations are illustrated in Fig. 4.5 which shows a view of the valves located in the cylinder head.

4.4.2 Swinging Link Mechanism

Mounting the probes on the piston crown also involves the extraction of the leads via the connecting rod and out through the sump to the engine casing. This presents a further problem since an engine operating at a speed of 1500 r.p.m. would quickly destroy any wiring bridging the gap between the big end bearing and the engine casing. Consequently a swinging link was designed which

could be attached between the big end bearing and the crank case wall and would allow the wires to undergo an extremely fast but predictable path whilst the engine was operating at speed. The connecting rod assembly, false piston crown and swinging link are illustrated in Fig. 4.6 and it may be observed that 6 leads terminate on the bearing of the connecting rod. Fig. 4.7 shows the swinging link and lower bearing shell wired and ready for installation on the engine. Again 6 individual leads are bound together on the link mechanism and when suitable connections are made with the probes, the mechanism will allow the signals from three separate probes to be taken from the engine.

4.4.3 Choice of Lead Material

When the engine is operated at speeds of 1500 r.p.m. the swinging link is subjected to high velocity and acceleration forces. Simple calculations performed for the mechanism revealed that a link machined from solid duraluminum bar would have adequate strength to stand up to the inertia forces developed but doubt existed with regard to the durability of the lead material. Investigations were made into various types of copper lead material and a special copper/tinsel wire (28) was found which could withstand excessive movement and still transmit a noise-free signal. Consequently, the copper tinsel wire (28) was adopted for all the swinging link leads.

4.4.4 Initial Experimental Tests using the Swinging Link

In order to justify the system developed for piston mounted probes, a single anemometer probe was mounted inside the combustion bowl and the necessary connections completed using the connecting rod

and link mechanism. The results for both gas temperature and bridge voltage were recorded using the same probe but different measuring equipment, refer (26), and a low engine speed of 500 r.p.m. was used for the initial tests. Excellent results were recorded for both bridge voltage and gas temperature and further tests were carried out which resulted eventually in an engine speed of 1750 r.p.m. being reached with no apparent noise imposed to the recorded signals by the rapid movement of the probe leads. Consequently, it was decided that the method of mounting probes on the piston crown and extracting the leads via the connecting rod and swinging link was feasible and yielded excellent results of the traces throughout the engine cycle.

4.4.5 Three Dimensional Velocity Measurements

Having justified the experimental apparatus and the feasibility of mounting a probe on the piston crown, consideration was given to the measurement of the three dimensional velocity vector. According to the conclusions of the literature survey, Section 2.5, it was anticipated that the air motion within the engine cylinder would be an orderly swirl in an anticlockwise direction (when viewed from above the cylinder head). Hence the probes were located mutually at right angles and in such a manner that the velocity vector formed an angle of incidence with each probe, refer Fig. 4.8 which illustrates three probes mounted within the combustion chamber of the engine. Experimental work was then undertaken at an engine speed of 500 r.p.m. to obtain both magnitude and direction of the overall velocity vector, at the various locations of the piston crown as illustrated in Fig. 4.5 and discussed in further detail in Section 4.5.

4.4.6 Bridge Voltage Measurement

Using each of the three probes in turn, a record was made of each bridge voltage signal from the three wire probe assembly and a typical trace is illustrated in Fig. 4.9. Curve a in Fig. 4.9 illustrates two complete cycles of the bridge voltage trace and reveals good cycle to cycle repeatability of the results. Curve b illustrates only one cycle of the trace but has included with it, the calibration lines necessary for the complete analysis of the results. After completion of the three traces, the probe assembly was rotated to a second predetermined location and a further series of experimental results recorded. It is important to point out that the method of recording the traces outlined above was necessary since the recording facilities available in the Mechanical Engineering Department were comparatively poor. Ideally, it was hoped that the signals could have been recorded directly on to magnetic tape and processed by the computer. This would have been advantageous since several cycles could have been statistically analysed for each measuring location. However, since the only facility available was the Southern Instruments Oscilloscope and Recording Camera, this had to be adopted for all the signal processing and analysis of the engine traces.

4.4.7 Gas Temperature Measurement

Theoretically, any one of the three wires could be used as a resistance thermometer to measure the gas temperature throughout the cycle, however, for the experimental work described here, the same probe was used at each of the five radial locations. This reduced the possibility of introducing any error into the gas temperature measurement and, by measuring the gas temperature at each location, helped justify the presence of a spatially uniform temperature distribution

within the section of the cylinder under investigation. Fig. 4.10a illustrates two gas temperature cycles and shows cycle to cycle repeatability is excellent for this measurement. The curve b shows a typical gas temperature trace used for analysis purposes.

4.4.8 Gas Pressure Measurement

The gas pressure measurement was made by mounting the Bell and Howel strain gauge pressure transducer into a specially constructed dummy injector and the measurement made at only one location within the engine. The sensing diaphragm of the transducer was located some distance from the actual cylinder area and connected via a 0.32 cm diameter passage. Initially, it was suspected that a 'passage effect' similar to that reported by Lyn (29) might be encountered due to this arrangement. However, observation of Fig. 4.11 illustrates that no such passage effect occurred since the trace is free from noise and comparison between the experimental trace and that computed using the polytropic expression $pV^{\dot{n}}$ = constant, where $\dot{n}$ = 1.35 for the compression and expansion periods showed excellent agreement. It was therefore concluded that the method of location for the pressure transducer was perfectly satisfactory. Again, Fig. 4.11a shows good repeatability of the pressure trace and b illustrates a typical pressure traced used in the analysis procedure.

4.5 Discussion of the Experimental Results

A series of results is illustrated in Figs. 4.12 to 4.17 which show the velocity vectors at a variety of radial locations and differing crank angle positions throughout the engine cycle. The vector represents the magnitude (refer particular scale on each Figure) and

is resolved into the horizontal plane. The vertical angle B, refer Fig. 3.5, associated with each vector is written at the side of that vector. The results illustrated here were computed from the signals obtained whilst the probe assembly was located at a height of 0.65 cm. above the piston crown, and, in order to avoid collision between the probe assembly and the cylinder head, small pockets were made in the latter. Thus, as the piston approached the top dead centre position, the probes plunged into the recesses formed in the cylinder head. Obviously, accurate records could not be made from the signals in the top dead centre positions but detailed analysis of the results revealed that the air motion in the later stages of the compression period (after 40 degrees before top dead centre) was basically two dimensional and a very low vertical angle B was recorded. Consequently, in order to complete the measurements in the top dead centre position, two probes were located within the clearance volume at a height of approximately .038 cm. above the piston crown. These two probes could then be used to measure the magnitude and direction of the air motion in the confined space between the cylinder head and piston crown.

Investigation was made as to the possibility of wall proximity errors resulting from the probes being mounted so close to the piston crown and reference was made to the work of Wills (30) which showed that a probe could be mounted within 0.025 cm. of a wall surface, the result being negligable heat loss to that surface, refer Appendix 4B. It was therefore decided that the mounting of the probes at a height of .038 cm. was perfectly acceptable and no correction was necessary for the signals obtained.

The results show that an orderly flow exists within the cylinder, except for the early part of the induction period when it

appears that the flow is particularly random as it enters through the inlet valve. However during the latter stages of the induction period and compression period, the flow may be described as orderly and several conclusions can be made regarding the air motion,

(i) an orderly swirl is developed during the induction period after approximately 90 degree crank angle,

(ii) the developed swirl exists throughout the compression period but with an increase in speed,

(iii) as the piston approaches within 40 degrees of the top dead centre position, the flow pattern reduces to a two dimensional system since a low vertical angle B (always less than 10 degrees) exists,

(iv) the air appears to spiral into the combustion chamber as the top dead centre position is approached and an ideal radial movement of the air was not found,

(v) the angular velocity is approximately constant along a cylinder radius and suggests the presence of a forced vortex velocity profile.

The successful demonstration of the orderly air motion and existence of a forced vortex velocity profile is supported by the work of Horvatin and Hussmann (11), Horvatin (31) and Stock (32), whose results are illustrated in Figs. 2.15, 4.18 and 4.19 respectively. However, in order to justify the assumption of a uniform pressure distribution to exist within the engine cylinder, a mathematical analysis was undertaken where the forces existing on a fluid element were investigated in detail. The analysis is presented in Appendix 4C

and concludes that a forced vortex profile existing within the engine cylinder will be accompanied by a negligable radial pressure gradient, thus justifying the assumption of uniform pressure distribution within the engine cylinder.

Consequently, in order to predict the air motion within the engine cylinder, the demonstration of an orderly air motion, forced vortex velocity profile and uniform pressure distribution were extremely important contributions and formed the basis of the mathematical model detailed in Section 5.0.

4.6 Conclusions of the Experimental Work Performed within a Motored Diesel Engine

Having undertaken an initial programme of experimental work using a hot wire anemometer system located on the piston crown within the cylinder of a motored Diesel Engine, the following important conclusions were made.

(i) Initial experimental work performed on the pre-chamber engine used by Hassan (16) provided valuable experience for the future cylinder investigation.

(ii) Three probes mounted mutually at right angles to each other and located at any one of five radial positions, refer Fig. 4.5, could be manufactured and fitted to a false piston crown. The probe leads were then extracted via the connecting rod and a specially designed swinging link mechanism.

(iii) The swinging link mechanism was used to record noise free signals up to a maximum engine speed of 1750 r.p.m.

(iv) An orderly air flow exists throughout the major part of the induction, compression and expansion periods and is accompanied by a rapid release of air from the engine cylinder as the exhaust valve opens.

(v) After 90 degrees crank angle during the induction period, the air motion may be represented by a forced vortex velocity profile and this is supported by the work of Horvatin and Hussmann (11), Horvatin (31) and Stock (32) whose results are illustrated in Figs. 2.15, 4.18 and 4.19 respectively.

(vi) Using the evidence of an orderly flow, forced vortex velocity profile and uniform pressure distribution existing during the majority of the induction and compression periods, it was concluded that a mathematical model could be developed in order to predict theoretically the air motion occurring within the engine cylinder during this part of the engine cycle.

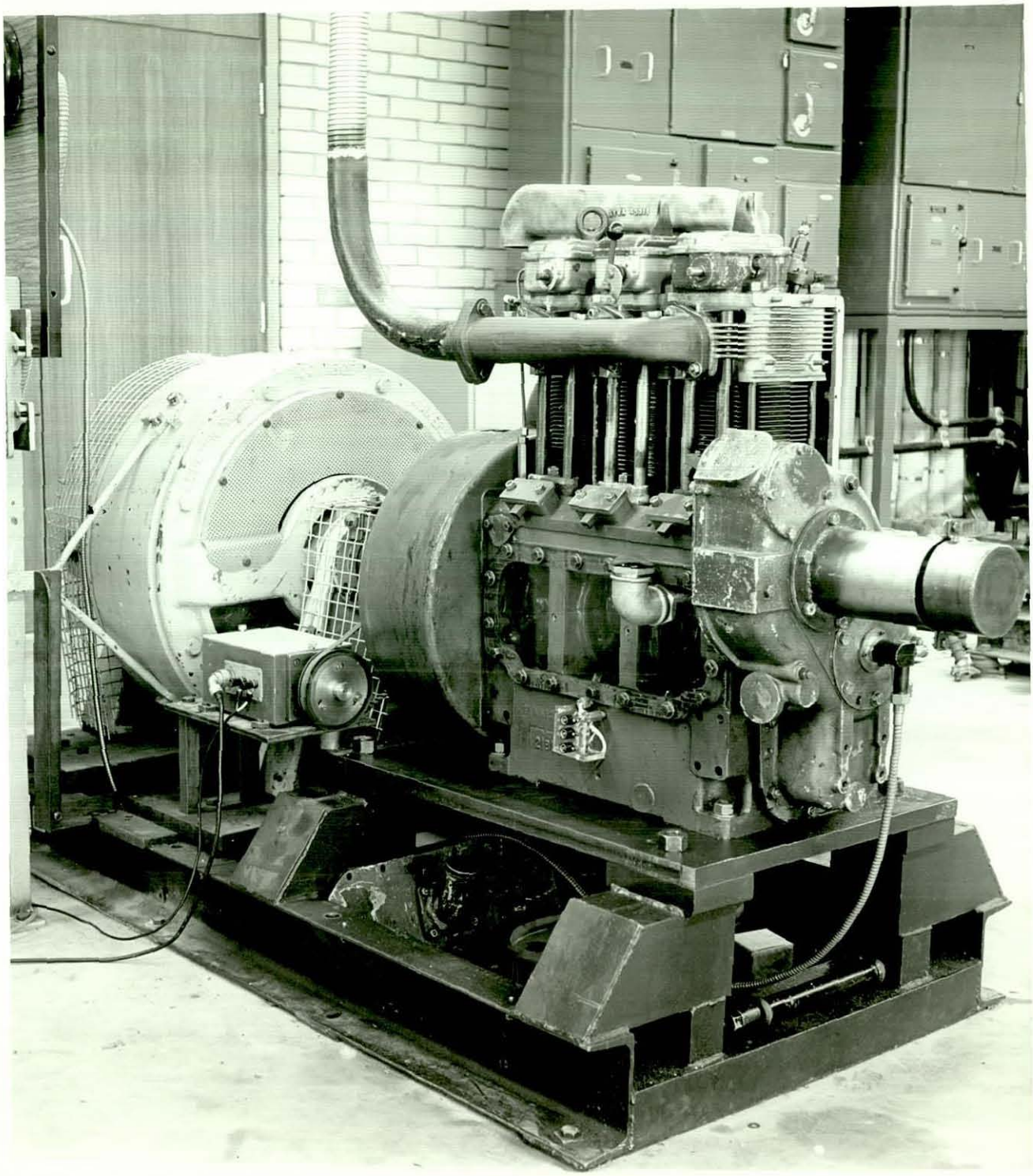

FIG. 4.1 3YWA ENGINE AND MOTORING FACILITY

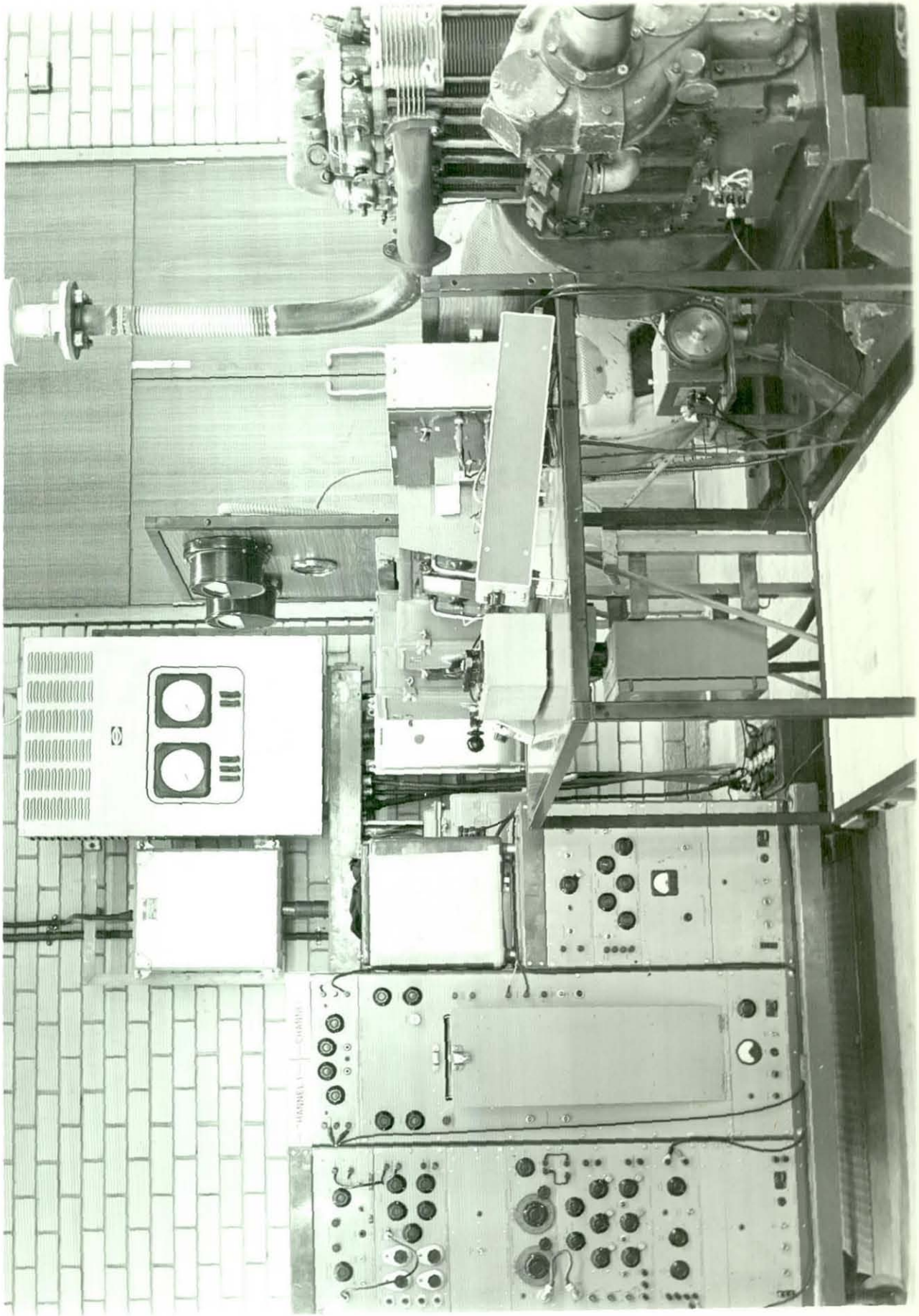

FIG. 4.2 GAS VELOCITY MEASURING AND RECORDING EQUIPMENT

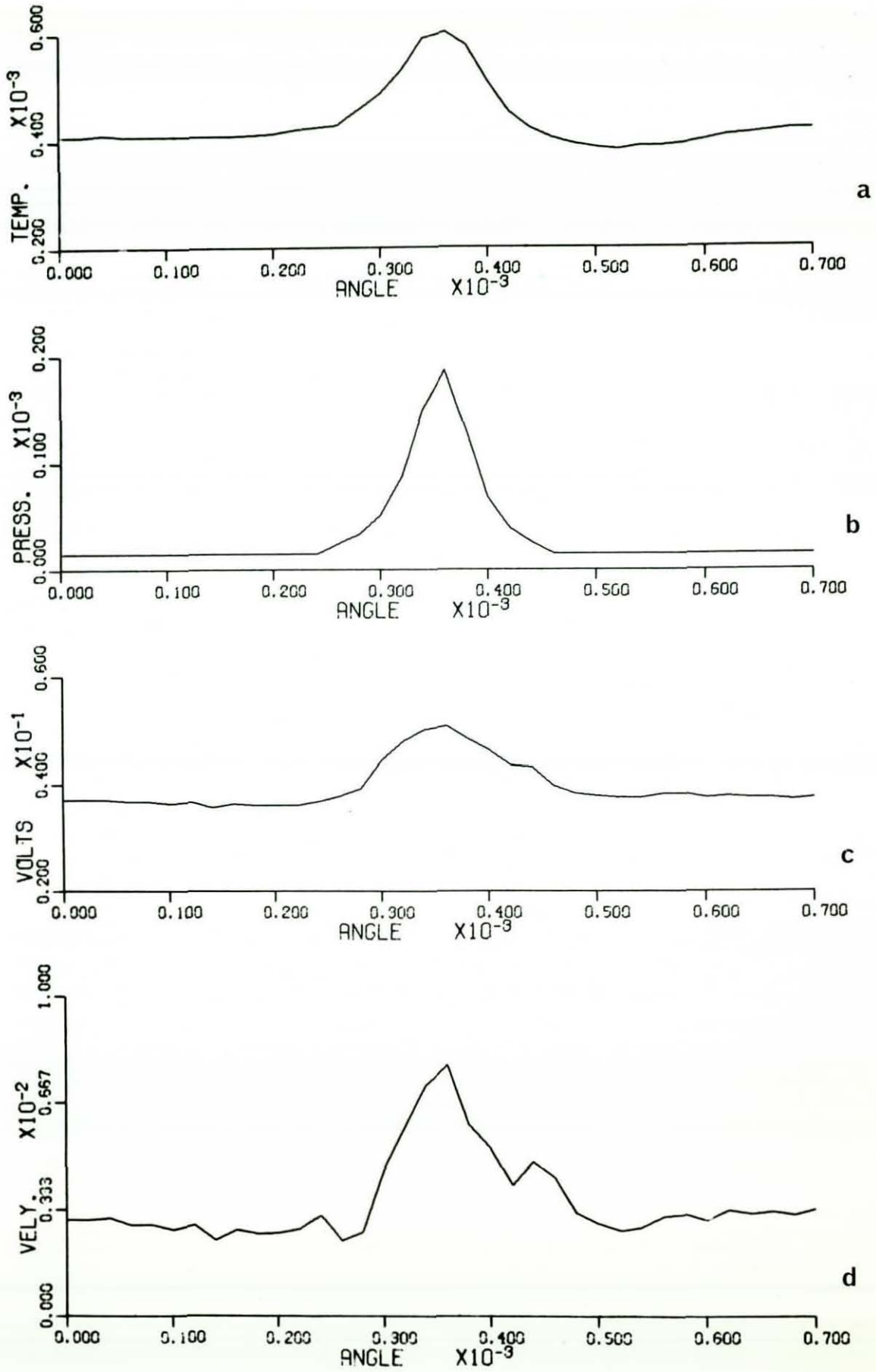

FIG. 4.3 RESULTS FROM A PRE-CHAMBER ENGINE MOTORED AT 1000 R.P.M.

FIG. 4.4 TYPICAL 'FALSE PISTON CROWN'

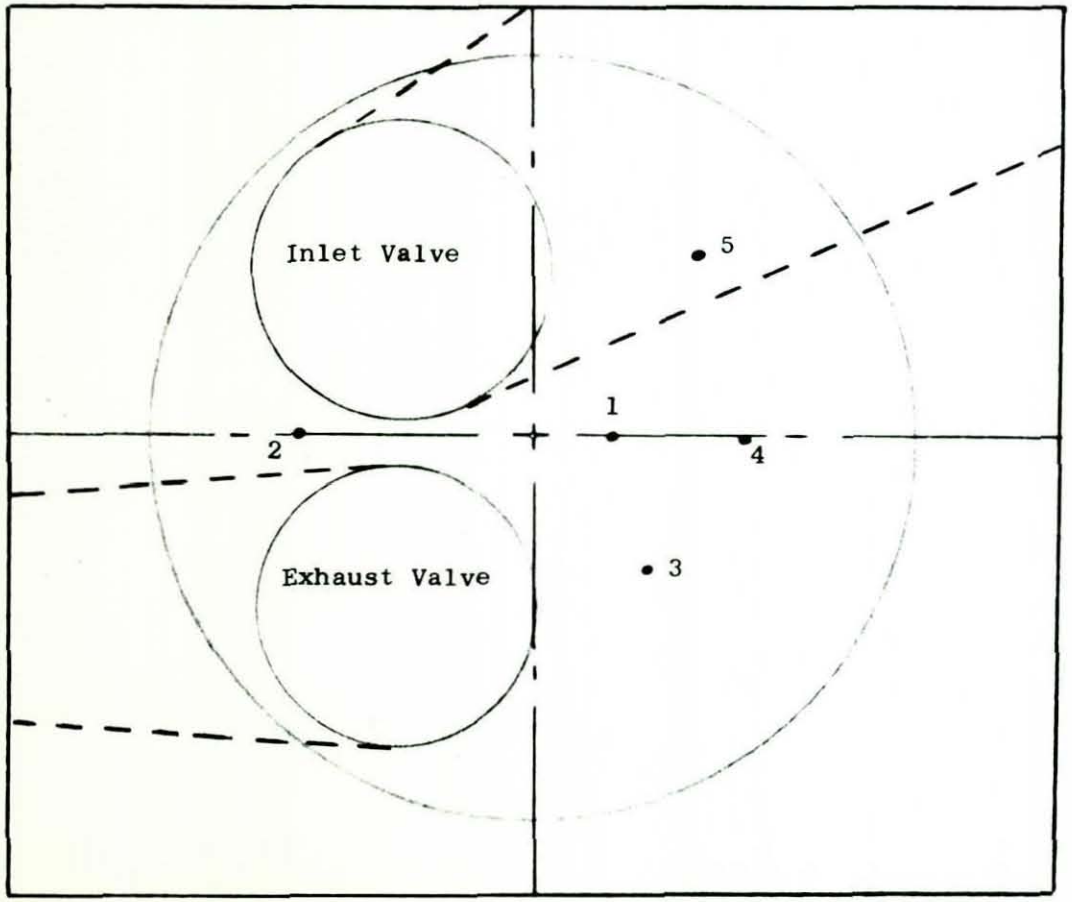

Position No.	Radius from Centre
1	1.27 cm.
2	2.49 cm.
3	3.18 cm.
4	3.49 cm.
5	3.81 cm.

FIG. 4.5 CYLINDER HEAD AND PROBE LOCATIONS

FIG. 4.6 CONNECTING ROD AND SWINGING LINK ASSEMBLY

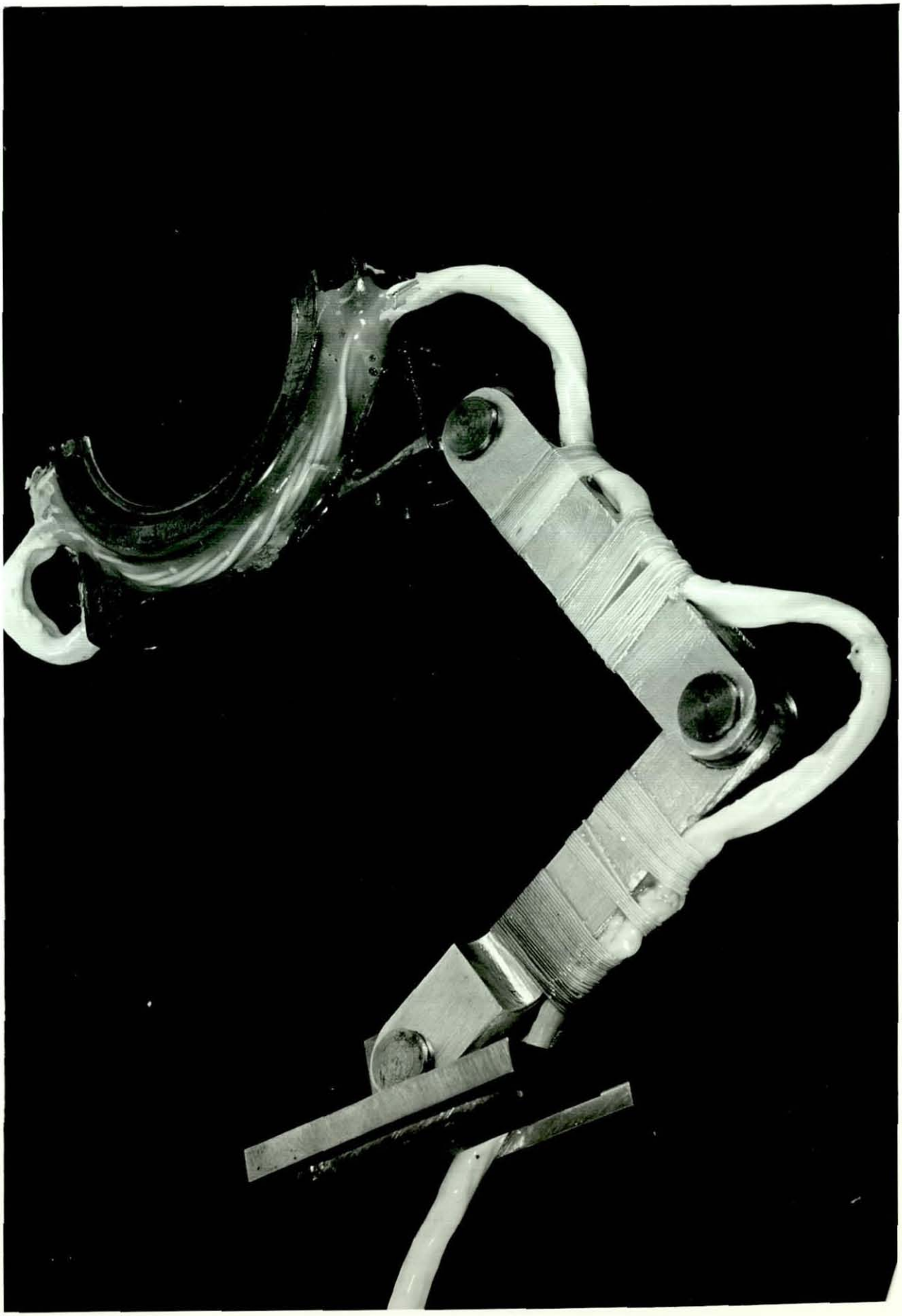

FIG. 4.7 COMPLETE SWINGING LINK UNIT

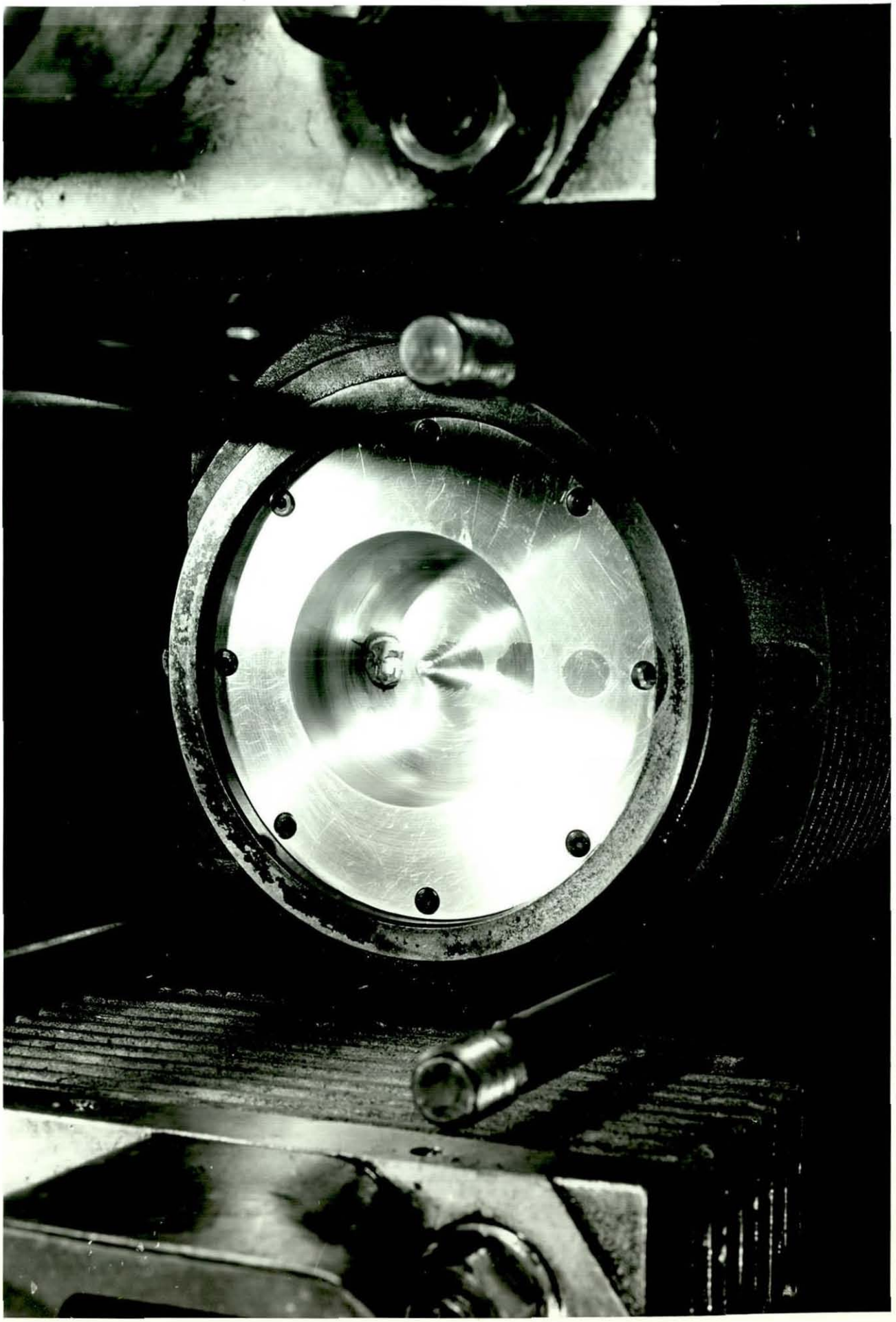

FIG. 4.8 THREE WIRE PROBE LOCATED INSIDE THE COMBUSTION CHAMBER

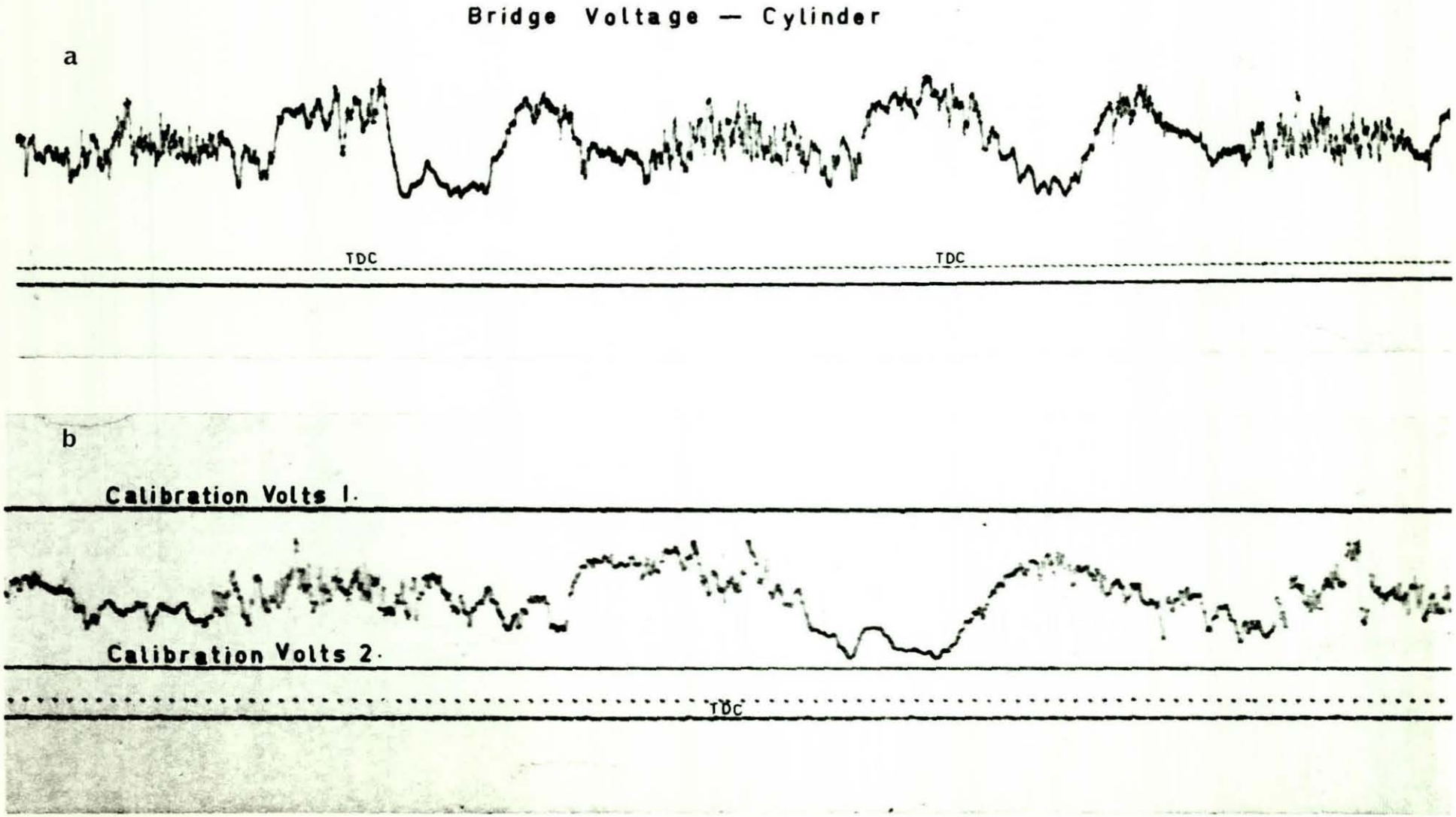

FIG. 4.9 BRIDGE VOLTAGE TRACE

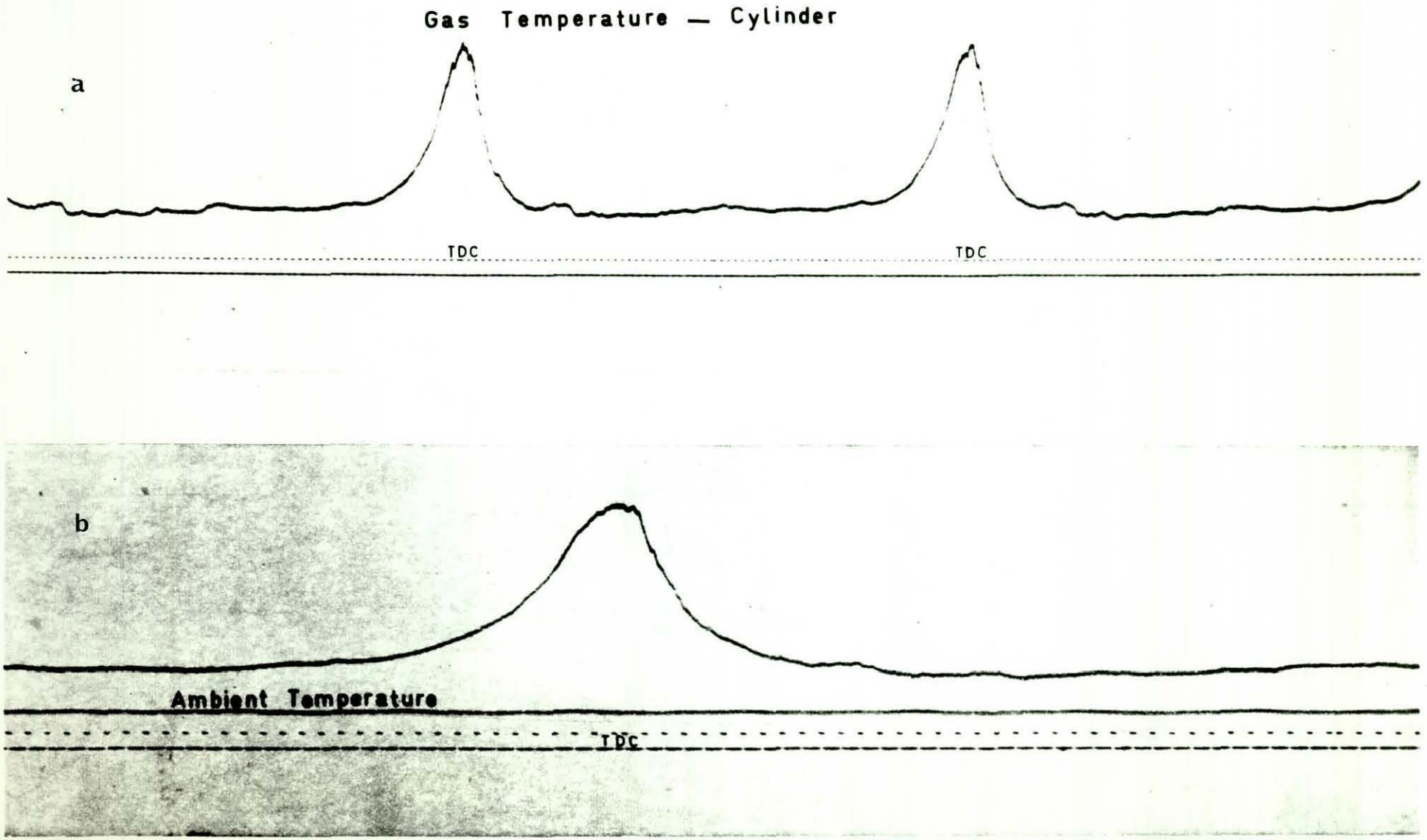

FIG. 4.10 GAS TEMPERATURE TRACE

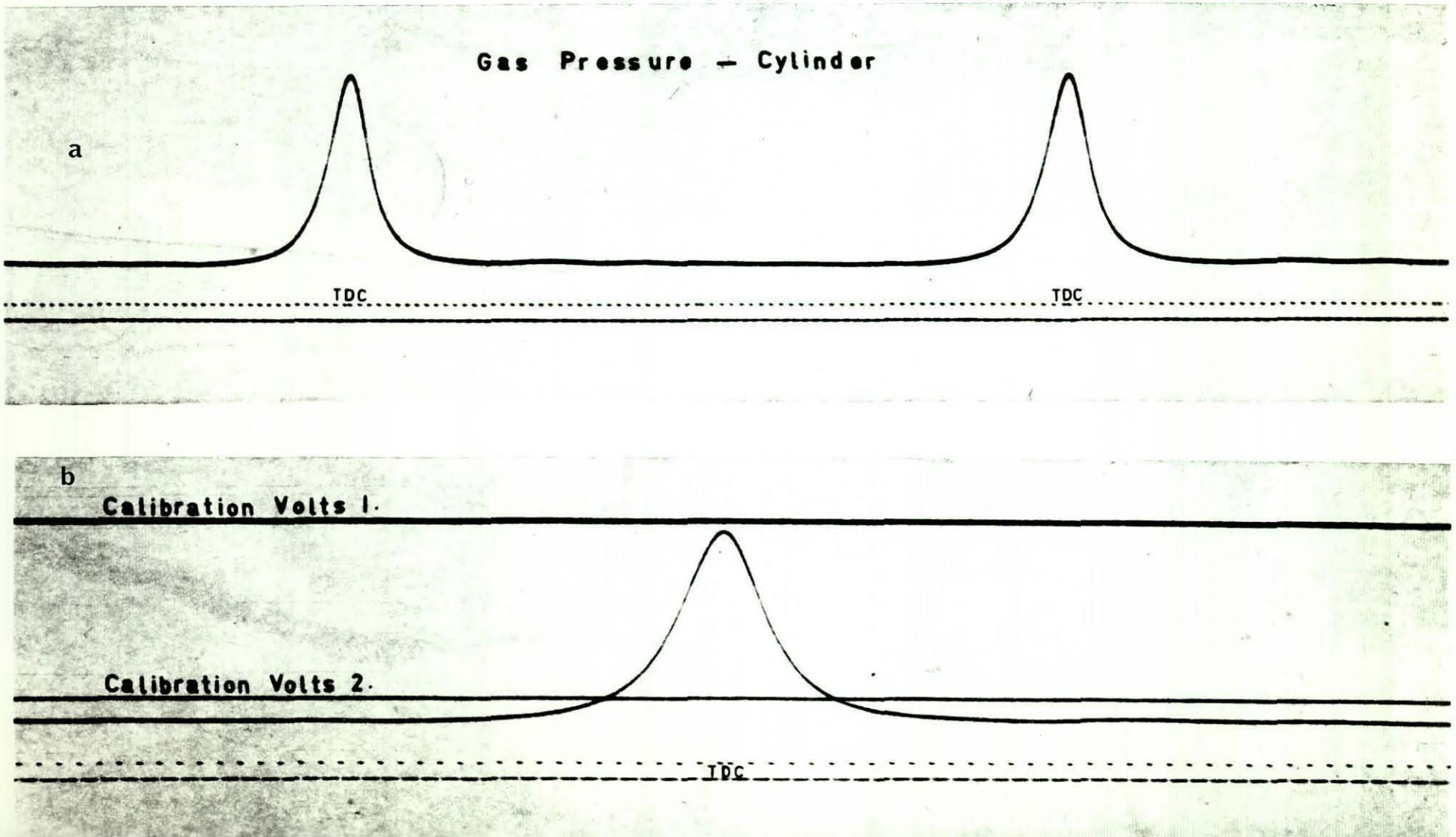

FIG. 4.11 GAS PRESSURE TRACE

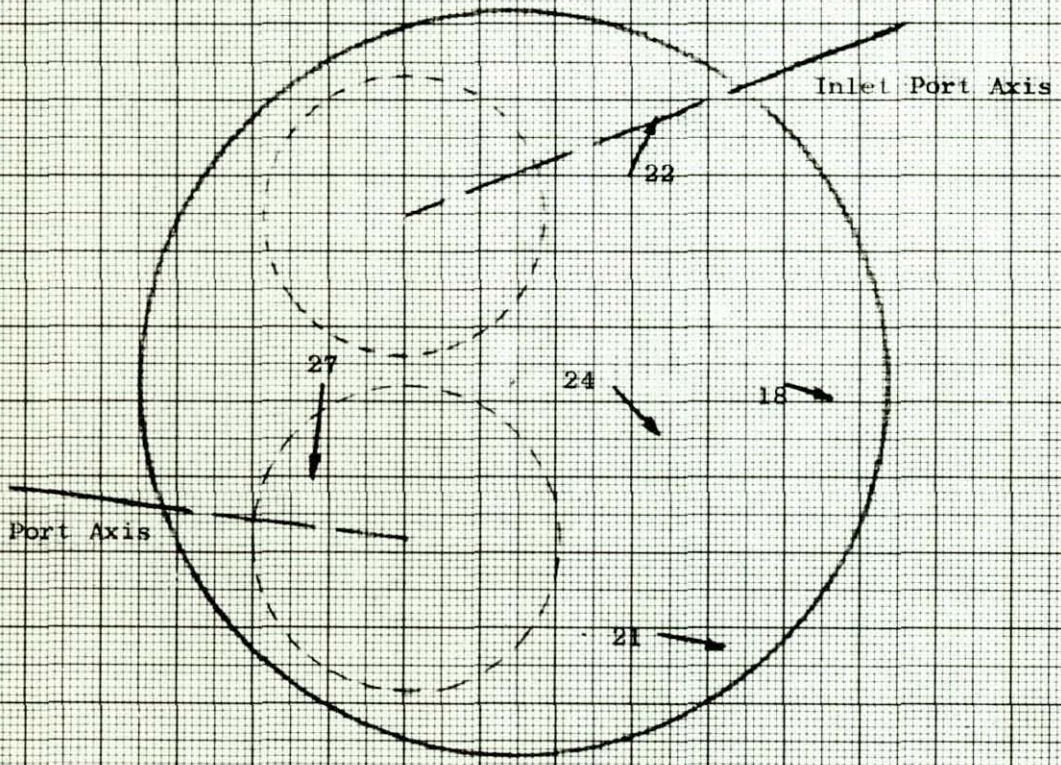

Crank Angle 20 degrees

Scale 1 cm = 10 m/s

FIG. 4.12 VELOCITY RESULTS AT 500 R.P.M.

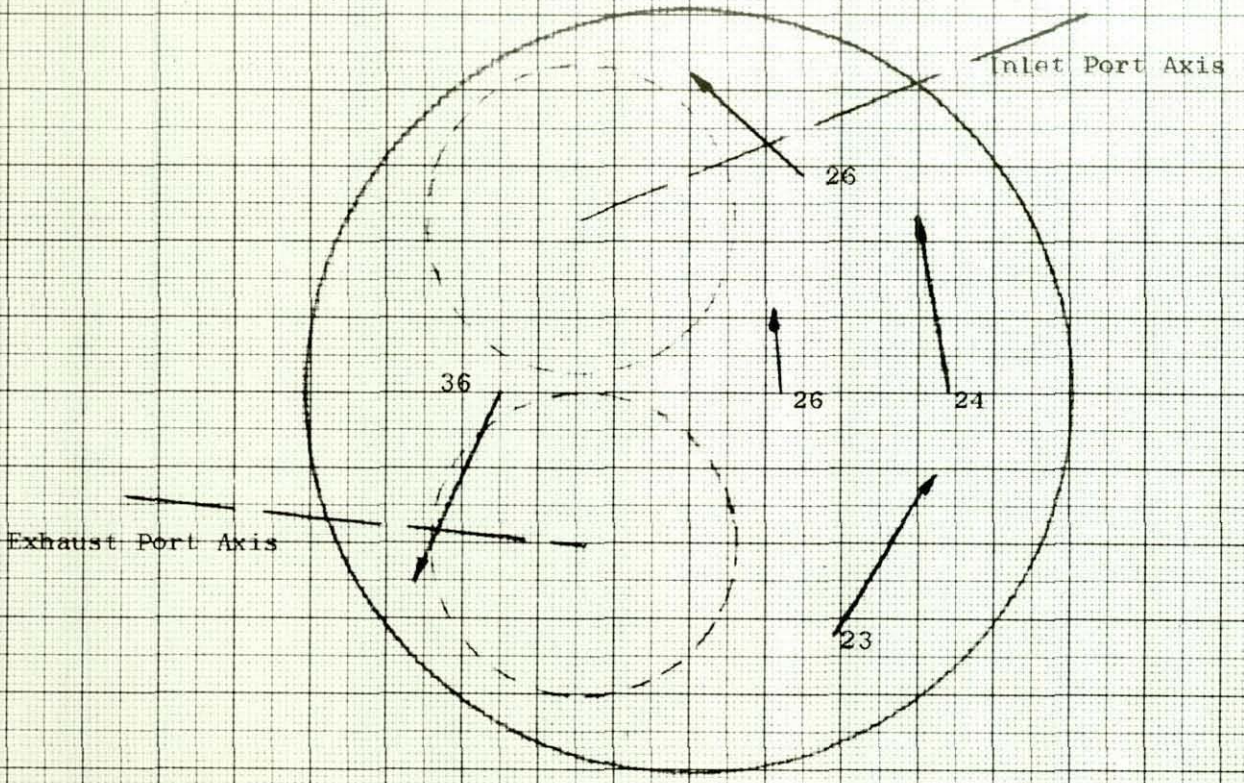

Crank Angle 90 degrees

Scale 1 cm = 10 m/s

FIG. 4.13 VELOCITY RESULTS AT 500 R.P.M.

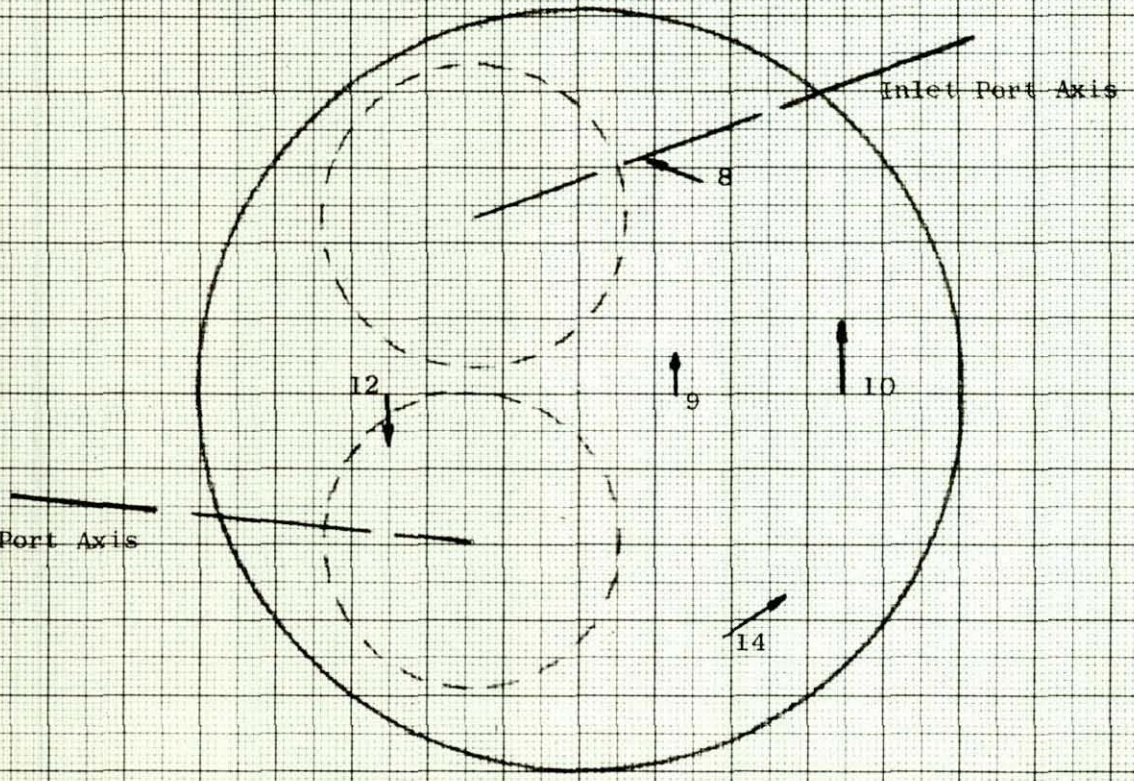

Crank Angle 180 degrees

Scale 1 cm = 10 m/s

FIG. 4.14 VELOCITY RESULTS AT 500 R.P.M.

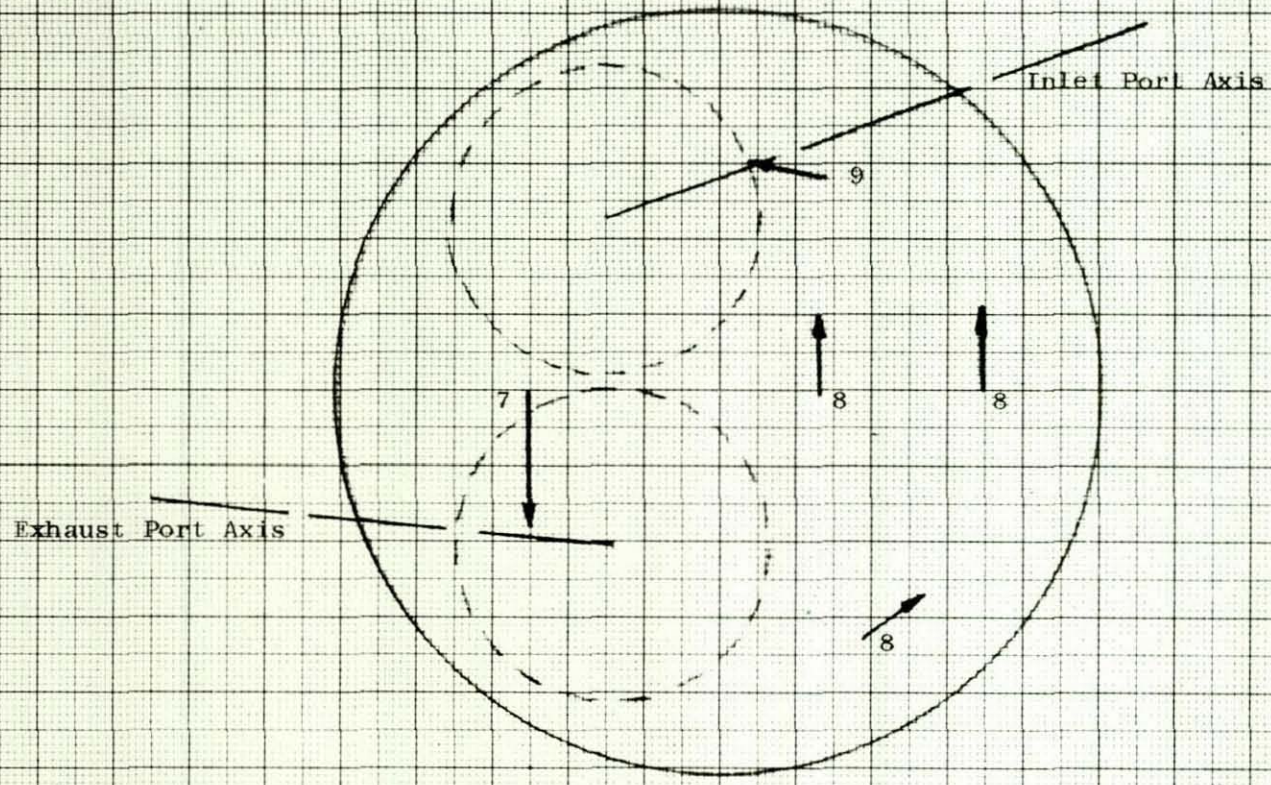

Crank Angle 340 degrees

Scale 1 cm = 10 m/s

FIG. 4.15 VELOCITY RESULTS AT 500 R.P.M.

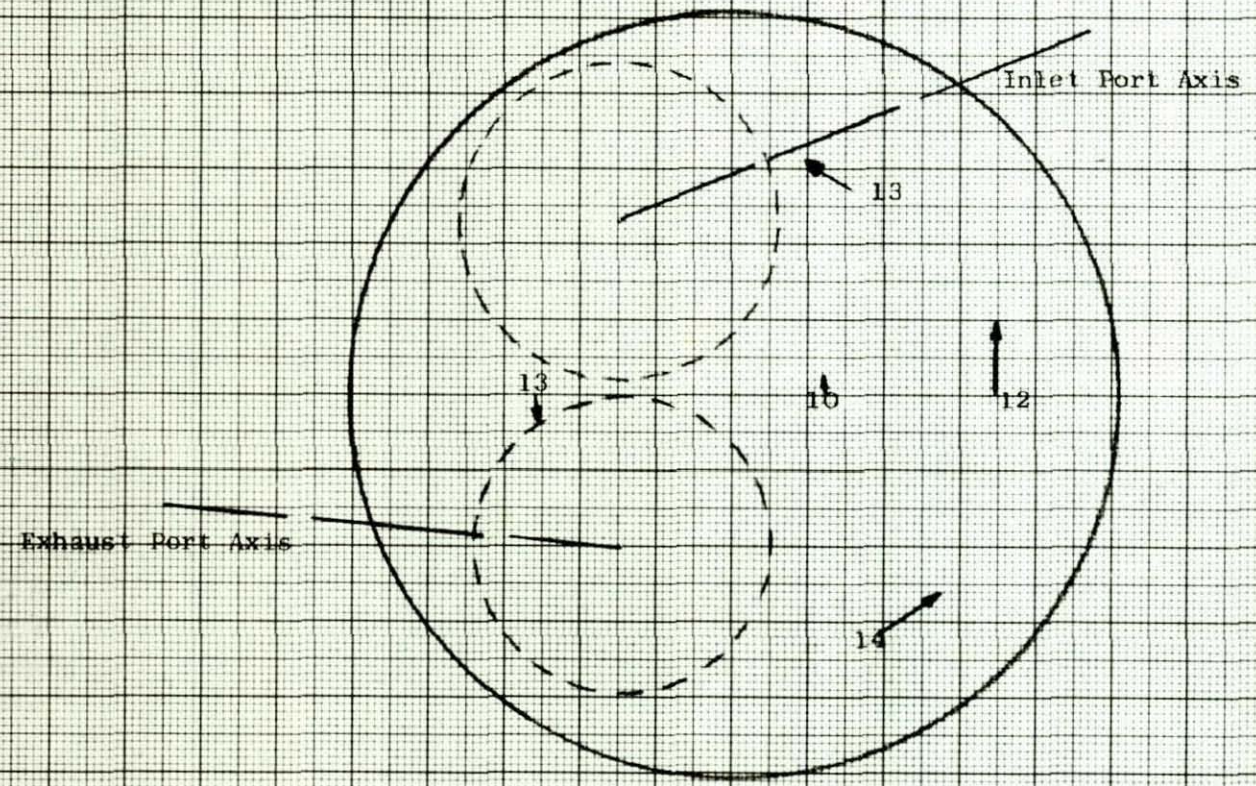

Crank Angle 450 degrees

Scale 1 cm = 10 m/s

FIG 4.16 VELOCITY RESULTS AT 500 R.P.M.

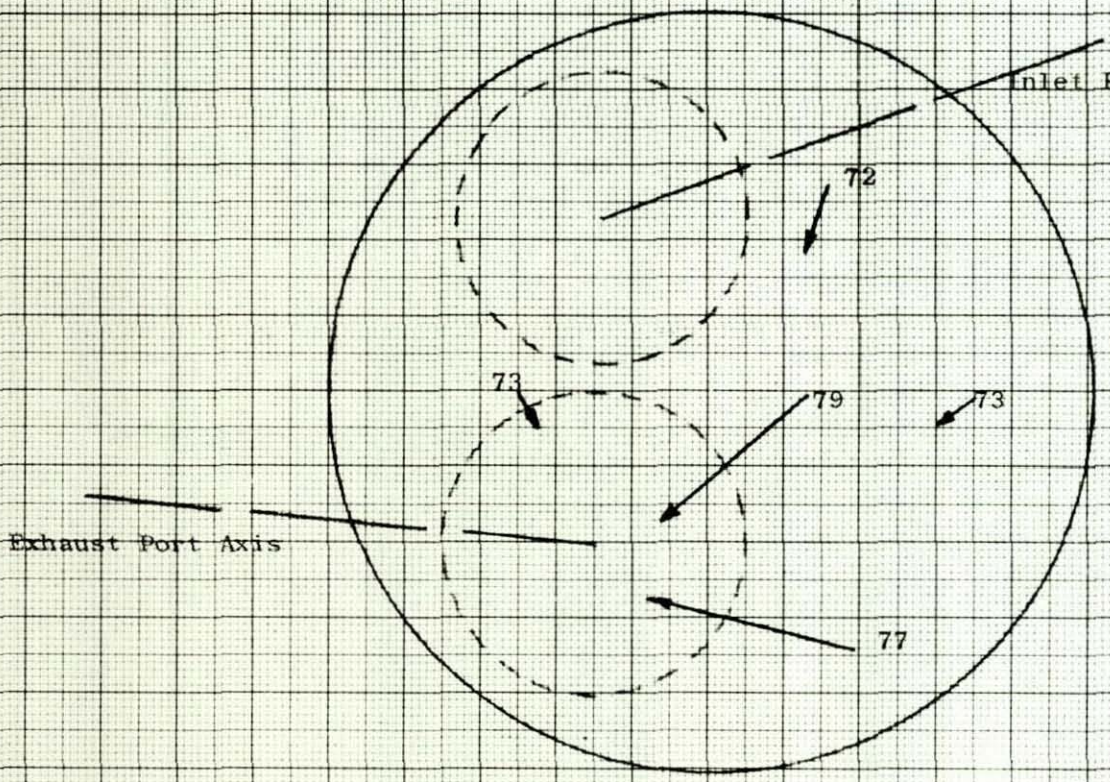

Crank Angle 540 degrees

Scale 1 cm = 10 m/s

FIG. 4.17 VELOCITY RESULTS AT 500 R.P.M.

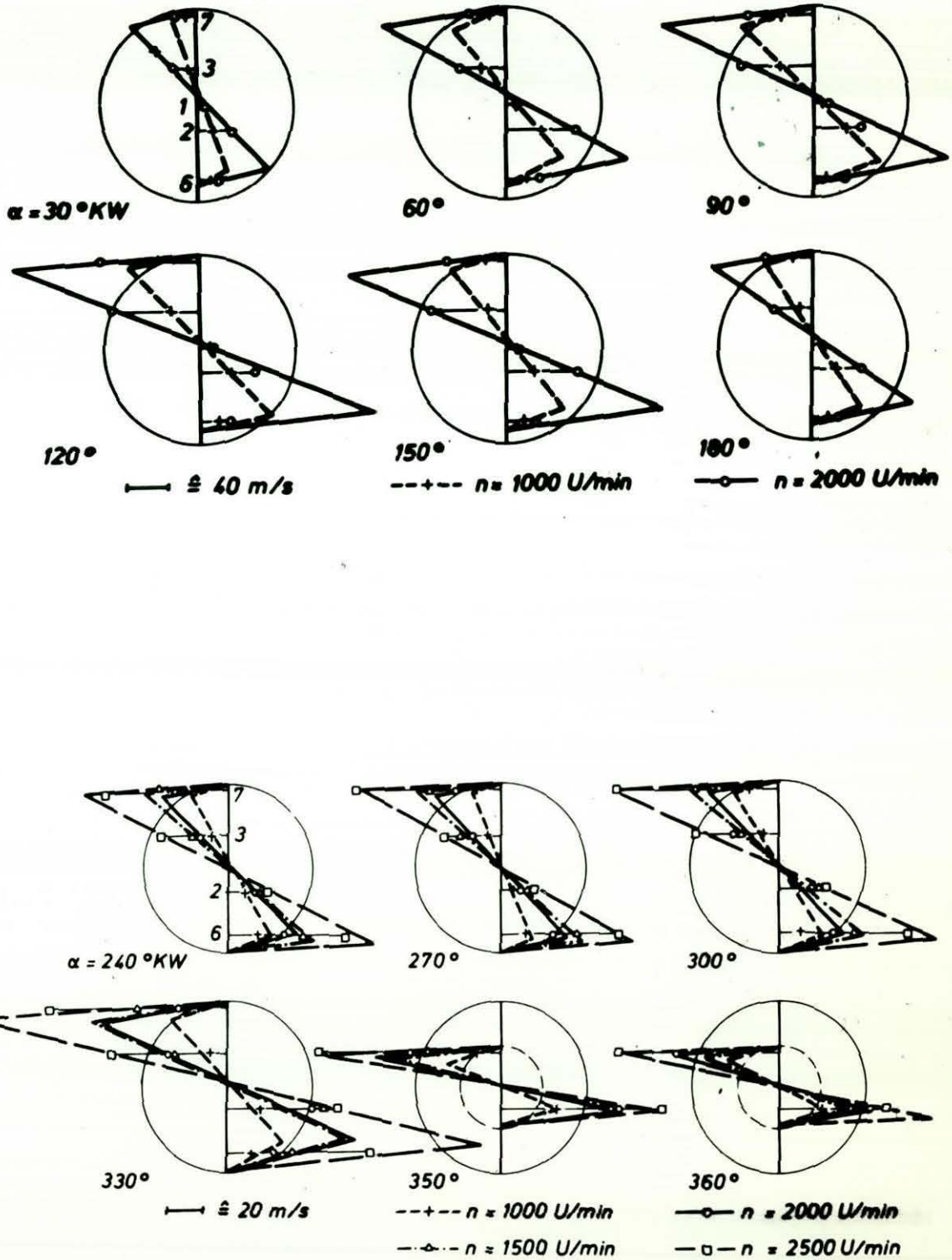

FIG. 4.18 HORVATIN'S (31) RESULTS FOR SWIRL

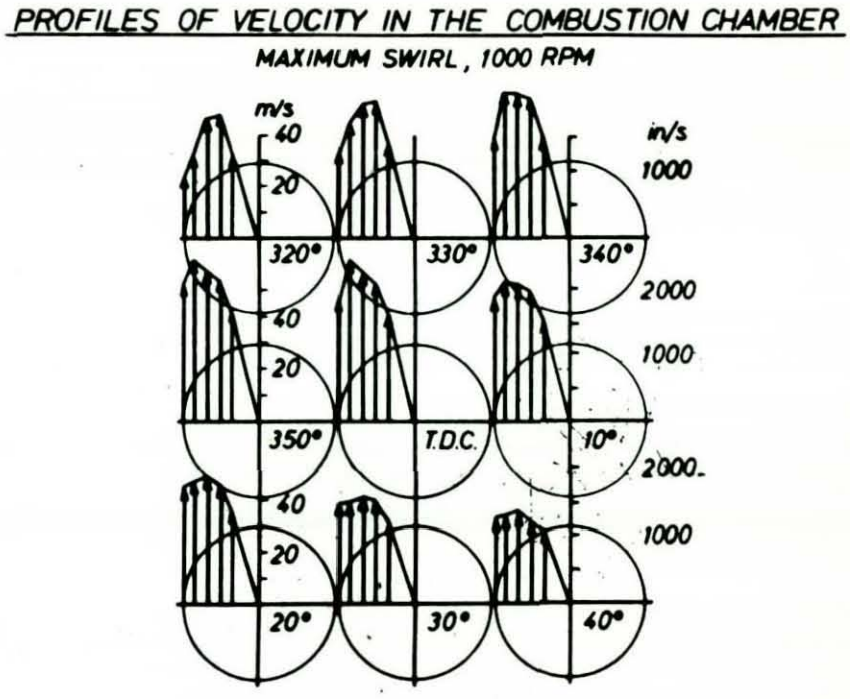

FIG. 4.19 STOCK'S (32) RESULTS FOR SWIRL

5.0 A MATHEMATICAL MODEL FOR THE PREDICTION OF AIR MOTION WITHIN AN ENGINE CYLINDER

5.0 A MATHEMATICAL MODEL FOR THE PREDICTION OF AIR MOTION WITHIN AN ENGINE CYLINDER

5.1 Introduction to the Mathematical Model

Following from conclusion (vi), Section 4.6, it was proposed that a mathematical model could be developed which would predict the air motion within the engine cylinder. The initial results, refer Figs. 4.12 - 4.17, suggest that after approximately 90 degrees crank angle during the induction period, an orderly swirl is developed and this continues to exist throughout the compression period. Similar results were found by Horvatin and Hussmann (11), Horvatin (31) and Stock (32) whose experimental results are illustrated in Figs. 2.15, 4.18 and 4.19 respectively. In order to predict the velocity at any particular location within the cylinder, it was anticipated that a forced vortex velocity profile would be a representative description of the air motion within the cylinder and this was supported by the initial experimental evidence of the present investigation, refer Figs. 4.12 to 4.17. Both Horvatin and Hussmann (11) and Horvatin (31) using a similar combustion chamber geometry, refer Fig. 2.14, support this assumption and the experimental work of Stock (32), which was performed on an engine having a combustion chamber similar to that used by Alcock (1) illustrated in Fig. 2.3, also suggests that the forced vortex profile is a good representation for the air motion within the engine cylinder. In order to develop the model using the basic information regarding the cylinder and engine geometry, it was concluded that the basic assumption proposed by Fitzgeorge and Allison (9) would be adopted; that is, the incoming momentum through the inlet port would be equal to the momentum conserved within the engine cylinder. During the compression period, the assumption of

conservation of angular momentum could be used, although it would be necessary to account for the friction loss occurring between the air and the cylinder surfaces, particularly when the surface to volume ratio for the cylinder increases during the latter part of the compression period. Dicksee (8), Alcock and Scott (10) and Horvatin and Hussmann (11) have all suggested that frictional forces might be considerable during the latter part of the compression period. Hence a mathematical model is proposed in Section 5.2 which computes the angular velocity throughout the induction period assuming momentum to be conserved, whilst Section 5.3 considers the entire compression period and the angular velocity is computed assuming that the angular momentum is conserved, whilst the effects due to friction caused by the cylinder wall, the piston crown and cylinder head are accounted for. A method of solution of the relevant equations for the angular velocity throughout the induction and compression periods is given in tabular form in Section 5.4. Section 5.5 outlines the necessary experimental work undertaken to support the mathematical model. A thorough discussion is made of the mathematical model in Section 5.6 and comparison is made between the angular velocity computed using the model and those measured experimentally using the hot wire anemometers at an engine speed of 1000 r.p.m. Finally, in Section 5.7, an analysis is made of the theoretical squish equation proposed by Fitzgeorge and Allison (9) and comparison is made between this computation and experimental work performed at the edge of the combustion chamber again at an engine speed of 1000 r.p.m.

5.2 Analysis of the Swirl during the Induction Period

The induction period may be regarded as the charging of a container from a reservoir where the conditions inside the cylinder are assumed uniform at any time and the reservoir and cylinder are filled with the same gas. The instantaneous mass flow, pressure and induced mass of air into the cylinder during the induction period may be computed on an energy transfer basis with the assumption of a reversible adiabatic process. The basic relationship is that the rate of entry of energy into the cylinder with the ingoing air is equal to the rate of increase of internal energy, plus the rate at which work is done on the piston (assuming work done on the system to be positive).

Therefore,

$$\begin{matrix}\text{Energy inflow/second} \\ \text{through inlet port}\end{matrix} = \begin{matrix}\text{Work done/second} \\ \text{on piston}\end{matrix} + \begin{matrix}\text{Increase in internal} \\ \text{energy in cylinder}\end{matrix} \qquad \text{——— 5.1}$$

At any time, the internal energy in the cylinder is $\frac{\dot{P}\dot{V}}{k-1}$, assuming a zero datum for the internal energy at the temperature $T = 0^{o}K$ and the rate of increase of internal energy is $\frac{1}{k-1}\left[\frac{\dot{P}\,dV}{dt} + \frac{\dot{V}\,dP}{dt}\right]$

The rate of work done on the piston is $P\frac{dV}{dt}$ and finally the rate of energy (enthalpy) inflow is $\frac{dm}{dt}\ C_pT$. Hence

$$\frac{dm}{dt}\,CpT = P\,\frac{dV}{dt} + \frac{1}{(k-1)}\left[P\,\frac{dV}{dt} + V\,\frac{dP}{dt}\right] \qquad \text{——— 5.2}$$

Equation 5.2 may be solved by expressing it in finite difference form with a sufficiently small time step Δ t over which the pressure and volume maintain some representative value, i.e.

$$\frac{\Delta m}{\Delta t} CpT = P \frac{\Delta V}{\Delta t} + \frac{1}{(k-1)} \left[P \frac{\Delta V}{\Delta t} + V \frac{\Delta P}{\Delta t} \right] \qquad \text{——— 5.3}$$

Rearranging equation 5.3 gives

$$P_{n+1} = P_n + \frac{(k-1)\, \dot{m}\, Cp\, T \Delta t}{V_n} + \frac{k\, P_n (V_{n+1} - V_n)}{V_n} \qquad \text{——— 5.4}$$

where n refers to the step under consideration and $\dot{m}$ is the mass flow rate into the cylinder and is equal to $\frac{\Delta m}{\Delta t}$.

The mass flow rate into the cylinder may be computed by treating the inlet port as an orifice and applying the reversible isentropic compressible flow equation, refer Houghton and Brock (38), whilst a suitable correction is made for friction through the inlet port, refer Section 5.6.2 for justification, i.e.

$$\dot{m} = A^* \left[\frac{P_n}{P_o} \right]^{\frac{1}{k}} \left[\left(\frac{2k}{k-1} \right) P_o \rho_o \left[1 - \left(\frac{P_n}{P_o} \right)^{\frac{k-1}{k}} \right] \right]^{\frac{1}{2}} \qquad \text{——— 5.5}$$

where O refers to atmospheric conditions and A^* is the effective area of the inlet port when friction is accounted for.

5.2.1 Momentum Considerations for the Induction Period

During the induction period of an engine, the mass flow, valve opening and consequently the swirl velocity vary from instant to instant. Assuming that momentum is conserved in the engine

cylinder, then the rate of change in angular momentum in the cylinder may be equated to the moment of momentum entering through the inlet port, i.e.

$$\frac{\Delta (I w)}{\Delta t} = \dot{m}\, r\, U \cos \phi \cos \psi \qquad \text{——————} \quad 5.6$$

where r is the distance of the inlet valve centre from the cylinder axis and U is the velocity of the air associated with the instantaneous mass flow rate $\dot{m}$ through the inlet port. ϕ is the angle between the cylinder head and the inlet port axis, refer Section 2.1 and Fig. 2.1 where the component $U\cos\phi$ is discussed in detail (the angle ϕ equals 30 degrees) and ψ is the angle formed between the inlet port axis and the line joining the cylinder axis to the inlet valve axis (the angle ψ equals 90 degrees for the cylinder head considered).

Now considering the mass flow rate to be a dependant variable as outlined in Section 5.2, then

$$\dot{m} = \rho_n U A^* \qquad \text{——————} \quad 5.7$$

and substitution for U into equation 5.6 gives

$$\frac{\Delta (Iw)}{\Delta t} = \frac{\dot{m}^2 r \cos \phi \cos \psi}{\rho_n A^*} \qquad \text{——————} \quad 5.8$$

Now the density inside the cylinder may be expressed by

$$\rho_n = \rho_o \left(\frac{p_n}{p_o}\right)^{\frac{1}{k}} \qquad \text{——————} \quad 5.9$$

where n and o refer to the cylinder and atmospheric conditions respectively.

Hence, the total angular momentum at time t may be found by integrating both sides of equation 5.8 and substituting for ρ_n i.e.

$$I\, w_{(t)} = \int_o^t \frac{\dot{m}^2\, r \cos\phi \cos\not{\phi}}{A^* \rho_o} \left(\frac{P_o}{P_n}\right)^{\frac{1}{k}} dt \qquad \text{——— 5.10}$$

where the upper limit t in equation 5.10 refers to the instantaneous time or crank angle position during the induction period (noting that $dt = d\theta/6N$ where N is the engine r.p.m.).

If now the air in the cylinder is regarded as two coaxial cylinders attached but located one above the other, the lower one of diameter d and volume V_b being the combustion chamber and the upper one of diameter D representing the cylinder, it will be noted that at the top dead centre position, the lower cylinder contains practically all the charge and the upper one having almost negligible capacity. At the bottom dead centre position however, the upper cylinder has its maximum capacity and the lower cylinder a small capacity by comparison. The effective diameter of the induced mass therefore varies with piston displacement.

For the assumption of a forced vortex velocity profile, wr = constant, where w is the angular velocity and r is the radius at a particular location. Hence, it may be shown, refer Appendix 5A, that the angular momentum of the total induced mass m_t at any instant is given by

$$I = \frac{m_t}{2}\left[\frac{\frac{\pi D^4 S(\theta)}{16 V_b} + \frac{d^2}{4}}{\frac{\pi D^2 S(\theta)}{4 V_b} + 1}\right] \qquad \text{——— 5.11}$$

Hence, using equations 5.10 and 5.11 and noting that the trapped mass m_t will vary throughout the induction period, the angular velocity may be computed at any instant of time throughout the induction period and details of this computation are given in Section 5.4.

5.3 Analysis of Swirl during the Compression Period

Having determined the angular velocity throughout the induction period using the assumption of conservation of angular momentum outlined in Section 5.2, it is reasonable to assume that the angular velocity throughout the compression period may be determined using the same assumption. However, it was mentioned in Section 5.1 that, in order to develop a more representative equation for the compression period, during which the surface to volume ratio increases as top dead centre is approached, the effects of friction between the air and the containing surfaces would have to be considered. Hence an investigation was made of the effects due to friction caused by

(i) the cylinder wall

(ii) the cylinder head and piston crown

(i) and (ii) were isolated from each other and investigated in detail in Section 5.3.1 and 5.3.2 and Section 5.3.3 then investigates the combined effect due to (i) and (ii) where a representative equation for the angular velocity throughout the compression period is derived. Finally, Section 5.3.4 considers the case where friction is neglected and a simplified equation is derived for the angular velocity throughout the compression period.

5.3.1 Frictional Effects caused by the Cylinder Wall

In order to compute the frictional effects due to the cylinder wall, it is necessary to consider the forces exerted on the cylinder wall and equate these to the change of angular momentum of the rotating mass inside the cylinder, i.e

$$\text{Momentum Change of the rotating fluid} = -\sum \text{of the restraining torque present} \qquad \text{——— 5.15}$$

Assuming that a forced vortex flow pattern exists and that the viscosity effects in the fluid bulk are negligible, then it may be shown that the shear torque exerted at the wall, on the rotating fluid at any crank angle position θ is given by,

$$-\frac{D}{2}\ \Pi\ D\ S(\theta)\ \tau \qquad \text{——— 5.16}$$

where D is the cylinder diameter,

$S(\theta)$ is the displacement of the piston crown from the top dead centre position at crank angle θ

τ is the frictional force per unit area acting on the cylinder wall.

It may also be shown that, by substituting $U = wD/2$, where U is the tangential velocity and w is the angular velocity,

$$\tau = \frac{C_f\ \rho\ w^2\ D^2}{8} \qquad \text{——— 5.17}$$

where C_f the skin friction factor may be approximated to that of a

flat plate where the characteristic length in the Reynolds Number is equal to the circumference of the cylinder πD,

i.e. $$C_f = 0.067\ Re^{-0.2} \qquad \text{——— 5.18}$$

where $Re = \rho w D^2/\mu$, and ρ and μ are the density and viscosity of the air respectively.

Substitution for τ into equation 5.16 gives,

$$\frac{-\ 0.067\ \pi\ D^{3.6}\ \rho^{0.8}\ \mu^{0.2}\ S(\theta)\ w^{1.8}}{16} \qquad \text{——— 5.19}$$

5.3.2 Frictional Effects caused by the Piston Crown and Cylinder Head

In order to compute the frictional effects caused by the cylinder head and piston crown, suppose the cylinder head and piston crown are approximated by two flat discs of diameter D and consider the torque force acting at the mean cylinder radius D/4, which may be equated to the incremental angular momentum change of the rotating mass inside the engine cylinder, refer equation 5.15, Section 5.3.1. Assuming that a forced vortex flow pattern exists, it may be shown that, for the two surfaces considered, the restraining torque due to the shear stress is

$$-\ \frac{D}{4}\ .\ 2\ \tau\ \text{Area} \qquad \text{——— 5.20}$$

Substitution for τ and noting that the expression for C_f for a flat disc with mean radius D/4 results in the expression

$$C_f = 0.088\ Re^{-0.2} \qquad \text{——— 5.21}$$

where $Re = \rho w D^2/\mu$ and the characteristic length is $\Pi D/2$.

Hence, the following equation may be derived from equations 5.20 and 5.21

$$\frac{-0.088\ \Pi\ D^{4.6}\ \rho^{0.8}\ \mu^{0.2}\ w^{1.8}}{256} \qquad \text{——— 5.22}$$

5.3.3 Computation of the Angular Velocity throughout the Compression Period assuming Friction is Present

Following from Sections 5.3.1 and 5.3.2 where the frictional effects due to the cylinder wall and cylinder head and piston crown were considered separately, it is now possible to combine 5.19 and 5.22 and derive a representative equation for the angular velocity throughout the compression period which accounts for friction caused by both the cylinder wall and the cylinder head and piston crown, and noting that the rate of change of angular momentum of the rotating fluid mass is $\frac{\Delta(Iw)}{\Delta t}$ then,

$$\frac{\Delta(Iw)}{\Delta t} = -\frac{\Pi\ D^{3.6}\ \rho^{0.8}\ \mu^{0.2}\ w^{1.8}}{16}\left[0.067\ S(\theta) + \frac{0.088\ D}{16}\right] \qquad \text{——— 5.23}$$

which may be expressed as,

$$I\frac{\Delta w}{\Delta t} + w\ \frac{\Delta I}{\Delta t} = -\frac{\Pi\ D^{3.6}\ \rho^{0.8}\ \mu^{0.2}\ w^{1.8}}{16}\left[0.067\ S(\theta) + \frac{0.088\ D}{16}\right]$$

——— 5.24

Equation 5.24 may now be solved by expressing it in finite difference form and noting that the suffix n refers to the next step in the engine cycle and suffix p refers to the previous step in the engine cycle, whilst the mean value of I and w are computed for the step under consideration. Hence we have,

$$\frac{(Ip + In)}{2}\left(\frac{wn - wp}{\Delta t}\right) + \left(\frac{wp + wn}{2}\right)\left(\frac{In - Ip}{\Delta t}\right) = -A\left(\frac{wp + wn}{2}\right)^{1.8} \qquad \text{5.25}$$

where $$A = \frac{\Pi D^{3.6} \rho^{0.8} \mu^{0.2}}{16}\left[0.067\, S(\theta) + \frac{0.088\, D}{16}\right]$$

Simple algebra reduces equation 5.25 to the following

$$In\ wn - Ip\ wp = -A\left(\frac{wp + wn}{2}\right)^{1.8} \Delta t \qquad \text{5.26}$$

and this may be solved for each crank angle position throughout the compression period and hence the angular velocity may be computed throughout the compression period with the frictional effects of the containing surfaces accounted for. Actual computational details are discussed in Section 5.4

5.3.4 Computation of the Angular Velocity throughout the Compression Period Neglecting the Effects of Friction

Suppose, however, that friction were neglected from the analysis of the angular velocity throughout the compression period, then the forces present acting at all surfaces, refer equation 5.23,

would be zero and hence the rate of change in angular momentum of the cylinder contents would be zero, i.e.

$$\frac{\Delta(Iw)}{\Delta t} = 0 \qquad \text{——————} \quad 5.27$$

Therefore, $I\,w = \text{constant}$

Hence $$I_{ivc}\ w_{ivc} = I_{\theta}\ w_{\theta} \qquad \text{——————} \quad 5.28$$

where the subscripts ivc and θ refer to the position of inlet valve closure and any crank angle θ throughout the compression period respectively. Hence, we may derive the simplified expression,

$$w_{\theta} = w_{ivc}\ \frac{I_{ivc}}{I_{\theta}} \qquad \text{——————} \quad 5.29$$

which may be used to obtain the angular velocity throughout the compression period, neglecting the effects of friction.

5.4 Solution of the Mathematical Model

In order to compute the angular velocity throughout the induction and compression periods, two computer programs were written in Fortran IV. The program listings are included in Appendix 5C along with a description of the input and output data parameters whilst a comprehensive flow chart may be found in Table 1 at the end of Section 5.0.

5.4.1 Induction Period

The first program N250 computes the angular velocity throughout the induction period and a tabular solution is outlined below.

1. Read in the engine data parameters associated with the effective inlet valve area A^* which are

COEF1, COEF2, COEF3	The coefficients obtained from a least squares fit performed on the curve of effective inlet valve area plotted against the ratio vlave lift/valve diameter and illustrated in Fig. 5.3.
DTH	Inlet valve rise and fall period (^{o})
Z	Maximum inlet valve lift (m)

2. Read in the engine data parameters which are,

S	Engine stroke (m)
G	Connecting rod length (m)
DC	Cylinder diameter (m)
DB	Combustion chamber diameter (m)
T	Ratio of the specific heats (-)
BVOL	Volume of the combustion chamber (m^3)
VRAD	Inlet valve radius (m)
AREAPORT	Area of the inlet port (m^2)

3. Read in the constants associated with the air in the inlet manifold which are,

CP	Specific heat of air at ambient temperature (J/kg^oC)
TO	Ambient temperature of the air (^oC)
PO	Ambient pressure of the air (N/m^2)
RHO	Density of the air at ambient temperature & pressure (kg/m^3
VCL	Clearance volume, comprising the combustion chamber and bump clearance volume (m^3)
ER1	Percentage error allowed in the Wegstein Iteration Procedur (-)
VA	Angle between the inlet port axis and the cylinder head (^{o}
DV	Diameter of the inlet valve (m)

4. Read in the final induction parameters which are

RPM	Engine speed (r.p.m.)
PCYl	Initial cylinder pressure assumed to be 101000N/m^2
FLOTO	Initial trapped mass inside the cylinder and computed to be .000053 kg from the clearance volume and initial density assuming atmospheric conditions.

5. Compute the cylinder parameters for the crank angle position considered, i.e. piston displacement from the top dead centre position, cylinder volume, inlet valve lift and effective inlet valve area. It is important to mention that in order to simulate the inlet valve timing, measurements were made of the actual timing (which was found to be 15 BTDC to 25 ATDC) and the inlet valve opening approximated by a sine wave beginning at top dead centre and extending over a period of 95 degrees crank angle. The inlet valve closure was simulated by a cosine wave, however the period of closure extended over 110 degrees crank angle.

6. Solution of equation 5.5, i.e.

$$\dot{m} = A^* \left[\frac{p_n}{p_o}\right]^{\frac{1}{k}} \left[\left(\frac{2k}{k-1}\right) p_o \rho_o \left[\left(1 - \left(\frac{p_n}{p_o}\right)\right]^{\frac{k-1}{k}}\right]^{\frac{1}{2}}$$

using the data computed from step 5 at the particular crank angle considered, (where p_n was assumed to be 101000 N/m^2 at the beginning of the computation).

7. Solution of equation 5.4, i.e.

$$p_{n+1} = p_n + \frac{(k-1)\,\dot{m}\,C_p\,T\,\Delta t}{V_n} + \frac{k\,p_n\,(V_{n+1} - V_n)}{V_n}$$

assuming a step length of one degree crank angle and noting that $\Delta t = \Delta\theta/6N$, where N is the engine r.p.m.

It should be mentioned that, during the initial stages of the induction period (approximately the first 10 degrees), the solution of equations 5.4 and 5.5 become unstable and therefore, even with a small step length of one degree crank angle, it was found necessary to introduce the Wegstein (39) Iteration procedure. This iteration permitted a computation to be made of the mass flow rate $\dot{m}$ using equation 5.5 and then the pressure was computed at step $n + 1$ using equation 5.4. A second estimation of the mass flow rate was then made at the same crank angle position using the latest value of cylinder pressure (P_{n+1}) computed from equation 5.4 and substituting this value for the cylinder pressure (P_n) in equation 5.5. Hence a further computation of the cylinder pressure (P_{n+1}) was made from equation 5.4 using the latest computation for the mass flow rate. Providing that the difference between these pressure computations was less than 0.0001, the computation of mass flow rate and pressure was assumed successful and the procedure continued to the next crank angle position. If, however, the difference between the computed pressures was greater than 0.0001, then the iteration procedure continued until such time that the specified condition was satisfied. The program then continued to the next crank angle position.

8. Having computed the instantaneous mass flow rate and pressure at each individual crank angle position throughout the induction period, the rate of change of angular momentum of the entering air was computed using equation 5.8, i.e.

$$\frac{\Delta (Iw)}{\Delta t} = \frac{\dot{m}^2 r \cos \phi \cos \psi}{\rho_n A^*}$$

and finally the angular velocity at each crank angle position throughout the induction period computed using equation 5.10, i.e.

$$I w_t = \int_0^t \frac{\dot{m}^2 r \cos \phi \cos \psi}{A^* \rho_o} \left(\frac{p_o}{p_n}\right)^{\frac{1}{k}} dt$$

The angular velocity may therefore be computed throughout the induction period.

5.4.2 Compression Period

The second program N260 computes the angular velocity throughout the compression period and assumes that the angular momentum is conserved whilst friction is accounted for between the air and the containing surfaces. In tabular form, the solution is as follows:-

1. Read in the pressure and temperature data at every 10 degrees crank angle throughout the compression period.

2. Read in the engine data parameters which are:

B	Connecting rod length (m)
S	Engine stroke (m)
VIS	Viscosity of air at ambient temperature ($gm/cm\ s^{\wedge}$)
DC	Cylinder diameter (m)
DB	Combustion chamber diameter (m)
BVOL	Volume of combustion chamber (m^3)
RPM	Engine speed (r.p.m.)
ASST	Mass trapped at the end of the induction period (kg)
WP	Angular velocity at the end of the induction period (r.p.m.)

3. Compute the pressure and temperature data at each individual crank angle position throughout the compression period assuming that the pressure and temperature vary linearly over the ten degree crank angle step. This latter assumption was justified since both the temperature and pressure traces (typical results illustrated in Figs. 4.10 and 4.11 respectively) were exceptionally clear and free from any electrical noise. Consequently, the ordinates could be accurately measured at ten degree intervals without difficulty.

4. Compute the moment of inertia at the point of inlet valve closure using equation 5.11, i.e.

$$I = \frac{m_t}{2}\left[\frac{\frac{\Pi D^4 S(\theta)}{16 V_b} + \frac{d^2}{4}}{\frac{\Pi D^2 S(\theta)}{4 V_b} + 1}\right]$$

and call this Ip.

5. Compute the moment of inertia at the next crank angle position using equation 5.11, but noting that $S(\theta)$ will have changed as the piston travels up the cylinder, and call this In

6. The angular velocity wn may now be computed at the particular crank angle position considered using equation 5.26, i.e.

$$In\ wn - Ip\ wp = -A\left(\frac{wp + wn}{2}\right)^{1.8}\Delta t$$

where $$A = \frac{\Pi D^{3.6} \rho^{0.8} \mu^{0.2}}{16}\left[0.067\ S(\theta) + \frac{0.088\ D}{16}\right]$$

It should be mentioned that equation 5.26 may be solved using an IBM iteration subroutine (41) which may be obtained from the ICL computing facilities at Loughborough University of Technology.

7. Transfer to the next crank angle position so that Ip = In and wp = wn and the computation continues from step 5 above for the next crank angle position during the compression period.

8. In order to compute the angular velocity neglecting friction, the modified form of equation 5.26 may be used, i.e.

$$In\ wn - Ip\ wp = 0$$

and hence the angular velocity computed throughout the compression period assuming friction is neglected.

5.4.3 Solution of the Angular Velocity throughout the Induction and Compression Periods

From the tabular solution outlined above, it may be observed how the relevant equations are adopted for the computation of angular velocity during both the induction and compression periods. However, further information regarding the computation of the angular velocity is provided in Table 1 in the form of a flow diagram and the program listings are included in Appendix 5C.

5.5 Experimental Justification of the Mathematical Model

5.5.1 Inlet Port Velocity Measurement

During the development of the mathematical model, it was considered necessary to measure the instantaneous air velocity in the inlet port at the junction between the inlet manifold and the cylinder head and compare this with the value at that same section obtained from the theoretical mass flow rate through the inlet port using equation 5.5. A hot wire anemometer system was adopted similar to that outlined in section 4.0, but here a one dimensional flow was anticipated and consequently only a single wire probe was used. A representative value of the inlet velocity was determined by measuring the velocity at several locations in the measuring section and the mean of the results computed and illustrated in Fig. 5.4 where comparison is made between the theoretical and experimental velocities through the inlet port and further discussion is presented in section 5.6.1. A typical example of the bridge voltage signal is illustrated in Fig. 5.1, where trace a illustrates good repeatability of the signal obtained when

the probe was rotated about its own axis and a maximum signal obtained with the probe sensing wire perpendicular to the flow. Measurements of the temperature and pressure of the air were also recorded at the measuring section of the inlet port but these measurements were found to be very similar to that of ambient temperature and pressure and therefore further measurements of temperature and pressure were neglected.

5.5.2 Cylinder Head and Inlet Port Suction Tests

In order to make an accurate estimation of the effective inlet port area A^* which is a major parameter in the solution of equations 5.5 and 5.10, a series of suction tests were performed using the Disa Wind Tunnel, refer Fig. 3.5. The tunnel had to be modified in order to accommodate the cylinder head, however the inlet diameter of the tunnel was approximately 7.5 cm. in diameter whilst the engine cylinder diameter was 10 cm. diameter and consequently it was considered more acceptable to modify the existing equipment rather than build a complete piece of new test equipment.

The inlet valve was located in the cylinder head and, whilst the latter was secured to the tunnel and sealed using plasticine to prevent any leakage, the inlet valve lift was adjusted using a specially designed dial gauge. The tunnel was then operated at a range of speeds so that the mass flow rate through the tunnel could be varied at each particular valve lift. From measurements made of the suction pressure at approximately 1.5 tunnel diameters downstream from the tunnel entrance, noting the pressure drop across the measuring section and assuming that the coefficient of discharge Cd for the tunnel to be unity, the mass flow rate through the tunnel was computed using equation 5.5. In order to justify the use of the tunnel with the cylinder head mounted

at the tunnel entrance, a measurement was made of the velocity at the measuring section of the tunnel using an anemometer and this agreed (within 5 to 10% error) with the theoretical velocity computed from the mass flow rate, thus justifying the use of the tunnel and confirming that the cylinder head did not have a detrimental effect to the tunnel performance.

Having computed the mass flow rate through the tunnel, it is reasonable to suppose that this is equal to the mass flow rate through the inlet port of the cylinder head during the suction test. Hence, by measuring the pressure difference across the inlet port, it is possible, using equation 5.5, to compute a value of A^*, the effective area of the inlet port at a particular valve lift assuming that friction is present. A typical family of values of A^* are plotted against the pressure ratio across the inlet port and these are illustrated in Fig. 5.2 for a variety of valve lift positions. Analysis of Fig. 5.2 reveals that, providing that the pressure ratio across the inlet port is less than 0.997, then the value of A^* is approximately constant for each value of valve lift, hence the curve illustrated in Fig. 5.3 was drawn and this provides a valid estimation of the effective area of the inlet port plotted against the ratio of inlet valve lift/inlet valve diameter. This data was therefore used in the computation of the angular velocity throughout the induction period.

5.5.3 Experimental Swirl Measurement

From the experimental program outlined in Section 4.0, the velocity vector was measured at several radial locations on the piston crown, refer Fig. 4.5, and typical results are illustrated in Figs. 4.12 to 4.17. The experimental velocity vectors were resolved into the horizontal plane parallel to the piston crown and then the

angular velocity computed at each radial location. Hence, by taking the mean of the five individual angular velocities, a mean representative value of the angular velocity was computed for particular crank angle positions throughout the induction and compressions periods. Fig. 5.5 illustrates a comparison between the theoretical model and the experimental results for an engine operating speed of 1000 r.p.m. and a comprehensive discussion of the results may be found in Section 5.6.

5.6 Discussion of the Mathematical Model

5.6.1 Inlet Port Velocity Measurement

As mentioned in Section 5.5.1, during the development of the mathematical model, it was considered necessary to check the velocity of the air computed from the theoretical mass flow rate at the junction of the cylinder head and inlet manifold and compare this with the measured velocity at that same section of the inlet port. Fig. 5.4 illustrates the comparison between the two sets of results for an engine speed of 1000 r.p.m. and it may be observed that the comparison is good throughout the entire induction period. Hence,the mass flow rate computed by the mathematical model was assumed to be correct and could be relied upon to compute the angular velocity within the engine cylinder.

5.6.2 Mean Angular Veocity

Fig. 5.5 illustrates the comparison made at an engine speed of 1000 r.p.m. between the computed velocity using the mathematical model outlined in Sections 5.2 and 5.3 and that measured

using the hot wire anemometers in a similar manner to that outlined in Section 5.5.3. Consideration of Fig. 5.5 reveals that the comparison between the computed and measured angular velocity is good throughout the majority of the induction and compression periods and the curve reaches a peak during the induction period at approximately 100 - 120 degrees crank angle and then decreases until the point of inlet valve closure. The curve then increases throughout the compression period and two curves are illustrated here, the upper one being the velocity profile assuming friction was neglected, whilst the lower curve is the profile derived from equation 5.26, when friction caused by the containing surfaces was accounted for. It may be observed that, during the compression period, the maximum frictional effect occurs at 360 degrees crank angle when the difference between the frictional and non-frictional curve is approximately 24% and the experimental results at this point in the engine cycle agree closely (within 6%) with the curve computed assuming friction to be present. Comparison of the results with the experimental work of Lee (7) and Horvatin and Hussmann (11), refer Figs. 2.8 and 2.15 confirm the general profile of the angular velocity throughout the induction and compression periods and provide additional experimental evidence in support of the mathematical model. However, it was impossible to make direct comparison of these latter experimental results with the proposed model owing to the lack of detailed information regarding the engine geometry on which the authors performed their experimentation.

Two important modifications to the original theory outlined in Section 5.2 were included in the computed results illustrated in Fig. 5.5 and these will be discussed in further detail.

(i) Throughout the induction period, the moment of inertia of the trapped mass of air inside the cylinder was approximated

by the expression $m_t D^2/8$, where m_t is the instantaneous trapped mass and D the cylinder diameter, instead of the more complicated expression given by equation 5.11, refer Section 5.2. Fig. 5.6 illustrates a comparison between this modified expression and that given by equation 5.11 and it may be observed that, during the first 20 degrees crank angle of the induction period, the difference between the two expressions is approximately 250%, whilst at 70 degrees crank angle, the difference has reduced to only 6%. In order to further justify the use of the expression $m_t D^2/8$ (which gives reasonable agreement with the experimental results) investigation was made of the velocity profile measured during the initial stages of the induction period. Fig. 5.7 illustrates the outward radial velocity component plotted at three different radial positions and for engine speeds of 500 r.p.m. and 1500 r.p.m. It may be observed that, during the first 40 degrees crank angle, there is a definite concentration of the trapped mass in the vicinity of the cylinder wall. Hence, it was considered acceptable to adopt the simplified expression $m_t D^2/8$ for the moment of inertia of the trapped mass, since this appeared to be a more representative expression than that given by equation 5.11, refer Section 5.2.

(ii) Also, during the induction period, it was found necessary to modify the effective area of the inlet port A^* by an increased factor of 10% in order to achieve good agreement with the experimental results and this modification was justified on the following basis. When the experimental work was performed to estimate the value of the effective inlet port area A^*, the suction pressure of the tunnel was measured at a location of only 1.5 diameters downstream from the tunnel entrance and therefore it was suspected that this pressure measurement was too low, since it was made in the

transition period before the streamline of the flow expands to the tunnel diameter. Hence, because the suction pressure was too low, the computation of A^* from equation 5.5 was consistently too low. In order to substantiate this argument, reference was made to Rouse (40) who considers in detail the effect of an abrupt enlargement in a conduit and for only a diameter ratio of 2, Rouse (40) shows that under prediction of the pressure may occur if the measuring section is not located sufficiently far downstream. Estimations of the ideal pressure location was made from Rouse's (40) work and it would appear that for the abrupt enlargement illustrated in Fig. 5.9, the measuring section should be located approximately 5 diameters downstream from the point of enlargement, where the diameter referred to is that of the enlarged section. Hence the value of the effective inlet port area A^* used in the computation of angular velocity was increased by a factor of 10% and this computation is illustrated in Fig. 5.5. Fig. 5.10 illustrates a comparison between the angular velocity computed using the original value of A^*, that computed using the modified value of A^* and the experimental results at an engine speed of 1000 r.p.m. It may be observed that, when the modified value of A^* was used, the agreement between the computed and experimental results were considerably improved.

During the initial stages of the induction period, the greatest errors occur between the computed and experimental results, these being approximately 20% and may be due to two important contributing factors:

(i) The model assumes ideally that the engine cycle is only just commencing at the top dead centre position during the induction period and hence the computed velocity is zero at this position. In reality, however, this is not the case and the experimental

measurements were made when the piston had attained a pre-determined operating speed, hence it is not unreasonable to suppose that the effect of the exhaust valve closure would contribute to the experimental results and no attempt was made to account for this in the mathematical model.

(ii) From the conclusions of Section 4.0, it was stated that the initial experimental results suggest that a uniform swirl pattern is only developed after approximately 90 degrees crank angle and hence the errors encountered before 90 degrees crank angle may be due to the poor development of the swirl pattern during this part of the engine cycle.

Investigation was also made using the model, of the effects of operating the engine at 4000 r.p.m. and, whilst this was physically impossible for the particular engine considered, since the engine was designed for an optimum operating speed of approximately 2000 r.p.m., it was interesting to note the effect of friction at this high speed. Fig. 5.8 illustrates the computed angular velocity throughout the induction and compression periods for an engine speed of 4000 r.p.m. Observation of the two curves drawn for the compression period, the upper one neglecting friction and the lower one accounting for the friction effects caused by the containing surfaces, suggests that friction results in a decrement of the swirl velocity of approximately 21%. Hence, it was concluded that no drastic change occurs due to the effect of friction as the engine speed was considerably increased. Indeed, for the two cases presented here, the effect friction has on the swirl velocity is reduced from approximately 24% at 1000 r.p.m. to approximately 21% at 4000 r.p.m. and this suggests the assumption of an approximately constant percentage decrement in swirl velocity due to friction as the engine speed varies.

In order to investigate further the effects of the modification to the effective inlet port area A^*, the mathematical model was used to compute the angular velocity during the induction period at an engine speed of 1500 r.p.m. (this was the highest engine speed anticipated for any of the experimental work) and the effective inlet port area A^* was increased by 25%. Observation of the results revealed that the maximum mass flow rate through the inlet port, which occurs at approximately 80 degrees crank angle, was only increased by approximately 2.5% and this suggests that, whilst alteration of the inlet port will have little effect upon the volumetric efficiency of the engine, it will contribute significantly to the angular velocity developed within the engine cylinder, refer Fig. 5.10. Hence it must be concluded that the angular velocity developed within the engine cylinder is particularly dependent upon the effective inlet port area and immediate increase in the angular velocity within the cylinder may be achieved by a reduction of the inlet port area. However, it must be stressed that continual reduction of the inlet port area is not possible since a critical position must be reached when the volumetric efficiency will be reduced considerably and thereby create a detrimental effect to the engine performance.

In conclusion, the initial comparison between the computed and measured angular velocity suggests that, for an engine operating speed of 1000 r.p.m., it is possible to compute the angular velocity using the mathematical model presented in Sections 5.2 and 5.3 where the induction and compression periods are considered in detail and friction was accounted for throughout the compression period. However, further discussion is presented in Section 6.0 where a range of engine speeds, inlet valve masking and supercharging are investigated.

5.7 Analysis of the Squish During the Compression Period

5.7.1 Fitzgeorge and Allison (9) Theoretical Analysis

Assuming that the air within the cylinder has a negligible swirl velocity and viscosity, Fitzgeorge and Allison (9) developed a theory for the prediction of the squish velocity assuming that the contents of the outer cylinder are transferred to the combustion chamber during the latter part of the compression period, refer Appendix 5B. The analysis neglects the effect of friction and assumes that the spatial pressure distribution is negligible within the cylinder whilst the radial transfer of the air occurs. This latter assumption was analysed in detail by Fitzgeorge and Allison (9) and the authors showed that, if the pressure increase P' is small compared with the pressure inside the combustion chamber, then the non-uniformity of pressure may be neglected and the compressibility effects omitted from the Bernoulli equation which reduces to:

$$P' = \frac{\rho U^2}{2} \qquad \text{5.30}$$

where ρ is the density and U the velocity. Using typical values of U from the squish computation P' was computed by the authors for a clearance volume of 0.075 cm. and the maximum error involved found to be approximately 0.5%. Hence the presence of a pressure distribution was ignored and the equation derived for squish is given by

$$U_r = \frac{1}{2r} \frac{(b^2 - r^2)}{(AS(\theta) + V_b)} \frac{V_b}{S(\theta)} \frac{dS(\theta)}{dt} \qquad \text{5.31}$$

where U_r is the radial velocity at radius r

A is the cross-sectional area of the cylinder

V_b is the volume of the combustion chamber

$S(\theta)$ is the displacement of the piston crown from the top dead centre position at crank angle θ

b is the cylinder radius

$\frac{dS(\theta)}{dt}$ is the piston speed.

5.7.2 Frictional Effects due to the Cylinder Head and Piston Crown

In order to consider the effects of friction caused by the cylinder head and piston crown on the squish velocity, a simple analysis was performed which equates the momentum change of the mass which is transferred from the outer cylinder into the combustion chamber, to the shear force due to friction acting on the piston crown and cylinder head.

i.e. $\dot{m} \Delta U$ = shear force ——————— 5.32

where $\dot{m}$ is the mass flow rate from the outer cylinder into the combustion chamber and ΔU is the decrease in velocity associated with $\dot{m}$ due to the shear force. Consideration of the cylinder geometry reveals that equation 5.32 may be written in the form,

$$\Pi \, dS(\theta) \rho \frac{U}{2} \Delta U = 2 \tau \frac{\Pi}{4} (D^2 - d^2) \qquad \text{——— 5.33}$$

where ρ is the density

d the diameter of the combustion chamber

$U/2$ is the arithmetric mean velocity of the mass flow into the combustion chamber (because the velocity at the cylinder wall is zero whilst that at the edge of the combustion chamber is a maximum)

ΔU is the change in velocity due to the shear force

τ is the frictional force per unit area

D is the cylinder diameter.

Now $$\tau = \frac{1}{2} C_f \rho \frac{U^2}{4} \qquad \text{.....} \quad 5.34$$

Again, considering U/2 to be the representative velocity of the mass flow and C_f may be approximated to a flat plate where the characteristic length in the Reynolds Number is $(D - d)/2$, the distance between the cylinder wall and the combustion chamber, hence,

$$C_f = 0.072\ Re^{-0.2} \qquad \text{.....} \quad 5.35$$

where $$Re = \frac{\rho U(D - d)}{4 \mu}$$

and μ is the viscosity.

Substitution for τ and C_f into equation 5.33 gives

$$S(\theta)\rho\Pi\, d\, \frac{U}{2}\, \Delta U = \frac{0.072\ \rho\ U^2 \Pi\ (D^2 - d^2)}{16} Re^{-0.2} \qquad \text{.....} \quad 5.36$$

which reduces to

$$\Delta U = \frac{0.072\ U\ (D^2 - d^2)}{8\ S(\theta)\ d} Re^{-0.2} \qquad 5.37$$

Equation 5.37 was solved for the worst possible condition assuming that, at an engine speed of 1000 r.p.m., the squish velocity was equal to 18 M/S as computed from Fitzgeorge and Allison (9), equation 5.31, and that the piston was in the top dead centre position (resulting in the smallest flow passage), whilst the Reynolds Number was computed using the actual pressure and temperature data at 350 degrees crank angle.

For an engine speed of 1000 r.p.m., it may be shown that the maximum error possible in the velocity is approximately 12%. The computation was repeated for an engine speed of 4000 r.p.m. and here the maximum error was approximately 10%. Thus, in a similar manner to the swirl, refer Section 5.6, it is apparent that the percentage decrease in velocity due to friction remains approximately constant with engine speed. Because the percentage change in velocity due to friction is of the same order of magnitude as the error in the anemometry system developed for detecting velocity magnitude and direction, it was decided that the squish computation could neglect the effect of friction.

5.7.3 Experimental Squish Measurement **

During the latter part of the compression period, it was anticipated that squish would be developed as the piston approached the top dead centre position and the mass of air was transferred from the outer cylinder into the combustion chamber. In order to measure the squish component, two anemometers were located at the edge of the combustion chamber at the same level as the piston crown. The probes were located so that the squish component would form an angle of incidence with each probe and the resultant magnitude could

** Experimental squish in this context refers to the radial component of the flow.

be computed using the relationship $U_{\theta} = U_{maximum} \sin \theta$ where θ is the angle between the anemometer sensing wire and any cylinder radius and was equal to 45 degrees. Using two probes instead of one permitted a check to be made on the computation.

5.7.4 Discussion of the Squish Velocity

Using the theoretical squish equation 5.31 developed by Fitzgeorge and Allison (9) and presented in detail in Appendix 5B, the squish velocity was computed for a radial location equal to 2.70 cm. (equal to the combustion chamber radius) and is illustrated in Fig. 5.11 for an engine speed of 1000 r.p.m. Observation of Fig. 5.11 reveals that for the engine geometry under consideration, the squish has a maximum computed value of approximately 18 M/S at 354 degrees crank angle. However, for the air being transferred from the outer cylinder area into the combustion chamber, it was suggested in Section 2.3.4 that the swirl and squish cannot be isolated from each other and that a spiral pattern is the more probable motion for the air as it enters the combustion chamber. Hence, the comparison between the experimental and theoretical squish is only included to illustrate that the air motion has a radial component during the latter stage of the compression period and the measured component agrees approximately with the theoretical squish computed using the equation presented by Fitzgeorge and Allison (9), refer Section 5.7.1, which neglects the effect of friction. From the simple analysis outlined in Section 5.7.2, where the momentum change of the mass transferred from the outer cylinder into the combustion chamber was equated to the shear force due to friction, it was shown that for an engine speed of 1000 r.p.m., the percentage decrement in the velocity was approximately 12%. This was computed for the worst possible case when the piston was in the top dead centre position and

hence for all crank angle positions before top dead centre, the frictional effect will be considerably reduced, since the surface to volume ratio of the cylinder and the squish velocities will be less than that at 354^{o} crank angle. When the piston is in the top dead centre position according to the theoretical computation, the squish velocity is zero, since the mass contents of the cylinder have now been transferred completely to the combustion chamber and this is not supported by the experimental evidence. It is possible, however, that the anemometer is responding to a component of the swirl velocity when the piston is in the top dead centre position and this would account for the discrepancy between the computed and experimental results in this position and thus justify the argument made previously that swirl and squish cannot be isolated from each other but obviously combine together and probably form a spiral pattern as the air is transferred into the combustion chamber during the latter stages of the compression period.

5.8 Conclusions of the Mathematical Model

In conclusion, the highest error encountered between the theoretical model and the experimental measurements is approximately $\pm$ 20%, however, observation of the results reveals that the majority of the comparisons are well within this error. The results do, however, show that the model predicts the general pattern of the air flow inside the engine cylinder with reasonable accuracy and justifies the assumption of a solid body rotation and a forced vortex velocity profile.

During the induction period, there are particularly high three dimensional components of the flow and these are illustrated in Figs. 4.12 and 4.13. Consequently, even with the assumption of only a horizontal component of the inlet momentum, refer Section 2.1 and Fig. 2.1 and the computation of the horizontal component (parallel to the piston crown) of the experimental measurements, it is impossible to predict exactly the theoretical pattern of the flow during the induction period.

The greatest error in the results appears during the initial stages of the induction period and this may be due to the effect of exhaust valve closure and the relatively poor flow development during the first 90 degrees crank angle of the engine cycle. Alternatively, this could also be due to a consequence of only one height above the piston crown being used for each radial location of the anemometers. Had the anemometers been located at different heights at each radial location and a mean value of the velocity determined from these results, a more satisfactory comparison might have been achieved. However, it was considered unnecessary to perform additional experimental work when a reasonable comparison had already been made throughout the compression period which was considered the most important part of the engine cycle.

Consideration of the compression period and in particular the region 330-360 degrees crank angle, reveals that the comparison between computed and experimental results is good providing that the frictional effects of the cylinder surfaces are accounted for, and here the error between the computed and experimental results is approximately 6%. This latter period is of particular importance regarding any future work investigating the fuel injection process for a Diesel Engine where an accurate knowledge of the air velocity

and its distribution would be required and using the mathematical model developed here, this information could be successfully obtained.

Considering the latter stages of the compression period, it was concluded that squish was present during this period and agreed approximately with the squish computed using Fitzgeorge and Allison (9) theory (which neglects the effect of friction). But when the piston is in the top dead centre position, a component of the swirl velocity was measured and this suggests that the swirl and squish velocities cannot be isolated from each other but, in fact, combine together to create a spiral flow as the air is transferred from the outer cylinder into the combustion chamber.

T A B L E 1

N250 INDUCTION PERIOD PROGRAM

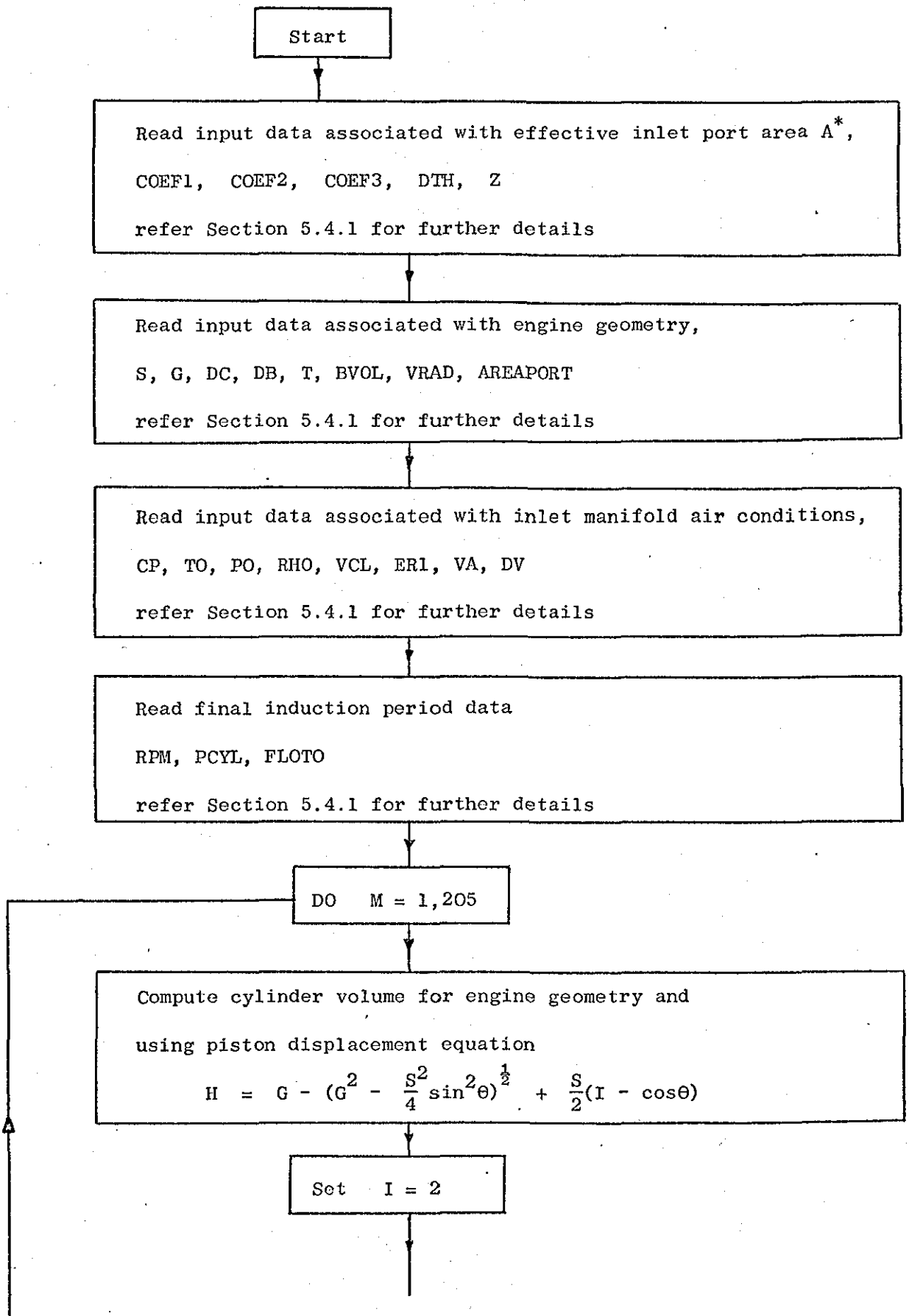

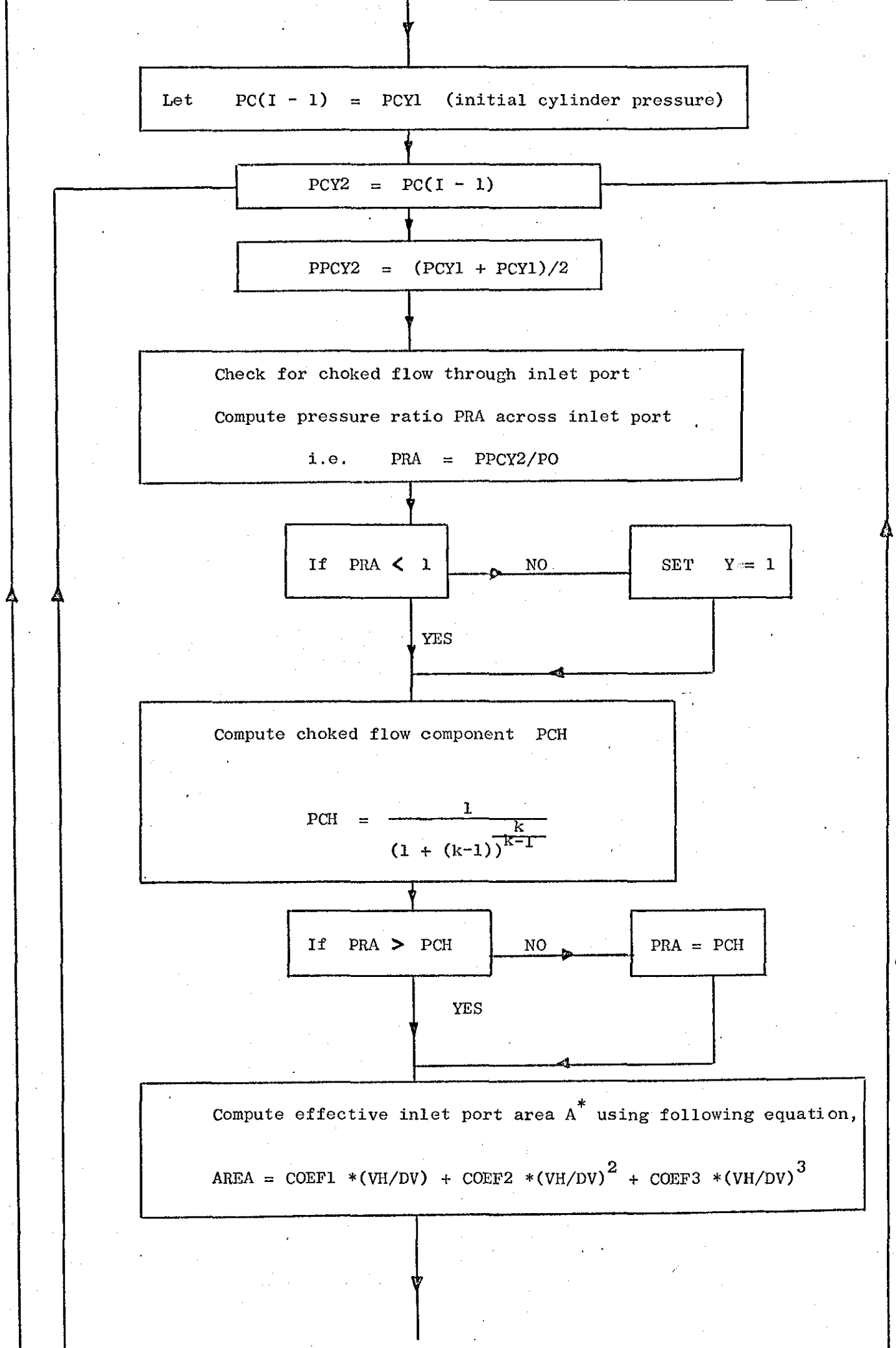
Let PC(I - 1) = PCY1 (initial cylinder pressure)
PCY2 = PC(I - 1)
PPCY2 = (PCY1 + PCY1)/2
Check for choked flow through inlet port
Compute pressure ratio PRA across inlet port
i.e. PRA = PPCY2/PO
If PRA < 1
NO
SET Y = 1
YES
Compute choked flow component PCH
PCH = 1 / (1 + (k-1))^(k/(k-1))
If PRA > PCH
NO
PRA = PCH
YES
Compute effective inlet port area A* using following equation,
AREA = COEF1 *(VH/DV) + COEF2 *(VH/DV)^2 + COEF3 *(VH/DV)^3

Compute instantaneous mass flow rate through inlet port using equation 5.5

$$\dot{m} = A^* \left(\frac{P_n}{P_o}\right)^{\frac{1}{k}} \left[\left(\frac{2k}{k-1}\right) P_o \rho_o \left[1 - \left(\frac{P_n}{P_o}\right)^{\frac{k-1}{k}}\right]\right]^{\frac{1}{2}}$$

Compute instantaneous pressure inside the cylinder using equation 5.4

$$P_{n+1} = P_n + \frac{(k-1)\dot{m}\, Cp\, T\, \Delta t}{V_n} + \frac{k\, P_n (V_{n+1} - V_n)}{V_n}$$

Check for reversed flow

IF Y = 1

YES → $\dot{m} = -\dot{m}$

NO

Let PX(I) = New cylinder pressure P_{n+1}

IF I = 2

YES → I = I + 1

PC(2) = PX(2)

NO

Compute new estimate of cylinder pressure according to Wegstein iteration (39)

$$PC(3) = PX(3) - \frac{(PX(3) - PX(2)) * (PX(3) - PC(2))}{PX(3) - PX(2) - PC(2) + PC(1)}$$

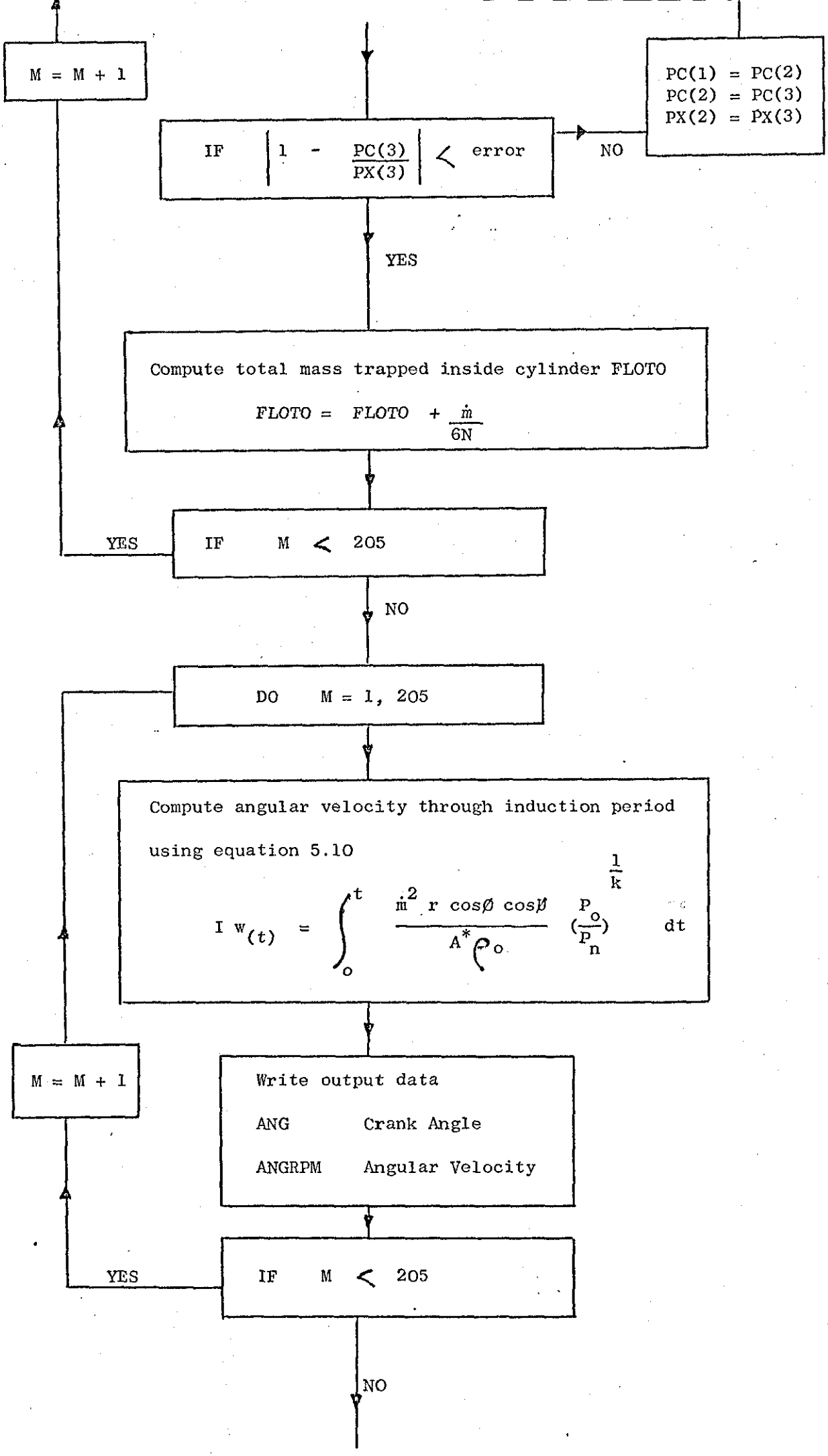
M = M + 1
PC(1) = PC(2)
PC(2) = PC(3)
PX(2) = PX(3)
IF | 1 - PC(3)/PX(3) | < error
NO
YES
Compute total mass trapped inside cylinder FLOTO
FLOTO = FLOTO + ṁ/6N
YES
IF M < 205
NO
DO M = 1, 205
Compute angular velocity through induction period
using equation 5.10
I w(t) = ∫ from o to t (ṁ² r cosØ cosβ / A* ρo) (Po/Pn)^(1/k) dt
M = M + 1
Write output data
ANG Crank Angle
ANGRPM Angular Velocity
YES
IF M < 205
NO

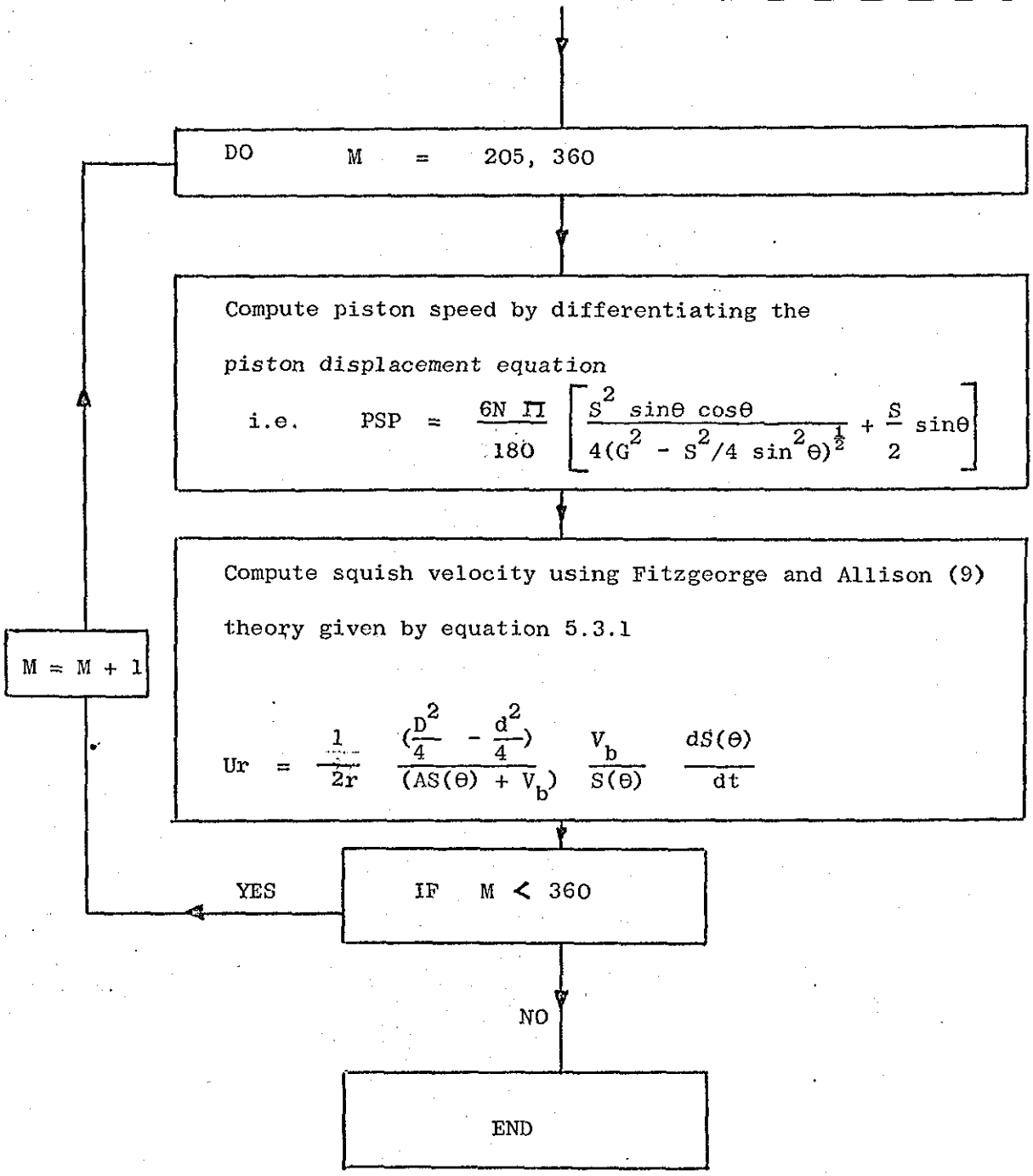
DO M = 205, 360
Compute piston speed by differentiating the
piston displacement equation
i.e. PSP = 6N Π/180 [S² sinθ cosθ / 4(G² - S²/4 sin²θ)^½ + S/2 sinθ]
Compute squish velocity using Fitzgeorge and Allison (9)
theory given by equation 5.3.1
Ur = 1/2r (D²/4 - d²/4) / (AS(θ) + V_b) V_b/S(θ) dS(θ)/dt
M = M + 1
YES
IF M < 360
NO
END

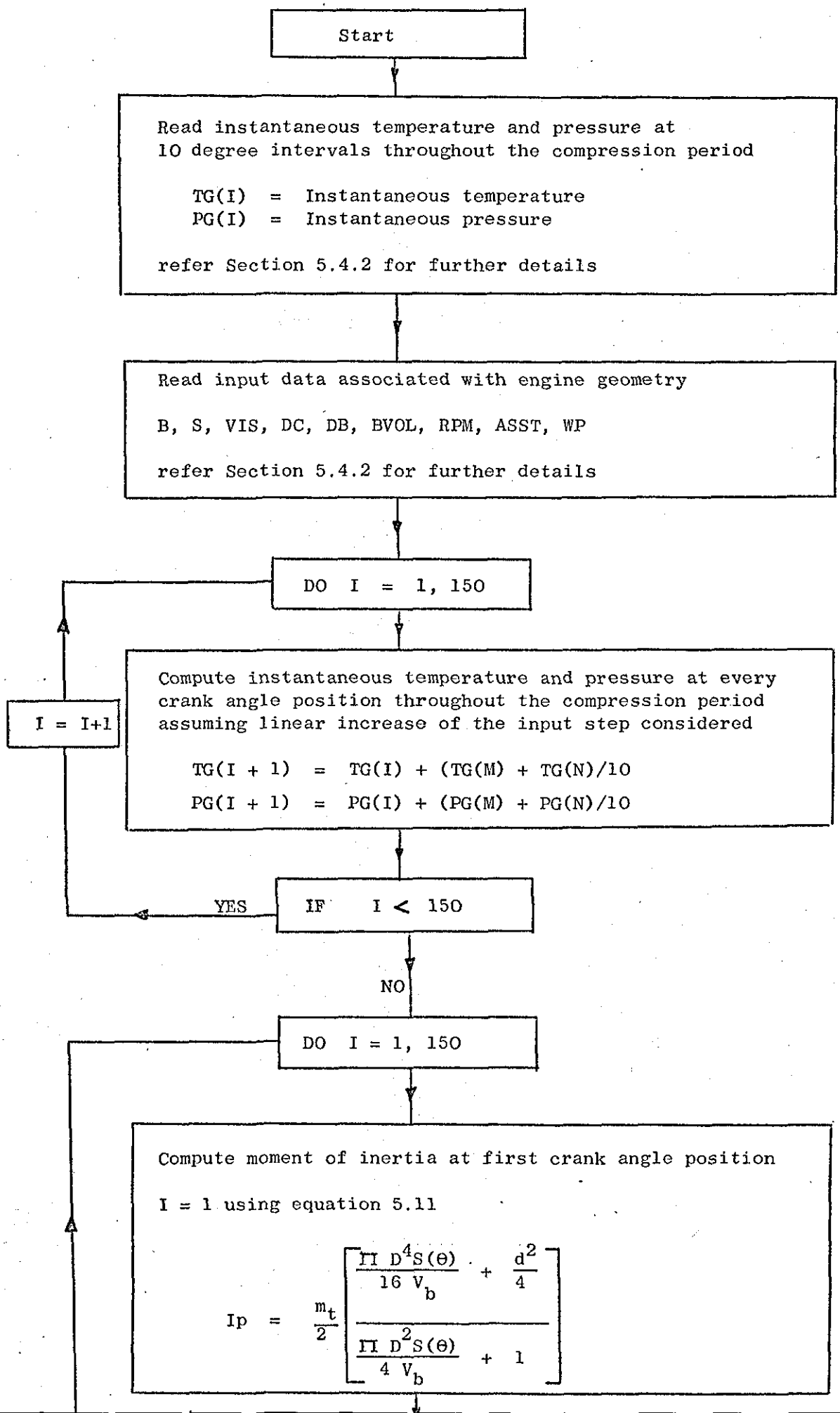
Start
Read instantaneous temperature and pressure at 10 degree intervals throughout the compression period
TG(I) = Instantaneous temperature
PG(I) = Instantaneous pressure
refer Section 5.4.2 for further details
Read input data associated with engine geometry
B, S, VIS, DC, DB, BVOL, RPM, ASST, WP
refer Section 5.4.2 for further details
DO I = 1, 150
Compute instantaneous temperature and pressure at every crank angle position throughout the compression period assuming linear increase of the input step considered
TG(I + 1) = TG(I) + (TG(M) + TG(N)/10
PG(I + 1) = PG(I) + (PG(M) + PG(N)/10
I = I+1
YES
IF I < 150
NO
DO I = 1, 150
Compute moment of inertia at first crank angle position
I = 1 using equation 5.11
Ip = m_t/2 [(ΠD^4 S(θ)/16 V_b + d^2/4) / (ΠD^2 S(θ)/4 V_b + 1)]

Compute moment of inertia at next crank angle position I = I + 1 using equation 5.11

$$In = \frac{m_t}{2}\left[\frac{\frac{\Pi D^4 S(\theta)}{16 V_b} + \frac{d^2}{4}}{\frac{\Pi D^2 S(\theta)}{4 V_b} + 1}\right]$$

Compute frictional torque due to friction acting on the cylinder surfaces using equation 5.25 where

$$A = \frac{\Pi D^{3.6} \rho^{0.8} \mu^{0.2}}{16}\left[0.067\, S(\theta) + \frac{0.088\, D}{16}\right]$$

I = I +1

Call subroutine DRTMI (41)

Compute angular velocity at crank angle position I = I + 1 using equation 5.26

$$In\ wn - Ip\ wp + A\left(\frac{wp + wn}{2}\right)^{1.8}\frac{\Delta\theta}{6N} = 0$$

Return to main segment

Write output data

X	Crank Angle Position
OMEGA	Angular Velocity
ZZZ	Ratio Ip/In

Set Ip = In

wp = wn

YES — IF I < 360

NO

END

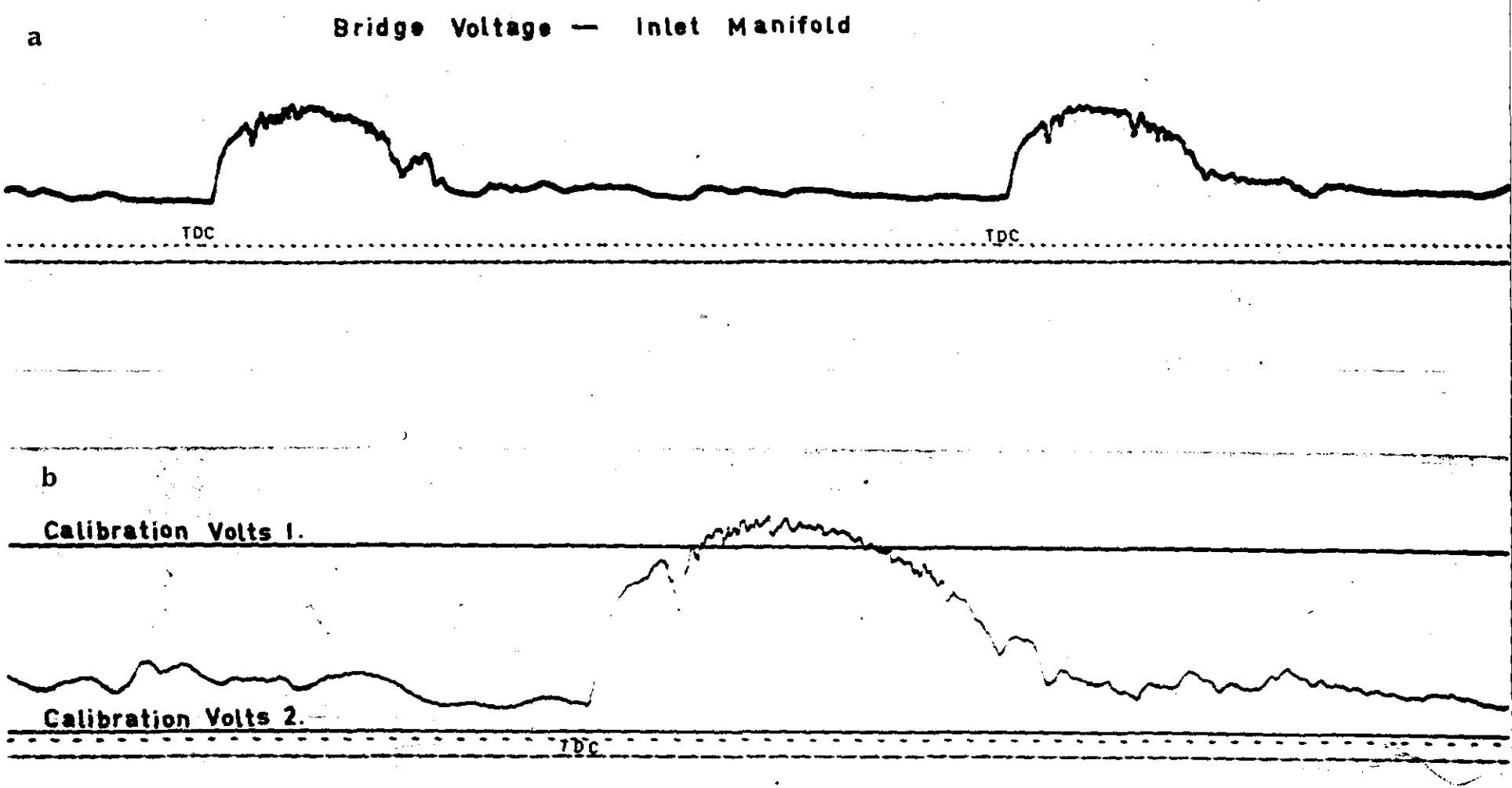

FIG. 5.1 INLET PORT VELOCITY TRACE

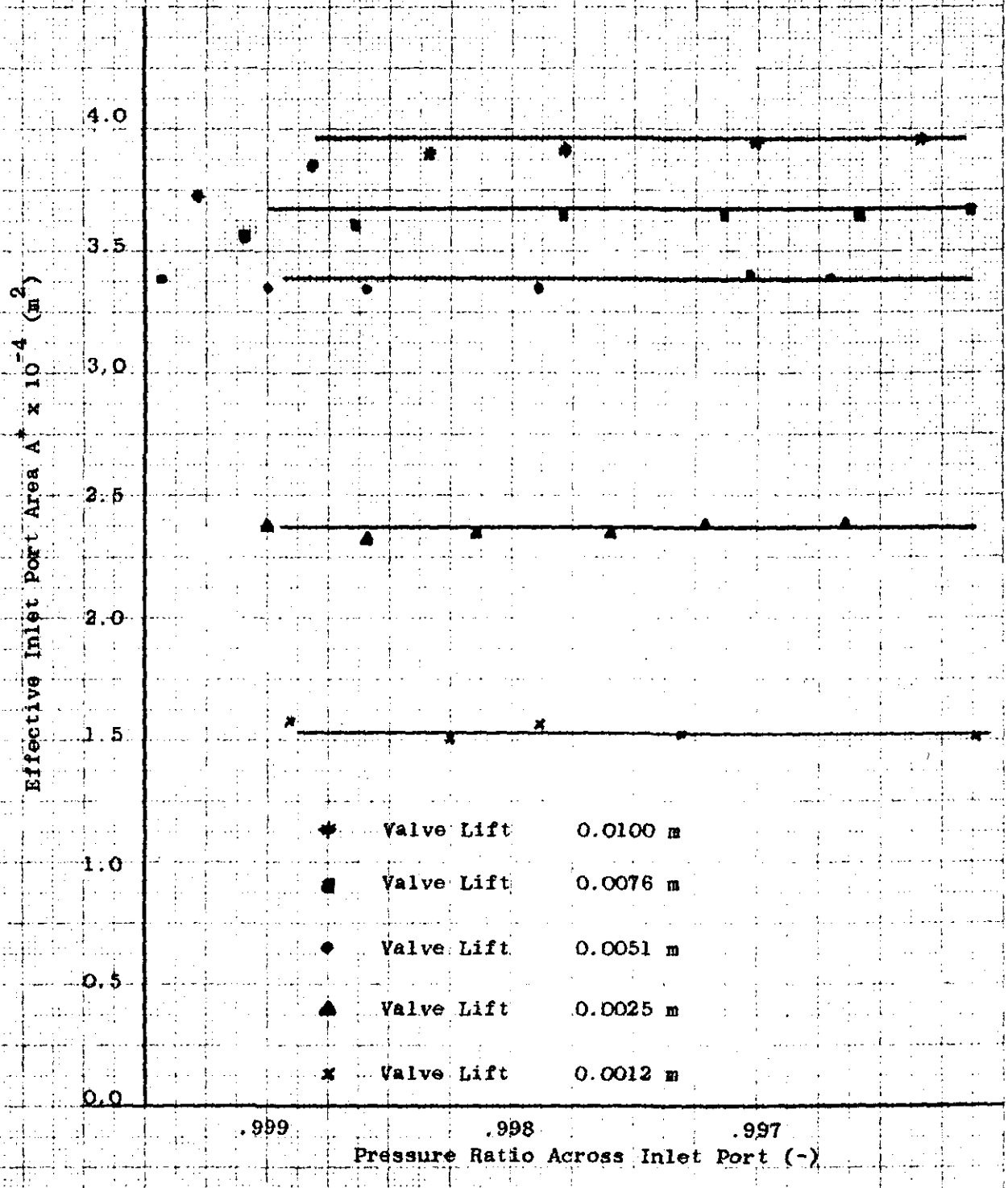

FIG. 5.2 EFFECTIVE INLET PORT AREA A^* PLOTTED AGAINST PRESSURE RATIO ACROSS THE INLET PORT

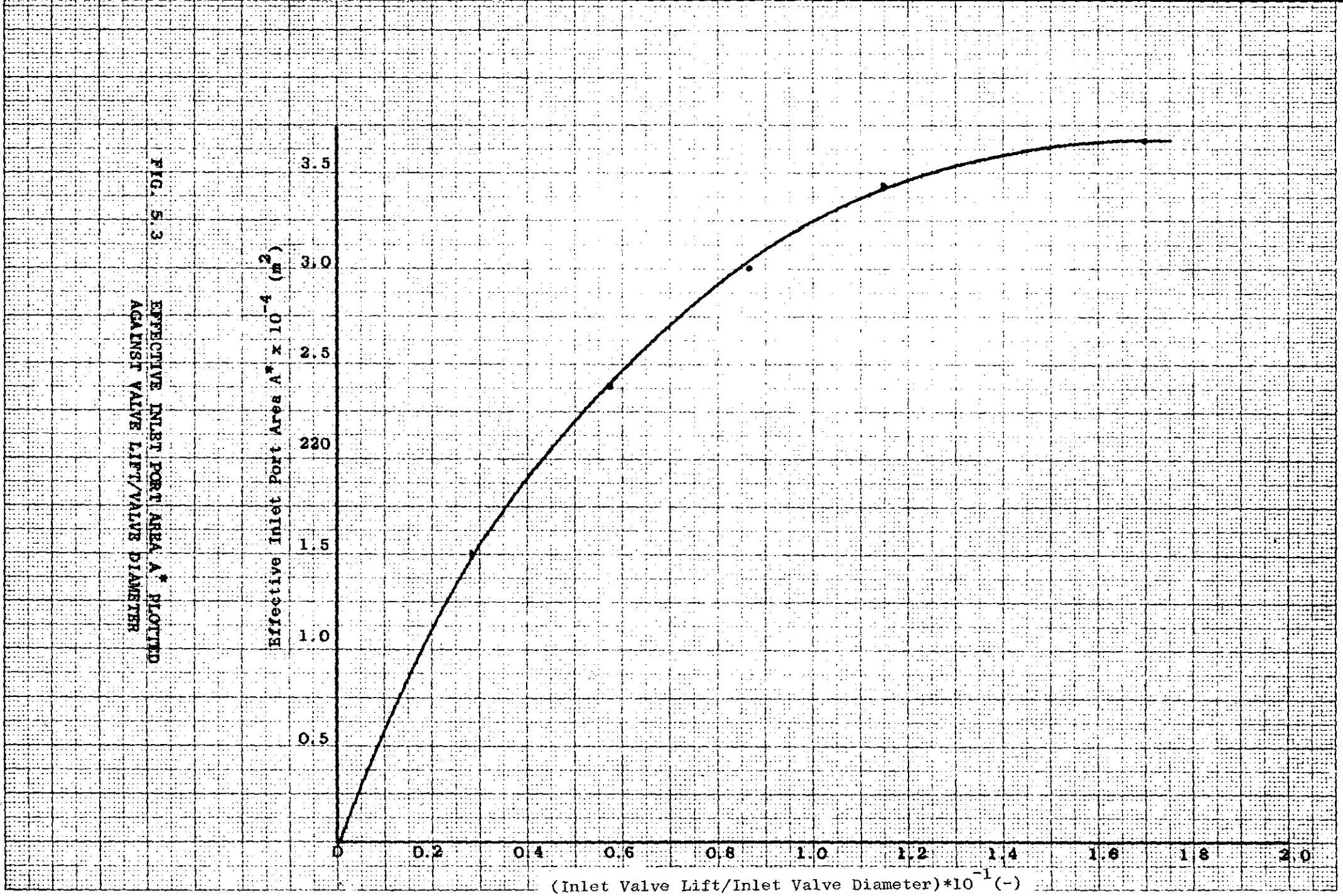

FIG. 5.3 EFFECTIVE INLET PORT AREA A* PLOTTED AGAINST VALVE LIFT/VALVE DIAMETER

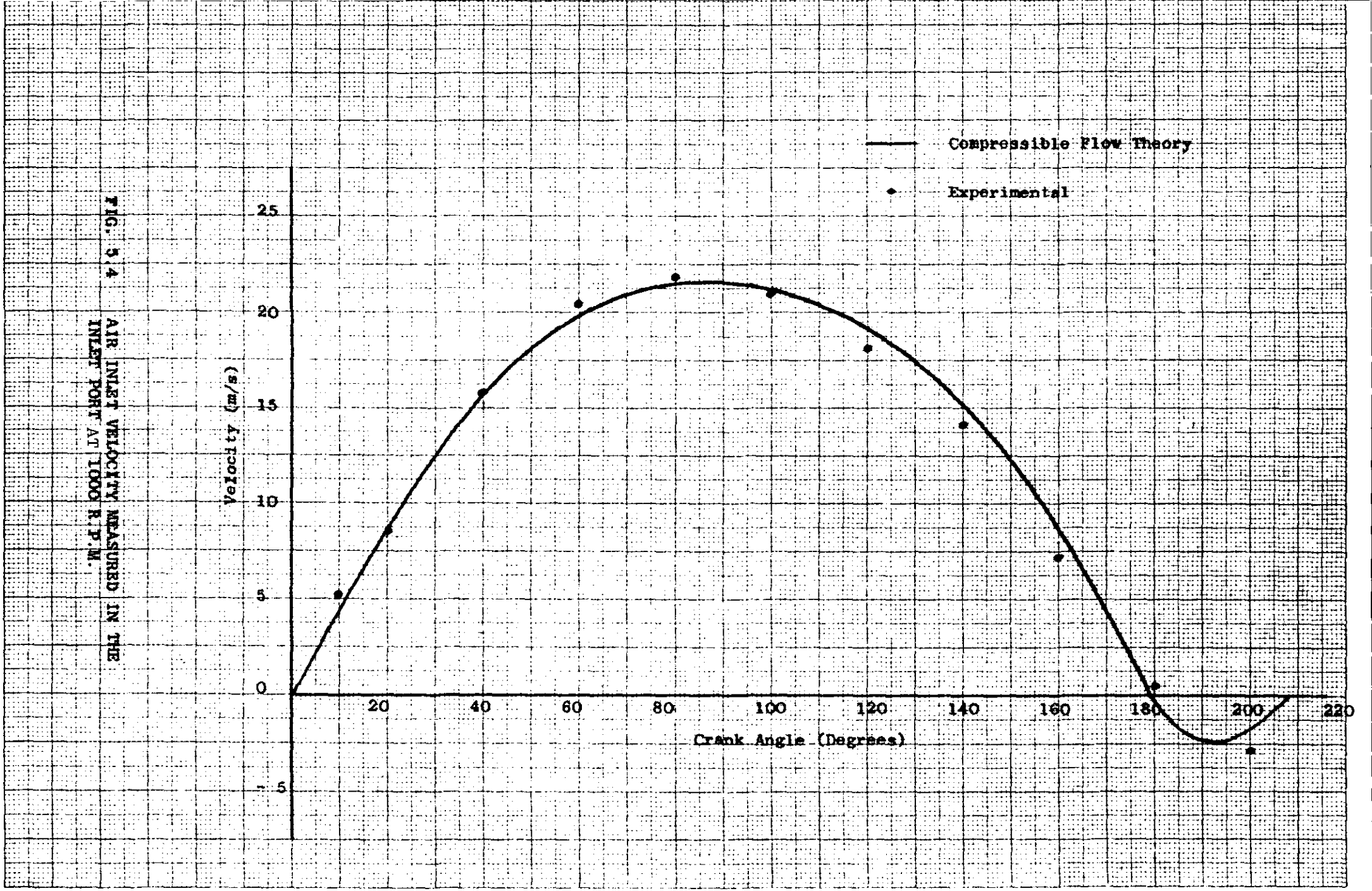

FIG. 5.4 AIR INLET VELOCITY MEASURED IN THE INLET PORT AT 1000 R.P.M.

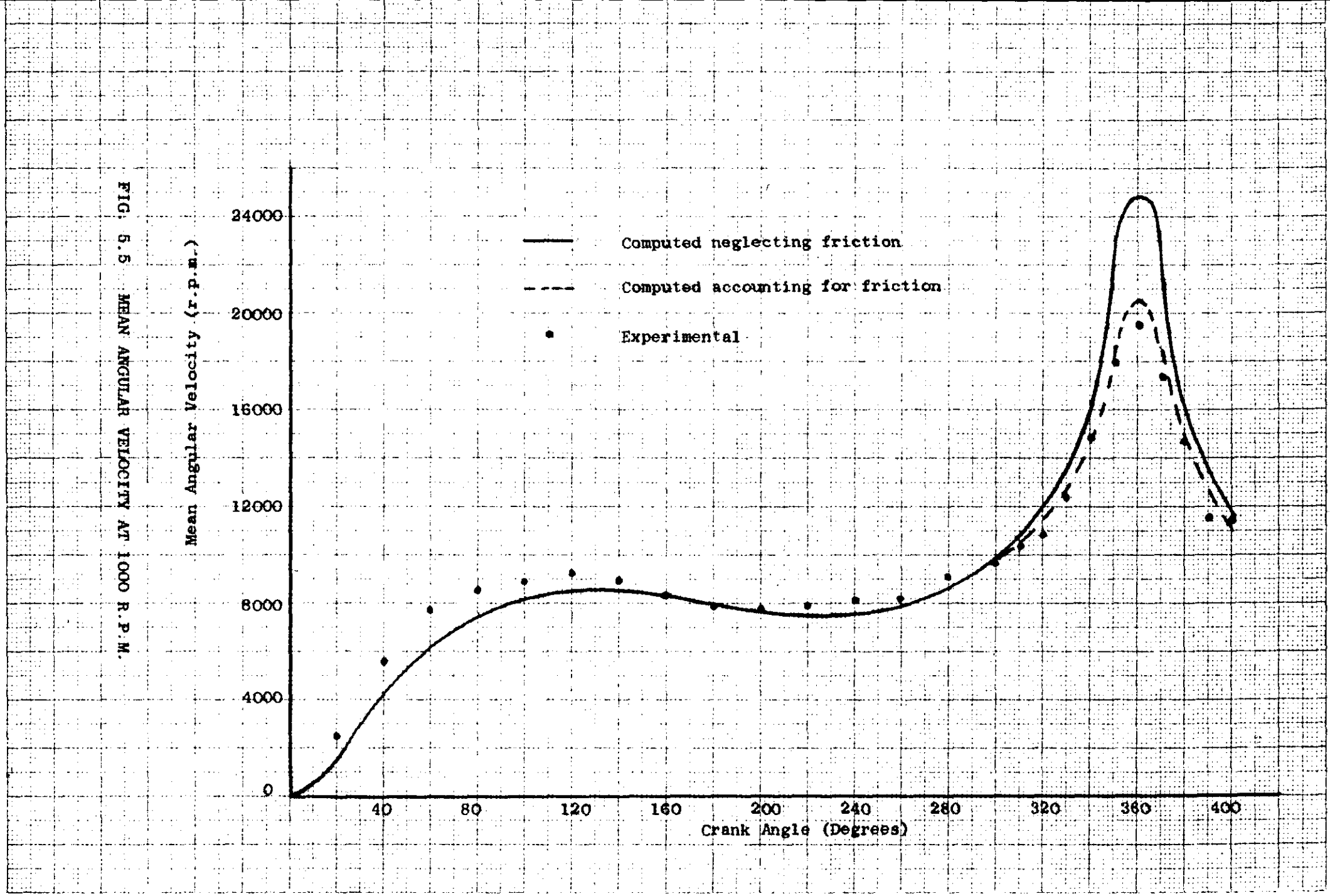

FIG. 5.5 MEAN ANGULAR VELOCITY AT 1000 R.P.M.

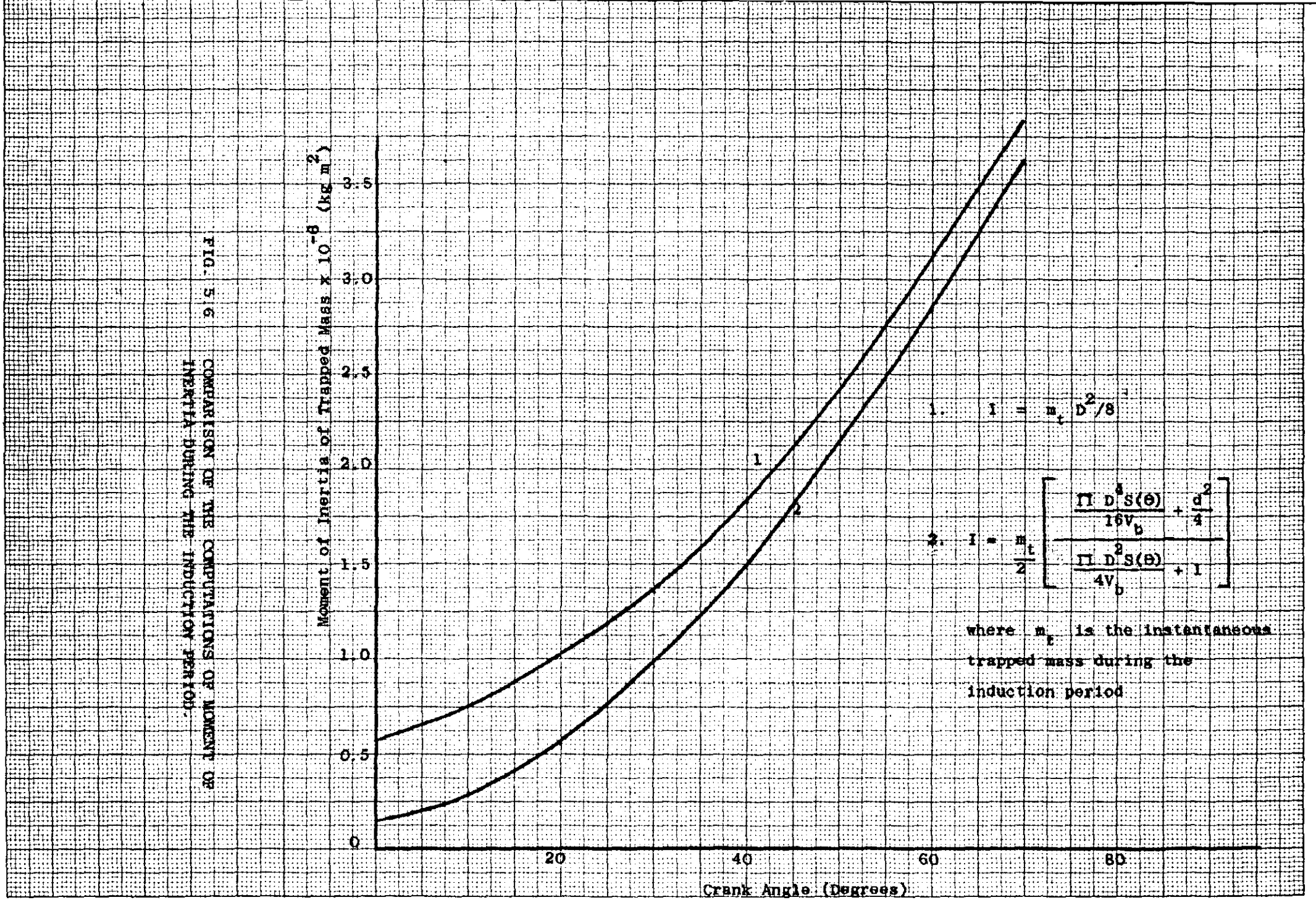

FIG. 5.6 COMPARISON OF THE COMPUTATIONS OF MOMENT OF INERTIA DURING THE INDUCTION PERIOD.

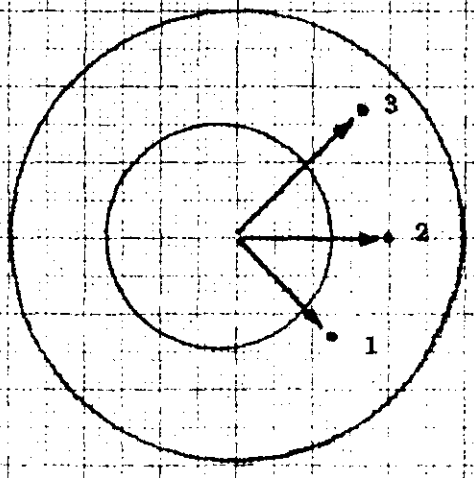

Radial Location

1 R = 3.18 cm.

2 R = 3.49 cm.

3 R = 3.81 cm.

1500 R.P.M.

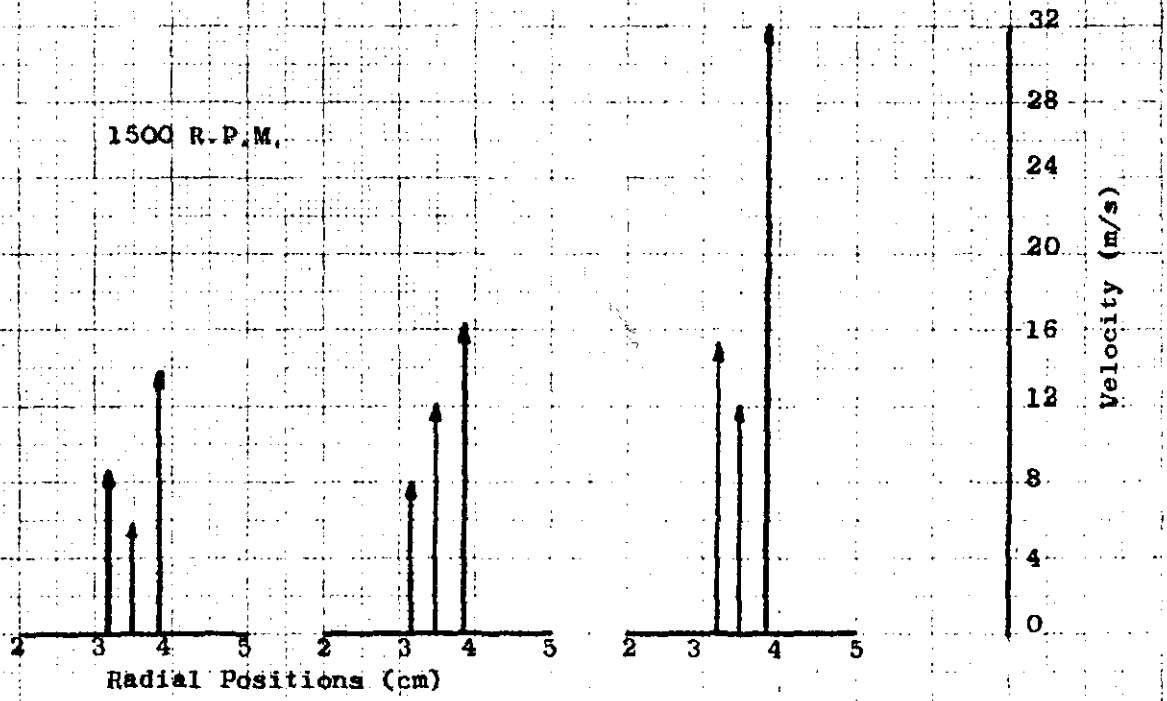

500 R.P.M.

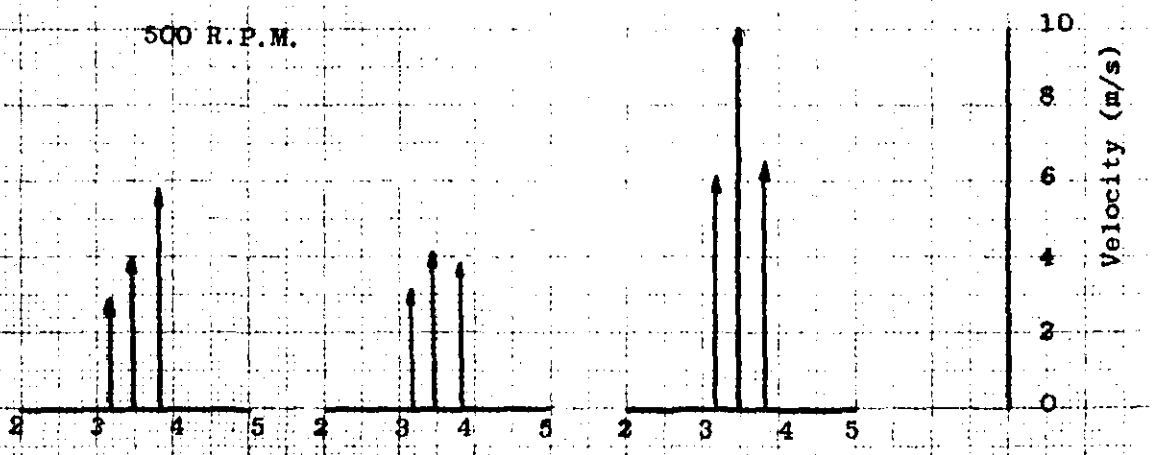

FIG. 5.7 OUTWARD RADIAL VELOCITY COMPONENTS OF FLOW AT THREE RADIAL POSITIONS AND THREE CRANK ANGLE POSITIONS FOR 500 AND 1500 R.P.M.

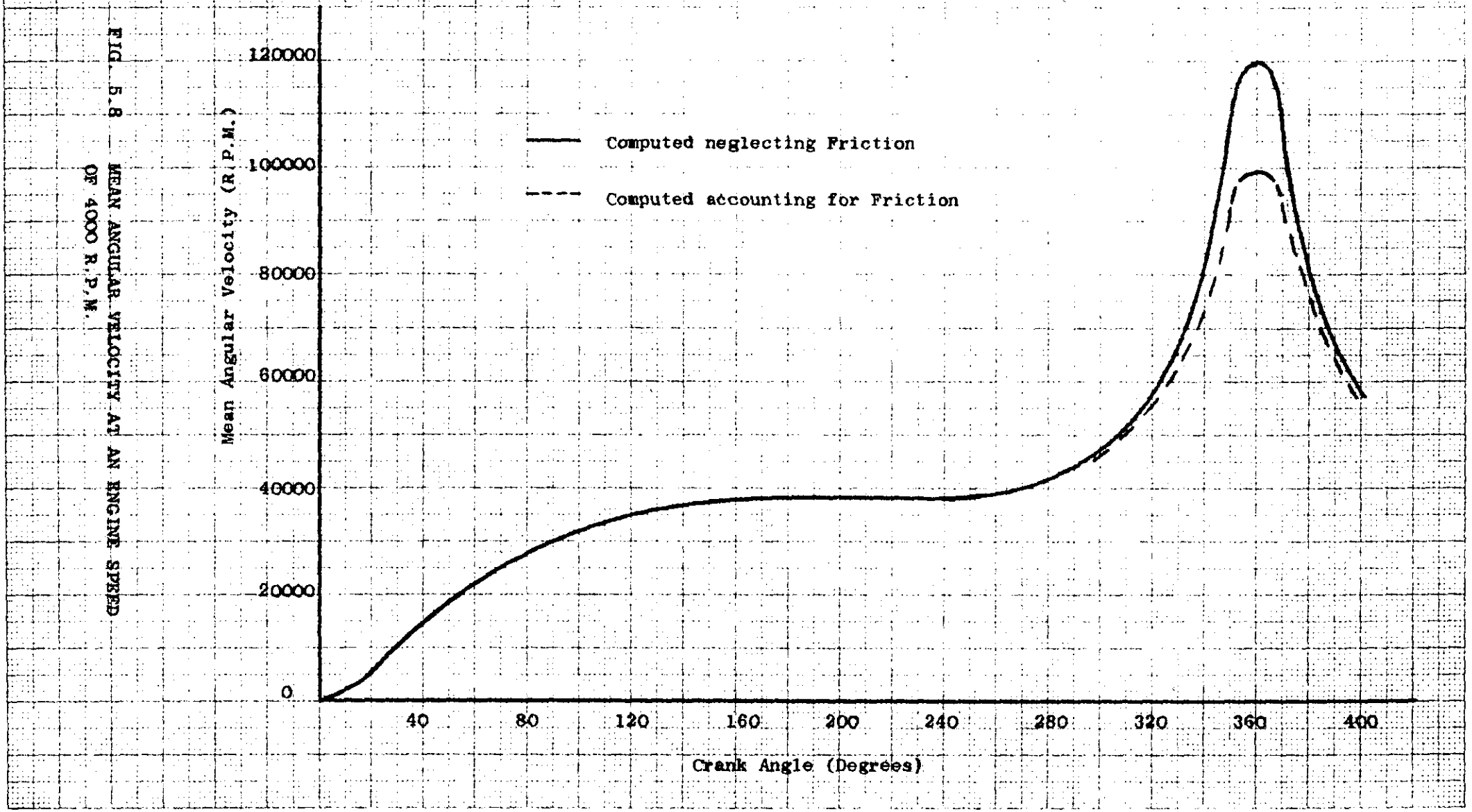

FIG. 5.8 MEAN ANGULAR VELOCITY AT AN ENGINE SPEED OF 4000 R.P.M.

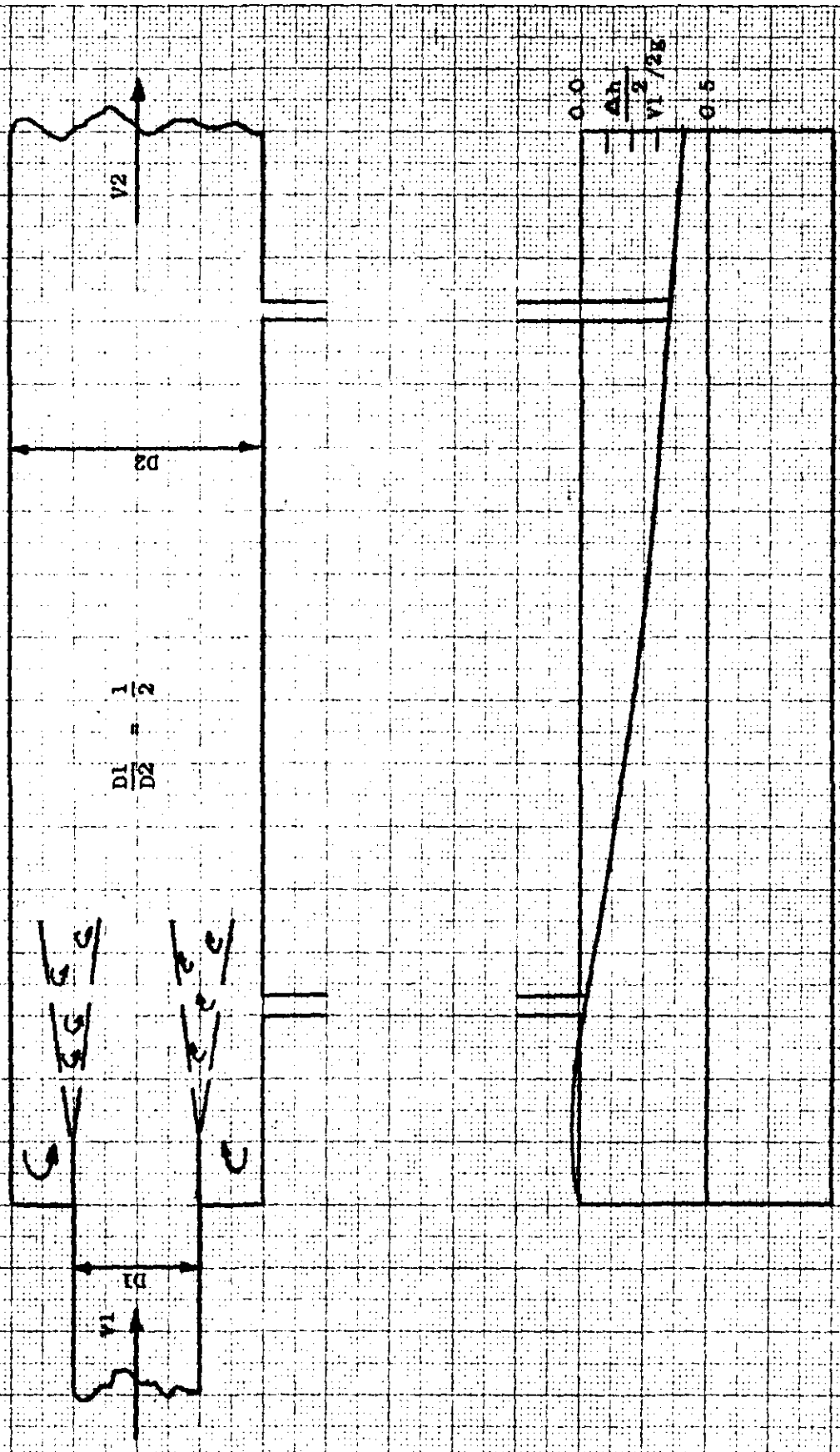

FIG. 5.9 VARIATION IN PRESSURE HEAD AT AN ABRUPT ENLARGEMENT (TAKEN FROM ROUSE (40))

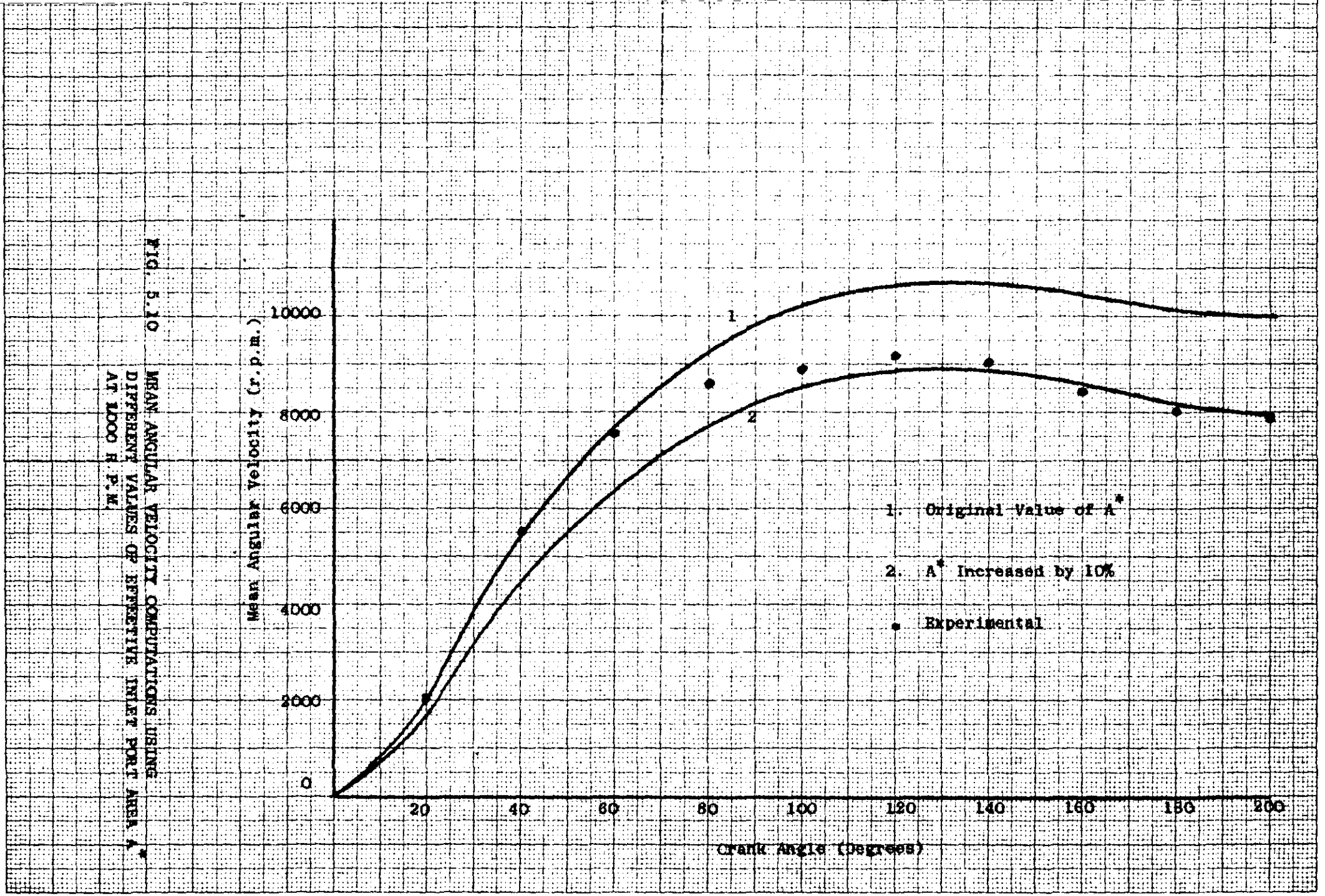

FIG. 5.10 MEAN ANGULAR VELOCITY COMPUTATIONS USING DIFFERENT VALUES OF EFFECTIVE INLET PORT AREA A* AT 1000 R.P.M.

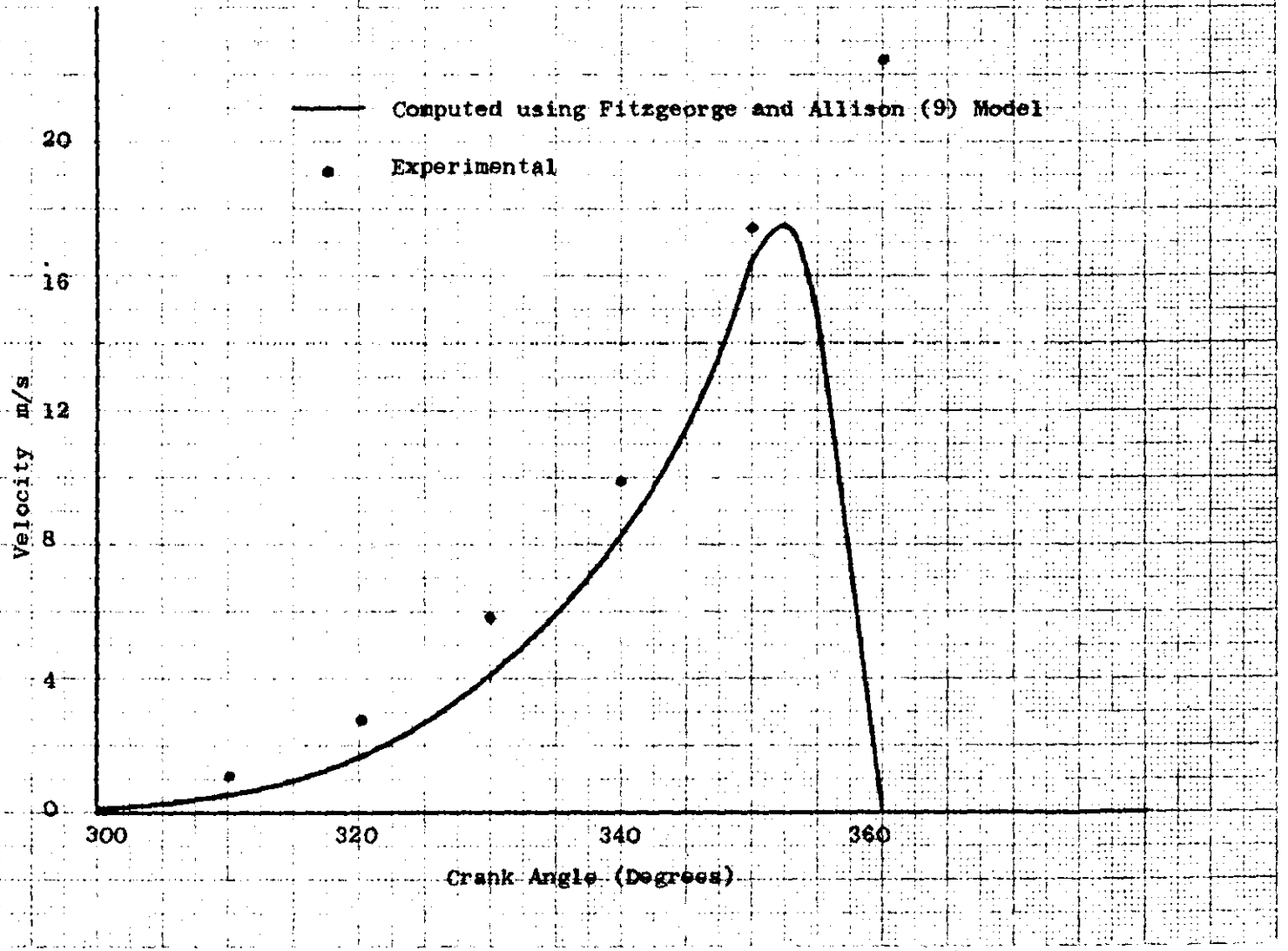

FIG. 5.11 SQUISH (INWARD RADIAL COMPONENT OF FLOW) AT 1000 R.P.M.

6.0 DISCUSSION OF THE INVESTIGATION

6.0 DISCUSSION OF THE INVESTIGATION

6.1 Introduction

Having outlined a system of hot wire anemometry and a technique for measuring a three dimensional velocity vector in both magnitude and direction, refer Sections 3.0 and 4.0, a mathematical model was proposed, refer Section 5.0, which assumed that momentum was conserved within the engine cylinder throughout the induction and compression periods whilst frictional effects caused by the containing surfaces of the cylinder were accounted for during the compression period. An initial comparison was made between the computed angular velocity using the mathematical model and that measured experimentally using the hot wire anemometer technique and this comparison, which was illustrated in Fig. 5.5, showed good agreement between the computed and experimental results, particularly during the latter stages of the compression period, where the difference between the results was approximately 6%. In order to justify the model and its usefulness to a design engineer wishing to investigate a variety of engine parameters, a programme of experimental work was undertaken to investigate the following parameters and the effect they have upon the air motion.

(i) Engine Speed

(ii) Inlet Valve Masking

(iii) Supercharging.

6.2 Variation of Engine R.P.M.

The engine was capable of a maximum operating speed of 2000 r.p.m. However, because of the restrictions imposed by the belt

drive, motoring facilities and the swinging link mechanism adopted for the extraction of the signals from the engine cylinder, a speed range of 500 - 1500 r.p.m. was investigated.

6.2.1 Velocity of the Induced Air in the Inlet Port

The inlet port velocities were measured at the junction of the cylinder head and inlet manifold in a similar manner to that outlined in Section 5.5.1 and three different engine speeds investigated, these being 500, 1000 and 1500 r.p.m. The three curves are illustrated in Fig. 6.1 and the experimental results compare well with the compressible flow theory developed for the mathematical model, thus showing that the theory may be relied upon to predict accurately the mass flow rate $\dot{m}$ into the engine cylinder through the inlet port. However, as mentioned in the discussion of Section 5.0, refer Section 5.6.2, whilst a good comparison may be made between the computed and measured inlet port velocity at a particular section of the inlet port, this could not be relied upon to justify the representative value derived for the effective inlet port area A^*. In section 5.6.2, it was mentioned that theoretical computations were performed using the mathematical model and, at an engine speed of 1500 r.p.m., the mass flow rate $\dot{m}$ into the cylinder was computed using (i) the representative value derived for the effective inlet port area A^* refer Section 5.5.2 and (ii) a value of A^* increased by 25%. The results of the computation showed an increase in the mass flow rate at 90 degrees crank angle (approximately the position of maximum mass flow rate) of approximately 2.5% and therefore it was concluded that an increase in the effective inlet port area of 25% had little effect upon the mass flow rate into the engine cylinder. Instead an increase in A^*, the effective inlet port area, obviously leads to an increase in cylinder pressure (i.e. the cylinder pressure is greater than that computed using the

original A^*) and this would account for the mass flow rate only increasing by approximately 2.5% for the particular valve lift considered.

6.2.2 Forced Vortex Velocity Profile

From the analysis of the results taken at various locations on the piston crown, refer Section 4.4, the velocity vectors were resolved into a horizontal plane parallel to the piston crown and the results plotted at several different crank angle positions throughout the induction and compression periods. It should be mentioned here that, whilst large vertical angles were measured for the air motion during the induction period, these vertical angles were found to be considerably smaller (less than 10 degrees) for the latter stages of the compression period and indeed it was concluded that the air motion was basically two dimensional particularly after 300 degrees crank angle. The results are illustrated in Fig. 6.2 and 6.3 for three different engine speeds, 500, 1000 and 1500 r.p.m., and justify the existence of a forced vortex velocity profile after approximately 90 degrees crank angle during the induction period and throughout the entire compression period. The errors encountered before 90 degrees crank angle may be due to a variety of contributory factors, two of which were outlined in considerable detail in Section 5.6.2 and may be summarised as:

(i) Effect of exhaust valve closure,

(ii) Non-uniformity of flow development.

Another factor which has not been mentioned so far may be observed in Fig. 6.2 and concerns the velocity vector measured for the location R = 2.54 cm., particularly between 60 and 150 degrees crank angle. Reference to Fig. 4.5 reveals that this location is positioned directly

adjacent to the inlet port and therefore it is not unreasonable to suppose that the high magnitudes of velocity may be associated with this location since it is almost directly in line with the inlet port axis. However, these are the only ambiguous points in Fig. 6.2 and the assumption of a forced vortex is supported by the experimental results generally. Figs. 6.2 and 6.3 also compare well with the results of Horvatin and Hussmann (11), Horvatin (31) and Stock (32) whose experimental results are illustrated in Figs. 2.15, 4.18 and 4.19 respectively. Hence, it may be concluded that, for the open combustion chamber similar to that under investigation, the assumption of a forced vortex velocity profile is justified by the experimental evidence.

6.2.3 Mean Swirl Results

In order to investigate the effect of the mean angular velocities of the air motion with engine speed, the experimental results were analysed, refer Section 5.5.3, and a mean angular velocity of the air motion in the cylinder computed assuming that a forced vortex velocity profile existed. These results are illustrated in Figs. 6.4 to 6.6 for engine speeds of 500, 1000 and 1500 r.p.m. and it may be observed that the comparison is good over the majority of the induction and compression periods. The most serious errors occur during the early stages of the induction period and these discrepancies were discussed in detail in Section 5.6.2 when it was found necessary to increase the effective area of the inlet port A^* by 10% for all three engine speeds considered. However, it may be observed that, for each engine speed, the experimental results are consistently below those of the model at the top dead centre position during the compression period and hence this discrepancy was investigated in further detail.

It was suggested in the literature survey, refer Section 2.0, by Alcock and Scott (10), Horvatin and Hussmann (11) and

Shimamoto and Akiyama (14) that considerable blowby of the air past the piston rings may occur whilst the piston approached the top dead centre position and this was a possible explanation for the discrepancy in the results mentioned above. The engine manufacturers supplied some data for blowby measurements made on a similar engine under normal running conditions at an engine speed of 1500 r.p.m. which was approximately 5×10^{-2} kg/s. When computed over a 5 degree crank angle step (i.e. the time during which blowby past the piston rings might occur with the piston approaching the top dead centre position) gives a total mass loss of 0.39×10^{-4} kg. Now the total mass trapped within the cylinder at top dead centre is 8.2×10^{-4} kg and therefore the percentage mass lost due to blowby is approximately 5%. However, because the engine in the present study was only motored for short periods of time and would not therefore attain a typical hot operating temperature, it was considered necessary to justify the quoted figure for blowby past the piston rings.

A single wire anemometer was located in a small diameter breather pipe attached to the crank case inspection cover and the mass flow rate measured from the crank case whilst the engine was motored under test conditions. From the results recorded from the anemometer, it was possible to make an estimation of the blowby loss and this was computed at crank angle positions of 355 and 360 degrees, from which it was concluded that the loss due to blowby was approximately 8.1% and 12.4% respectively. Hence, the mean blowby loss over the last 5 degrees crank angle of the compression period was computed and found to be approximately 10%. This value appeared high compared to that derived from the manufacturer's figures, which resulted in a blowby loss of only 5%. However, considering that under motoring conditions the engine would not attain a normal operating temperature, it was concluded that a figure of 10% blowby loss was not unjustified. In order to

estimate the effect of the blowby loss upon the angular swirl velocity, a further computation was performed adopting the mean blowby loss over the last 30 degrees crank angle of the compression period and this resulted in a maximum decrement in angular velocity of approximately 5% when the piston was in the top dead centre position. Hence the chain curve in Figs. 6.4 to 6.6, which was drawn accounting for friction between the air and the containing surfaces of the cylinder, could be reduced by approximately 5%. However, no attempt was made to include this reduction on Figs. 6.4. to 6.6 in order to avoid confusion, but having computed a total decrement in angular velocity of approximately 5% due to blowby, it may be observed that the computed and experimental results would agree very closely, particularly during the latter part of the compression period. Whilst the angular velocity may be adjusted to account for blowby using the technique outlined above, it must be emphasised that this was only an estimation of the engine blowby losses and hence was only relied upon to give a first approximation of the decrement of angular velocity due to blowby.

6.2.4 Conclusions of the Effect of Engine Speed

Consideration of the various results presented in Figs. 6.1 to 6.6 illustrate that,

(i) The induced velocity through the inlet port,

(ii) The velocities measured at various radial locations,

(iii) The mean angular swirl velocity.

all increase approximately linearly with engine speed. Fig. 6.1 illustrates that the curves of induced velocity through the inlet port follow similar profiles but with an increased magnitude as the engine speed increased. For the velocity inside the engine cylinder, it would appear that for the range of engine speeds considered (500 - 1500 r.p.m.)

a forced vortex velocity profile is a representative description of the air motion after approximately 90 degrees crank angle during the induction period and throughout the compression period, whilst the magnitude of the velocity increases almost linearly with engine speed. This is supported by Fig. 6.7, where the experimental mean angular velocities (computed as outlined in Section 5.5.3) are plotted against engine speed for several crank angle positions throughout the induction and compression periods and this is further supported by the comments of Alcock (1), refer Section 2.3.1 and also the experimental results of Lee (7), Fig. 2.8; Horvatin and Hussmann (11), Fig. 2.15; Ohigashi et. al. (15), Fig. 2.18; and Horvatin (31), Fig. 4.18. Hence it is reasonable to conclude that the air motion may be represented by a forced vortex velocity profile for the cylinder and combustion chamber system under consideration and the magnitude of the swirl increases approximately linearly with engine speed.

6.3 Effect of a Masked Inlet Valve

In order to estimate the effect of a masked inlet valve on the angular velocity of the air within the engine cylinder, the inlet valve was modified to incorporate a 90 degree included angle mask which could be positioned so that the mask centre formed a range of angles from + 45 degrees to - 30 degrees with the inlet port axis, refer Fig. 6.8. Whilst the engine was motored under test conditions, the masked inlet valve was secured in order to prevent it from rotating on the valve seat and a summary of the results using the mask at several locations is illustrated in Fig. 6.8. Observation of Fig. 6.8 reveals that rotation of the mask centre about the inlet port axis has a definite effect upon the angular velocity and that the angular velocity has a

maximum value when the mask centre is positioned in line with the inlet port axis. Figs. 6.9 to 6.11 illustrate the comparison made between the experimental results for optimum mask position and those computed using the mathematical model. It may be observed that the comparison is good and the inclusion of a 90 degree mask did not cause the experimental results to depart from the assumption made for the model and illustrated to hold true for the plain inlet valve in Figs. 6.4 to 6.6. Incidentally, it should be made clear that the inclusion of the masked inlet valve also required the estimation of an effective inlet port area A^* for the valve and this representative value was obtained in an identical manner to that outlined in Section 5.5.2. Consequently, it was not surprising to find that a similar correction had to be made to the value of A^* according to the argument presented in Section 5.6.2 which corrected for the error encountered due to measuring the suction pressure at a location only approximately 1.5 diameters downstream from the tunnel entrance. However, having increased the value of A^* by 10% (as was the case for the plain inlet valve), the comparison between the computed and experimental results was good over the speed range 500 - 1500 r.p.m. Fig. 6.12 also illustrates a comparison between the plain and masked inlet valve results (experimental results for masked inlet valve only) for an engine speed of 1000 r.p.m. and it may be observed that the masked inlet valve results in an increase of the angular velocity by a factor of approximately 1.25.

6.3.1 Conclusions on the Use of the Masked Inlet Valve

It may be concluded that the masked inlet valve increases the angular velocity of the air depending upon the position of the mask centre and that an optimum position exists for the mask centre when the angular velocity will be a maximum. This optimum position

occurs when the mask centre is positioned in line with the inlet port axis and in this position the direction of the air motion is unaffected by the mask and follows a pattern similar to that created by the plain inlet valve. Comparison may be made between Fig. 6.8 and the work of Ohigashi et.al. (15) whose work is presented in Section 2.6.4 and illustrated in Fig. 2.19 and it may be observed that similar conclusions can be made from this work when considering the effect of the masked inlet valve upon the magnitude and direction of the air motion.

6.4 Effect of Engine Supercharging at 10 p.s.i.g.

Recommendation (v) of Section 2.5 suggested that the air swirl within the engine cylinder might be increased if the quantity of air induced into the cylinder were increased and this suggestion led to the possibility of supercharging the engine. A supercharge system was developed which utilised a high pressure air supply to charge the reservoir illustrated in Fig. 6.13 to a pressure of 10 p.s.i.g. The reservoir was then connected to the inlet port of the cylinder under investigation and the assembly used to supply air at a pressure of 10 p.s.i.g. to the inlet port. During the preliminary tests with the engine, it was found that a suitable operating range for the engine was 750 r.p.m. - 1250 r.p.m. since below 750 r.p.m. unnecessary oscillation of the air within the inlet port occurred, whilst above 1250 r.p.m., the reservoir pressure could not be maintained sufficiently accurately at 10 p.s.i.g. by the high pressure supply. This latter problem could have been overcome had larger diameter supply piping been available but, under the circumstances, it was concluded that the speed range of 750 - 1250 r.p.m. was adequate to check the validity of the mathematical model under supercharge conditions.

As a preliminary check of the capabilities of the model, the velocity of the induced air in the inlet port was measured whilst the engine was operated using the supercharge system and the results are illustrated in Fig. 6.14. It may be observed that the curve profiles are very similar to those illustrated in Fig. 6.1 and the agreement between the experimental and theoretical points of Fig. 6.14 is good throughout the induction period, thus justifying that the mathematical model will predict accurately the mass flow rate into the engine cylinder under supercharge conditions. The mean angular velocities were also computed for the induction and compression periods in a similar manner to that outlined in Section 6.2.3 and observation of Figs. 6.15 to 6.17 illustrates that the agreement between the experimental and theoretical results is good during the induction and compression periods. In Fig. 6.18 a comparison is made between the results for the supercharge and non-supercharge (plain inlet valve used) at an engine speed of 1000 r.p.m. and it may be observed that supercharging at 10 p.s.i.g. results in an increase in the angular velocity of the air by a factor of approximately 2.0.

6.4.1 Conclusion on the Inlet Manifold Supercharge System

From the results illustrated in Figs. 6.15 to 6.17 it may be concluded that the mathematical model may be used to predict the air motion within the engine cylinder when the engine is supercharged at 10 p.s.i.g. The magnitude of the angular velocity is increased by a factor of approximately 2 and the assumption of conservation of momentum and a forced vortex velocity profile are shown to be reliable assumptions for the supercharge condition.

6.5 Squish Velocity

Referring to Section 5.7, a comparison was made between the theoretical squish velocity computed using the model developed by Fitzgeorge and Allison (9) (which neglects friction) and that measured experimentally at the edge of the combustion chamber using the hot wire anemometer. Fig. 5.11 shows that the agreement between the experimental and computed results at an engine speed of 1000 r.p.m. is good and suggests that, whilst the air motion may be described by a forced vortex velocity profile, during the latter 40 degrees of the compression period a definite radial component of velocity exists as the air is transferred from the outer cylinder into the combustion chamber. In order to investigate the squish velocity (inward radial component of flow) in further detail, the velocity components at the radial locations R = 3.18 cm, 3.49 cm. and 3.81 cm., refer Fig. 4.5, were resolved into (a) the horizontal plane (parallel to the piston crown) and (b) into the radial direction. These were then compared to the computed squish velocity using the Fitzgeorge and Allison (9) model at the particular locations concerned. Figs. 6.19 to 6.21 illustrate these comparisons and it may be observed that the comparisons illustrated in Figs. 6.19 and 6.20 at R = 3.18 cm. and 3.49 cm. is reasonable and again justify the adoption of a simple model such as that of Fitzgeorge and Allison (9) to obtain the radial inward component of the flow. However, the comparison illustrated in Fig. 6.21 is poor, particularly for the engine speeds of 1000 and 1500 r.p.m. when the experimental results are approximately 400% greater in magnitude than the computed results at 350 degrees crank angle. This error may be attributed to several factors.

(i) According to the theory developed for the squish velocity, the velocity would be zero at the cylinder wall. However, due to the effect of blowby past the piston rings, there is a strong possibility that there is a velocity component in the radial direction towards the cylinder wall, which may be described as a reversed squish velocity during the compression period. This phenomena was not recorded by Shimamoto and Akiyama(14) in their experimental squish investigation, refer Section 2.6.3, and Fig. 2.17 as the authors only measured the squish at the inside edge of the combustion chamber and would therefore not encounter this phenomena. Hence, one explanation of the high experimental results may be attributed to the proposed reversed squish during the compression period.

(ii) A more plausible explanation for the poor comparison between computed and experimental results at R = 3.81 cm. may be due to the possibility of the spiral flow pattern into the combustion chamber postulated in Section 2.3.4. If the air spiralled into the combustion chamber during the latter stage of the compression period, obviously there is a position where the air will actually enter the chamber. Observation of the actual velocity profiles illustrated in Figs. 6.24 and 6.25 and the colour photograph of the piston crown subjected to a paint test, Fig. 6.26, suggests that the air does spiral into the combustion chamber and that the point of entry is in the vicinity of the location R = 3.81 cm., refer Fig. 4.5. Hence, this could be a further explanation of the high experimental results obtained when this swirl velocity was resolved into the radial direction.

As mentioned previously, however, the results illustrated that the air certainly has a radial component of velocity and when the mean of the resolved swirl results was compared to the mean of the computed results, refer Fig. 6.22, then a reasonable comparison is

obtained. Fig. 6.23 also illustrates the comparison made between the experimental results measured at the edge of the combustion chamber, refer Section 5.7, and these computed at this position. Again, the agreement between the computed and experimental results is good and justified the use of the simple model for computing the radial flow component. It must be emphasised, however, that due to the extremely simple assumptions of the model (assumes a purely radial transfer of the cylinder contents from the outer cylinder area into the combustion chamber) it is not possible to predict the precise radial velocity component at all radial locations on the piston crown as Fig. 6.21 illustrates. There is evidence, however, refer Fig. 6.23, that at the edge of the combustion chamber, the radial velocity component may be computed with reasonable accuracy (greatest error between computed and experimental results is approximately 20%, neglecting the 360 degree position which was discussed in considerable detail in Section 5.7).

In conclusion, it would appear reasonable to compute the swirl velocity assuming momentum to be conserved throughout the induction and compression periods whilst a forced vortex velocity profile exists and friction is accounted for particularly when the surface to volume ratio increases. The squish may be computed using the Fitzgeorge and Allison (9) model, neglecting friction since the comparisons illustrated in Figs. 6.22 and 6.23 are reasonable, and it should then be possible to compute both the radial and tangential velocities at any crank angle position. The tangential and radial velocities may then be combined by simple vector addition (assuming a two dimensional flow since the vertical angle was shown to be less than ten degrees during the latter part of the compression period) to obtain both the magnitude and direction of the air motion at the edge of

the combustion chamber. This vector may then be taken as a representative value of the air velocity and direction and be used in subsequent computation of heat transfer and/or fuel spray investigations.

6.6 Air Motion During the Induction and Compression Periods

Summarising the discussion for the air motion during the induction period, it was concluded that, before 90 degrees crank angle, the air motion was three dimensional in nature and a forced vortex velocity profile had not developed, refer Figs. 4.12 and 4.13. Several arguments were postulated for the poor development of a forced vortex velocity profile during the early part of the induction period and these may be summarised by,

(i) Effect of exhaust valve closure,

(ii) Poor development of an orderly flow about the cylinder axis,

(iii) Location of one measuring position adjacent to and directly in line with the inlet port axis.

However, during the latter part of the induction period and throughout the compression period, the air motion may be described by a forced vortex velocity profile and this was justified by the experimental results illustrated in Figs. 6.2. and 6.3. Referring to the criticism of the work of Fitzgeorge and Allison (9), Section 2.3.4, where the authors postulated the presence of a rotary toroidal motion of the air within the combustion chamber as the piston approached

the top dead centre position, it was suggested that this pattern of air motion might not occur if the swirl were of greater magnitude than the squish (radial inward component of the flow). This hypothesis (already outlined in considerable detail in Section 2.3.4) was supported by Alcock and Scott (10), refer Section 2.3.5, who found little evidence of any toroidal motion in their combustion films but instead suggested that the air spirals into the combustion chamber as the top dead centre position was approached and photographic evidence was presented by the authors which supported this condusion, refer Fig. 2.13. Observation of the present investigation at 1000 r.p.m. illustrates that the maximum angular swirl velocities are high and of the order of 60 m/s (20000 r.p.m.) at the combustion chamber radius whilst the squish velocity (radial component of the velocity vector) at the same combustion chamber radius is approximately 16 M/S when the piston is at 353 degrees crank angle. Consequently, it is reasonable to presume that the swirl, being greater in magnitude than the squish by a factor of approximately 4.0, would result in the air spiralling into the combustion chamber and continuing to rotate within the chamber in accordance with the conservation of angular momentum (friction being accounted for). This hypothesis certainly supports that of Alcock and Scott (10) and is also justified by the experimental evidence illustrated in Figs. 6.24 and 6.25 where the individual velocity vectors of the air motion are drawn accurately in the horizontal plane and it may be observed that, as top dead centre is approached during the compression period, the air does spiral into the combustion chamber. This spiral motion is also illustrated by the photograph of the piston crown, refer Fig. 6.26, which was subjected to a paint and motoring test similar to that adopted by Dicksee (8), refer Section 2.33, and Alcock and Scott (10), refer Section 2.3.5, Indeed, the comparison between Figs. 6.24 and 6.25 and Fig. 6.26 are good and justify the

hypothesis presented for the spiral motion of the air into the combustion chamber as the piston approaches the top dead centre position.

Further consideration was given to the air motion during the compression period and the swirl ratio, defined by Alcock (1) as the air motion r.p.m./engine r.p.m., was computed for several crank angle positions during the compression period. The results are illustrated in Fig. 6.27 and it may be observed that the swirl ratio is approximately constant (within a tolerance of 25%) as the engine speed is varied in the range 500 - 1500 r.p.m. This is in accordance with the experimental results recorded by Alcock (1) in 1934 and summarised in conclusion (ii), refer Section 2.3.1. From the experimental results of the present investigation, the magnitude of the swirl ratio is approximately 20 at the top dead centre position and this value compares well with the experimental results of Horvatin (31) and Stock (32) whose experimental results are illustrated in Figs. 4.18 and 4.19 and result in swirl ratios at the top dead centre position of approximately 18 and 20 respectively. It was concluded, therefore, that the swirl ratios of the present investigation were not exceptionally high but compared favourably with the results of other investigations performed on engines of similar design and size.

Finally, investigation was made of the increase in magnitude of the angular velocity throughout the compression period. Ideally, assuming that the inlet valve closes at 180 degrees crank angle and angular momentum is conserved throughout the compression period, then the increase in angular velocity would be equal to the ratio D^2/d^2, where D is the cylinder diameter and d the combustion chamber diameter. Dicksee (8) suggested that, because of the effect of friction between the air and the containing surfaces of the cylinder and the possibility of blowby past the piston rings, the increase in angular velocity would not be equal to D^2/d^2 but a more realistic estimate would be the ratio D/d.

For the engine considered in the present investigation, the ratio $D^2/d^2 = 3.5$ and $D/d = 1.86$ whilst investigation of Figs. 6.4 to 6.6 reveals that, for the compression period, the experimental angular velocity increases by a factor of approximately 2.5 (taking the mean of the 3 curves considered). Hence, it may be concluded that, for the particular engine under investigation, the increase in angular velocity throughout the compression period is not equal to either the ratio D^2/d^2 or D/d, but instead a representative value is the mean of these two ratios, i.e. increase in swirl ratio during the compression period $= \frac{1}{2}\left(\frac{D^2}{d^2} + \frac{D}{d}\right)$.

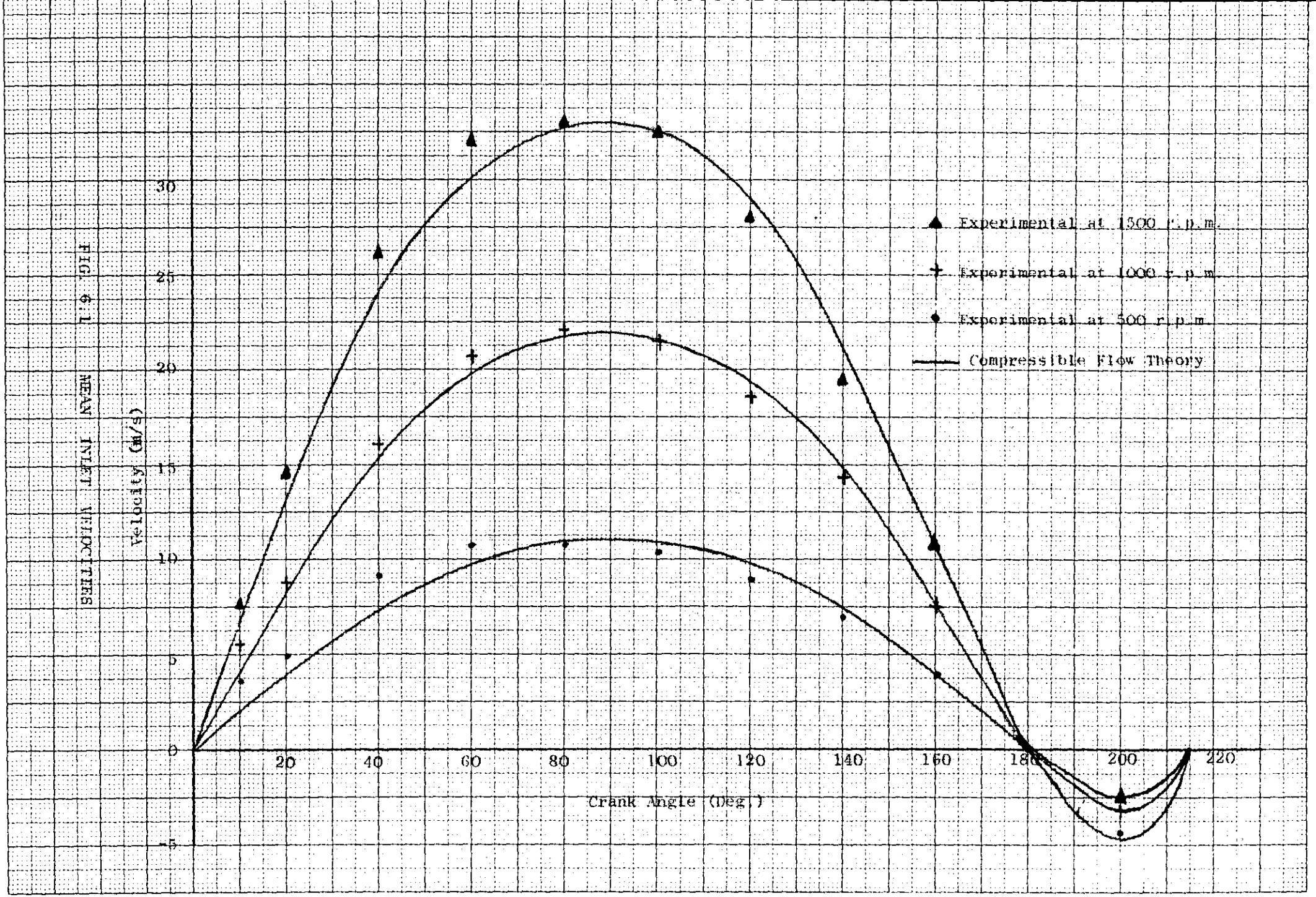

FIG. 6.1 MEAN INLET VELOCITIES

▲ 500 r.p.m. + 1000 r.p.m. ▲ 1500 r.p.m. Scale 1 cm = 20 m/s

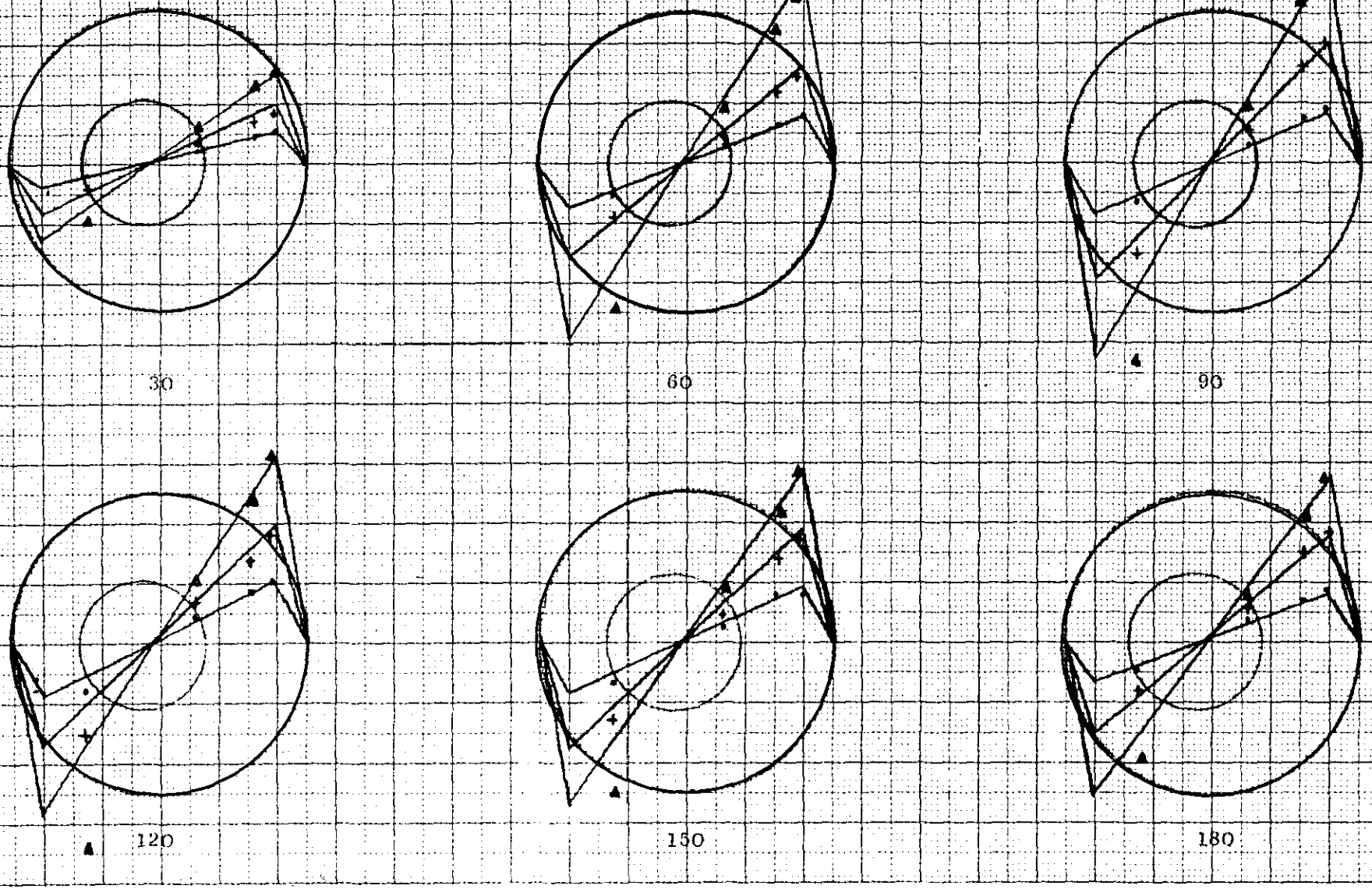

FIG. 9.2 VELOCITY PROFILES THROUGHOUT THE INDUCTION PERIOD

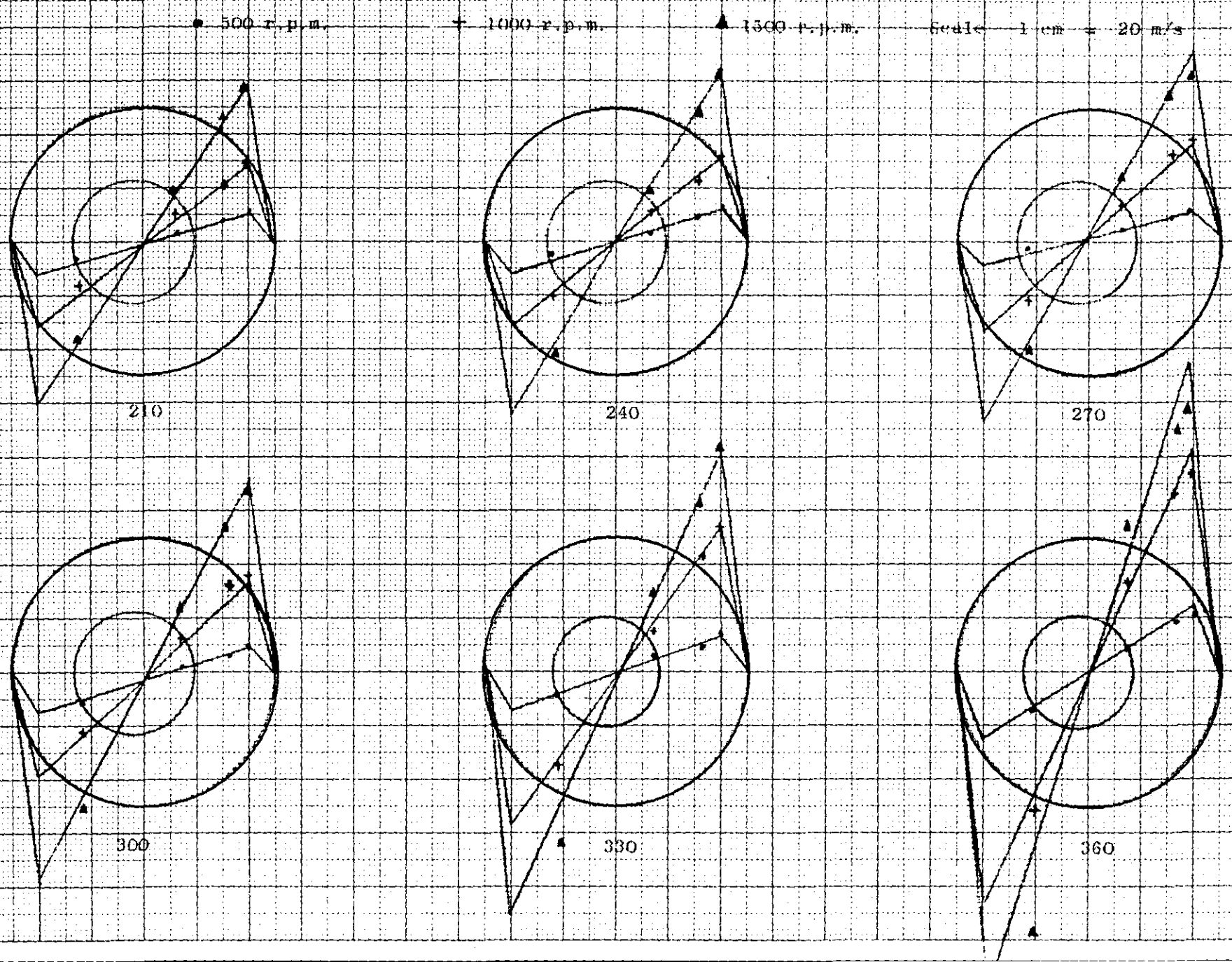

FIG. 6.3 VELOCITY PROFILES THROUGHOUT THE COMPRESSION PERIOD

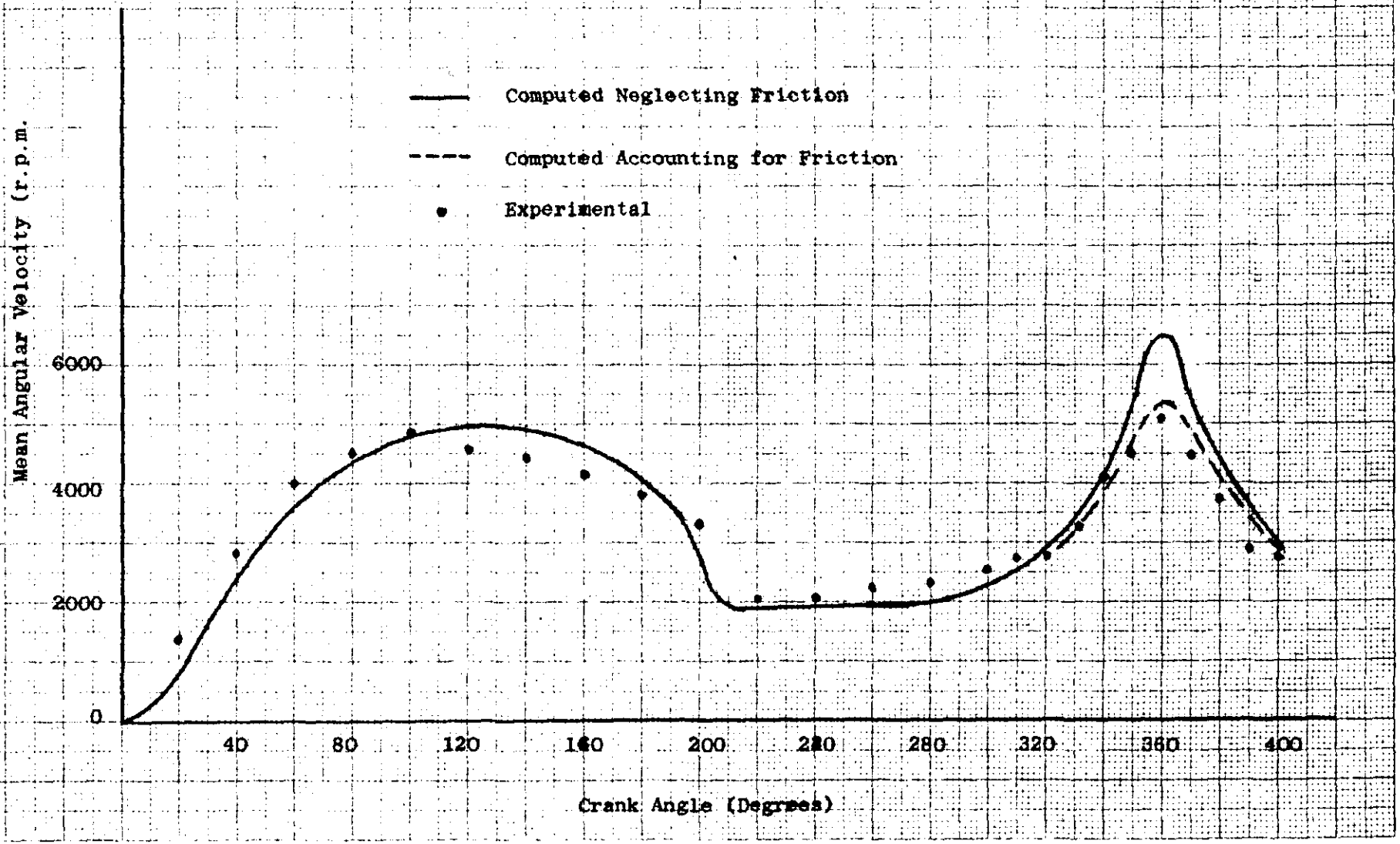

FIG. 6.4 MEAN ANGULAR VELOCITY USING A PLAIN INLET VALVE AND ENGINE RUNNING NORMALLY AT 500 R.P.M.

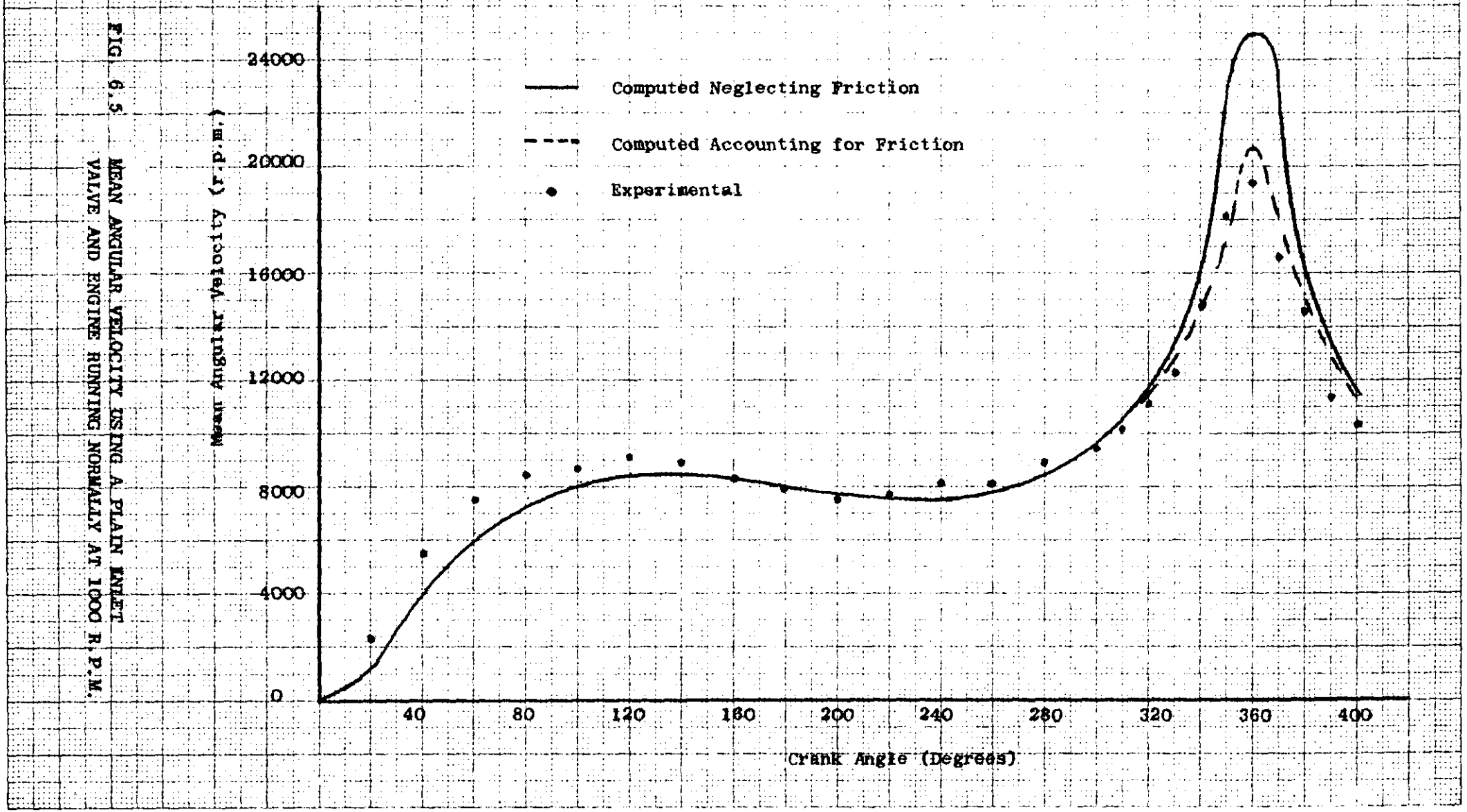

FIG 6.5 MEAN ANGULAR VELOCITY USING A PLAIN INLET VALVE AND ENGINE RUNNING NORMALLY AT 1000 R.P.M.

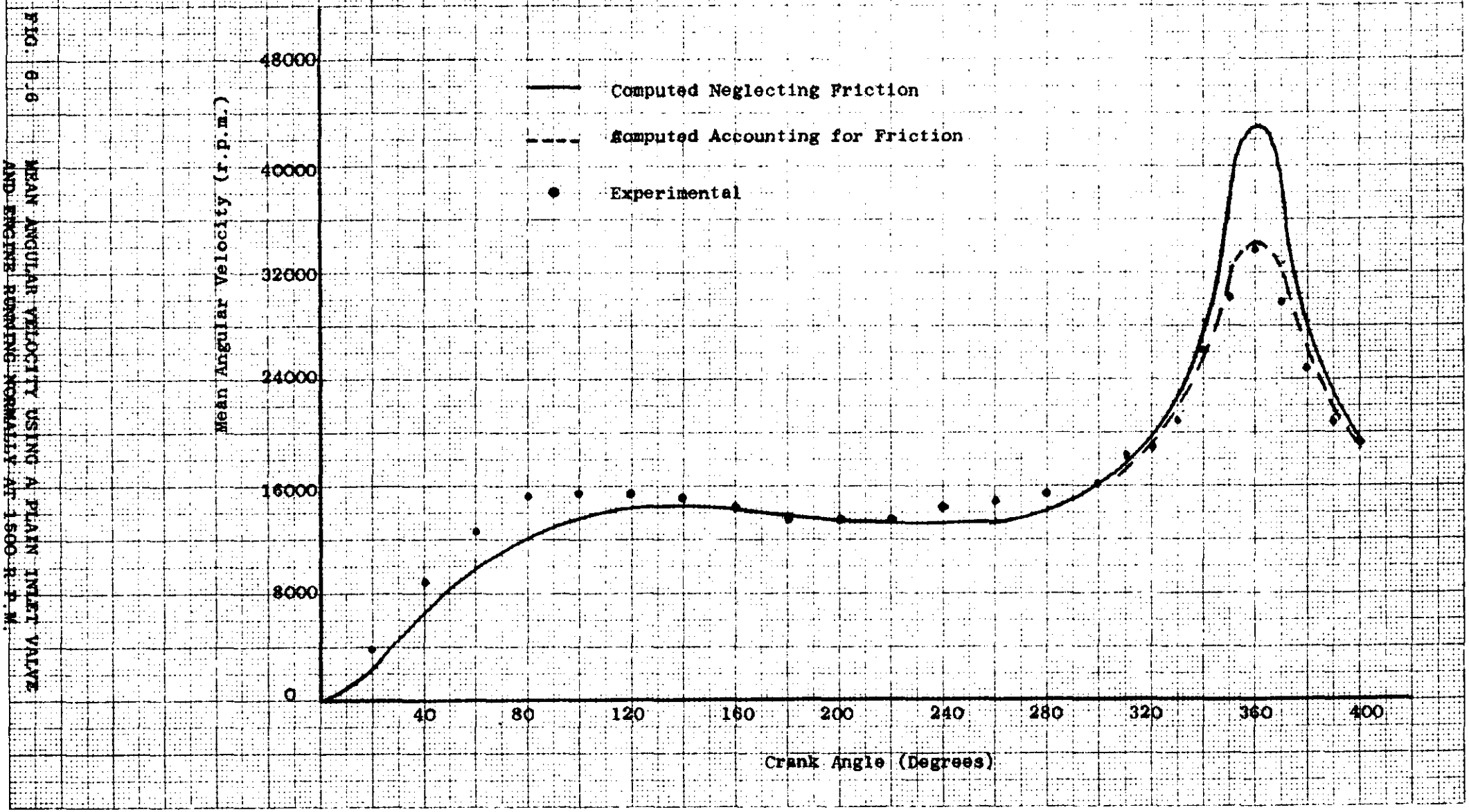

FIG. 8-6 MEAN ANGULAR VELOCITY USING A PLAIN INLET VALVE AND ENGINE RUNNING NORMALLY AT 1500 R.P.M.

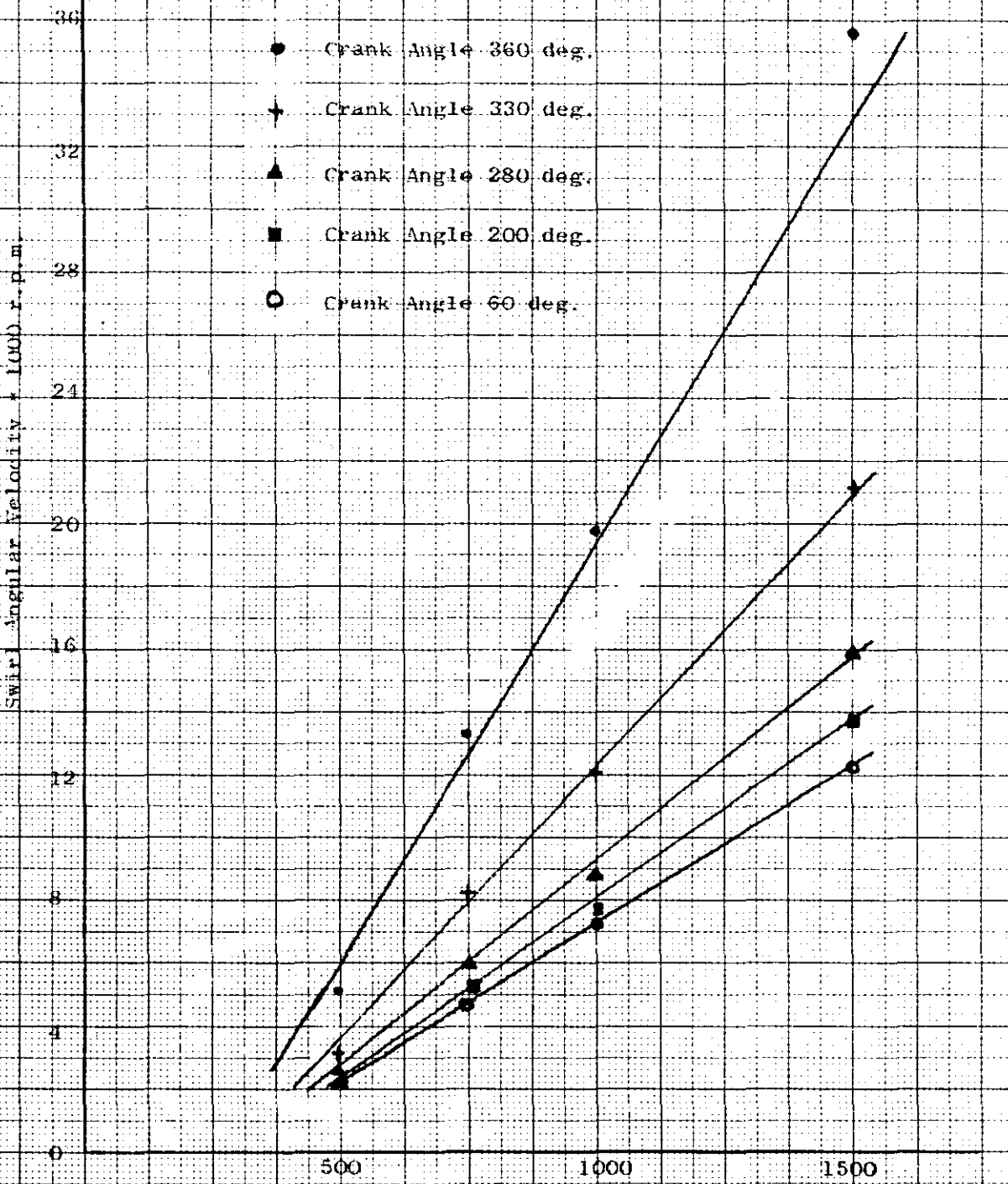

FIG. 6.7 SWIRL R.P.M. PLOTTED AGAINST ENGINE R.P.M. AT DIFFERENT CRANK ANGLE POSITIONS

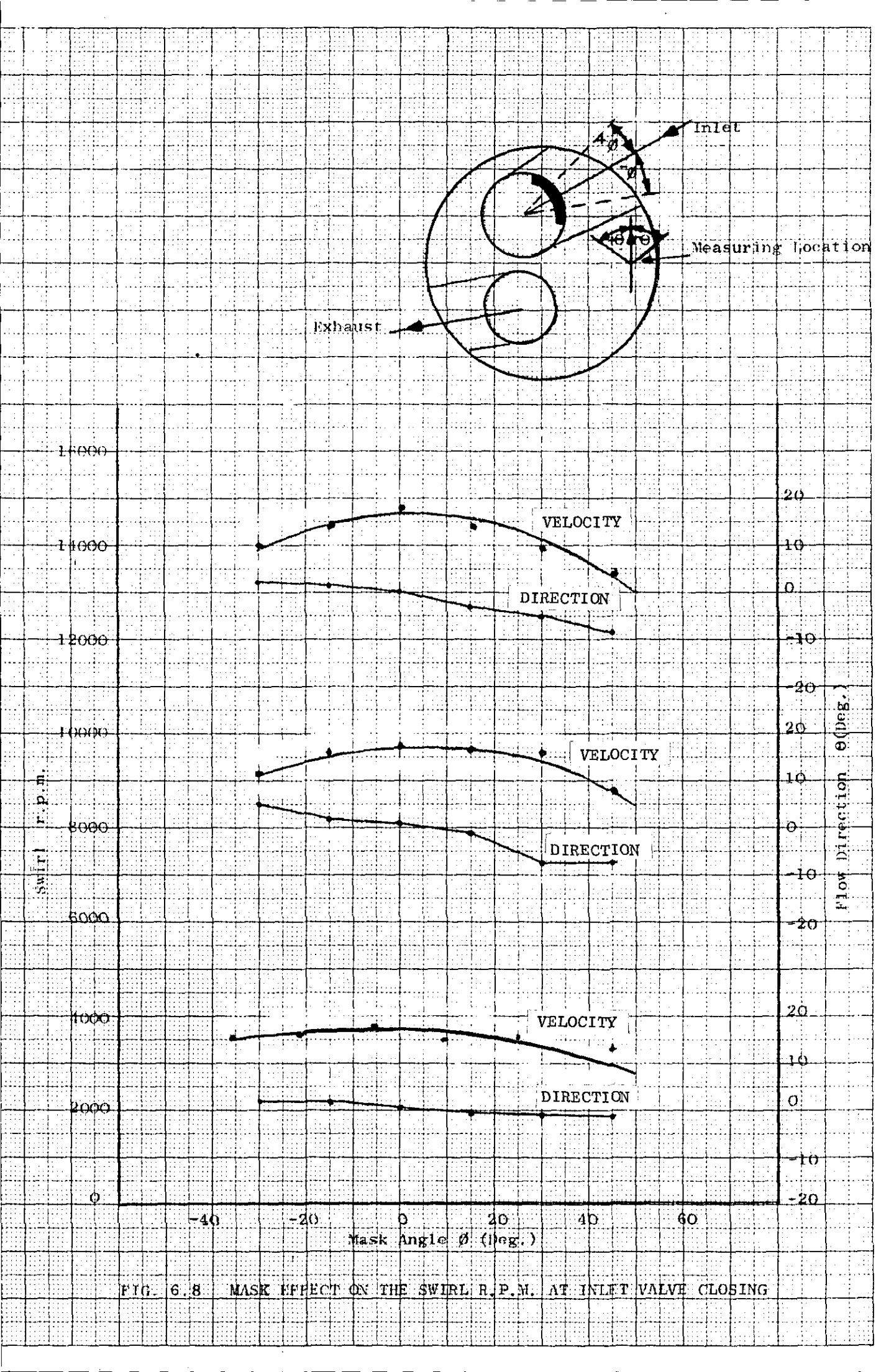

FIG. 6.8 MASK EFFECT ON THE SWIRL R.P.M. AT INLET VALVE CLOSING

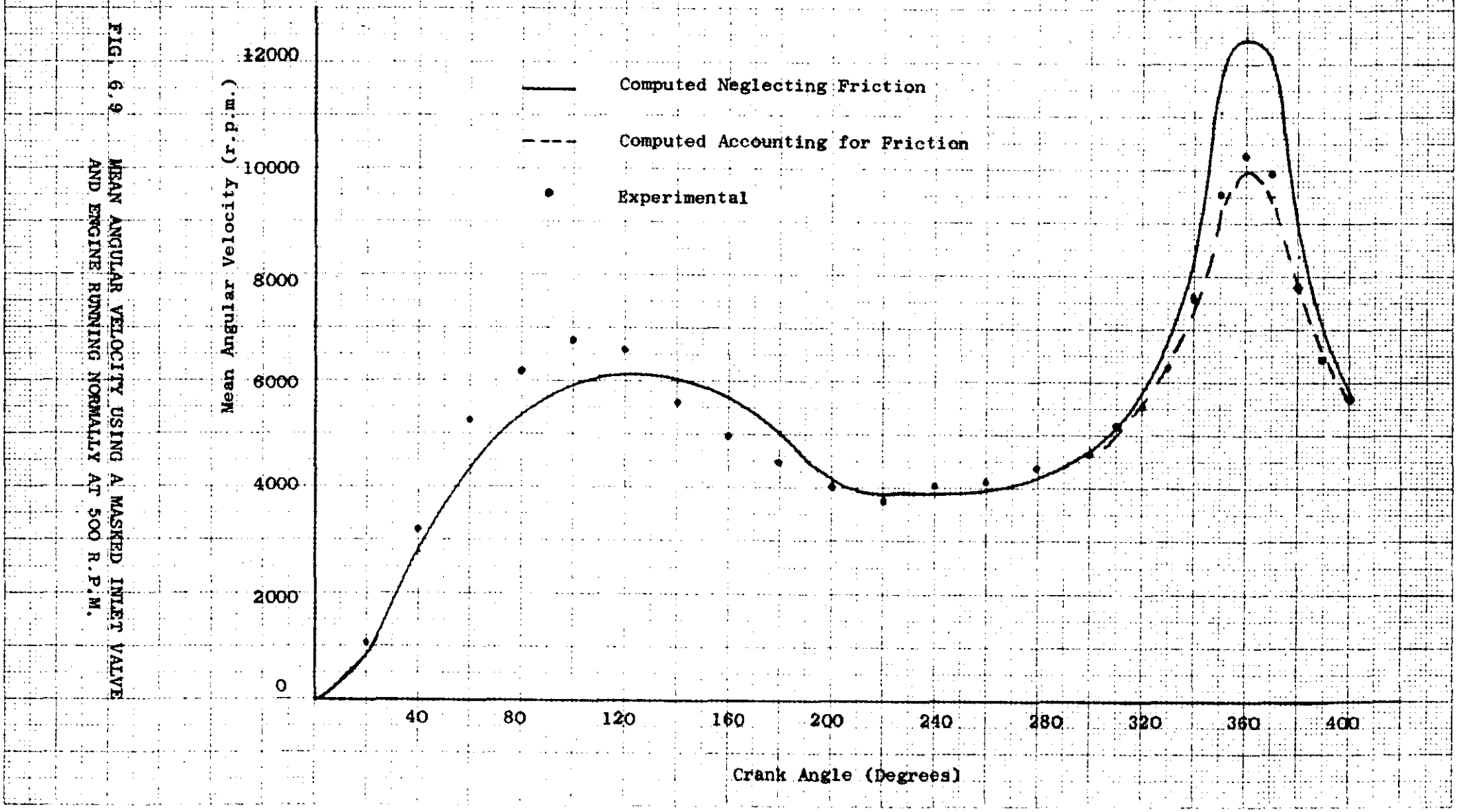

FIG. 6.9 MEAN ANGULAR VELOCITY USING A MASKED INLET VALVE AND ENGINE RUNNING NORMALLY AT 500 R.P.M.

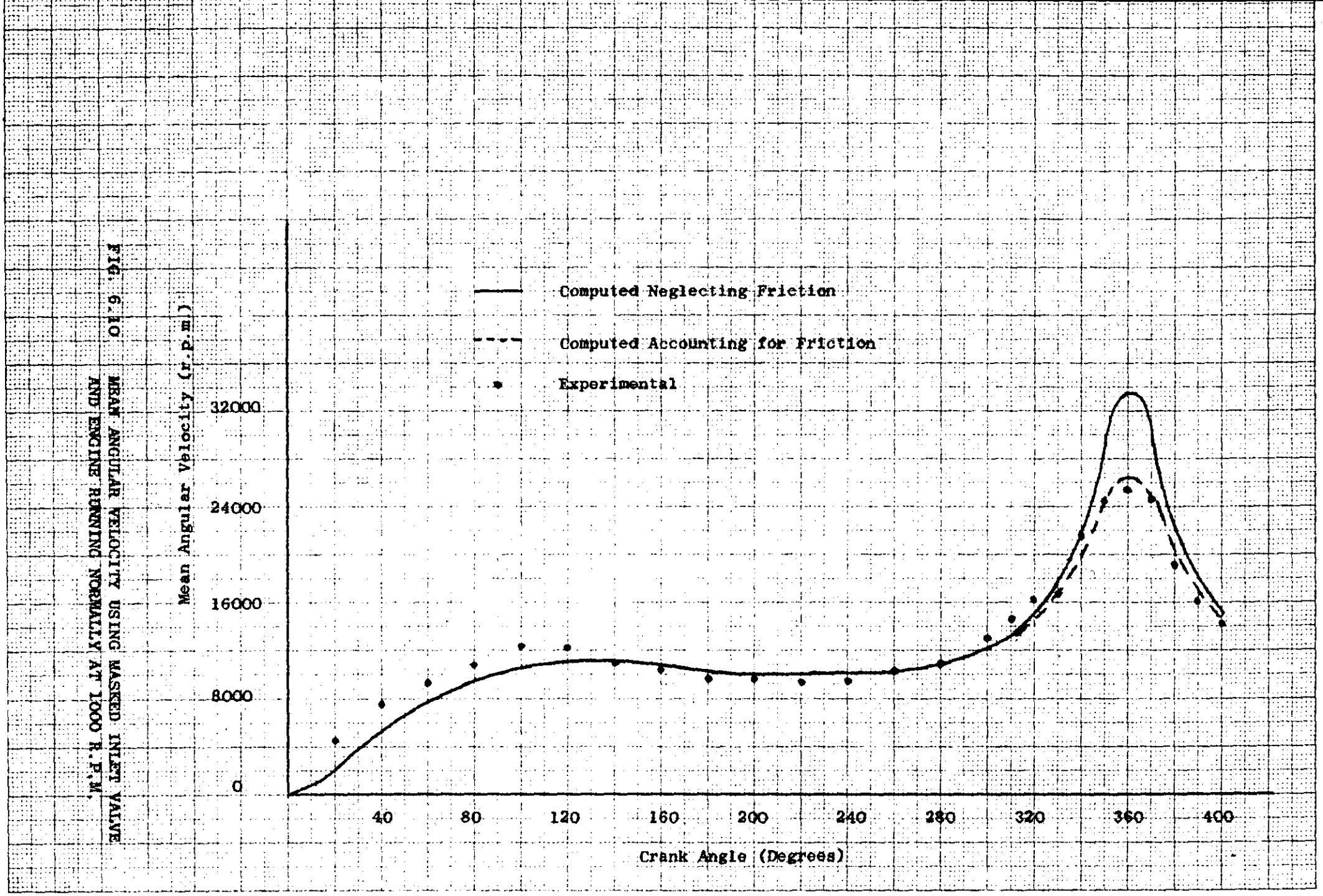

FIG. 6.10 MEAN ANGULAR VELOCITY USING MASKED INLET VALVE AND ENGINE RUNNING NORMALLY AT 1000 R.P.M.

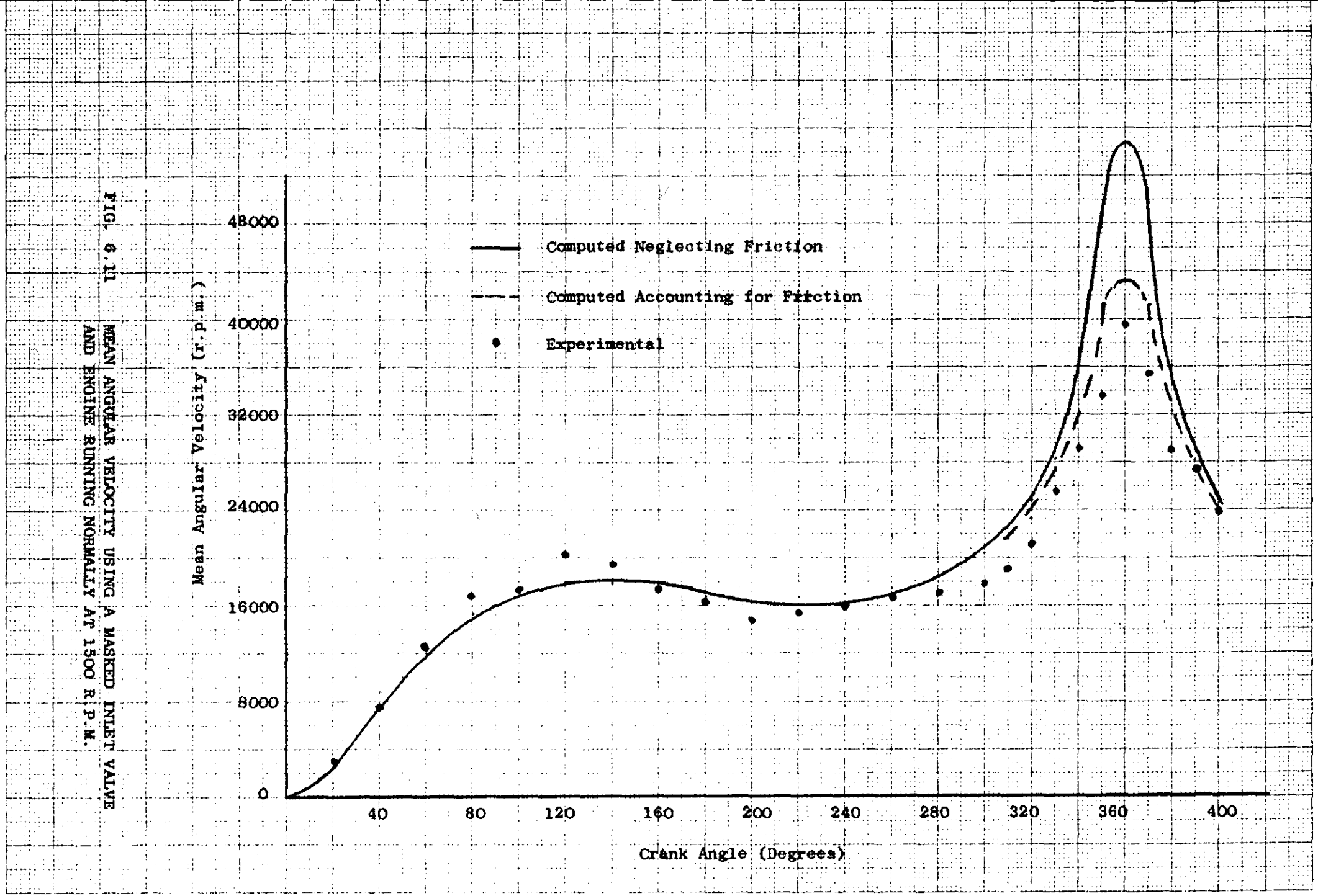

FIG. 6.11 MEAN ANGULAR VELOCITY USING A MASKED INLET VALVE AND ENGINE RUNNING NORMALLY AT 1500 R.P.M.

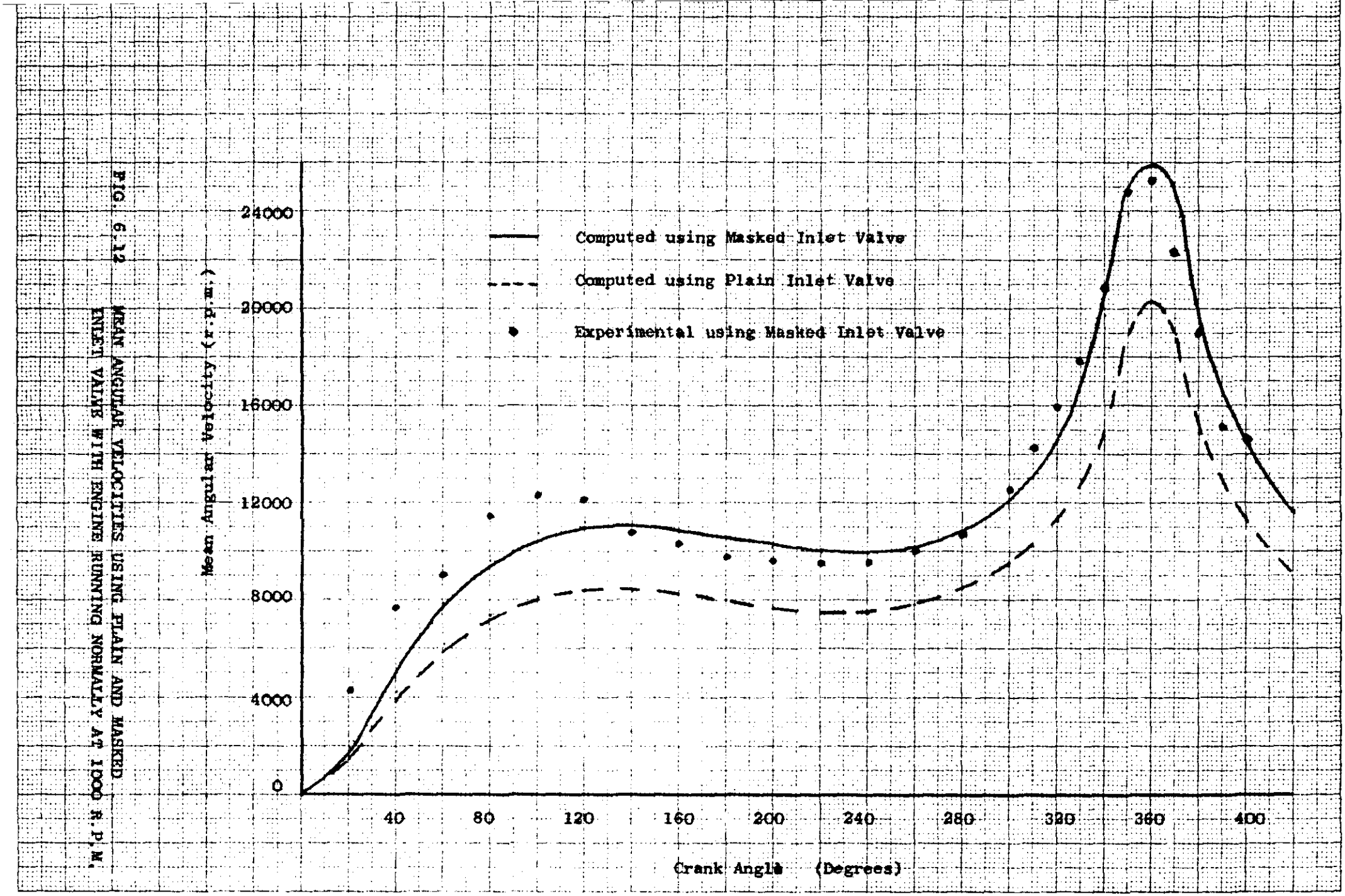

FIG. 6.12 MEAN ANGULAR VELOCITIES USING PLAIN AND MASKED INLET VALVE WITH ENGINE RUNNING NORMALLY AT 1000 R.P.M.

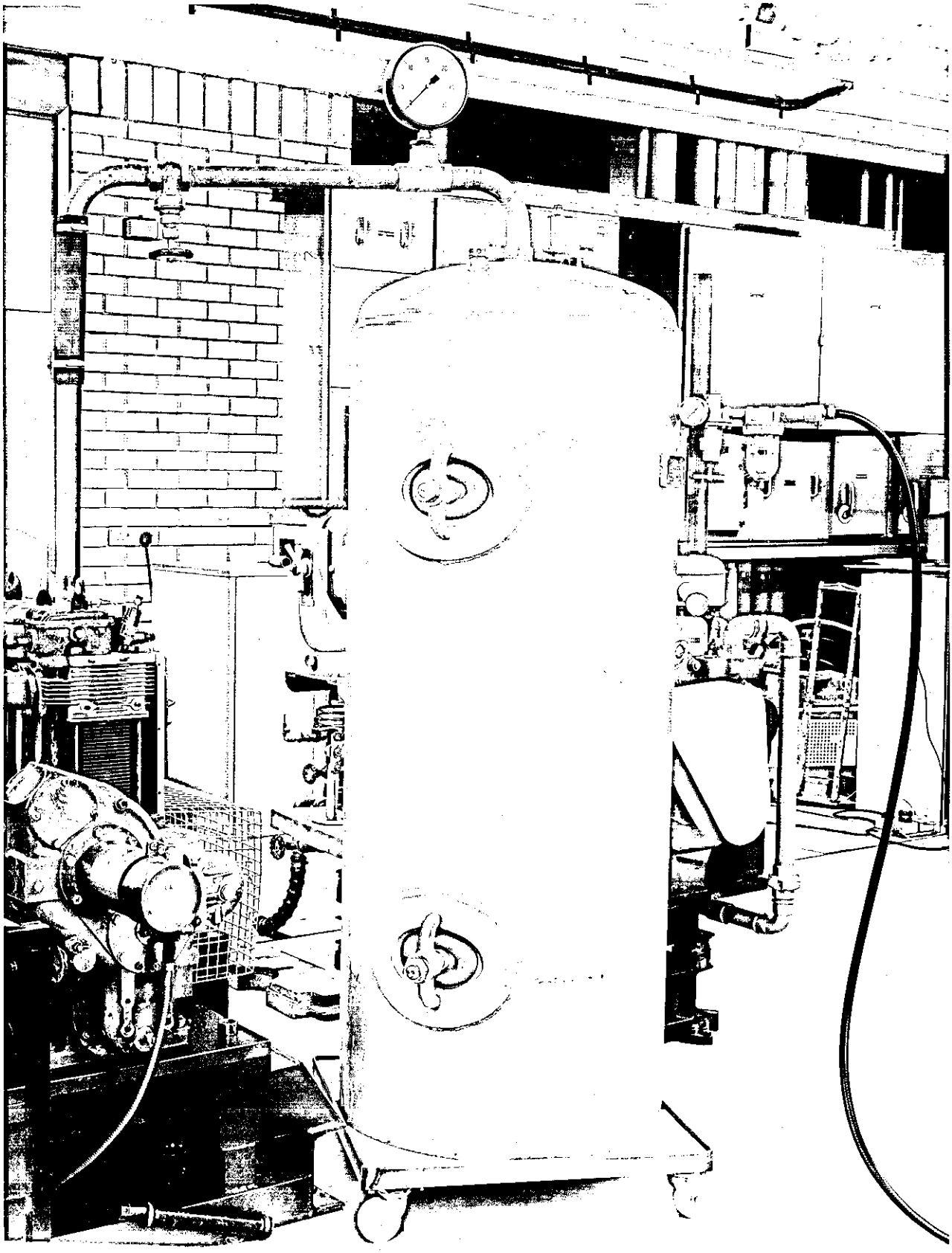

FIG. 6.13 EXPERIMENTAL SUPERCHARGE SYSTEM

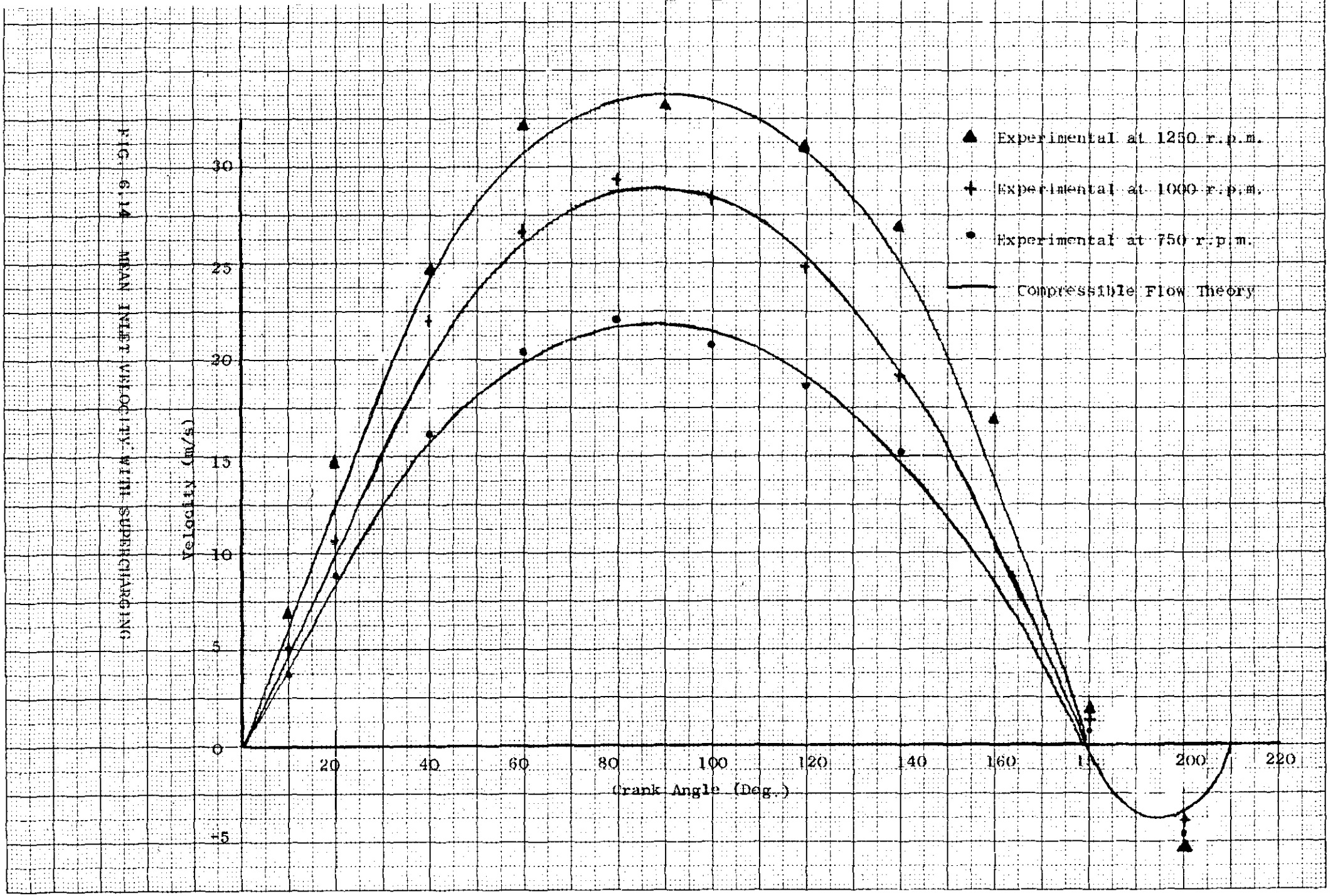
FIG. 6.14 MEAN INLET VELOCITY WITH SUPERCHARGING
Experimental at 1250 r.p.m.
Experimental at 1000 r.p.m.
Experimental at 750 r.p.m.
Compressible Flow Theory
Velocity (m/s)
30
25
20
15
10
5
0
-5
20
40
60
80
100
120
140
160
180
200
220
Crank Angle (Deg.)

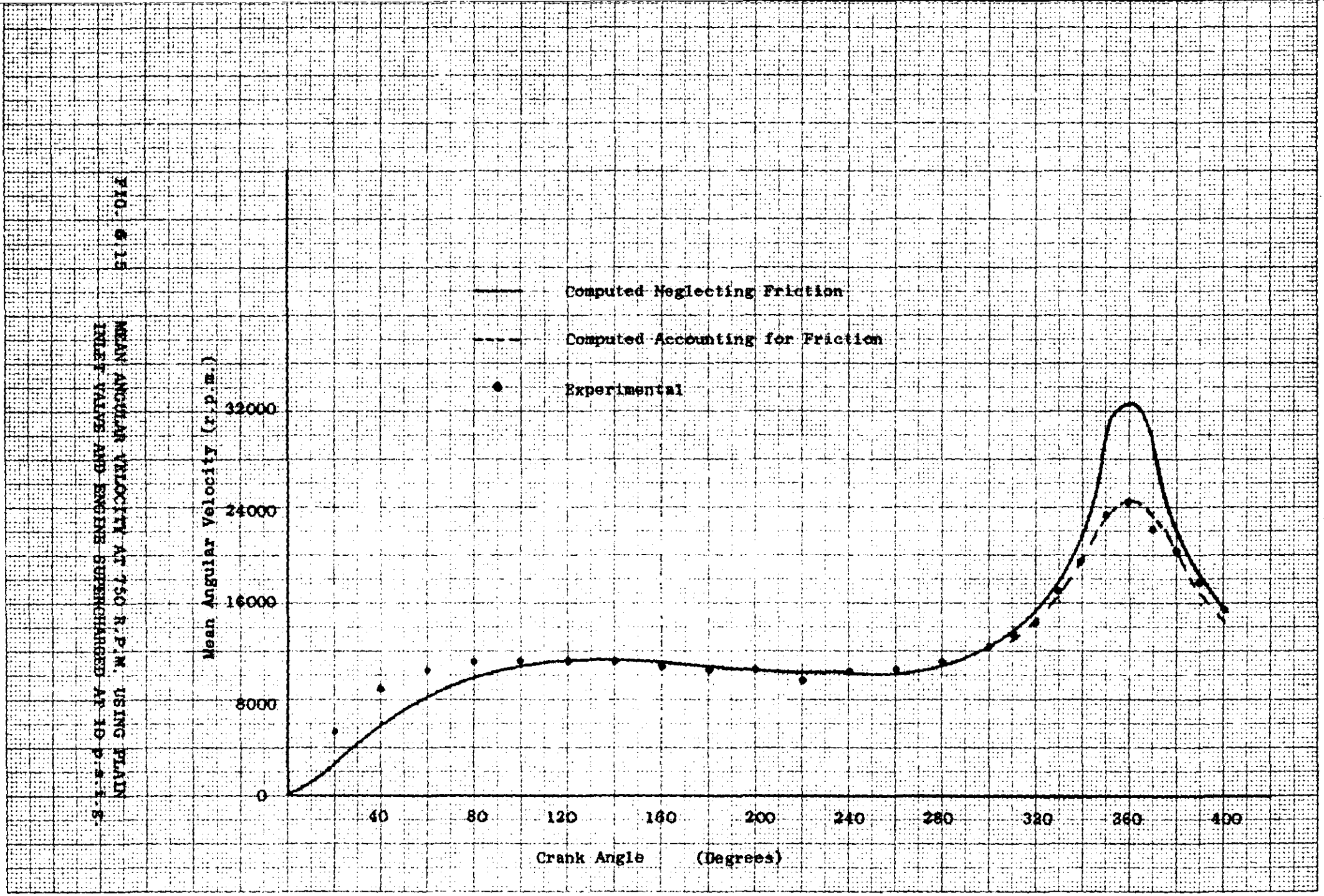

FIG. 115. MEAN ANGULAR VELOCITY AT 750 R.P.M. USING PLAIN INLET VALVE AND ENGINE SUPERCHARGED AT 10 P.S.I.G.

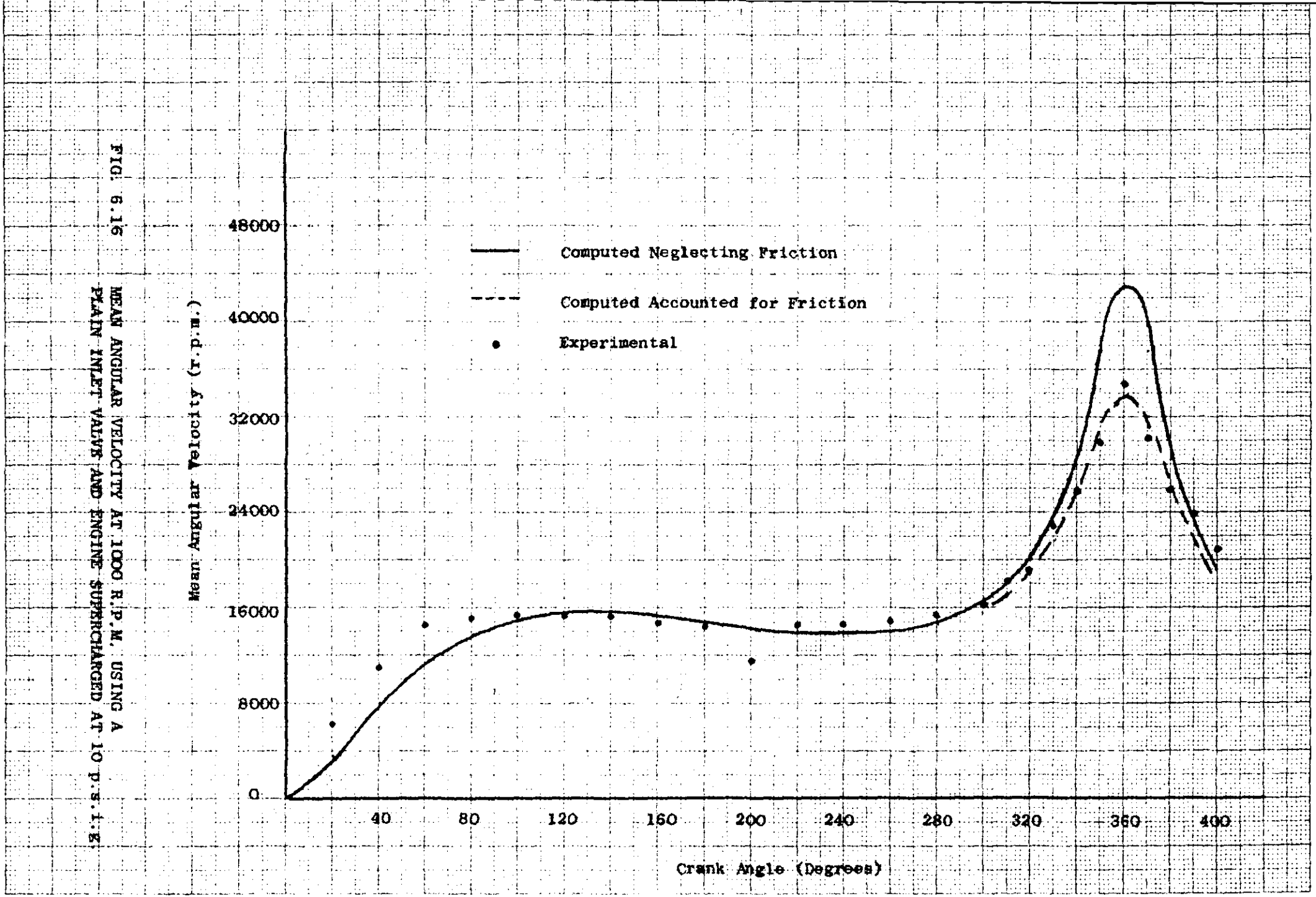

FIG. 6.16 MEAN ANGULAR VELOCITY AT 1000 R.P.M. USING A PLAIN INLET VALVE AND ENGINE SUPERCHARGED AT 10 p.s.i.g.

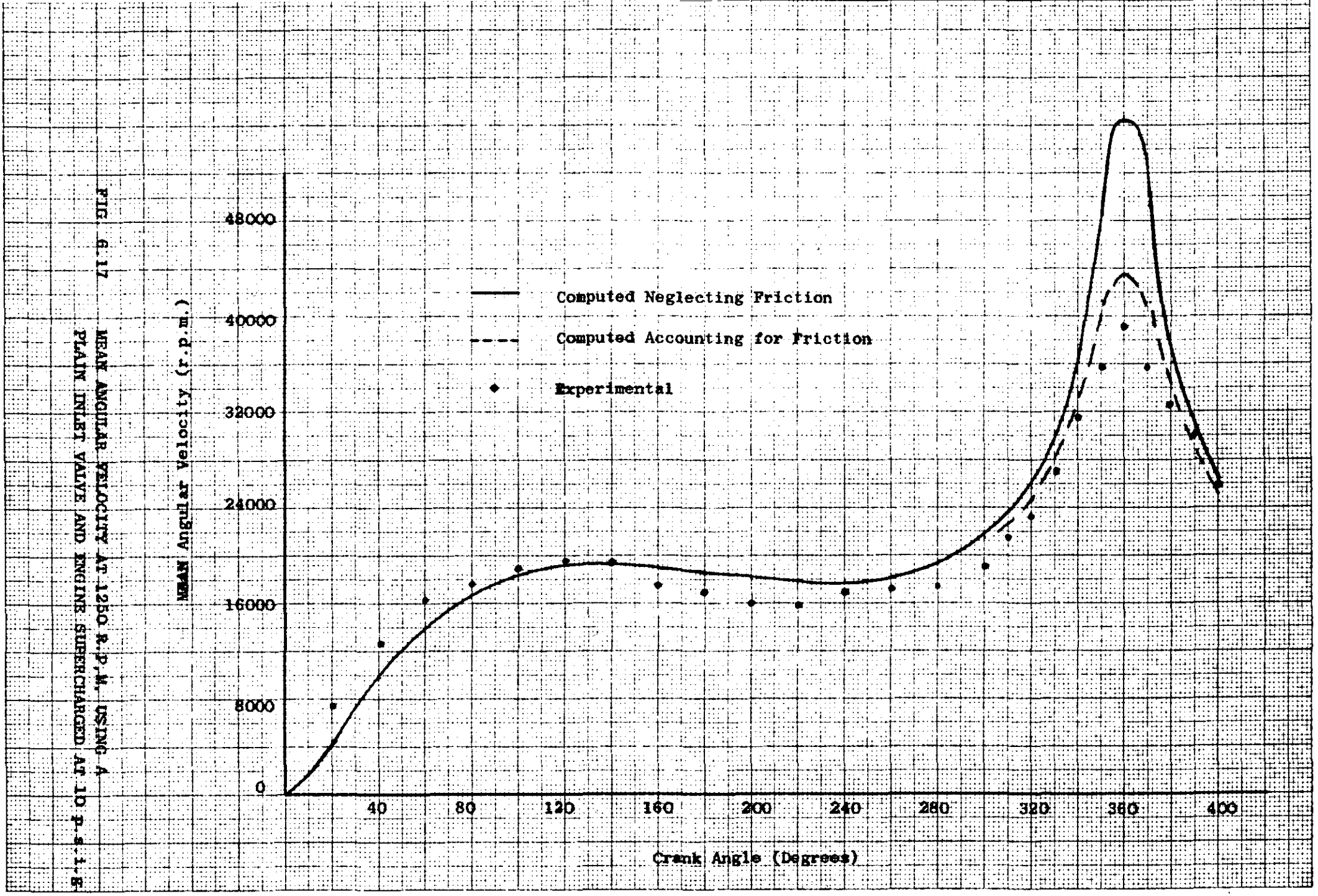

FIG. 6.17 MEAN ANGULAR VELOCITY AT 1250 R.P.M. USING A PLAIN INLET VALVE AND ENGINE SUPERCHARGED AT 10 p.s.i.g.

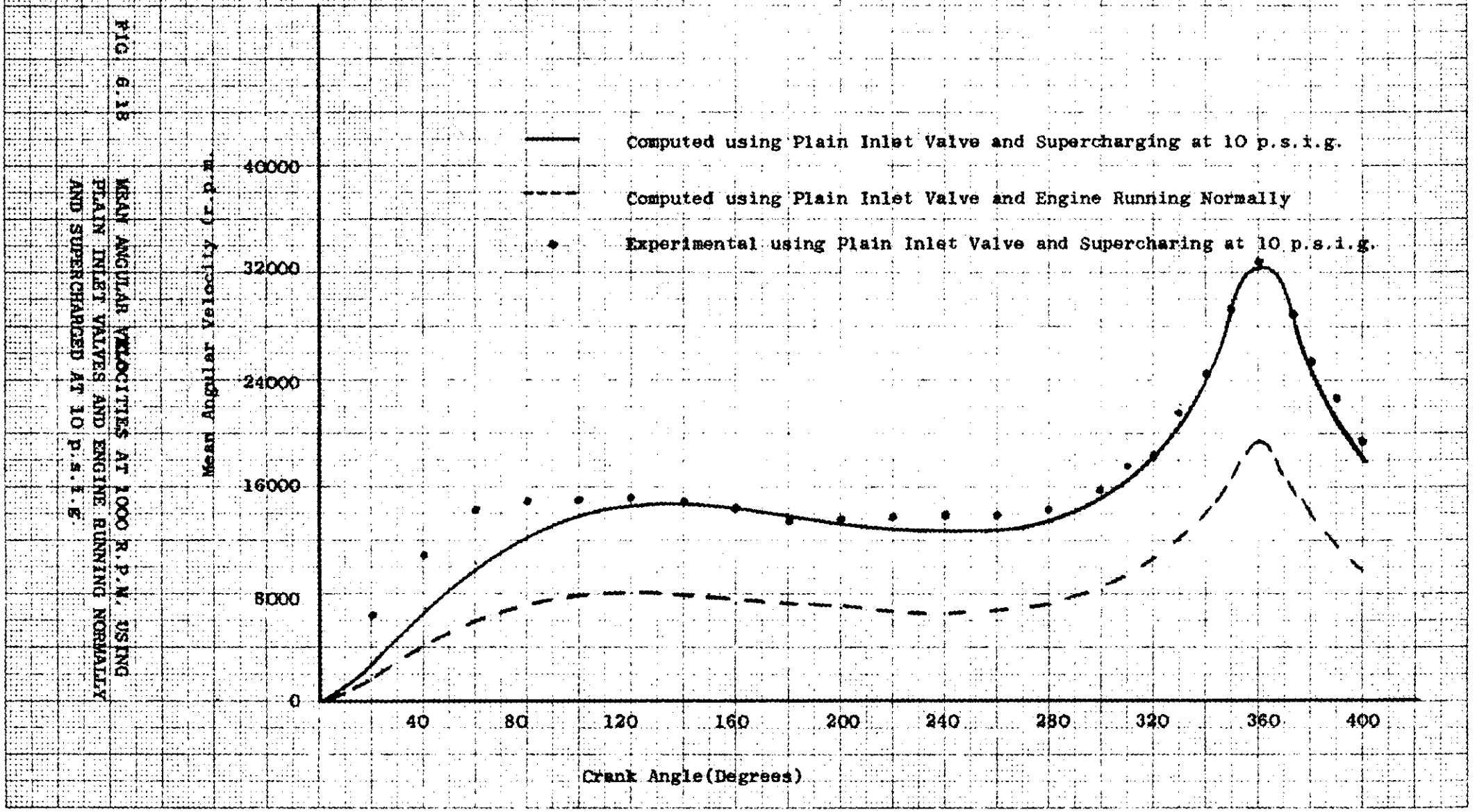

FIG. 6.18 MEAN ANGULAR VELOCITIES AT 1000 R.P.M. USING PLAIN INLET VALVES AND ENGINE RUNNING NORMALLY AND SUPERCHARGED AT 10 p.s.i.g.

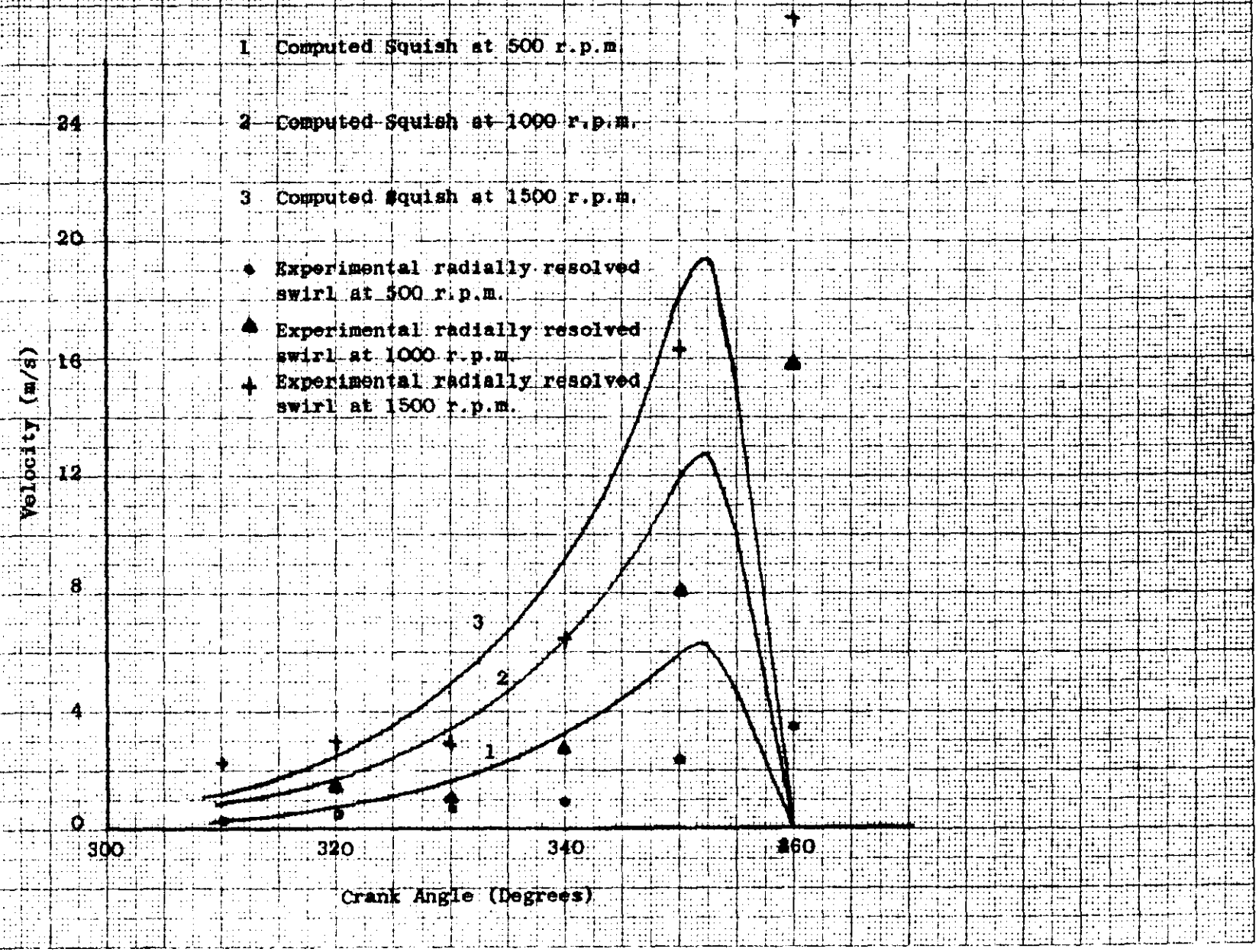

FIG. 6.19 RADIALLY RESOLVED SWIRL MEASUREMENTS AT R/B= 3.18 cm

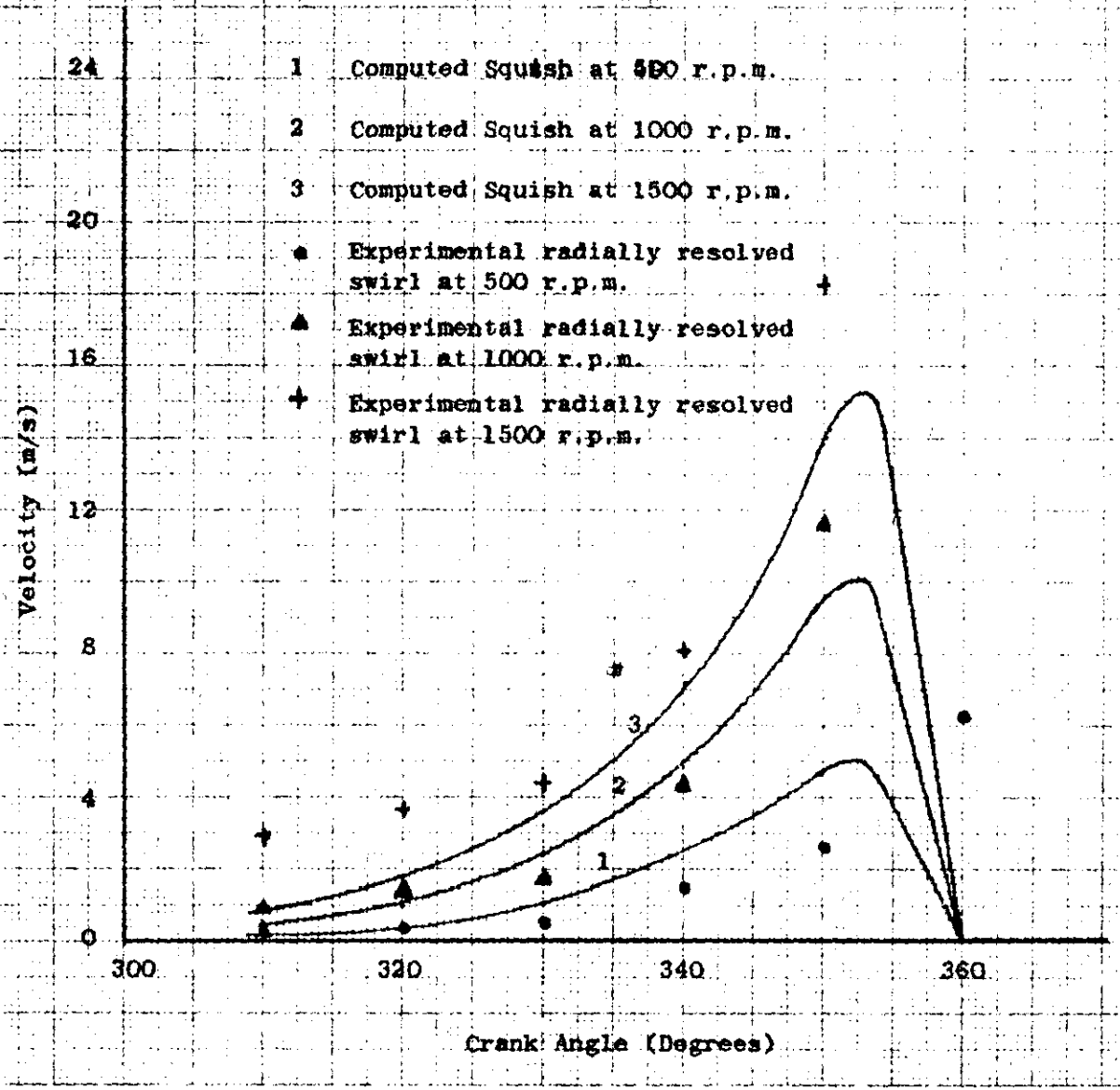

FIG. 6.20 RADIALLY RESOLVED SWIRL MEASUREMENTS AT R = 3.49 cm

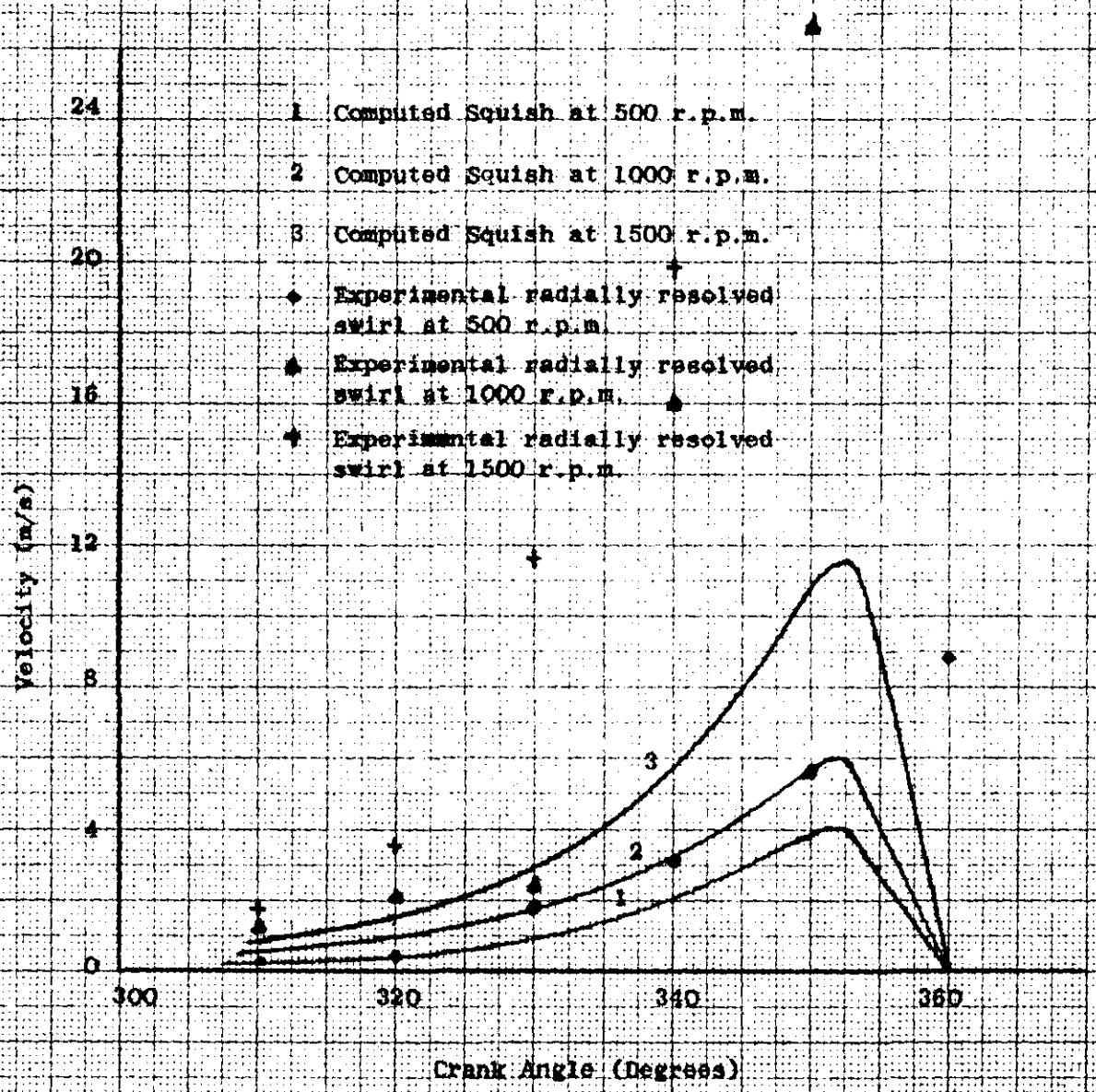

FIG. 6.27 RADIALLY RESOLVED SWIRL MEASUREMENTS AT R = 3.81 cm.

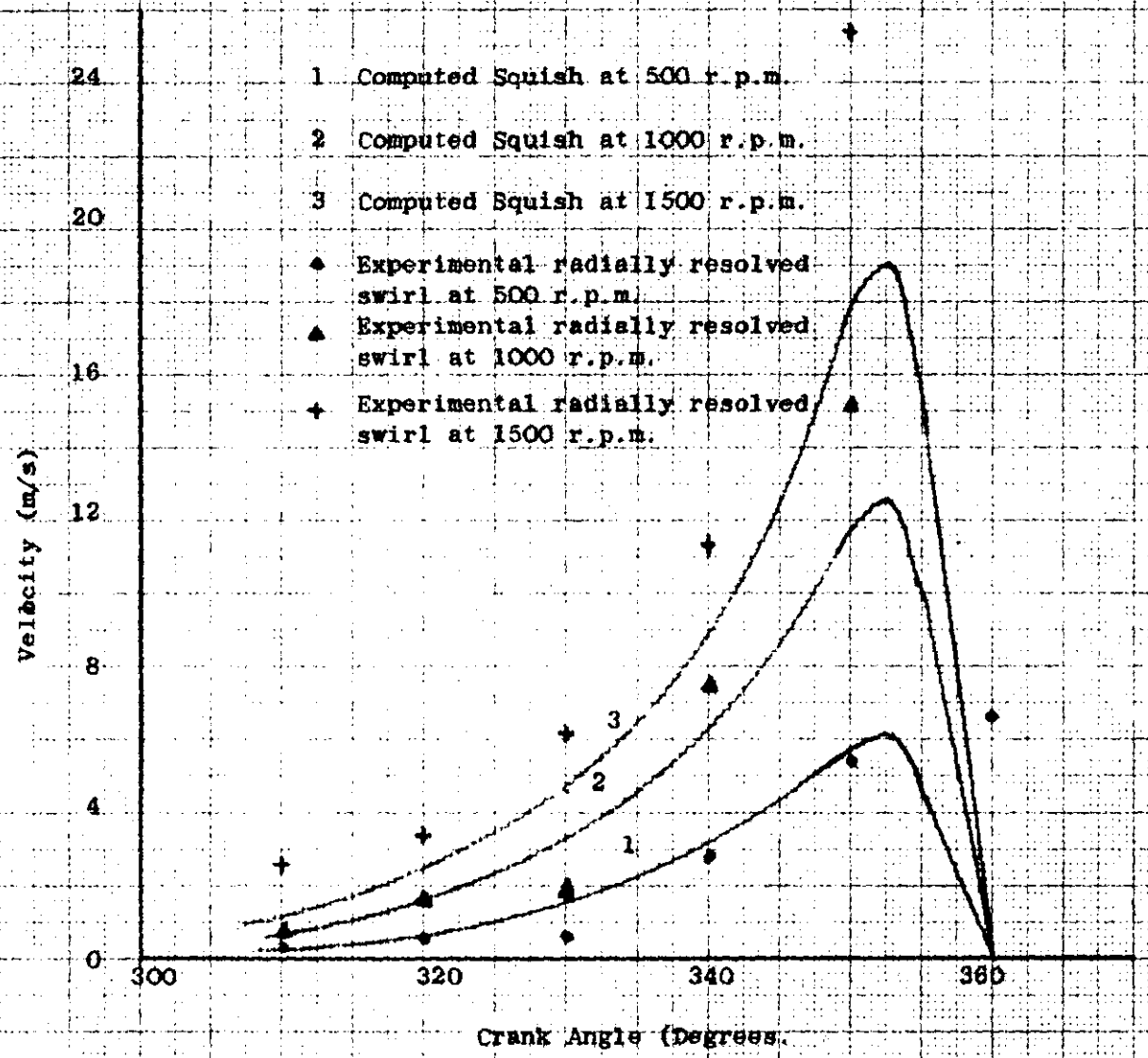

FIG. 6.22 MEAN RADIALLY RESOLVED SWIRL MEASUREMENTS AT R = 3.08 cm.

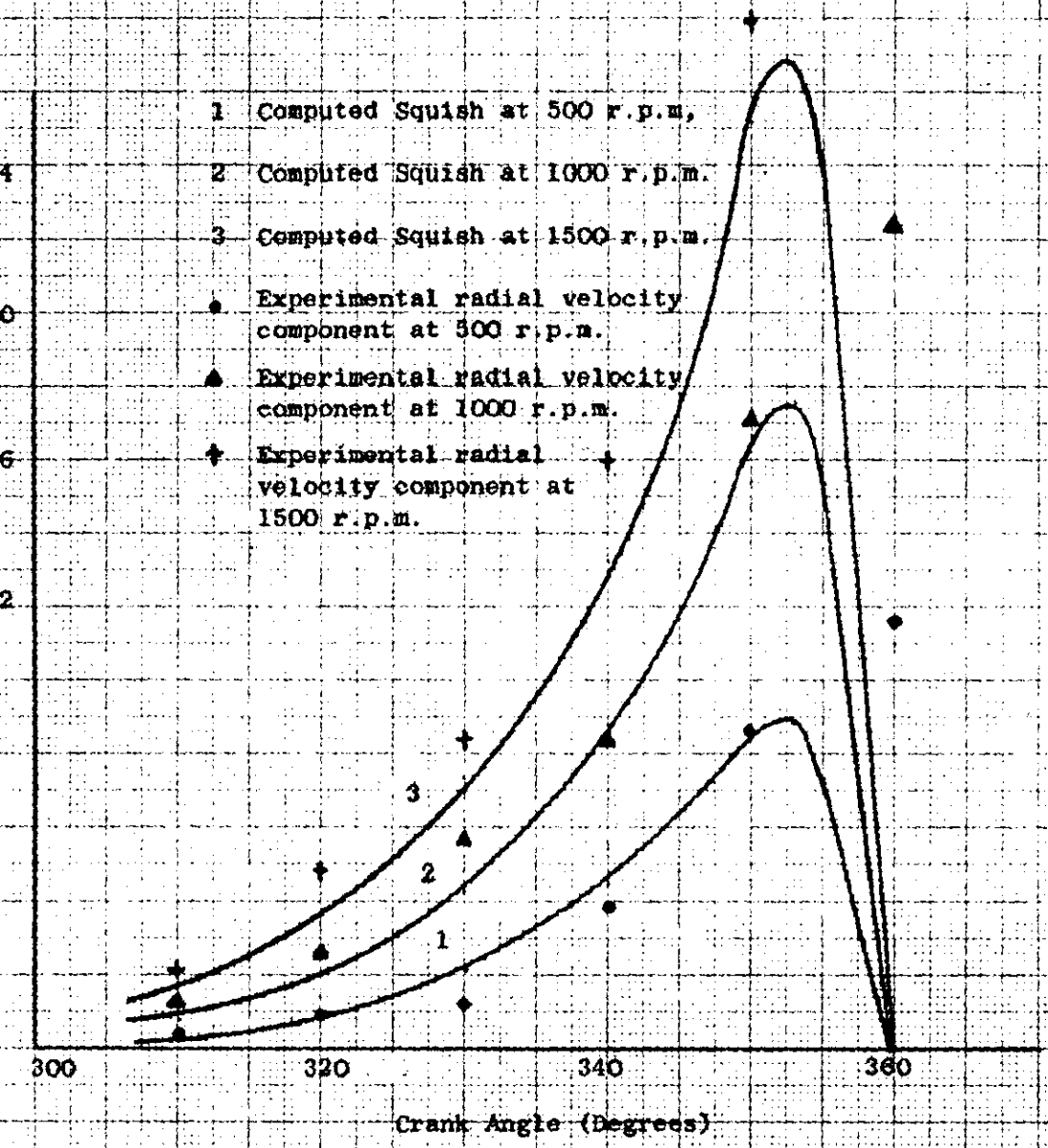

FIG. 6.23 RADIAL VELOCITY COMPONENT MEASURED AT R = 2.70 cm.

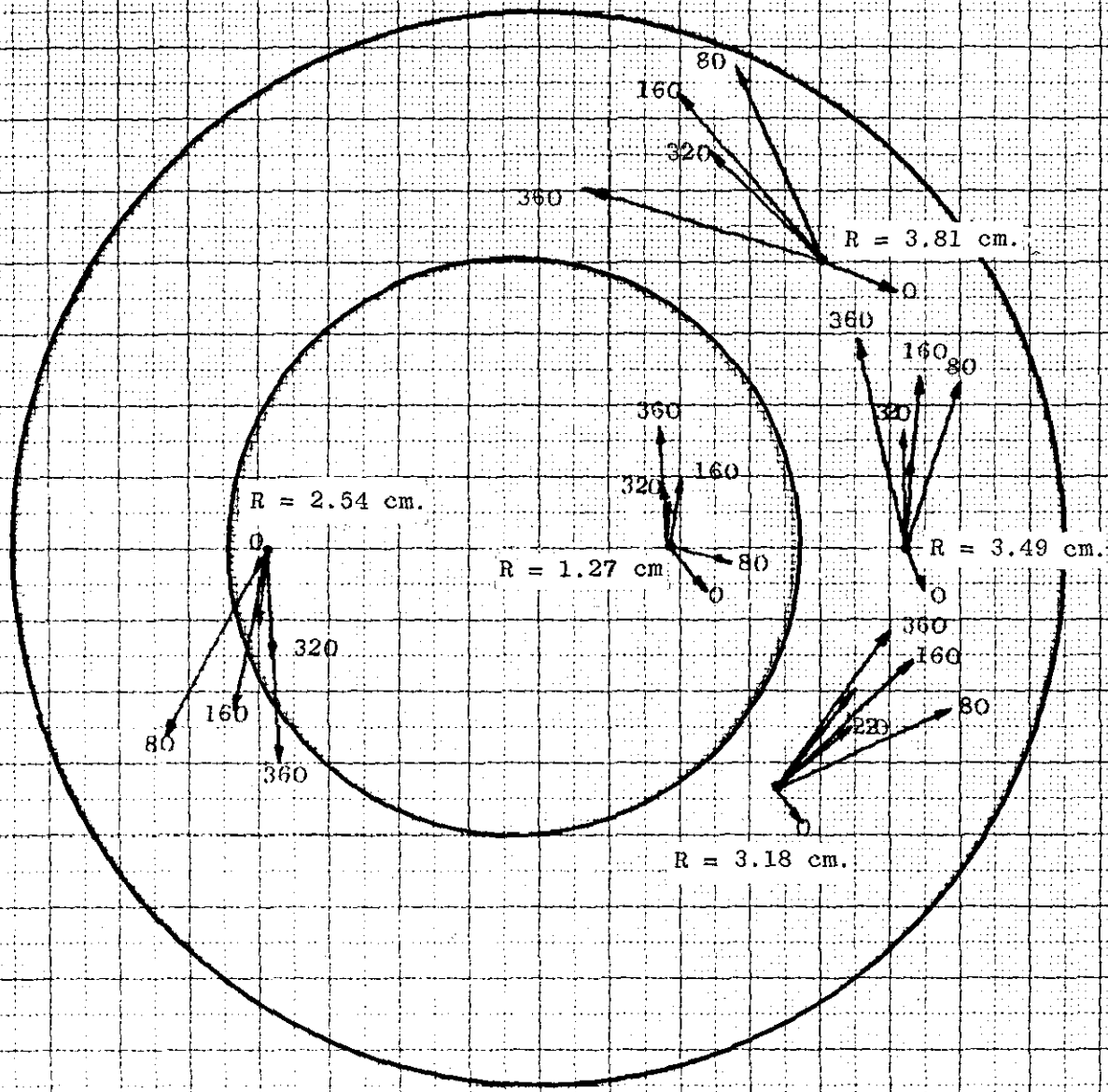

FIG. 6.24 VELOCITY PROFILES AT 500 R.P.M.

Scale 1 cm = 20 m/s

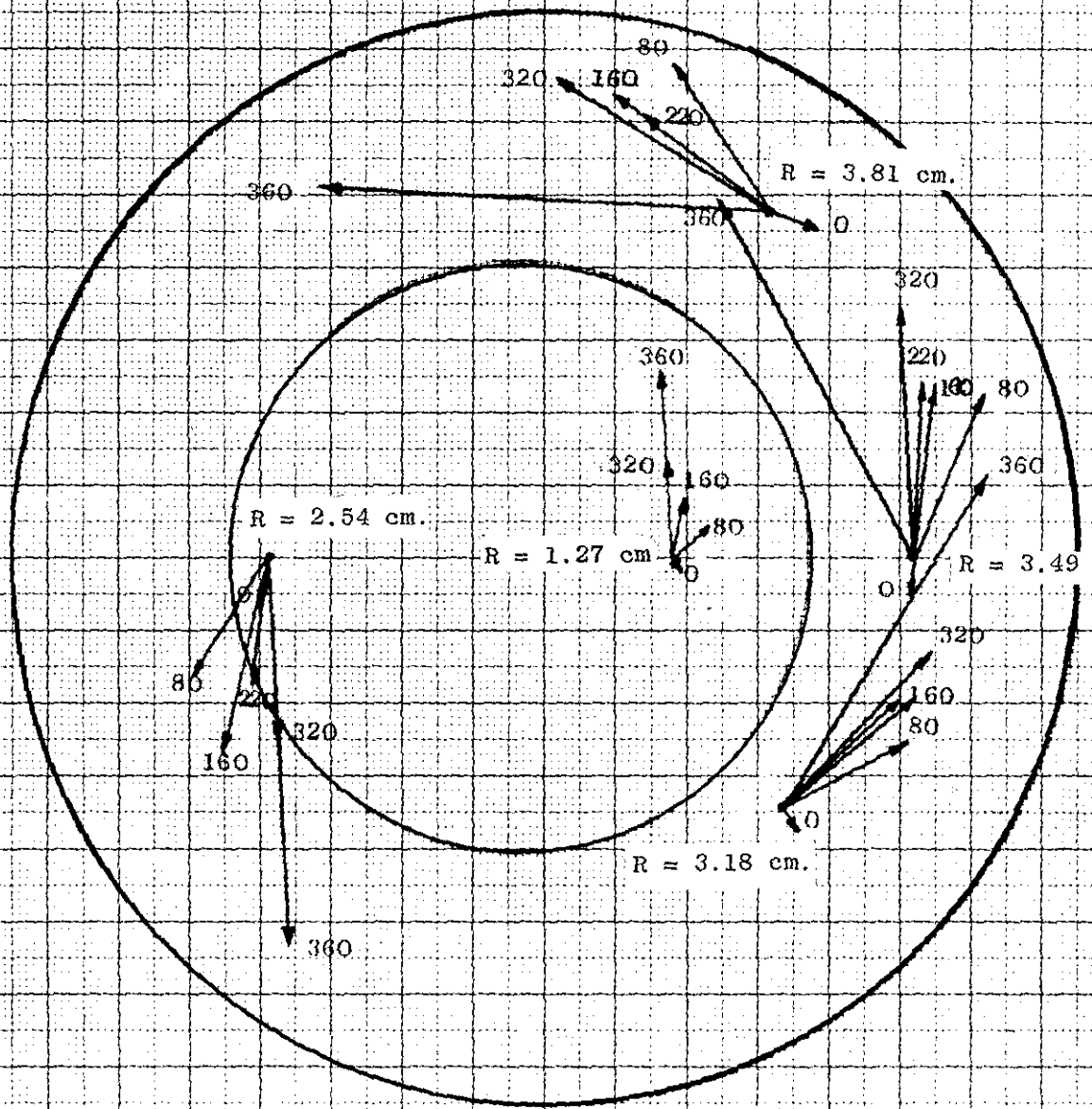

FIG. 6.25 VELOCITY PROFILES AT 1500 R.P.M.

FIG. 6.26 SWIRL PATTERN DEVELOPED USING FINE PAINT DROPS AND MOTORING THE ENGINE

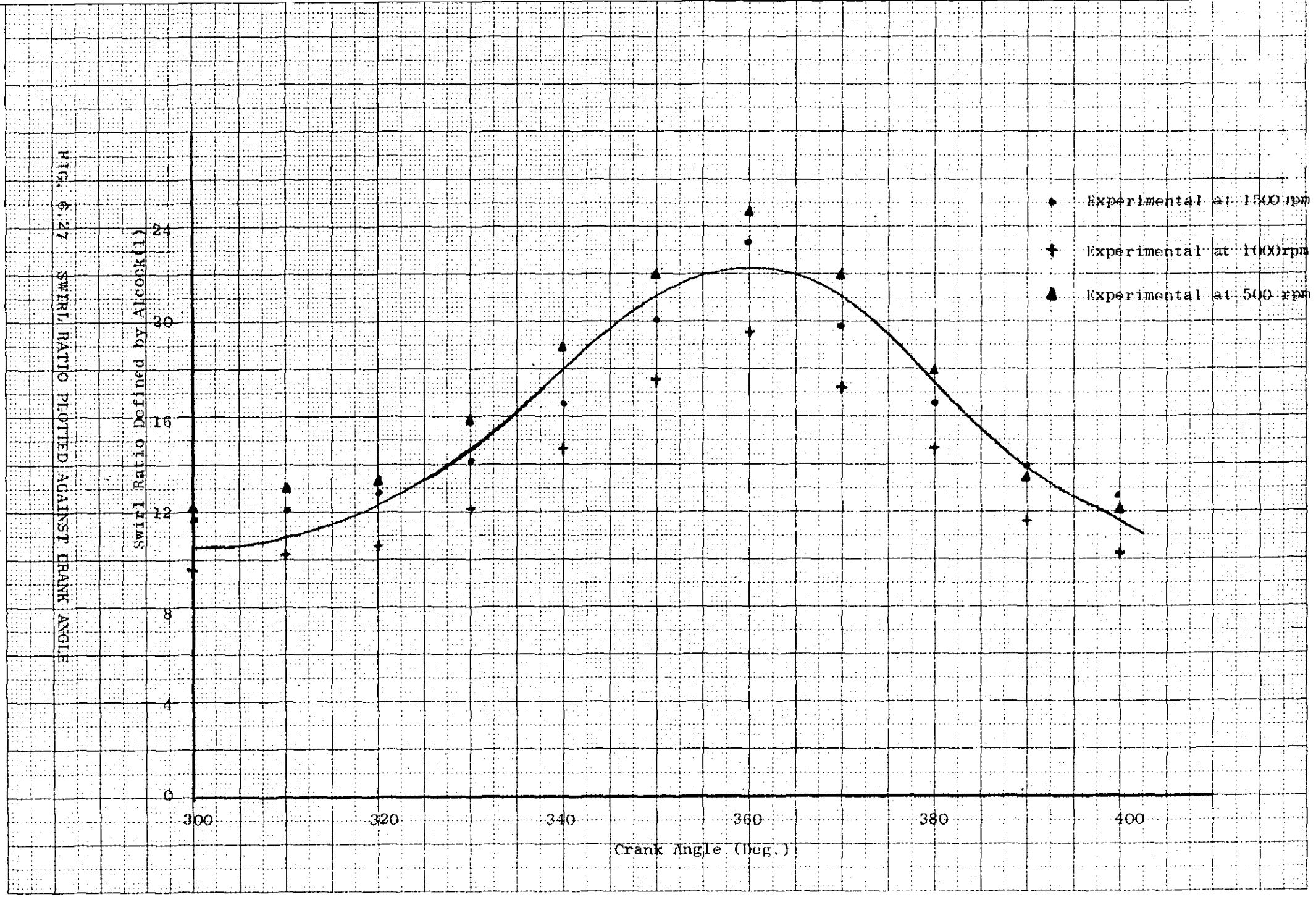

FIG. 6.27 SWIRL RATIO PLOTTED AGAINST CRANK ANGLE

7.0 CONCLUSIONS AND RECOMMENDATIONS FOR FURTHER WORK

7.0 CONCLUSIONS AND RECOMMENDATIONS FOR FURTHER WORK

7.1 Conclusions

From the experimental work undertaken and presented in the preceeding sections, the following major conclusions may be made regarding the adoption of hot wire anemometry and its use in justifying the mathematical model presented in Section 5.0, which attempts to predict the air motion throughout the induction and compression periods of a motored, four stroke, direct injection Diesel Engine.

(i) A three probe anemometer, with sensing wires mounted mutually at right angles to each other may be satisfactorily installed within a motored engine cylinder and relied upon to give measurements which result in the accurate determination of the magnitude and direction of the overall velocity vector within the engine cylinder.

(ii) From the experimental programme undertaken in a wind tunnel and the error analysis outlined in Appendix 3A, it was concluded that the three dimensional velocity vector may be determined in magnitude with an accuracy of $\pm$ 9.0%, whilst its direction may be determined with an accuracy of $\pm$ 12.0%.

(iii) The hot wire anemometer system adopted may be relied upon to predict the velocity in a variable density flow using a theoretical analysis similar to Davies and Fisher (17), providing that the temperature correction factor $(Tw/Tg)^{0.3}$, refer Appendix 3B, is included in the computation of the velocity.

(iv) The mathematical model developed assuming that momentum is conserved throughout the induction and compression period and a forced vortex velocity profile existing within the engine cylinder resulted in a good estimation (maximum error approximately 20%) of the air motion. It was concluded, therefore, that a forced vortex velocity profile is a representative description for the air motion within the cylinder and that providing frictional losses are accounted for between the air and the containing surfaces of the cylinder, then the assumption of conservation of momentum to exist throughout the induction and compression period is justified.

(v) The use of a masked inlet valve had little effect upon the general air motion within the engine cylinder but an optimum position of the mask exists (when the mask centre was located along the axis of the inlet port) when the swirl was increased by a factor of approximately 1.25 times that of the unmasked valve condition.

(vi) Supercharging the engine to a pressure of 10 p.s.i.g. had little effect upon the air motion within the cylinder but, in a similar manner to conclusion (v), the swirl was increased by a factor of approximately twice that of the non-supercharged condition.

(vii) Because the angular swirl velocity was considerably greater than the squish velocity (radial inward component of flow) the resultant motion of the air as the piston approached the top dead centre position on the compression stroke was a spiral pattern as the air entered the combustion chamber from the outer cylinder area. The air then continued to rotate inside the combustion chamber in accordance with the conservation of angular momentum and little evidence of the

theoretical toroidal motion postulated by Alcock (1), Dicksee (8) and Fitzgeorge and Allison (9) could be found. Instead the results supported those previously reported by Alcock and Scott (10), Horvatin and Hussmann (11) and Horvatin (31) which are illustrated in Figs. 2.13, 2.15 and 4.18 respectively.

7.2 Recommendations for Future Work

Having established that a forced vortex velocity profile is a representative description of the air motion inside the engine cylinder and that the basic assumption of conservation of angular momentum throughout the induction and compression periods exists, then the mathematical model presented in Section 5.0 may be adopted to predict the magnitude of the air motion throughout the induction and compression periods. However, should further experimental work be required to justify the assumptions presented in Section 5.0, then it is recommended that a single hot wire anemometer should be used, the probe being inserted through the cylinder head and located at various radial positions and depths inside the cylinder whilst facility would have to be made for the probe to plunge into the piston as the latter approached the top dead centre position. This latter technique, which is almost identical to that adopted by Horvatin and Hussmann (11) and Horvatin (31) may be justified since,

(i) The use of a three wire probe, whilst giving satisfactory results (maximum error of $\pm$ 9.0% for the magnitude and $\pm$ 12.0% for its direction) is very difficult and complicated to install on the piston crown and cannot be used for engine speeds in excess of 1500 r.p.m. due to the lead wires becoming damaged.

(ii) Interpretation of the results is difficult and requires not only the extremely accurate calibration of individual probes but also the matching of the three individual probes used for the determination of the velocity vector.

(iii) Installation of a piston mounted probe requires the continual stripping down of the cylinder head assembly and, whilst this is feasible for a single cylinder head, it would become extremely laborious should the technique of hot wire anemometry be applied to a multi-cylinder engine.

(iv) For the engine considered in the present investigation, it has been conclusively shown that the air motion is basically two dimensional during the latter part of the compression period (after 300 degrees crank angle) and therefore, regarding the magnitude of the air motion in this period (which must be the most important part of the engine cycle from a design engineer's point of view) a single anemometer would give the magnitude of the air motion. Rotation of the probe assembly about its own axis and observing the position of the probe which results in a maximum output signal would give the direction of the air motion, since by its very nature the anemometer will have a maximum output signal when its sensing wire is located perpendicular to the air flow.

Hence, a single probe anemometer is proposed for any future investigation and, by locating the anemometer so that a variety of radial locations and depths into the cylinder may be achieved, it is proposed that it would be a simple procedure to estimate the magnitude and direction of air motion within the engine cylinder.

Regarding the question of the air motion during the induction period, it is apparent from the experimental results illustrated in Figs. 4.12 and 4.13 that the air motion is three dimensional and to obviate all doubt as to this motion, two suggestions are proposed.

(i) A perspex suction and/or blowing rig could be developed which would incorporate the actual cylinder head and false engine cylinder with smoke introduced throughout the inlet port. Hence, by using high speed photography, it is anticipated that the air motion could be recorded on film for the induction period, depending upon the position of the inlet valve. Alternatively, the rig could be developed in order to accommodate a dynamic inlet valve lift and hence the induction cycle could be simulated on the rig.

(ii) The flow rig proposed by Fitzgeorge and Allison (9) must be investigated in far greater detail since this is an obviously simple rig to operate and because of its simplicity is favoured in industrial practice. Certainly, the flow rig may be used far more quickly and easily than the hot wire anemometer and when investigations are required into the development of inlet port systems incorporating one or even two inlet ports per cylinder, it must be concluded that a flow rig would ultimately be the most versatile tool for swirl investigations.

In conclusion, it is anticipated that the comments outlined above will be useful and an aid to further investigation regarding the problem of air motion established inside the engine cylinder. The proposals for easy visualisation of the air motion using injected smoke through the inlet port and the adoption of a paddle wheel to determine the magnitude of the air motion during the induction period are definitely the most simple and obvious techniques for future investigations.

8.0 REFERENCES AND APPENDICES

REFERENCES

1. ALCOCK, J.F.
Air Swirl in Oil Engines
Proc. Inst. Mech. Eng., 1934, 128.

2. SASS, F.
Kompressorlose Dieselmaschinen.

3. HURLEY, T.F.
Discussion to Alcock's (1) Paper.

4. COOKE, R.
Discussion to Alcock's (1) Paper.

5. CAVE-BROWN-CAVE, T.R.
Discussion to Alcock's (1) Paper.

6. BAKER, P.M.
Communication to Alcock's (1) Paper.

7. LEE, D.W.
A Study of Air Flow in an Engine Cylinder.
Report No. 653, National Advisory Committee for Aeronautics, 1939.

8. DICKSEE, C.B.
Open Combustion Chamber Diesel Engines in Britain
S.A.E., Jan. 1949, Vol. 3, No. 1.

9. FITZGEORGE, D. and ALLISON, J.L.
Air Swirl in a Road-Vehicle Diesel Engine
Proc. Inst. Mech. Eng. (A.D.), No. 4, 1962-63.

10. ALCOCK, J.F. and SCOTT, W.B.
Some More Light on Diesel Combustion
Proc. Inst. Mech. Eng. No. 5, 1962-63.

11. HORVATIN, M. and HUSSMANN, A.W.
Measurement of Air Movements in Internal Combustion Engine Cylinders
Disa Information No. 8, July, 1969.

12. WATTS, R. and SCOTT, W.B.
Air Motion and Fuel Distribution Requirements in High-Speed Direct-Injection Diesel Engines.
Proc. Inst. Mech. Eng., Symposium, Lond, 1968.

13. HEUBNER, K.H. and McDONALD, A.T.
A Dynamic Model and Measurement Technique for Studying Induction Air Swirl in an Engine Cylinder
Trans. A.S.M.E., 192, April, 1970.

14. SHIMAMOTO, Y. and AKIYAMA, K.
A Study of Squish in Open Combustion Chambers of a Diesel Engine
Bulletin of the J.S.M.E., Vol. 13, No. 63, 1970.

15. OHIGASHI, S., HAMMAMOTO, Y. and TANABE, S.
Swirl - Its Measurement and Effect on Combustion in a Diesel Engine.
Proc. Inst. Mech. Eng., Symposium, 1972.

16. HASSAN, H.
Unsteady Heat Transfer in a Motored Internal Combustion Engine
Ph.D. Thesis, Loughborough University of Technology, 1968.

17. DAVIES, P.O.A.L. and FISHER, M.J.
Heat Transfer from Electrically Heated Cylinders
Proc. Roy. Soc., A280, 1964.

18. HASSAN, H. and DENT, J.C.
Correction for Temperature Loading and High Gas Pressure Effects for the Constant-Temperature Hot-Wire Anemometer
J.Phys.D., Appl. Phys. 2, 1969.

19. LOBO, P.
The Determination of Velocity Patterns in Engine Cylinders by means of the Hot Wire Anemometer.
Ph.D. Thesis, Kings College, London University, 1966.

20. ULSAMER, J.
Die Grundlagen der Messung der Geschwindigheit Nacht Grosse und Richtung mit dem Hitzdrahtinstrument.
Forsch - Ing. Wes. V4 1933.

21. HINZE, J.O.
Turbulence
McGraw-Hill, New York, 1959.

22. KOVASNAY, L.S.C.
Development of Turbulence Measuring Equipment
N.A.C.A. Tech. Note 880, 1943.

23. NEWMAN, B.G. and LEARY, B.G.
The Measurement of Reynolds Stresses in a Circular Pipe as a means of Testing a Hot Wire Anemometer
Report A 72, Aeronautical Sci. Lab., Sydney, Australia, 1950.

24. PEARSON, C.E.
Measurement of Instantaneous Air Velocity Vectors by Hot Wire Methods.
Jour. Aero. Sci., Vol. 19, No. 2, 1952.

25. DENT, J.C. and DERHAM, J.A.
A Method for Checking the Consistency of Velocity Computations from Hot Wire Anemometer Measurements in Variable Density Flows.
J. Phys. E., Scientific Instruments, 1972, Volume 5.

26. DERHAM, J.A.
Measurement of Air Velocity in a Variable Density Flow.
Internal Report, Loughborough University of Technology, 1971.

27. D. MAC DIGITISER
Operating Instructions
Computer Centre Communications, Loughborough University of Technology

28. TINSEL WIRE
8 Ends Tinsel Core, Specification CW180
British Insulated Callender's Cables Ltd., Helsby.

29. LYN, W.T., STOCKWELL, A.J. and WANG, C.H.T.
Accuracy in Cylinder Pressure Measurements
Proc. Inst. Mech. Eng., Symposium Automobile Division, Jan. 1966.

30. WILLS, J.A.B.
The Correction of Hot Wire Readings for Proximity to a Solid Boundary.
J. Fluid Mech., Vol. 12, No. 3, 1962.

31. HORVATIN, M.
Beitrag Zur Awendung Des Hitzdraht-Anemometers Für Strömungs Und Turbulenzmessungen in Ver Brennungsmotoren.
Dr. Ing. Thesis, Technical University, Munich, 1971.

32. STOCK, D.
Untersachungen Der Gemischbildungs - ,
Zund und Verbrennungsvoränge, Eines Direkteinspritzenden Dieselmotors Mit Hilff Der Toepler'schen Schlierenmethode und der Hochgeschwindigeitsfotographic.
Dr. Ing. Thesis, Technical University, Berlin, 1970.

33. PIERCY, N.A.V. and RICHARDSON, E.G.
On the Flow of Air Adjacent to the Surface of an Aerofoil
Aero. Res. Council, London, Report and Memo 1224, 1928.

34. HEGGE ZIJNEN, B.G. VAN DER
Measurement of the Velocity Distribution in the Boundary Layer along a Plane Surface.
Thesis, Delft, 1924.

35. DRYDEN, H.L.
Air Flow in the Boundary Layer near a Plate
Nat. Adv. Comm. Aero., Wash., Tech. Rep. No. 562, 1936.

36. REICHARDT, H.
Die Wärmeübertragung in turbulenten Reibungschichten
Zeit Ang. Math. Mech. 20, 1940.

37. COLLIS, D.C. and WILLIAMS, M.J.
Two Dimensional Convection from Heated Wires at
Low Reynolds Numbers.
J. Fluid Mech. 6, 1959.

38. HOUGHTON, E.L. and BROCK, A.E.
Tables for the Compressible Flow of Dry Air
Edward Arnold Ltd., London, 1961.

39. WEGSTEIN, J.H.
Accelerating Convergence of Iterative Processes
Comm. Assoc, Comp. Mach. Vol. 1, No. 6, 1968.

40. ROUSE, H.
Elementary Mechanics of Fluids
John Wiley & Sons, New York

41. KRISTIANSEN, G.K.
Zero of Arbitrary Function
B.I.T., Vol. 3 (1963) pp 205-206

APPENDIX 3A

3.A.1 ERROR ANALYSIS FOR THE VELOCITY COMPUTATIONS

Using the theoretical computation of Davies and Fisher (17) outlined in Section 3.3.1, a theoretical calibration may be obtained for an anemometer probe operated at a particular hot wire temperature and the sensing wire having exact pre-determined dimensions. Assuming that the theoretical computations are correct, refer Davies and Fisher (17), the error encountered in the velocity measurement depends upon the ability to operate the probe at the theoretical conditions and in particular the hot wire operating temperature. The errors encountered in this latter requirement are those pertaining to accurate measurement of the resistance values of the probe and these are investigated in further detail.

In order to operate the bridge voltage circuit designed by Davies and Fisher (17), a Sullivan and Griffiths non-reactive decade resistance box was used which had an accuracy in the 0 - 20 ohms measuring range of $\pm$ 0.1%.

The probe cold lead resistance was measured using a Kelvin bridge which had an accuracy of $\pm$ 0.1 to 0.5% in the measuring range 1 to 10 ohms.

Having manufactured a probe using 10 μm platinum/30% iridium wire and spot welded this to the probe supports, analysis was made regarding the errors involved in the measurement of the sensing wire dimensions. The wire diameter was obtained from Johnson Mathey and the diameter quoted to be correct within $\pm$ 0.1 μm or $\pm$ 1% of the nominal diameter.

Measurement of the wire length was not so easy to determine since some deformation occurs at the points where the sensing wire is spot welded to the supports. However, using a vernier microscope, the sensing wire length was determined to within $\pm$ 0.05 mm and this results in an error of $\pm$ 2.5% when considered for a total wire length of 2 mm.

In order to make an assessment of the overall error involved in the velocity measurement, an error analysis was computed in a similar manner to the case outlined below.

Consider the case of a result R which is some function of three measured variables X, Y and Z, then

$$R = f(X,Y,Z) \qquad \text{——————} \quad 3.A.1$$

If, X, Y and Z are the errors in the determination of the variables, then

$$\begin{aligned} X &= X_c + x \\ Y &= Y_c + y \\ Z &= Z_c + z \end{aligned} \qquad \text{——————} \quad 3.A.2$$

where X_c, Y_c and Z_c are the correct values of the variables.

The error in the derived result is r, therefore $R = R_c + r$ and from equation 3.A.1, we have

$$R_c + r = f(X_c + x, Y_c + y, Z_c + z) \qquad \text{——————} \quad 3.A.3$$

If the function f is continuously differentiable, it may be expanded in a Taylor's Series and using the first two terms of the

expansion, the following equation is obtained for $R_c + r$.

$$R_c + r = f(X_c, Y_c, Z_c) + \left(\frac{\partial f}{\partial X_c}\right) \frac{X_c + x - X_c}{1!} + \left(\frac{\partial f}{\partial Y_c}\right) \frac{Y_c + y - Y_c}{1!} + \left(\frac{\partial f}{\partial Z_c}\right) \frac{Z_c + z - Z_c}{1!}$$

$$= R_c + \left(\frac{\partial R}{\partial X_c}\right) x + \left(\frac{\partial R}{\partial Y_c}\right) y + \left(\frac{\partial R}{\partial Z_c}\right) z \qquad \text{———3.A.4}$$

Therefore $$r = \left(\frac{\partial R}{\partial X_c}\right) x + \left(\frac{\partial R}{\partial Y_c}\right) y + \left(\frac{\partial R}{\partial Z_c}\right) z \qquad \text{———3.A.5}$$

Since errors x, y and z can be positive or negative, equation 3.A.5 is squared and the sum of the terms containing cross products will tend to zero since any particular cross product is as likely to be positive as negative.

Therefore $$r^2 = \left(\frac{\partial R}{\partial X_c}\right)^2 x^2 + \left(\frac{\partial R}{\partial Y_c}\right)^2 y^2 + \left(\frac{\partial R}{\partial Z_c}\right)^2 z^2 \qquad \text{———3.A.6}$$

The percentage error in the final results will then be obtained from

$$\frac{r}{R} \times 100 = \frac{100}{R} \left(\left(\frac{\partial R}{\partial X_c}\right)^2 x^2 + \left(\frac{\partial R}{\partial Y_c}\right)^2 y^2 + \left(\frac{\partial R}{\partial Z_c}\right)^2 z^2 \right)^{\frac{1}{2}} \qquad \text{———3.A.7}$$

3.A.2 SINGLE HOT WIRE ANEMOMETER

Davies and Fisher (17) employed a modified form of the Reynolds analogy to relate the convective heat transfer coefficient at the wire surface to the flow velocity, refer Section 3.3.1 and their results may be shown as

$$\frac{hd}{k_w} = \frac{2.6}{\gamma\Pi} \left(\frac{\rho_g U d}{\mu_g}\right)^{1/3} \left(\frac{Cp_g \rho_g}{k_g}\right) \qquad \text{——————3.A.8}$$

where h is the heat transfer coefficient from the wire,

d is the wire diameter,

k_w is the thermal conductivity of the gas at the wire temperature

k_g is the thermal conductivity of the gas,

Cp_g is the specific heat of the gas at constant pressure,

μ_g is the viscosity of the gas,

γ is the ratio of the specific heats

ρ_g is the density of the gas

U is the gas velocity.

Equation 3.A.8 may be arranged so that

$$U = B^3 h^3 d^2 \qquad \text{——————3.A.9}$$

where $$B = \left(\frac{k_g \gamma \Pi}{2.6 k_w Cp_g}\right)^3 \left(\frac{1}{\mu_g}\right)^2 \frac{1}{\rho_g}$$

and substitution for h, where $h = I^2 R_H R_c \alpha / R_H - R_c$ and I is the heating currents R_H and R_c the hot and cold probe resistance values and α the temperature coefficient of resistance of the wire material gives,

$$U = B^3 d^2 I^6 \alpha^3 \left(\frac{R_H R_c}{R_H - R_c}\right)^3 \qquad \text{——————3.A.10}$$

Equation 3.A.10 may be easily differentiated with respect to d, the sensing wire diameter, R_H the hot wire operating resistance and R_c the probe cold resistance. Hence the partial differentials may be obtained and substituted into equation 3.A.7 which will permit the computation of the overall error for a single hot wire anemometer.

Substitution of the following values into equation 3.A.7 was made in order that the error could be computed.

$$\left(\frac{\partial U}{\partial d}\right)^2 = 0.136 \quad , \quad d = .1\ \mu m$$

$$\left(\frac{\partial U}{\partial R_c}\right)^2 = 0.537 \quad , \quad r_c = .3\ \Omega$$

$$\left(\frac{\partial U}{\partial R_H}\right)^2 = 0.031 \quad , \quad r_H = .01\ \Omega$$

For a low velocity of 10 m/s, where the error is likely to be highest, the percentage error is given by,

$$\text{error} = \frac{100}{10} \left(.136 \times .1 + .537 \times .3 + .031 \times .01\right)^{\frac{1}{2}}$$

Therefore, the percentage error for a single hot wire anemometer is $\pm$ 4.30%.

3.A.3 ERROR ENCOUNTERED IN THE DETERMINATION OF THE VELOCITY VECTOR MAGNITUDE

In order to compute the error incurred using the three wire method, refer Section 3.2.3, for the determination of the magnitude of the velocity vector, equation 3.A.7 can be used. Basically, the error will be comprised of three simultaneous errors from three individual probes and also the error resulting from the spatial location of the

three probe sensing wire. The three wires should ideally be mutually at right angles to each other, and using a rotary engineers table and a travelling microscope, this configuration was aligned within $\pm$ 2 degrees. According to equation 3.1, Section 3.2.1, the signal from a probe wire will respond to the expression $U_\theta = U_{maximum} \sin \theta$ where θ is the angle of incidence of the velocity vector to the probe sensing wire, therefore the following expressions were substituted into equation 3.A.7.

$$\left(\frac{\partial U_V}{\partial U_{\text{single wire}}}\right)^2 (\text{error single wire})^2 = 3 \times .185$$

from the analysis in Section 3.A.2.

and

$$\frac{\partial (U_\theta / U)}{\partial \theta} = 1.00 \quad , \quad \theta = 2.0$$

For a low velocity vector of 25 m/s, the percentage error is,

$$\text{error} = \frac{100}{25} \left(3 \times .185 + 1.0 \times 4 \right)^{\frac{1}{2}}$$

Therefore, the percentage error encountered in the determination of the three dimensional velocity vector was $\pm$ 8.56%.

3.A.4 ERROR ENCOUNTERED IN THE DETERMINATION OF THE VELOCITY DIRECTION

Estimation of the errors in measuring the horiztonal and vertical angles A and B respectively in Fig. 3.5 requires consideration of the following equations:

$$\text{Cos A} = \frac{U_x}{(U_x^2 + U_y^2)^{\frac{1}{2}}}$$

$$\text{Cos B} = \frac{(U_x^2 + U_y^2)^{\frac{1}{2}}}{U_v}$$

where x and y refer to individual sensing wires in the x and y co-ordinate system and v refers to the overall velocity vector. Obviously, the expression for Cos B will contain the greater error since this expression is dependent upon the overall vector magnitude and this is not the case with the expression for Cos A.

Using equation 3.A.7, the following estimated errors were substituted in order to computer the error.

$$\left(\frac{\partial \cos B}{\partial U_x}\right)^2 (\text{error single wire})^2 = 2 \times .185$$ from the single wire analysis.

$$\left(\frac{\partial \cos B}{\partial U_v}\right)^2 (\text{error velocity vector})^2 = 4.55$$ from the three wire analysis.

For an angle of 20 degrees, the percentage error is,

$$\text{error} = \frac{100}{20} (4.55 + 2 \times .185)^{\frac{1}{2}}$$

Therefore the percentage error in the determination of the direction of the velocity vector is $\pm$ 11.1%.

3.A.5 CONCLUSIONS OF THE ERROR ANALYSIS

It may be observed from the analysis computed above that the following errors are likely to be encountered when using the hot wire anemometer system outlined in this investigation:

(i) for a single wire anemometer, the velocity perpendicular to the probe sensing wire will have an error of approximately $\pm$ 5.0%.

(ii) using the three wire method, detailed in Section 3.2.3, the determination of the overall vector magnitude is likely to have an error of approximately $\pm$ 9.0%.

(iii) the direction of the velocity vector may be computed accurately with a maximum error in the vertical plane, perpendicular to the piston surface, of approximately $\pm$ 12.0%.

Observation of the calibration curve, refer Fig. 3.6, illustrates that the error involved in measuring a velocity which is perpendicular to the probe sensing wire is within the computed error of $\pm$ 5%. Further analysis of Fig. 3.8 also illustrates that the magnitude of three dimensional velocity vector and the angles A and B can also be measured within the computed errors which are approximately $\pm$ 9.0% for the magnitude and $\pm$ 12.0% for the direction.

A method for checking the consistency of velocity computations from hot wire anemometer measurements in variable density flows

J C Dent and J A Derham
Department of Mechanical Engineering, University of Technology, Loughborough, Leics

MS *received 26 April 1971, in revised form 8 December 1971*

Abstract A method is presented for checking the consistency of air velocity calculation from hot wire anemometer measurements in an air flow which undergoes a continuous variation of density with time. The method gives a means of checking correction factors applied to ambient wind tunnel calibration tests to allow for variable density conditions. A particular application of the method to air velocity measurement in a motored internal combustion engine is discussed.

1 Introduction

The use of the hot wire anemometer for the measurement of velocity in variable density flows is of importance generally. A particular application in this field has been the study of air motion in motored internal combustion engines (Horvatin and Hussmann 1969, Hassan and Dent 1970.)

The use of the hot wire anemometer for engine applications necessitates knowledge of the local gas temperature and pressure in the vicinity of the anemometer probe throughout the engine cycle. Therefore, it is necessary to calibrate the hot wire anemometer at conditions of pressure and temperature prevailing in the engine. An alternative would be calibration of the anemometer in a wind tunnel under steady ambient conditions, with the correction of the results for continuous variation of gas pressure and temperature which occur throughout the engine cycle.

The first method, whilst being preferable, is expensive. The second method has been partially proven (Hassan and Dent 1969) by showing that correction factors could be applied to steady state wind tunnel tests at ambient conditions to predict velocity in a steady flow of air at elevated pressure and temperature. However, the range of velocities covered in the high pressure and temperature tests were narrow (67–75 ft s^{-1}), and are approximately three times lower than the peak velocities encountered in the engine study of Hassan and Dent (1970).

In this paper, it is proposed to show how the variation of output voltage of the constant temperature hot wire anemometer bridge, with choice of wire operating temperature, can be used in a variable density flow to check the efficacy of a correction factor applied to steady state wind tunnel tests at ambient conditions.

The approach adopted here differs from that of Horvatin and Hussmann (1969) in two important ways. Firstly, the variation of temperature along the hot wire element is considered in a more exact way, through a detailed differential analysis as discussed by Davies and Fisher (1964), rather than by use of a mean wire temperature deduced from an integral analysis with an assumed parabolic temperature distribution. The boundary conditions in both cases are the same. The second major difference in approach in this paper is the use of a correction factor to allow for the effects of elevated gas and wire temperatures on the computed gas velocity.

2 Constant temperature hot wire anemometer operation

2.1 *Steady state ambient conditions*

The constant temperature hot wire anemometer operates in the following manner. The wire probe, of known resistance at ambient temperature, forms the unknown resistance arm of a Wheatstone bridge. The balancing resistance arm of the bridge is then set at a value to give the required operating temperature of the wire probe, since the remaining two resistance arms of the bridge are of constant and equal value.

When the anemometer probe is inserted into a steady air flow at constant temperature and pressure, and the anemometer circuit energized, the out of balance in the Wheatstone bridge is detected and fed back to a power circuit which drives the bridge back to balance, by passing a heating current through the probe wire, so increasing its resistance to that of the balancing arm. Analysis of the heat transfer processes at the wire and their relation with the air motion over the wire, yields the air velocity.

2.2 *Variable density conditions*

When the anemometer probe is operating in a flow with continuously varying pressure and temperature – as in the engine study – the cooling effect of the air flow over the wire is reduced as the air temperature increases. In the case where the wire operating temperature is of the same order of

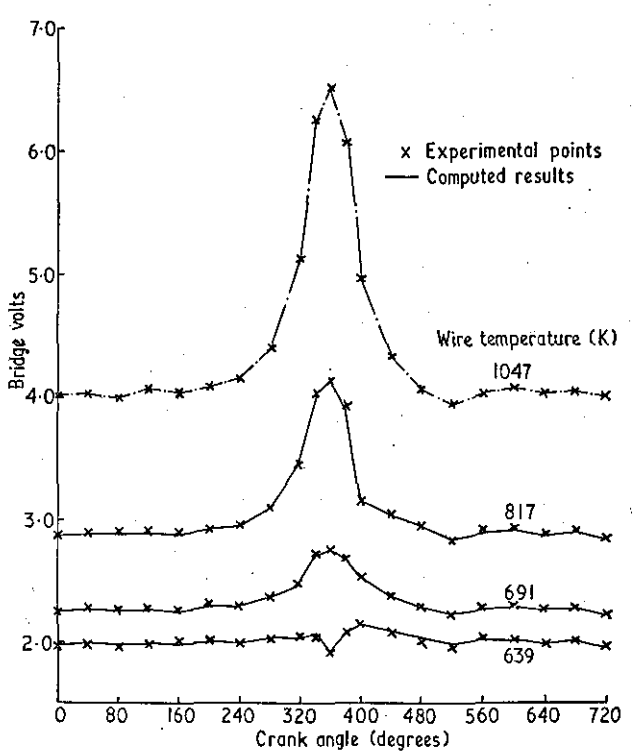

Figure 1 The effect of wire operating temperature on the variation of anemometer bridge output voltage with crank angle on a motored internal combustion engine

magnitude as the peak air temperature at TDC of the compression stroke, the heating current through the wire is reduced, and so also is the voltage drop across the wire. The effects of operating the hot wire at various temperatures in a variable pressure and temperature flow are shown in figure 1. These results were obtained with a 10 μm platinum–30% iridium wire of 2 mm length. The wire probe was inserted perpendicular to the air flow in the prechamber of a motored internal combustion engine operating at 800 rev min^{-1}. The anemometer output voltage over the engine cycle and engine crank angle were displayed on a twin beam oscilloscope, and permanent records obtained with a drum camera.

The prechamber used in this study was of the cylindrical disc type of 2 in diameter and $\frac{3}{8}$ in thickness. (The chamber was mounted on the top of the cylinder head with its axis perpendicular to that of the engine cylinder. Connection between the prechamber and engine cylinder was through a $\frac{3}{8}$ in diameter port, tangential to the prechamber and inclined at 135° to the engine cylinder axis. The gas motion produced in this type of chamber has the characteristics of a forced vortex.) The anemometer wire was perpendicular to the horizontal radius of the prechamber and was positioned 0·1 in from the chamber wall.

The gas pressure in the prechamber was determined over the engine cycle with the aid of a Bell & Howell type 4–361 strain gauge pressure transducer, an oscilloscope and the drum camera. Because the cycle to cycle variation of gas temperature in the prechamber was negligible (Hassan and Dent 1970), the hot wire element was used as a resistance thermometer. With the aid of a simple Wheatstone bridge circuit, and the recording equipment mentioned, the gas temperature during the engine cycle was obtained.

The peak gas temperature in the engine cycle was constant at 580 K. The wire temperatures at which the data shown in figure 1 were obtained, were decreased from 1047 to 639 K.

2.3 *Response of the constant temperature hot wire anemometer used*

Davies and Fisher (1964) showed that an anemometer circuit identical to that used in this study, but operating with a 5 μm diameter 2 mm long tungsten wire, had a frequency response of about 50 kHz.

In the study mentioned here, the same bridge circuit was used in conjunction with a 10 μm diameter 2 mm long platinum–30% iridium wire, the circuit having a transconductance of 60 A V^{-1}. From Davis (1970), the frequency response for the constant temperature hot wire anemometer (bridge and element together) can be computed from

$$\omega_c = \omega_n [1 - \zeta^2]^{1/2} \tag{1}$$

where ω_n is the natural frequency of the system, ζ is the damping and ω_c is the damped frequency. ω_n and ζ were evaluated for the system discussed above using the procedure of Davis (1970). From this, it was found that ω_c is of the order of 25 kHz.

The engine operating speed in this study was 800 rev min^{-1} (13·3 Hz). The cyclic gas velocity variation follows the engine operating frequency, with higher harmonics up to about 100 superimposed, due to the effects of turbulence. The anemometer system used would therefore be quite capable of this order of response. Because of this, the heat transfer analysis of the wire at any engine crank angle position can be considered on a steady state basis, using measured values of instantaneous gas pressure and temperature to compute fluid properties. Therefore, the analysis of wire heat transfer and its relation to flow velocity follows the method discussed by Davies and Fisher (1964), with correction of the velocity for gas density and wire operating temperature as indicated by Hassan and Dent (1969) where it was shown that

$$U_{\text{flow}} = U_{DF} [T_w/T_g]^{0.3} \tag{2}$$

where U_{flow} is the gas velocity, U_{DF} the velocity according to Davies and Fisher, T_w the mean wire temperature and T_g the gas temperature.

3 Analysis of Davies and Fisher

The Davies and Fisher (1964) method of computing flow velocity is based on the steady state, one dimensional analysis of the hot wire as an extended surface with heat generation, and convection to the surroundings at the instantaneous gas temperature T_g. The boundary conditions placed on the analysis are: (i) maximum temperature occurs at the half length of the wire so that $dT_w/dx = 0$ at that point, (ii) at the wire supports, the wire is at the instantaneous gas temperature T_g. Calculations have shown that the effect of wire support response to gas temperature fluctuations has a negligible effect on the mean wire temperature.

From the analysis of Davies and Fisher (1964), the mean wire temperature T_w is obtained in terms of properties of the gas, the wire, and the heat transfer coefficient h_{DF}. This expression is

$$T_w = \frac{K_2}{K_1}\left[\frac{\tanh(|K_1|^{1/2} l)}{(|K_1|^{1/2} l)} - 1\right] + T_g \tag{3}$$

where

$$K_1 = \frac{I^2 \lambda_g \alpha}{k_t A_r^2} - \frac{\pi h_{DF} d}{k_t A_r}$$

and

$$K_2 = \frac{I^2 \lambda_g}{k_t A_r^2}.$$

I is the heating current in the wire, λ_g the electrical resistivity of the wire at gas temperature, α the temperature coefficient of resistance of probe wire, k_t the thermal conductivity of the wire, A_r the cross sectional area of the probe, d the probe diameter and $2l$ the probe wire length.

Davies and Fisher (1964) employed a modified form of the Reynolds analogy to relate the convective heat transfer coefficient at the wire surface to the flow velocity. Their results can be shown in rearranged form as

$$\frac{h_{DF} d}{k_w} = \frac{2{\cdot}6}{\gamma\pi}\left[\frac{\rho_g U_{DF} d}{\mu_g}\right]^{1/3}\left[\frac{Cp_g \mu_g}{k_g}\right] \tag{4}$$

which is valid in the range

$$0 \leqslant \left[\frac{\rho_g U_{DF} d}{\mu_g}\right] \leqslant 50$$

where k_w is the thermal conductivity of the gas at the wire temperature, γ the ratio of the specific heats, ρ_g the density of the gas, Cp_g the specific heat of the gas at constant pressure, μ_g the viscosity of the gas and k_g the thermal conductivity of the gas.

In setting the balance arm of the anemometer bridge, the mean wire temperature T_w is fixed. Hence, for a given probe, wire temperature T_w and heating current I, obtained from the solution of the Wheatstone bridge circuit at balance, equation (3) can be solved by iteration to yield h_{DF} for given conditions of gas density and temperature. Finally, h_{DF} may be related to U_{DF} through equation (4).

4 Scheme for consistency check–engine study

The scheme for the consistency check is based on the voltage characteristics of the hot wire shown in figure 1.

A wire operating temperature is chosen through setting the balance arm of the Wheatstone bridge – say this results

in a value of $T_{w1} = 1047$ K. The anemometer output voltage V is obtained over the engine cycle figure 1 plot for $T_w = 1047$ K. Measurements of instantaneous gas temperature T_g and pressure P_g are also made over the engine cycle. Hence U_{DF} and thence U_{flow} can be computed (at the particular probe location in the prechamber) for the whole engine cycle.

Now if the wire is operated at some other mean temperature T_{w2} – say 691 K, and measurements of anemometer output voltage V are obtained as before, then, since the mean flow velocity of gas over the wire at any instant during the engine cycle is essentially the same as that measured at T_{w1} (because cycle to cycle variation has been shown to be negligible), U_{flow} obtained with the 1047 K wire temperature computation is used through equations (3) and (2) to compute the wire heating current and hence the bridge voltage for a wire temperature of 691 K. The computed bridge voltages at 691 K are then checked against the measured values with the probe operating at $T_{w2} = 691$ K. The accuracy of the correction term $(T_w/T_g)^{0.3}$ can now be assessed more effectively than in the tests of Hassan and Dent (1969). A comparison between measured and computed values of bridge voltage are shown in figure 1 for a range of wire operating temperatures. The flow velocity U_{flow} was evaluated with the wire temperature of 1047 K and used in the subsequent calculations.

It will be seen from figure 1 that agreement between computed and measured voltages are generally very good. The fluctuating signal of much lower output voltage when operating the wire at a temperature of 639 K also shows good agreement, though there is a tendency to more scatter in the results as would be expected.

The effect of neglecting the correction term $(T_w/T_g)^{0.3}$ is shown in figure 2.

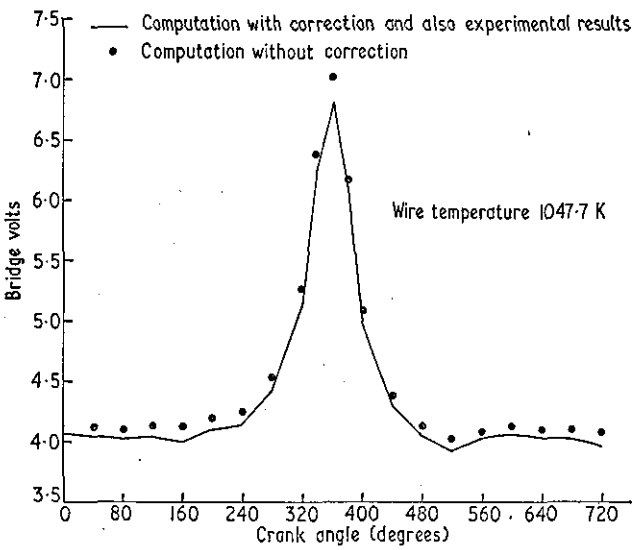

Figure 2 The effect of neglecting correction term $(T_w/T_g)^{0.3}$ on computed anemometer bridge output voltage

5 Conclusion

A method has been presented for checking the consistency of air velocity calculation from hot wire anemometer measurements in a variable density flow. The method gives a means of checking correction factors applied to wind tunnel calibration tests at ambient conditions, to allow for density variations in the flow. In the particular application of the method to measurements in the precombustion chamber of a motored internal combustion engine, it was found that the correction $(T_w/T_g)^{0.3}$ applied to the velocity computed by the method of Davies and Fisher (1964) was quite justified.

References

Davies P O A L and Fisher M J 1964 *Proc. R. Soc.* A **280** 486–527

Davis M R 1970 *J. Phys.* E: *Sci. Instrum.* **3** 15–20

Hassan H and Dent J C 1969 *J. Phys.* D: *Appl. Phys.* **2** 85–92

Hassan H and Dent J C 1970 *Proc. Instn. Mech. Engrs* **185** 583–92

Horvatin M and Hussmann A W 1969 *DISA Information* (1969) No 8 July pp 13–22

A P P E N D I X 4 A

4.A.1 THREE DIMENSIONAL VELOCITY VECTOR PROGRAM

In order to compute the three dimensional velocity vector, the following computer program was written in Fortran IV and, considering that execution time must be kept to a minimum, the program was subdivided into a main segment and two subroutines which are listed below.

(i) MAIN SEGMENT, which computes the overall velocity vector magnitude and direction from the three individual velocity readings,

(ii) Subroutine VELOCITYCALCULATION, which computes the individual velocity vectors using the instantaneous bridge voltage, pressure and temperature,

(iii) Subroutine COORDS, which is used to translate the paper tape output from the D Mac Pencil Follower (27) into numerical values of bridge voltage, pressure and temperature.

A listing of the program is included and the input and output data explained in detail.

INPUT DATA

D	Wire diameter (μm)
ELP	Temperature coefficient for the wire material ($/^{o}C$)
VIS	Viscosity of air at $0^{o}C$ (gm/cm s)
TGMIN	Minimum gas temperature within the cylinder (^{o}K)
SCP	Pressure Scale (psi/cm)

SCT	Temperature Scale (^{o}C/cm)
SCV1	Voltage Scale 1 (volts/cm)
SCV2	Voltage Scale 2 (volts/cm)
SCV3	Voltage Scale 3 (volts/cm)

OUTPUT DATA

N	Crank angle position (deg.)
U1(K)	Velocity 1 (m/s)
U2(K)	Velocity 2 (m/s)
U3(K)	Velocity 3 (m/s)
UV	Overall velocity vector (m/s)
UHORZ	Overall velocity vector resolved horizontally (m/s)
UVERT	Overall velocity vector resolved vertically (m/s)
BVT	Vertical Angle B (Deg.)
AH	Horizontal Angle A (Deg.)
TG(K)	Gas temperature (^{o}K)
PO(K)	Gas Pressure (KN/m^{2})

```
      MASTER N207
      DIMENSION U1(100),U2(100),U3(100),A1(100),A2(100),A3(100),MOR(100)
     1,ICHNO(100),TG(100),PO(100),UVT(200,2),HG(100)
      COMMON D,ELP,VIS,PO,TG,TGMIN
      READ(1,10)D,ELP,VIS,TGMIN,SCP,SCT,SCV1,SCV2,SCV3
   10 FORMAT(9F0.0)
      LP=2
      NTR=3
      M=1
      CALL COORDS(NTR,LP,M,TX,TY,NSCAN)
      M=2
      DO 11 K=1,3
      CALL COORDS(NTR,LP,M,TX,TY,NSCAN)
      PO(K)=TY*SCP
   11 CONTINUE
      M=1
      CALL COORDS(NTR,LP,M,TX,TY,NSCAN)
      M=2
      DO 12 K=1,3
      CALL COORDS(NTR,LP,M,TX,TY,NSCAN)
      TG(K)=TY*SCT
      TG(K)=TG(K)+TGMIN
   12 CONTINUE
      NCOUNT=0
   13 NCOUNT=NCOUNT+1
      M=1
      CALL COORDS(NTR,LP,M,TX,TY,NSCAN)
      M=2
      DO 14 K=1,3
      CALL COORDS(NTR,LP,M,TX,TY,NSCAN)
      A1(K)=TY*SCV1
   14 CONTINUE
      M=1
      CALL COORDS(NTR,LP,M,TX,TY,NSCAN)
      M=2
      DO 15 K=1,3
      CALL COORDS(NTR,LP,M,TX,TY,NSCAN)
      A2(K)=TY*SCV2
   15 CONTINUE
      M=1
      CALL COORDS(NTR,LP,M,TX,TY,NSCAN)
      M=2
      DO 16 K=1,3
      CALL COORDS(NTR,LP,M,TX,TY,NSCAN)
      A3(K)=TY*SCV3
   16 CONTINUE
      CALL VELOCITYCALCULATION(A1,U1)
      CALL VELOCITYCALCULATION(A2,U2)
      CALL VELOCITYCALCULATION(A3,U3)
      WRITE(2,17)
   17 FORMAT(10X,5HANGLE,5X,2HU1,5X,2HU2,5X,2HU3,5X,2HUV,5X,6HUHORZ.,2X,
     16HUVERT.,4X,9HVERT.ANG.,3X,9HHORZ.ANG.,2X,9HGAS TEMP.,4X,10HGAS PR
     1ESS./)
      DO 19 K=1,3
      A=(-U1(K)**2+U2(K)**2+U3(K)**2)/2
      B=(U1(K)**2-U2(K)**2+U3(K)**2)/2
      C=(U1(K)**2+U2(K)**2-U3(K)**2)/2
      UV=SQRT(A+B+C)
      UX=SQRT(ABS(A))
      UY=SQRT(ABS(B))
      UZ=SQRT(ABS(C))
      X=UX/UV
```

```
      Y=UY/UV
      Z1=UZ/UV
      ALFA=ACOS(X)
      BETA=ACOS(Y)
      GAMMA=ACOS(Z1)
      ALFA=ALFA*180/3.1415
      BETA=BETA*180/3.1415
      GAMMA=GAMMA*180/3.1415
      COSA=(UX/UV)/(SQRT((UX/UV)**2+(UY/UV)**2))
      AH=ACOS(COSA)
      AH=AH*180/3.1415
      COSB=(UX/UV)/COSA
      BVT=ACOS(COSB)
      BVT=BVT*180/3.1415
      WRITE(2, 18)N,U1(K),U2(K),U3(K),UV,UHORZ,UVERT,BVT,AH,TG(K),PO(K)
   18 FORMAT(11X,I3,2X,4F7.2,2X,F7.2,1X,F7.2,6X,F6.2,6X,F6.2,4X,F7.2,6X,
     1F7.2)
   19 CONTINUE
      STOP
      END



      SUBROUTINE VELOCITYCALCULATION(A,U)
      DIMENSION PO(100),TG(100),A(100),U(100)
      COMMON D,ELP,VIS,PO,TG,TGMIN
      READ(1,10)Z,RH,RS
   10 FORMAT(3F0.0)
      AREA=3.1415*(D**2)/4.
      ROWO=36.441/10**6
      RC=ROWO*Z/AREA
      TO=293
      Z=Z/2.
      TW=(RH-RC)/(RC*ELP)+TO
      CAW=(2.56+(7.3*(TW-54.)/1000.))/10.**4.
      ROWT=ROWO*(1.+ELP*(TW-TO))
      TCWT=(2.23*TW)/(ROWT*10.**8)
      DO 27 K=1,3
      TS=TG(K)
      ROWS=ROWO*(1+ELP*(TS-293))
      TCWS=(2.23*TS)/(ROWS*(10.**8.))
      DEN=(2.31*PO(K))/(96.5*TG(K))
      RG=RC*(1+ELP*(TG(K)-TO))
      DT=TW-TG(K)
      CAG=(2.56+(7.3*(TG(K)-54)/1000))/10.**4
      VSY=(VIS*390*(TG(K)/273)**1.5)/(TG(K)+117)
      CV=(.1715+.02788*DEN)*4.1813
      CUR=A(K)/(2*RS)
      CONST=(RH-RG)*CUR**2/(2*3.1415*Z*CAW*DT)
      HWP=6.
      HWN=0.

C         SOLVING FOR K1.

C         MAIN ITERATION.

      CAY1=(4.*CAW)/(TCWT*D**2)
   11 CAYP=HWP*D/CAW-CONST
      CAYN=HWN*D/CAW-CONST
      CAYP3=ABS(CAY1*CAYP)
      CAYN3=ABS(CAY1*CAYN)
      CAYP4=(SQRT(CAYP3))*Z
      CAYN4=(SQRT(CAYN3))*Z
```

```
      DIF1=CUR**2*RH/(D*3.1415*2*Z*DT)
      IF(CAYP4.GT.50) GO TO 12
      EP=(EXP(2.*CAYP4)-1.)/(EXP(2.*CAYP4)+1.)
      GO TO 13
   12 EP=1
   13 IF(CAYN4.GT.50) GO TO 14
      EN=(EXP(2.*CAYN4)-1.)/(EXP(2.*CAYN4)+1.)
      GO TO 15
   14 EN=1
   15 DIFP2=1.-(RG*TCWS*EP)/(RH*TCWT*CAYP4)
      DIFN2=1.-(RG*TCWS*EN)/(RH*TCWT*CAYN4)
      FUP=HWP-DIF1*DIFP2
      IF(FUP-.0000001)25,25,16
   16 CONTINUE
      FUN=HWN-DIF1*DIFN2
      IF(ABS(FUN)-.0000001)17,17,18
   17 H=HWN
      GO TO 26
   18 CONTINUE
      HWM=(HWN*FUP-HWP*FUN)/(FUP-FUN)
      CAYM=HWM*D/CAW-CONST
      CAYM3=ABS(CAY1*CAYM)
      CAYM4=(SQRT(CAYM3))*Z
      IF(CAYM4.GT.50) GO TO 19
      EM=(EXP(2.*CAYM4)-1.)/(EXP(2.*CAYM4)+1.)
      GO TO 20
   19 EM=1
   20 DIFM2=1.-(RG*TCWS*EM)/(RH*TCWT*CAYM4)
      FUM=HWM-DIF1*DIFM2
      IF(FUM)21,25,22
   21 HWN=HWM
      GO TO 23
   22 HWP=HWM
   23 IF(ABS(HWP-HWN)-.001)25,25,24
   24 GO TO 11
   25 H=HWP
   26 CONTINUE
      U(K)=((H*3.1415*CAG)/(2.6*CV*CAW))**3*(D/VSY)**2/(DEN)
      U(K)=U(K)/100
      U(K)=U(K)*(TW/TG(K))**.3
   27 CONTINUE
      RETURN
      END



      SUBROUTINE COORDS (NTR,LP,M,TX,TY,NSCAN)
   10 FORMAT(F0.0)
   11 FORMAT(3I0)
      IF (M.NE.1) GO TO 13
      READ(3,10)A
      READ(3,10)B
      READ(3,10)A1
      READ(3,10)B1
      READ(3,10)A2
      READ(3,10)B2
      READ(3,11)N1,N2,N3
      X = N1
      Y = N2
      READ(3,11)N1,N2,N3
      X1 = N1
      Y1 = N2
      READ(3,11)N1,N2,N3
```

```
      X2 = N1
      Y2 = N2
      RADS = 57.296
      XANG = ATAN2 ((Y1-Y),(X1-X))
      BXANG = XANG*RADS
      YANG = ATAN2 ((X-X2),(Y2-Y))
      BYANG = YANG*RADS
      DIFANG = XANG-YANG
      DIFRAD = DIFANG*RADS+90.0
      IF (DIFANG.GT.0.02) WRITE (2,12)DIFRAD
   12 FORMAT (1X,45HERROR IN READING SCALE FACTORS - AXES ARE AT ,F7.3,
     1 8H DEGREES)
      ANG = (XANG+YANG)/2
      YSCALE = (B2-B)/SQRT((X-X2)**2+(Y2-Y)**2)
      XSCALE = (A1-A)/SQRT((X1-X)**2+(Y1-Y)**2)
      NSCAN = N3
      RETURN
   13 READ(3,11)N1,N2,N3
      NSCAN = N3
      H = N1
      V = N2
      TY=((V-Y)*COS(ANG)-(H-X)*SIN(ANG))*YSCALE+B
      TX=((H-X)*COS(ANG)+(V-Y)*SIN(ANG))*XSCALE+A
      RETURN
      END
      FINISH
```

APPENDIX 4B

4.B.1 WALL PROXIMITY ESTIMATIONS

When using a hot wire anemometer for velocity measurements close to a solid boundary, errors may be introduced if the effect of the boundary on the rate of heat loss from the wire is ignored. The proximity of an infinite, flat, solid boundary having a much higher thermal conductivity than the fluid affects the heat loss from a wire by modification of the temperature and velocity fields. The boundary is effectively at ambient temperature and so additional heat is extracted from the fluid that is heated by the wire. This effect will increase rapidly as the wire approaches the boundary.

Piercy and Richardson, 1928, (33) measured the heat loss from a hot wire attached to a whirling arm rotating uniformly in still air. The whirling arm was co-axial with a fixed metal cylinder and supported the hot wire close to the surface of the cylinder and parallel to its axis.

Van der Hegge Zijnen, 1924, (34) obtained a form of correction by assuming that the effect of the wall could be represented by an additional heat loss independent of the stream velocity and dependent only on the distance of the wire from the wall. The correction was obtained by measuring the total heat loss from the wire at a large distance from the wall and then continuing to make measurements as the wire approaches the wall surface, all the measurements being taken in still air. The extra heat loss so obtained was then used to correct the experimental velocity measurements. The same method was used by Dryden, 1936, (35) to correct hot wire readings in a boundary layer.

He found by experiment that the extra heat loss to the wall in still air was given by:

$$H = \text{constant} \times l \, (\theta_w - \theta_a)^2 / b \qquad \text{——————} \quad 4.B.1$$

where θ_w and θ_a are wire and ambient temperatures respectively,

l is the wire length

b is the distance of the wire from the wall.

The success of this method of correction depends on the assumption that the wire loses heat to the wall only by conduction, which is true only for very small Reynolds numbers based on the wire diameter.

A more accurate method was that used by Reichardt, 1940 (36) who calibrated his wires close to the wall in a laminar flow channel and used the calibration in a channel with a turbulent flow having the same value of wall shear stress. Wills' (30) results are illustrated in Fig. 4.B.1, and it must be mentioned that the experimental work performed was limited to a maximum Reynolds number of 1.0. However, when $Nu(\theta_w/\theta_a)^{-0.17}$ was plotted again $R_w^{0.45}$, Wills obtained a series of parallel lines (depending upon the b/a value) which had the equation,

$$Nu(\theta_w/\theta_a)^{-0.17} = A + 0.56 \, R_w^{0.45} \qquad \text{——————} \quad 4.B.2$$

where $A = 0.26$ as $b/a \rightarrow \infty$.

Equation 4.B.2 was obtained by Collis and Williams (37) (for Reynolds number in the range 0 - 44) from an extensive series of measurements of two dimensional convection from hot wires far from a solid boundary and as mentioned above, fitted Wills' results very accurately. Consequently, it was assumed that the curves illustrated in Fig. 4.B.1 remained parallel up to a Reynolds Number of 44.0.

Using a 10 μm diameter wire in the engine studies, a maximum Reynolds number of approximately 35.0 was encountered and assuming that the b/a curve equal to 50 is adopted and assumed to be sufficiently close to the case of negligible heat loss due to a solid boundary, then we have

$$\frac{b}{a} = 50, \qquad 2a = 0.00101 \text{ cm.}$$

i.e. $b = 0.025$ cm.

Therefore, a 10 μm diameter wire may be located within 0.025 cm. of a solid boundary and does not require correction for wall proximity. Consequently, it was concluded that the mounting of the anemometer probes within the cylinder head and piston crown space at approximately 0.038 cm. from either surface was perfectly justified and the measured results would not require correction.

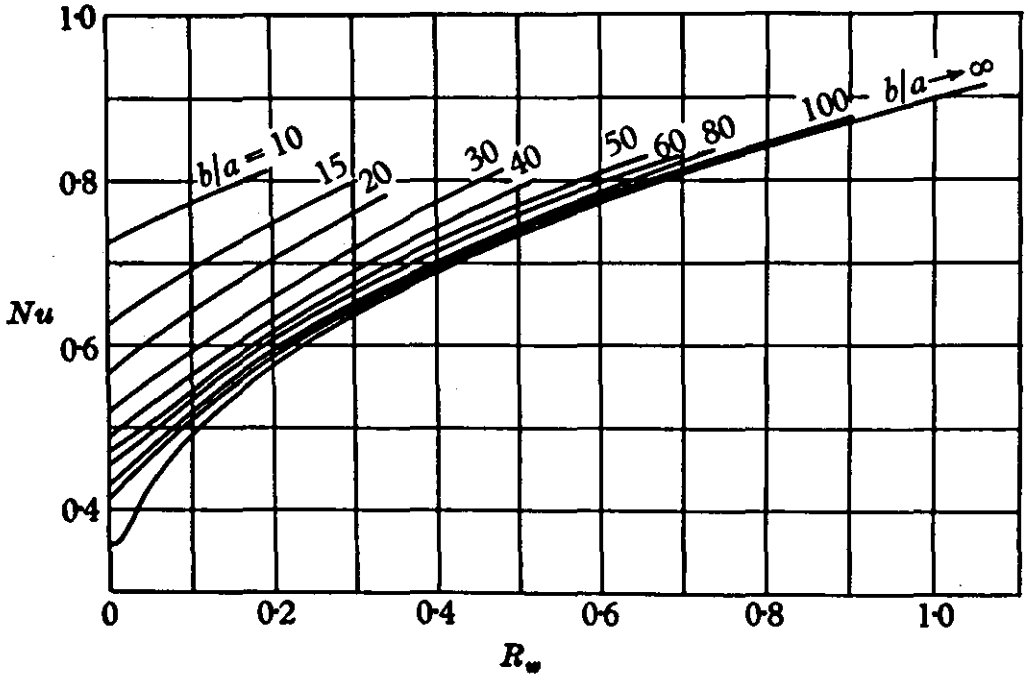

FIG. 4B1 WILLS' (30) RESULTS

A P P E N D I X 4 C

4.C.1 FORCED VORTEX THEORY

Vortex theory is based on the fact that radial pressure forces are required to act on the air elements in order to provide the necessary centripetal accelerations associated with the swirl velocity U. The basic equation for radial equilibrium may be derived from consideration of the pressure forces acting on a fluid element as illustrated in Fig. 4.C.1. As the acceleration in the radial direction is high and may amount to several thousand times the acceleration due to gravity, gravitational forces may be neglected and hence resolving in the radial direction we have,

$$(P + dP)(r + dr)d\theta - Prd\theta - Pdr^2 \frac{d\theta}{2} = \rho dr\, r\, d\theta \frac{U^2}{r} \qquad 4.C.1$$

where P, ρ, U, and r are the pressure, density, swirl velocity and radius respectively.

From equation 4.C.1 we have,

$$dP = \rho dr \frac{U^2}{r} \qquad 4.C.2$$

In curved flow, the pressure increases with the radius and there is a fall in pressure per unit radial distance towards the centre of curvature by an amount $\rho U^2/r$. The pressure gradient $dP/dr = \rho U^2/r$.

Imagine now a vertical cylindrical vessel with fluid rotating about a central vertical axis. The streamlines will be concentric circles and if the fluid rotates as a solid body, such a flow is

called a forced vortex, where the linear velocity U at any radius is given by $U = wr$ (where w is the angular velocity).

Substituting the relation $U = wr$ into equation 4.C.2 and integrating between the limits 1 and 2, where 1 refers to the cylinder axis and 2 refers to the outer cylinder radius, gives,

$$\int_1^2 dP = \rho w^2 \int_1^2 r\,dr$$

$$\text{i.e. } P_2 - P_1 = \frac{\rho w^2}{2}(r_2^2 - r_1^2) = \frac{\rho}{2}(U_2^2 - U_1^2) \qquad \text{4.C.3}$$

Substitution into equation 4.C.3 for some typical values, for an engine speed of approximately 1500 RPM, where $P_1 = 2510$ kN/m^2, $\rho = 12.0$ kg/m^3, $U_2 = 100$ m/s, and $U_1 = 0$ m/s, gives,

$$P_2 = (251 + 6) \times 10^4 \text{ N/m}^2$$

$$\therefore P_2 = 257 \times 10^4 \text{ N/m}^2$$

The percentage error between the pressures P_1 and P_2 is therefore given by,

$$\text{Percentage error} = \frac{(257 - 251) \times 10^6}{251 \times 10^4}$$

i.e. Percentage error = 2.4%

Hence, it may be concluded that pressure distribution is spatially uniform within the cylinder when the developed flow pattern is characterised by a forced vortex velocity profile.

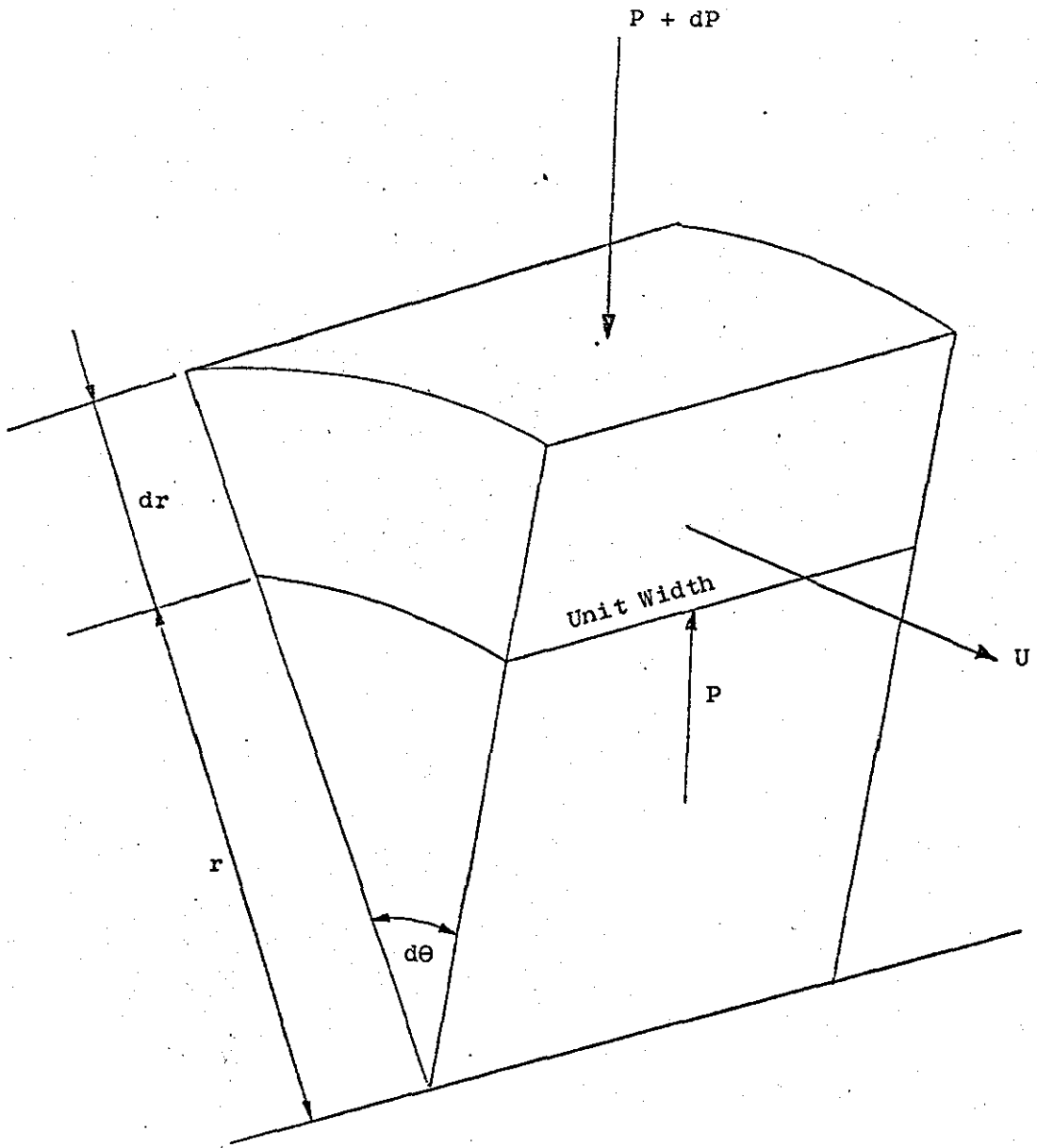

FIG.4.C.1. PRESSURE FORCES ACTING ON A FLUID ELEMENT

APPENDIX 5A

5.A.1 MOMENTUM ANALYSIS FOR THE INDUCED AIR IN THE CYLINDER

Conservation of angular momentum about an axis occurs if the sum of the moments of the external forces about that axis is zero. This follows because there is then no angular impulse about that axis and hence no change in angular momentum can occur.

Consider the piston and cylinder configuration outlined in Fig. 5A.1. The outer chamber has diameter D and at B.D.C. contains practically all the induced mass, whilst the smaller chamber has diameter d and volume V_b and contains practically all the induced mass at T.D.C.

From Fig. 5A.1, it may be observed that the mass moment of inertia of the contents of the outer chamber, assuming solid body rotation of the gas is given by,

$$I_c = m_c \frac{D^2}{8} \qquad \text{——— 5.A.1}$$

where m_c is the instantaneous mass trapped inside the outer chamber. The mass moment of inertia for the smaller chamber, assumed here to be cylindrical, (and to obey the solid body rotation assumption above), is given by,

$$I_b = (m_t - m_c) \frac{d^2}{8} \qquad \text{——— 5.A.2}$$

where m_t is the total mass induced into the cylinder at any crank angle, after inlet valve opening.

Therefore, the total mass moment of inertia is given by the sum of equations 5.A.1 and 5.A.2, i.e.

$$I = I_c + I_b = m_t \frac{m_c D^2}{m_t 8} + 1 - \frac{m_c}{m_t} \frac{d^2}{8} \qquad \text{——————5.A.3}$$

Assuming that the pressure and temperature are spatially uniform throughout the induction and compression periods and the angular velocity is the same for each particle of charge, then the angular momentum at any instant can be derived from equation 5.A.3 providing that the ratio m_t/m_c can be derived at any instant.

Because the volume of the smaller chamber is negligible in comparison to the cylinder swept volume, the ratio m_t/m_c may be written in terms of the volumes, i.e.

$$\frac{m_t}{m_c} = \frac{V_c + V_b}{V_c} = 1 + \frac{V_b}{V_c} \qquad \text{——————5.A.4}$$

or

$$\frac{m_t}{m_c} = 1 + \frac{V_b}{\frac{\Pi D^2 S(\theta)}{4}} \qquad \text{——————5.A.5}$$

where $S(\theta)$ is the piston displacement from T.D.C. at any crank angle θ. Substitution for m_t/m_c in to equation 5.A.3 gives

$$I_{(\theta)} = \frac{m_t}{2}\left[\frac{\frac{\Pi D^4 S(\theta)}{16 V_b} + \frac{d^2}{4}}{\frac{\Pi D^2 S(\theta)}{4 V_b} + 1}\right] \qquad \text{——————5.A.6}$$

The idea may be extended for the compression period, since it is necessary to determine the ratio $I_{(205)}/I_{(\theta)}$ where $I_{(205)}$ is the mass moment of inertia at the closure of the inlet valve.

Hence

$$\frac{I_{(205)}}{I_{(\theta)}} = \left[\frac{\frac{\Pi D^4 S(205)}{16 V_b} + \frac{d^2}{4}}{\frac{\Pi D^2 S(205)}{4 V_b} + 1}\right]\left[\frac{\frac{\Pi D^2 S(\theta)}{4 V_b} + 1}{\frac{\Pi D^4 S(\theta)}{16 V_b} + \frac{d^2}{4}}\right] \qquad \text{5.A.7}$$

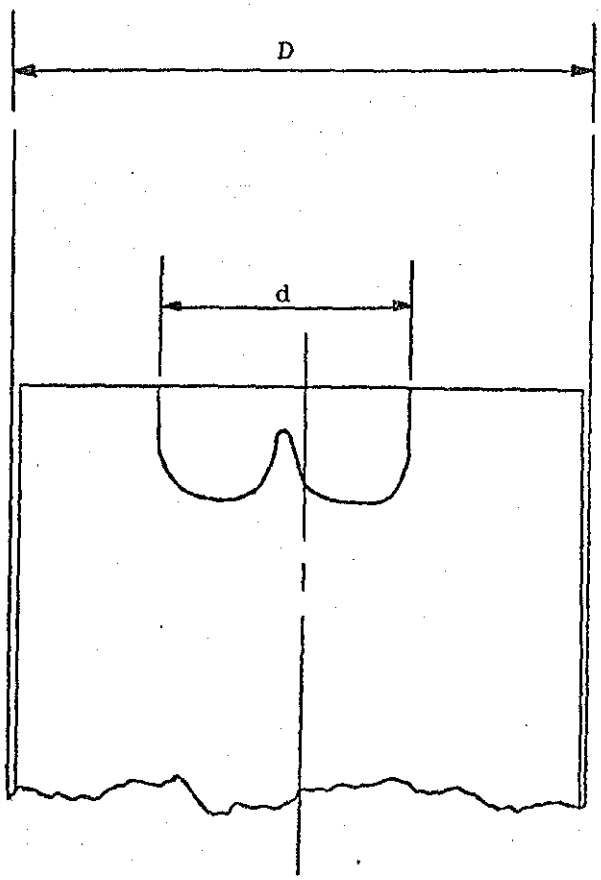

FIG. 5.A.1 CYLINDER AND PISTON GEOMETRY

APPENDIX 5 B

5.B.1 DETERMINATION OF SQUISH VELOCITY WHEN CYLINDER PRESSURE IS UNIFORMLY DISTRIBUTED

This appendix relates to a gas which has negligible inertia and viscosity and is not subject to surface friction effects. The instantaneous pressure during the compression stroke may then be assumed to be uniformly distributed throughout the gas volume.

Referring to Fig. 2.2 consider a small upward movement of the piston, reducing the distance between the annular face and the cylinder head from x to $x - dx$. Now let the area of that part of the annular face between the general radius r and the outer radius b be represented by A_r such that

$$A_r = (b^2 - r^2) \qquad \text{——— 5.B.1}$$

The volume swept by this annular area during the displacement dx is $A_r dx$, while the change in total volume of the cylinder is $A\,dx$. Since the pressure is spatially uniform, the density is also uniform, provided that temperature variation due to heat transfer is negligible; the high speed of rotation of the gas should prevent any appreciable temperature variation. Representing the total mass of gas in the cylinder by m, the mass in the outer annular space is

$$\frac{mA_r x}{Ax + v}$$

initially, and

$$\frac{mA_r(x - dx)}{A(x - dx) + v}$$ finally.

(where v is the volume of the combustion chamber).

The flow dm from the outer annular space across the cylindrical surface represented by $R'R''$ is the difference of these two expressions, that is,

$$dm = mA_r \left(\frac{x}{Ax + v} - \frac{x - dx}{A(x - dx) + v}\right)$$

The instantaneous density is $m/(Ax + v)$ and the volume flow across $R'R''$ may be written

$$dV = mA_r \left(\frac{x}{Ax + v} - \frac{x - dx}{A(x - dx) + v}\right)\left(\frac{Ax + v}{m}\right)$$

$$= \frac{A_r v\, dx}{Ax - A\, dx + v}$$

Omitting the term A dx, we have

$$\frac{dV}{dx} = \frac{A_r v}{Ax + v} \qquad \text{——— 5.B.2}$$

To obtain the rate of volume flow with respect to time, dV/dx must be multiplied by the piston velocity dx/dt. To obtain the linear velocity of the air, the flow rate dV/dt must be divided by the area of flow, that is, by the cylindrical area $2\pi rx$ at radius r. The mean air velocity is then given by

$$U_r = \frac{1}{2\pi r} \frac{A_r v}{x(Ax + v)} \frac{dx}{dt} \qquad \text{——— 5.B.3}$$

or

$$U_r = \frac{1}{2r} \frac{(b^2 - r^2)v}{(Ax + v)x} \frac{dx}{dt}$$

A P P E N D I X 5 C

5.C.1 MATHEMATICAL MODEL PROGRAM

In order to compute the instantaneous angular velocity for the mathematical model outlined in Section 5.0, two computer programs were written in Fortran IV. The two programs, N250 for the induction period and N260 for the compression period were presented in tabular solution form in Section 5.4 and the flow charts are included in Table 1 at the end of Section 5.0. Included below is a listing of the major input and output statements used in the program along with a complete listing of the two programs.

N250 Induction Period

Input Data

COEF1	First polynomial coefficient from the suction test (-)
COEF2	Second polynomial coefficient from the suction test (-)
COEF3	Third polynomial coefficient from the suction test (-)
DTH	Inlet Valve rise and fall time (^{o})
Z	Inlet valve lift (m)
S	Piston Stroke (m)
G	Connecting Rod length (m)
DC	Cylinder diameter (m)
DB	Combustion chamber diameter (m)
T	Polytropic exponent (-)
BVOL	Volume of the combustion chamber (m^3)
VRAD	Distance of inlet valve centre from the cylinder axis (m)

AREAPORT	Area of the inlet port at the velocity measuring section (m^2)
CP	Specific heat of air at constant pressure (kJ/kg^oC)
TO	Ambient air temperature (^oK)
PO	Ambient air pressure (N/m^2)
RHO	Air density in the inlet port (kg/m^3)
VCL	Clearance volume between cylinder head and piston crown (including the combustion chamber) (m^3)
ER1	% error in Wegstein iteration procedure (-)
VA	Inlet valve seat angle (^{o})
DV	Inlet valve diameter (m)
RPM	Engine speed (r.p.m.)
PCY1	Pressure inside the cylinder at top dead centre (N/m^2)
FLOTO	Mass of air trapped inside the cylinder at beginning of the computation.

Output Data

FLO1	Instantaneous mass flow rate (kg/s)
PCY1	Instantaneous cylinder pressure (N/m^2)
FLOTO	Total mass contained inside the cylinder (kg)
ANGRPM(M)	Instantaneous angular velocity (r.p.m.)
PSP(M)	Instantaneous piston speed (m/s)
USQ(M)	Instantaneous squish velocity (m/s)
AN6	Instantaneous crank angle (^{o})

N260 Compression Period

Input Data

B	Connecting rod length (m)
S	Piston Stroke (m)
VIS	Viscosity of air at ambient temperature gm/cm s
DC	Diameter of cylinder (m)
DB	Diameter of combustion chamber (m)
BVOL	Volume of combustion chamber (m^3)
RPM	Engine Speed (r.p.m.)
ASST	Total trapped mass inside the cylinder (kg)
WP	Angular velocity at the end of the induction period (r.p.
TG(I)	Instantaneous gas temperature (^oK)
PG(I)	Instantaneous gas pressure (p.s.i.)

Output Data

X	Crank angle position (^{o})
OMEGA	Instantaneous angular velocity (r.p.m.)

```
      MASTER N250
      DIMENSION PRES(450),FLOM(450),FLOMT(450),DEN(450),VEL(450)
      DIMENSION ENTLM(500),ANGV(500),ANGRPM(500),VEL1(500),VEL2(500)
      DIMENSION VEL3(500),VEL4(500),VEL5(500),ERTIA(500),PSP(500)
      DIMENSION USQ(500),AT1(500),PX(10),PC(10),DENTLM(500),X(500)
      DIMENSION X1(500),X2(500),X3(500)
      READ(1,10)COEF1,COEF2,COEF3,DTH,Z
   10 FORMAT(5F0.0)
      READ(1,11)S,G,DC,DB,T,BVOL,VRAD,AREAPORT
   11 FORMAT(8F0.0)
      READ(1,12)CP,TO,PO,RHO,VCL,ER1,VA,DV
   12 FORMAT(8F0.0)
      J=0
   13 J=J+1
      WRITE(2,14)
   14 FORMAT(1H1)
      READ(1,15)RPM,PCY1,FLOTO
   15 FORMAT(3F0.0)

C     CALCULATION OF CONSTANTS

      A=1/T
      B=(T-1)/T
      C=1/B
      P=0
      SA=SIN(P)
      S2A=SA*SA
      CA=COS(P)
      H=G-(G*G-S*S/4*S2A)**.5+S/2*(1-CA)
      VOL1=3.1415*DC*DC*H/4+VCL
```

```
      DO 26 M=1.205
      K=K+1
      P=M*3.1415/180
      P2=M*90*3.1415/(95*180)
      P3=(M-95)*90*3.1415/(110*180)
      SA=SIN(P)
      S2A=SA*SA
      CA=COS(P)
      H=G-(G*G-S*S/4*S2A)**.5+S/2*(1-CA)
      VOL2=3.1415*DC*DC*H/4+VCL
      VM=(VOL1+VOL2)/2
      VA=VA*3.1415/180

C     WEGSTEIN ITERATION PROCEDURE

      I=2
      PC(I-1)=PCY1
   16 PCY2=PC(I-1)
      PPCY2=(PCY2+PCY1)/2
      PRA=PPCY2/PO

C     TEST FOR CHOKED FLOW

      IF(PRA.LT.1)GO TO 17
      Y=1
      PRA=1/PRA
   17 Z3=(1+(Y-1)/2)**C
      PCH=1/Z3
      IF(PRA.GE.PCH)GO TO 18
       PRA=PCH
```

```
   18 IF(M.GE.95) GO TO 19
      VH=Z*SIN(P2)
      GO TO 20
   19 VH=Z*COS(P3)
   20 AREA=COEF1*(VH/DV)-COEF2*(VH/DV)**2+COEF3*(VH/DV)**3
      AREA=AREA/10000

C     MASS FLOW CALCULATION FOR COMPRESSIBLE FLOW

      A1=AREA
      A2=PRA
      A3=A2**A
      A4=2*Y/(Y-1)
      A5=PO*RHO
      A6=1-PRA**B
      A7=SQRT(A4*A5*A6)
      A8=A1*A3*A7
      FLO2=A8

C     CHECH FOR REVERSED FLOW

      IF(Y.EQ.1)GO TO 21
      GO TO 22
   21 FLO2=-FLO2
      Y=2

C     ENERGY CALCULATION FOR CYLINDER PRESSURE

   22 B1=PCY1
      TEMP=TO/(PO/PCY1)**B
```

```
      B2=(T-1)*A8*TEMP*CP*1/(6*RPM*VM)
      B3=PPCY2*(VOL2-VOL1)/VM
      B4=B1+B2-B3
      PX(I)=B4
      IF(I.EQ.2)GO TO 23
      GO TO 24
   23 PC(2)=PX(2)
      I=I+1
      GO TO 16
   24 PC(3)=PX(3)-(PX(3)-PX(2))*(PX(3)-PC(2))/(PX(3)-PX(2)-PC(2)+PC(1))
      RA=PC(3)/PX(3)
      ER=ABS(1-RA)
      IF(ER.LT.ER1)GO TO 25
      PC(1)=PC(2)
      PC(2)=PC(3)
      PX(2)=PX(3)
      GO TO 16
   25 PCY2=PC(3)
      PCY1=PCY2
      FLO1=FLO2
      VOL1=VOL2
      ANG=M
      FLOTO=FLOTO+FLO1*1/(6*RPM)

C     VELOCITY CALCULATION

      PRES(M)=PCY1
      FLOM(M)=FLO1
      DEN(M)=RHO*(PRES(M)/PO)**A
      VEL(M)=ABS(FLOM(M))/(AREA*DEN(M))
```

```
      DENTLM(M)=FLO1*VEL(M)*VRAD
      FLOMT(M)=FLOTO
      VELIN=FLOM(M)/(RHO*AREAPORT)
   26 CONTINUE
      ENTLM(1)=0.
      DO 27 M=1,215
      ENTLM(M+1)=ENTLM(M)+DENTLM(M)
      ENTLM(M)=ENTLM(M)/(6*RPM)
   27 CONTINUE
      DO 28 M=1,205
      ERTAA=DC*DC/8
      ANGV(M)=ENTLM(M)/(ERTAA*FLOMT(M))
      ANGRPM(M)=ANGV(M)*60/(2*3.1415)*COS(VA)
      VEL1(M)=ANGV(M)*.0127*COS(VA)
      VEL2(M)=ANGV(M)*.0254*COS(VA)
      VEL3(M)=ANGV(M)*.0349*COS(VA)
      VEL4(M)=ANGV(M)*.0318*COS(VA)
      VEL5(M)=ANGV(M)*.0381*COS(VA)
   28 CONTINUE
      K=0
      DO 31 M=1,200
      K=K+1
      ANG=M
      IF(K.EQ.10) GO TO 29
      GO TO 31
   29 WRITE(2,30)ANG,ANGRPM(M)
   30 FORMAT(2E20.8)
      K=0
   31 CONTINUE
```

```
C       CALCULATION OF PISTON SPEED AND SQUISH VELOCITY

        DO 32 M=205,360,1
        P1=M*3.1415/180
        SA=SIN(P1)
        S2A=SA*SA
        CA=COS(P1)
        H=G-(G*G-S*S/4*S2A)**.5+S/2*(1-CA)
        S1=DC*DC/4
        S2=DB*DB/4
        S3=3.1415*DC*DC*H/4
        S4=3.1415*DB*DB*DB/(8*H)
        S5=4*(B*B-S*S/4*S2A)**.5
        S6=S*S*SA*CA/S5+S*SA/2
        PSP(M)=6*RPM*3.1415/180*S6
        USQ(M)=(S1-S2)/(S3+BVOL)*BVOL*PSP(M)/(H*DB)
        PSP(J.I)=ABS(PSP(M))
        USQ(J.I)=ABS(USQ(M))
   32   CONTINUE
        IF(J.LT.4) GO TO 13
        STOP
        END
        FINISH
```

```
      MASTER N260
      DIMENSION TG(200),PG(200)
      EXTERNAL FN
      COMMON/FUN/WP,ERN,ERP,STV
      K=0
    9 K=K+1
      READ(1,10)(TG(I),I=1,151,10),(PG(I),I=1,151,10)
   10 FORMAT(8F0.0)
      READ(1,11)B,S,VIS,DC,DB,BVOL,RPM,ASST,WP
   11 FORMAT(9F0.0)
      WP=WP*2*3.1415/60
      N=1
      M=11
      DO 12 I=1,150
      IF(I.EQ.M) N=N+10
      M=N+10
      TG(I+1)=TG(I)+(TG(M)-TG(N))/10
      PG(I+1)=PG(I)+(PG(M)-PG(N))/10
   12 CONTINUE
      A=209*3.1415/180
      SA=SIN(A)
      S2A=SA*SA
      CA=COS(A)
      A1=B-(B*B-S*S/4*S2A)**.5+S/2*(1-CA)
      VOLR=1+4*BVOL/(DC*DC*A1)
      ERP=DC*DC/(8*VOLR)+(1-1/VOLR)*DB*DB/8
      ERP=ERP*ASST
      ZZ=ERP
      J=0
      DO 16 I=1,151
```

```
      IF(K.GT.8) PG(I)=PG(I)*1.8
      J=J+1
      X=I+209
      A=X*3.1415/180
      SA=SIN(A)
      S2A=SA*SA
      CA=COS(A)
      A1=B-(B*B-S*S/4*S2A)**.5+S/2*(1-CA)
      A2=VIS*390*(TG(I)/273)**1.5/(TG(I)+117.0)/10
      A3=2.31*PG(I)/(96.5*TG(I))*1000
      VOLR=1+4*RVOL/(DC*DC*A1)
      ERN=DC*DC/(8*VOLR)+(1-1/VOLR)*DB*DB/8
      ERN=ERN*ASST
      ZZ1=ERN
      ZZZ=ZZ/ZZ1
      A7=3.1415*A3**0.8*A2**0.2*DC**3.6/16
      A8=A7*0.067+A1
      A9=A7*0.088*DC/16
      A10=A9/(6*RPM)
      A11=A8/(6*RPM)
      STV=A10
      WP1=WP
      CALL ORTMI(WN,F,FN,0.0,55000.0,.0001,100,IER)
      OMEGA=WN*60/(2*3.1415)
      IF(J.EQ.11) GO TO 13
      GO TO 15
   13 WRITE(2,14)X,OMEGA,ZZZ
   14 FORMAT(25X,3E14.6)
      J=1
   15 ERP=ERN
```

```
      WP=WN
   16 CONTINUE
      WRITE(2,17)
   17 FORMAT(1H1)
      IF(K.LT.11) GO TO 9
      STOP
      END


      FUNCTION FN(WN)
      COMMON/FUN/WP,ERN,ERP,STV
      FN=WN*ERN-WP*ERP+STV*(((WN+WP)/2)**1.8)
      RETURN
      END


      SUBROUTINE DRTMI(X,F,FN,XLI,XRI,EPS,IEND,IER)
      IER=0
      XL=XLI
      XR=XRI
      X=XL
      TOL= X
      F=FN(TOL)
      IF(F) 1,16,1
    1 FL=F
      X=XR
      TOL= X
      F=FN(TOL)
      IF(F) 2,16,2
    2 FR=F
```

```
      IF(SIGN(1.00,FL)+SIGN(1.00,FR)) 25,3,25
    3 I=0
      TOLF= 100.0*EPS
    4 I=I+1
      DO 13 K=1,IEND
      X= 0.5*(XL+XR)
      TOL=X
      F=FN(TOL)
      IF(F) 5,16,5
    5 IF(SIGN(1.00,F)+SIGN(1.00,FR)) 7,6,7
    6 TOL= XL
      XL=XR
      XR= TOL
      TOL= FL
      FL=FR
      FR= TOL
    7 TOL= F-FL
      A= F*TOL
      A=A+A
      IF(A-FR*(FR-FL)) 8,9,9
    8 IF(I-IEND) 17,17,9
    9 XR=X
      FR=F
      TOL= EPS
      A= ABS(XR)
      IF(A-1.00) 11,11,10
   10 TOL= TOL*A
   11 IF(ABS(XR-XL)-TOL) 12,12,13
   12 IF(ABS(FR-FL)-TOLF) 14,14,13
   13 CONTINUE
```

```
14 IF(ABS(FR)-ABS(FL)) 16,16,15
15 X=XL
   F=FL
16 RETURN
17 A=FR-F
   DX=(X-XL)*FL*(1.00+F*(A-TOL)/(A*(FR-FL)))/TOL
   XM=X
   FM=F
   X=XL-DX
   TOL=X
   F=FN(TOL)
   IF(F) 18,16,18
18 TOL= EPS
   A=ABS(X)
   IF(A-1.00) 20,20,19
19 TOL= TOL*A
20 IF(ABS(DX)-TOL) 21,21,22
21 IF(ABS(F)-TOLF) 16,16,22
22 IF(SIGN(1.00,F)+SIGN(1.00,FL)) 24,23,24
23 XR=X
   FR=F
   GOTO 4
24 XL=X
   FL=F
   XR=XM
   FR=FM
   GOTO 4
25 IER= 2
   RETURN
   END
```